Exploring Redox-driven Self-Assembly of Mixed Metal Polyoxometalates

Charikleia Sartzi

A Thesis submitted to the University of Glasgow for the degree of Doctor of Philosophy

School of Chemistry

April 2016

This research was funded by the University of Glasgow

True Knowledge exists

in knowing that you know nothing

-Socrates

«Ἓν οἶδα ὅτι οὐδὲν οἶδα»

-Σωκράτης

Acknowledgements

This project was carried out between May 2012 and September 2015 in the School of Chemistry at the University of Glasgow, during which time I received the help and advice of many people.

In particular, I would like to thank Professor **Lee Cronin**, for giving me the opportunity to do research in his group, for sharing the motivation and endless enthusiasm in his unique way to think and do chemistry, and for his constant support, patience and understanding.

Dr. **De-Liang Long** and Dr. **Ross Winter** for their support and help with Crystallography.

I own a great thanks to Dr. **Haralampos N. Miras**, for his patient and continuous support during these three years, for being such an amazing mentor from day one and for sharing his huge chemistry knowledge and experience.

In addition, I would like to thank Dr. **Christoph Busche**, for all the help with EPR and UV-vis measurements, Dr. **Laia Vilà-Nadal** for her help with DFT calculations, Dr. **Andrew MacDonell** for his help with the design programs and for the English classes. I want to thank Dr. **Andreu Ruiz** for introducing the world of flow systems and for helping me with the LabView software.

Dr. **Geoffrey J. T. Cooper**, for all his support with computers and software.

Dr. **Weimin Xuan** for being such a great "bench neighbour" and patient enough to teach me Badminton.

I extent my thanks to the people with whom I have shared an office- Dr. Ross Winter, Dr. Philip Kitson, Phil Robbins, Mercè Martin, James Taylor, Dr. Mo Hezwani, Jaun Manuel Parilla Gutierrez, Dr. Chaihong Zang, Vasilios Duros for having interesting conversations - you have all made my life in the group happier.

I extend my thanks to **Jim McIver** and **Dania Castro Spencer** for their continuous help and support in the laboratory.

Also, the technical staff of the University of Glasgow; Michael Beglan for FAAS, Kim Wilson for EA and Andy Monaghan for the TGA.

Finally, I would like to thank The Whole Cronin Group, a fascinating, amusing and talented of people to work with.

Table of Contents

Publications

"Trapping the δ Isomer of the Polyoxometalate-Based Keggin Cluster with a Tripodal Ligand", Harikleia Sartzi, Haralampos N. Miras, Laia Vilà-Nadal, De-Liang Long, and Leroy Cronin, *Angew. Chem. Int. Ed.*, **2015**, *54*, 15488-15492.

"Controlling the Self-Assembly of a Family of Mixed metal Mo/V Polyoxometalates utilizing Pyramidal Heteroanions", Harikleia Sartzi, Laia Vilà-Nadal, De-Liang Long, Leroy Cronin and Haralampos N. Miras, *Chem. Eur. Jour.*, in preparation.

Abstract

How can we control the experimental conditions towards the isolation of specific structures? Why do particular architectures form? These are some challenging questions that synthetic chemists try to answer, specifically within polyoxometalate (POM) chemistry, where there is still much unknown regarding the synthesis of novel molecular structures in a controlled and predictive manner. This work covers a wide range of POM chemistry, exploring the redox self-assembly of polyoxometalate clusters, using both "one-pot", flow and hydrothermal conditions. For this purpose, different vanadium, molybdenum and tungsten reagents, heteroatoms, inorganic salts and reducing agents have been used.

The template effect of lone-pair containing pyramidal heteroatoms has been investigated. Efforts to synthesize new POM clusters displaying pyramidal heteroanions (XO_3^{2-}, where X= S, Se, Te, P) are reported. The reaction of molybdenum with vanadium in the presence of XO_3^{2-} heteroatoms is explored, showing how *via* the cation and experimental control it is possible to direct the self-assembly process and to isolate isostructural compounds. A series of four isostructural (two new, namely $\{Mo_{11}V_7P\}$ and $\{Mo_{11}V_7Te\}$ and two already known, namely $\{Mo_{11}V_7Se\}$ and $\{Mo_{11}V_7S\}$ disordered egg-shaped Polyoxometalates have been reported. The compounds were characterized by X-ray structural analysis, TGA, UV-Vis, FT-IR, Elemental and Flame Atomic Absorption Spectroscopy (FAAS) analysis and Inductively Coupled Plasma Optical Emission Spectroscopy (ICP-OES). Cyclic Voltammetry measurements have been carried out in all four compounds showing the effect of the ionic density of the heteroatom on the potential. High-Resolution ESI-MS studies have revealed that the structures retain their integrity in solution.

Efforts to synthesize new mixed-metal compounds led to isolation, structural, and electronic characterization of the theoretically predicted, but experimentally elusive δ-isomer of the Keggin polyoxometalate cluster anion, $\{H_2W_4V_9O_{33}(C_6H_{13}NO_3)\}$, by the reaction of tungstate(VI) and vanadium(V) with triethanolammonium ions (TEAH), acting as a tripodal ligand grafted to the surface of the cluster. Control experiments (in the absence of the organic compound) have proven that the tripodal ligand plays crucial role on the formation of the isomer. The six vanadium metal centres, which consist the upper part of the cluster, are bonded to the "capping" TEA tripodal ligand. This metal-ligand bonding directs and stabilises the formation of the final product. The δ-Keggin species was characterized by single-crystal X-ray diffraction, FT-IR, UV-vis, NMR and ESI-MS spectrometry. Electronic structure and structure-stability correlations were evaluated by means of DFT calculations.

The compounds exhibited photochromic properties by undergoing single-crystal-to-single-crystal (SC-SC) transformations and changing colour under light.

Non-conventional synthetic approaches are also used for the synthesis of the POM clusters comparing the classical "one-pot" reaction conditions and exploring the synthetic parameters of the synthesis of POM compounds. Reactions under hydrothermal and flow conditions, where single crystals that depend on the solubility of the minerals under hot water and high pressure can be synthesized, resulted in the isolation of two isostructural compounds, namely, $\{Mo_{12}V_3Te_5\}$. The compound isolated from a continuous processing method, crystallizes in a hexagonal crystal system, forming a 2D porous plane net, while the compound isolated using hard experimental conditions (high temperature and pressure) crystallizes in monoclinic system, resulting in a different packing configuration. Utilizing these alternative synthetic approaches, the most kinetically and thermodynamically compounds would possibly be isolated. These compounds were characterised by single-crystal X-ray diffraction, FT-IR and UV-vis spectroscopy.

Finally, the redox-controlled driven oscillatory template exchange between phosphate (P) and vanadate (V) anions enclosed in an $\{M_{18}O_{54}(XO_4)_2\}$ cluster is further investigated using UV-vis spectroscopy as a function of reaction time, showed that more than six complete oscillations interconverting the capsule species present in solution from $\{P_2M_{18}\}$ to $\{V_2M_{18}\}$ were possible, provided that a sufficient concentration of the TEA reducing agent was present in solution. In an effort to investigate the periodicity of the exchange of the phosphate and vanadate anions, time dependent Uv-vis measurements were performed for a period at a range of 170-550 hours. Different experimental conditions were also applied in order to investigate the role of the reducing agent, as well as the effect of other experimental variables on the oscillatory system.

Abbreviations

POM	Polyoxometalate
BVS*av*	Bond valence sum average
LFS	Linear Flow System
CN	Coordination Number
HPOM	Heteropolyoxometalate
TGA	Thermogravimetric analysis
Acac	acetylacetonato
TBA	Tetra-*n*-butyl ammonium
TEA	Triethanol amine
TPP	Tetraphenylphosphonium
CSI-MS	Cryospray ionization mass spectroscopy
NMR	Nuclear magnetic resonance
UV-VIS	Ultraviolet-visible Spectroscopy
XRD	X-ray Diffraction
FT-IR	Fourier-transformation infra-red
ESI-MS	Electrospray ionization mass spectroscopy
SMM	Single Molecule Magnet

1. Introduction

1.1 Polyoxometalates

Polyoxometalates (POMS) are discrete clusters of metal-oxide units, perhaps the largest non-biologically derived molecules structurally characterized, with a large diversity of nanoscale structure and diverse properties. They are constructed from early transition metals in their highest oxidation states, most commonly vanadium, molybdenum and tungsten[1] and less commonly niobium[2], tantalum[3] and palladium.[4] They are assembled from the aggregation of mononuclear MO_x polyhedral units (M = W, Mo, V, Nb, Ta, or Cr; x = 4 – 7) linked via edge, corner and occasionally face sharing modes. The increasing interest in POMs (in the last 25 years, from 1991 to date) is centred on two features: the structural diversity due to the coordination flexibility in their metal-oxo structures ranging from tetrahedral to pentagonal bipyramid and the number of elements of the periodic table that can be incorporated inside POM clusters.[5] Due to these features POMs possess a wide range of composition, structures and charge distribution and have an unmatched range of physical and chemical properties. The list of potential properties includes, magnetism[6], catalysis[7] medicinal properties[8], and materials design.[9]

1.2 History of Polyoxometalates

Polyoxometalates have been known for more than two centuries. However the lack of appropriate analytical methods, the field remained the most confusing in inorganic chemistry. We could agree that the history of POMs started in 1793 Scheele investigated reduced molybdenum salts and discovered what are now known to be the first examples of Molybdenum Blues.[10] The next step in POM history came in 1826 when Jöns Jacob Berzelius reported the $(NH_4)_3[PMo_{12}O_{40}]\cdot xH_2O$, as "yellow precipitate" produced when ammonium molybdate $(NH_4)_2MoO_4$ is added in excess to phosphoric acid H_3PO_4 , with the so-called 12:1 composition.[11] It was not until 1864 when the analytical composition of the 12:1 heteropoly species was precisely determined through the discovery of the tungstosilicic acids and their salts (now known as $[H_4SiW_{12}O_{40}]\cdot xH_2O$) by Galissard de Marignac.[12] In the early 20th century, Werner himself tried to explain the structures of 12:1 species as an attempt to understand the composition of heteropolyanions.[13] In the following years Miolati,[14] Rosenheim[15] and Pauling[16] each gave a structural hypothesis that the clusters were shared metal-oxygen polyhedra. Specifically, in the Miolati-Rosenheim hypothesis, the 12-

molybdophosphoric acid was viewed as deriving from the hypothetical acid $H_7[PO_6]$ through the replacement of the oxygen atoms by Mo_2O_7 groups. After that hypothesis Pauling proposed a different theory in which the central tetrahedral XO_4 heteroatoms were surrounded by MO_6 octahedra. The structures he elaborated turned out to be incorrect because he did not consider the possibility of edge-sharing between MO_6 octahedra. A few years after Pauling's ideas, in 1933, with the development of single crystal X-ray diffraction (XRD), the crystal structure of $H_3[PW_{12}O_{40}]\cdot 5H_2O$ was solved by Keggin [17]. This structure which is named by its discoverer, is comprised of WO_6 octahedra, contains both corner and edge sharing of oxo ligands. In 1937, Anderson predicted the structure of $[Te^{VI}Mo_6O_{24}]^{6-}$ [18], which was crystallographically determined by Evans almost 10 years later.[19] The structure was revealed to be a planar ring of edge-shared MoO_6 octahedra around a central TeO_6 octahedron and it is now known as the Anderson or Anderson-Evans structure. Then, another common structure – the Wells-Dawson heteropoly anion (18:2) was proposed by Wells in 1945 and later confirmed by Dawson in 1953 [20]. The structure comprises two Keggin fragments connected together via corner sharing of oxygen ligands. The rapid development of X-Ray Crystallography [21] as well as the computer technology has followed by the rapid development of the field of polyoxometalates. In the mid-1990s, Müller and co-workers were able to isolate a few single crystals from a Mo blue solution obtained with NH_2OH as reducing agent. [22] The structure was revealed to be a giant wheel-shaped polyoxomolybdate, comprising 154 molybdenum atoms embedded in a network of oxygen atoms, with the general formula $[Mo_{154}(NO)_{14}O_{448}H_{14}(H_2O)_{70}]^{28-}$ or $[Mo^{VI}_{126}Mo^{V}_{28}]$ or $\{Mo_{154}\}$. With the publication of a review by Pope and Müller in 1991, [1] POM chemistry entered the modern era. The developments in POM chemistry were later reported in Chemical Reviews in 1998,[2] which presented the history, developments, and applications in many areas of POMs chemistry. The incredible wealth and diversity of modern POM research has been exemplified by several recent reviews and special editions of leading journals. [23]

1.3 General Formation and Bonding in Polyoxometalates

As was mentioned, POMs can be considered as a set of polynuclear clusters that consist of transition metals (also called *addenda*), mainly of Mo, W and V and shared oxygen atoms. [24] They are formed under acidic aqueous conditions and can be controlled by several synthetic parameters (e.g. the counterion, pH, temperature, solvent, ionic strength, type of acid, concentration of the metal oxide units, time of reaction, etc.). It is worth mentioning that control of the pH of the metal oxides solution is required in order to avoid the formation

of infinite powder solid oxides (MO_3 lattices). [25] It is thus understood that the POM clusters can be "trapped" between mononuclear metal ions and the infinite metal oxides, (Figure 1.1). These metal-oxide species are constructed *via* the condensation of different $\{MO_x\}$ units into larger aggregates where x is between 4 and 7, in which metal atoms are located at the centre and the oxygen atoms act as the vertices.

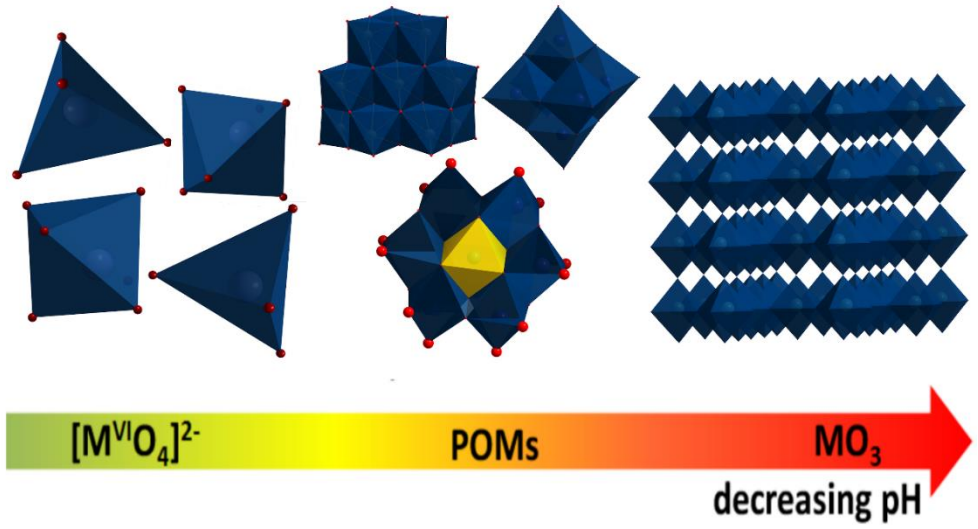

Figure 1.1 POM chemistry encapsulates a fertile region between small molecule solution chemistry and infinite solid oxide materials. Dark teal polyhedra: $\{MO_4\}$ and $\{MO_6\}$, light yellow polyhedron: $\{XO_4\}$, red spheres: O.

The formation of $\{MO_x\}$ units are mainly ruled by the charge (electrostatics) and the ionic radii of the metal centres.[26] The ratio between the ion charge and the ionic radii of the metal/ligands derive from the formation of tetrahedral $\{MO_4\}$, square base pyramid $\{MO_5\}$, octahedral $\{MO_6\}$ and pentagonal bipyramid $\{MO_7\}$ units (Table 1). However, the ion charge and the ionic radii are not the only important consideration to take about $\{MO_x\}$ units. The ability of the metal centre to form π metal-oxygen bonds is also an important parameter that directly affects the stability of the POMs.[27] The charge neutrality is most frequently provided by the association of alkali metal (e.g. K^+, Na^+, Li^+, etc.) or bulky organic cations (i.e. TEAH, TBA, TPP, etc.).

Table 1.1 The most common metal centres in POMs, their ionic radii and their coordination number with O^{2-} ligand.

Metal Centre (M^{n+})	Ionic Radii (Å)	Coordination Number {MO_x}
W^{6+}	0.60	6
Mo^{6+}	0.59	4, 6, 7
V^{5+}	0.54	4, 5, 6, 7
Ta^{5+}	0.64	6
Nb^{5+}	0.64	6

Further, normally the polyhedra are linked together by three possible modes, (a) corner-sharing, (b) edge-sharing and (c) face-sharing, Figure 1.2. The various size of POM clusters is a result of the different bonding and aggregation modes in POM compounds. For example, the Lindqvist polyanions containing as few as six metal atoms are relatively small,[28] whilst the "blue lemon" {Mo_{368}} is extremely large (diameter ~ 6 nm).[8] As mentioned, the versatility of POM structures is due to the ability of transition metals to coordinate to different numbers of oxygen atoms. Depending on different classification methods, the POM clusters usually fall into more than one category, such as isopolyanions and heteropolyanions; lacunary and plenary POMs; pure-inorganic and inorganic-organic hybrid POMs; homo-metallic and hetero-metallic POMs, decided by the types of addenda in the architectures. [29]

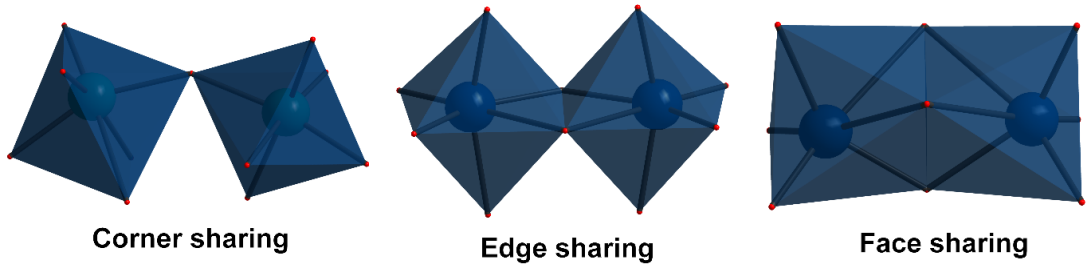

Figure 1.2 Representation of connecting modes of metal oxide polyhedra: (a) corner-sharing; (b) edge-sharing; (c) face-sharing. Dark teal polyhedra: {MO_6}, dark teal spheres: M, red spheres: O.

1.4 Polyoxometalates: Classical Features and Isomers

The majority of POMs can be identified as one of the four distinct structural families; Lindqvist, Anderson, Keggin and Well-Dawson-type clusters. Such architectures are dominant in the field because of their reproducibility and the fact that they can be formed by several types of addenda metals. Apart from M and O, other elements present in POMs structure are called heteroatoms (X). Their nature is diverse and nearly all elements of the periodic table have been included as heteroatoms, but the most common are transition metals as iron, copper, nickel, zirconium, ruthenium, etc. or elements from the p-block, as phosphorous, silicon, aluminium, etc. [30] Based on the POM nature and structure, the coordination of heteroatoms can be either tetrahedral or octahedral. The presence of heteroatoms in the structure classifies the POMs in two major families: isopolyoxoanions $\{[M_nO_y]^{p-}\}$ when no additional elements are present in the POM structure (e.g. Lindqvist) and heteropolyoxoanions $\{[X_zM_nO_y]^{p-}\}$ with $z \leq n$) when there are one or more heteroatoms (Anderson, Keggin and Wells-Dawson). [31] The stability of these classical POMs has made them excellent candidates as starting materials for the manufacture of new POM based clusters.

1.4.1 Lindqvist Structure

This hexametalate isopolyoxoanion is the smallest of the four POM types and it was first reported in 1950. [32] The structure has the general formula $[M_6O_{19}]^{n-}$ and it can be isolated from the early transition metals V, Mo, W, Nb and Ta. [33-36] The six addenda are coordinated to the central μ_6-O atom giving an overall O_h symmetry (Figure 1.3).

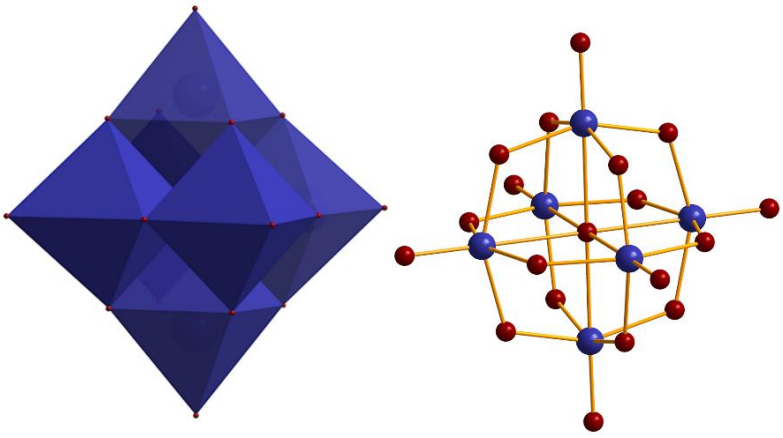

Figure 1.3 The Lindqvist structure $[M_6O_{19}]^{n-}$: Polyhedral (left) and ball-and-sticks (right) representation. Colour code: M: indigo, O: red.

1.4.2 Anderson-Evans Structure

The Anderson-Evans structure (or more commonly Anderson structure) is the smallest of the common heteropolyoxoanions, incorporating a single octahedral heteroatom, *X*, within a hexagonal planar ring of edge-sharing [MO_6] octahedra to yield a heptametalate D_{3h} species of the general formula $[H_yXM_6O_{24}]^{n-}$ (y = 0 - 6) (Figure 1.4). [17] Unlike the Lindqvist ion, the Anderson cluster may only be synthesised using the group VI addenda metals (predominately Mo and, less commonly, W) however a wide variety of (mainly 1st row) transition metal[37-41] and p-block elements [42-46] may act as the central heteroatom, significantly expanding the compositional diversity of this class of compounds. The Anderson structure, unlike the vast majority of POMs, has no useful redox chemistry associated with the d^0 addenda metal centres and the nature of the heteroatom may therefore play a key role in defining the properties of each species. The structure was first predicted by Anderson in 1937 and first solved by Evans in 1948. [18, 19]

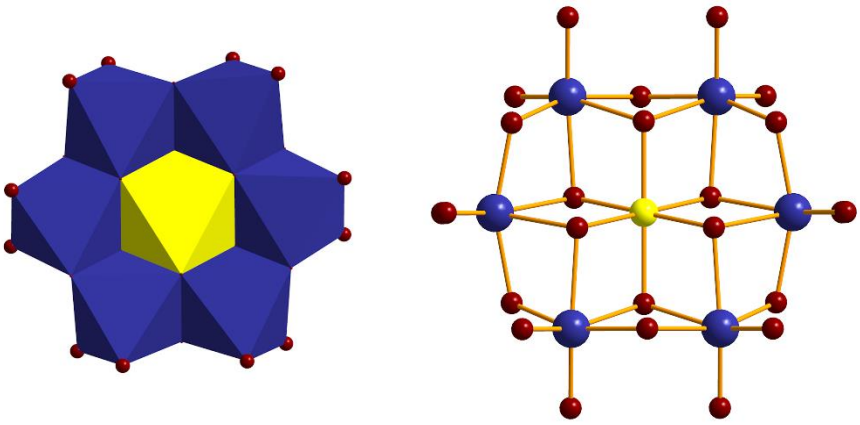

Figure 1.4 The Anderson structure $[XM_6O_{24}]^{n-}$: Polyhedral (left) and ball-and-sticks (right) representation. Colour code: M=indigo, X= green O=red.

1.4.3 Keggin Structure

Four $\{M_3O_{13}\}$ triads, where M=addenda, are organised tetrahedrally around a central heteroatom (Figure 1.5) forming the Keggin structure. The $\{MO_6\}$ octahedra within each triad are edge sharing and the triads are connected to each other *via* corner sharing of oxygen ligands. Each addendum has only one terminal M=O. For Keggin structures the most common heteroatoms (X) are p-block elements like B, Si, Ge, P and S [47], but in rare occasions the heteroatom can be a transition metal. [48] The heteroatom for Keggin POMs is in a tetrahedral coordination mode; however there is a unique example of a Keggin structure possessing an octahedral heteroatom. In 2011, Newton *et al.* reported a $\{Mn_{13}\}$ structure in which all the triads were composed of 12 Mn^{III} and a central octahedral Mn^{IV} cations, is held together by organic capping ligands, namely 2,6-bis[N-(2-hydroxyethyl)iminomethyl]-4-methylphenol (H_3bemp). [49]

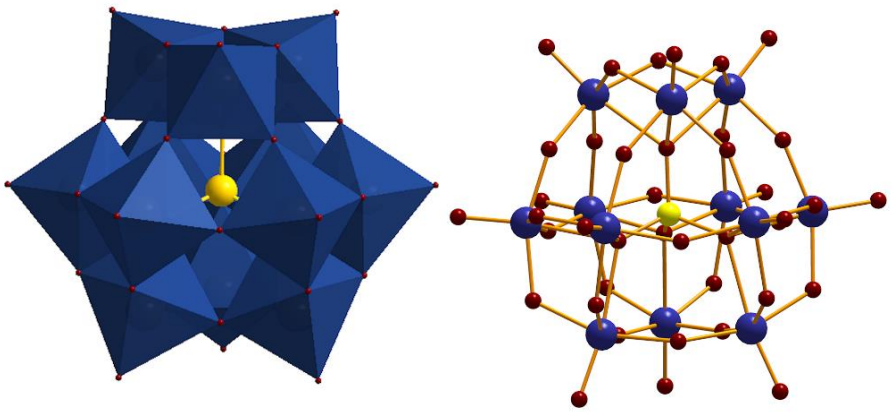

Figure 1.5 The Keggin structure $[XM_{12}O_{40}]^{n-}$: Polyhedral (left) and ball-and-sticks (right) representation. Colour code: M: indigo, X: yellow, O: red.

The different way in which the triads can be arranged relative to the heteroatom, give the Keggin structure the potential to exist in five isomers (including the α-Keggin structure). Investigations of the Keggin structure revealed four additional isomers, each resulting from the 60° rotation of the four basic $\{M_3O_{13}\}$ units, giving α, β, γ, δ and ε isomers as reported by Baker and Figgis, [50] see Figure 1.6b. With the α and β -isomers, the four building blocks are linked together in a corner-shared fashion, whilst in the case of γ, δ and ε the corner-shared linkages are replaced by one, three and six edge-shared, respectively. [51] These isomers can be experimentally distinguished by electrochemical techniques and vibrational spectroscopy, e. g. IR and Raman spectroscopy and of course by X-Ray Diffraction spectroscopy. This is due to the different orientation of the triads in the Keggin isomers, with the α-Keggin containing all triads in staggered conformation. Each subsequent rotation of a

tri-metallic cap leads to it in adapting an eclipsed conformation followed by the change from corner-sharing to edge-sharing mode between neighbouring triads (Figure 1.6a). Since the first report of the most common α- and β-Keggin isomers [52], many researchers have investigated their properties [53], whilst others reported families of transition metal substituted derivatives of α-, β- and γ- isomers. [54] The first Keggin species containing an ε-core was reported almost 60 years later as a Rh-substituted oxomolybdenum(V) complex [55], followed by the report of a mixed-valence Mo^{V}/Mo^{VI} iso-polyanion[56] and the La and Ni-substituted oxomolybdenum ε-Keggin isomers, respectively [57] and recently the Bi-substituted vanadium-based ε isomer. [58] The first δ-Keggin polyanionic polyoxometalate-based isomer consisted of four W^{VI} and nine V^{V} metal ions, was isolated by Cronin *et al.*[59], following the only related δ-Keggin cationic species; the $\{Al_{13}\}$ cation [60] and the "reverse-Keggin" ions incorporating either p-block elements (Sb^{5+}) or first row transition metal ions (Co^{2+}, Mn^{2+}, or Zn^{2+}). [61]

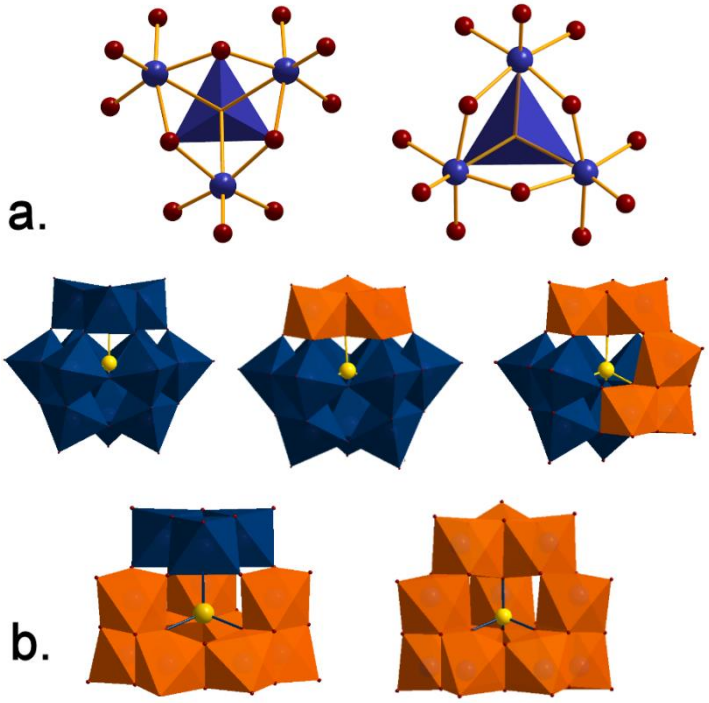

Figure 1.6 a) The regular 'staggered' conformation (left) of one tri-metallic triad relative to the central heteroatom moiety and the 'eclipsed' configuration (right) which has been rotated by 60°; (b) Polyhedral representation of the crystal structures of all the isomers of the Keggin ion: α, β and γ (top from the left), δ and ε (bottom from the left). The orange polyhedra show the $\{M_3O_{13}\}$ units which have been rotated the 60° with respect to the α-isomer. The yellow spheres are the heteroatom templates, the small red spheres are the oxo-ligands.

1.4.4 Wells-Dawson Structure

The first crystal structure of the Wells-Dawson (or simply known as Dawson) cluster was solved by Dawson in 1953 [20] and it has the generalised formula $\{X_2M_{18}O_{62}\}^{n-}$ (X= P, Si, As, etc., M=V, Mo, W). The structure can be viewed as a connection of two Keggin units that have had a $\{M_3O_{13}\}$ unit removed from each Keggin and the resulting moieties are connecting in a corner-sharing mode. The removed addenda come from three separate triads, generating a Keggin with one complete triad (or cap) and three incomplete triads. The two fragments are joined together *via* corner sharing of oxo ligands to create a belt of twelve addenda (Figure 1.7). It is worth noting that the electron transfer properties are different in the "cap" and "belt" positions of the Dawson [62], which impacts the chemical properties of the cluster. Finally, the hetero-anion, XO_4^{n-} links to the three metals of a $\{M_3O_{13}\}$ cap through a μ_3-O coordination mode and to six of the belt octahedra.

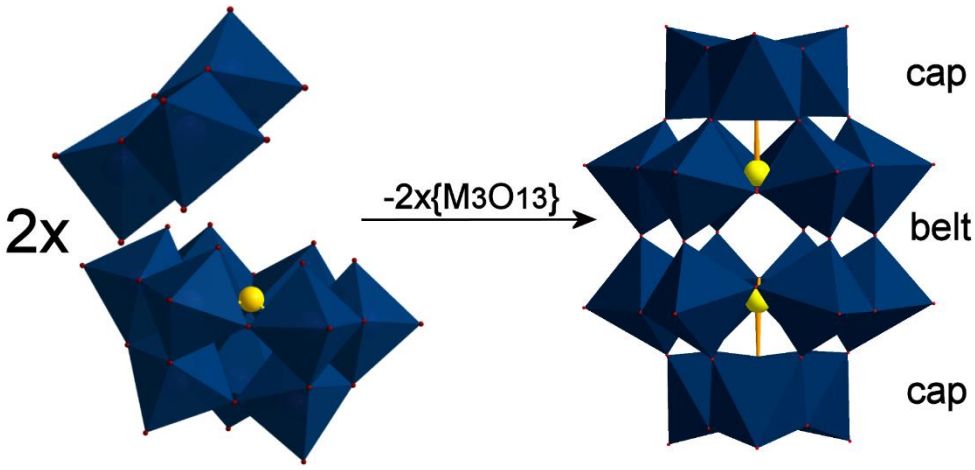

Figure 1.7 The formation of The Dawson-Wells structure $[X_2M_{18}O_{62}]^{n-}$ (right) as derived from the combination of two Keggin structures with a loss of two $\{M_3O_{13}\}$ units. Colour Code: MO_6 units: Indigo polyhedral, X: yellow, O: red.

Similar to the Keggin structure, the different orientation of the hetero-template of the Dawson cluster leads to the formation of six different isomers (α, α*, β, β*, γ and γ*), Figure 1.8. However, only the α [63], β [63-64], γ [64] and γ* [65] isomers have been synthesized and structurally characterized to date. One type of isomerism involves the rotation of the $\{M_3\}$ cap regions by 60° to give α-, β- and γ- forms. In the α-isomer the terminal M=O oxo ligands of both caps align with the corner shared bridging oxo ligands of the belt region. The β-isomer has one $\{M_3\}$ unit rotated by 60° so that the terminal oxo ligands now align with the edge shared bridging oxo ligands of the belt and the γ-isomer has both$\{M_3\}$caps rotated by

60° (Figure 1.8, top row). In all of these isomers the belt region contains a horizontal plane of symmetry so that the corner and edge shared oxo ligands of each hexagonal ring are located "in line" with one another. Similarly the heteroatomic tetrahedral $\{XO_4\}$ of each half of the molecule eclipse one another. The second form of isomerism breaks this symmetry by rotating one half unit $\{XM_9O_{36}\}$ through 60° and the heteroatomic polyhedra are now staggered relative to one another (Figure 1.9, bottom row). This imagined rotation of a half unit converts α to α*, β to β* and γ to γ*. DFT (Density Functional Theory) computational studies have revealed the order of stability for Dawson isomers is α > β > γ > γ* > β* > α* which goes some way to explain why certain isomers have not yet been discovered. [66]

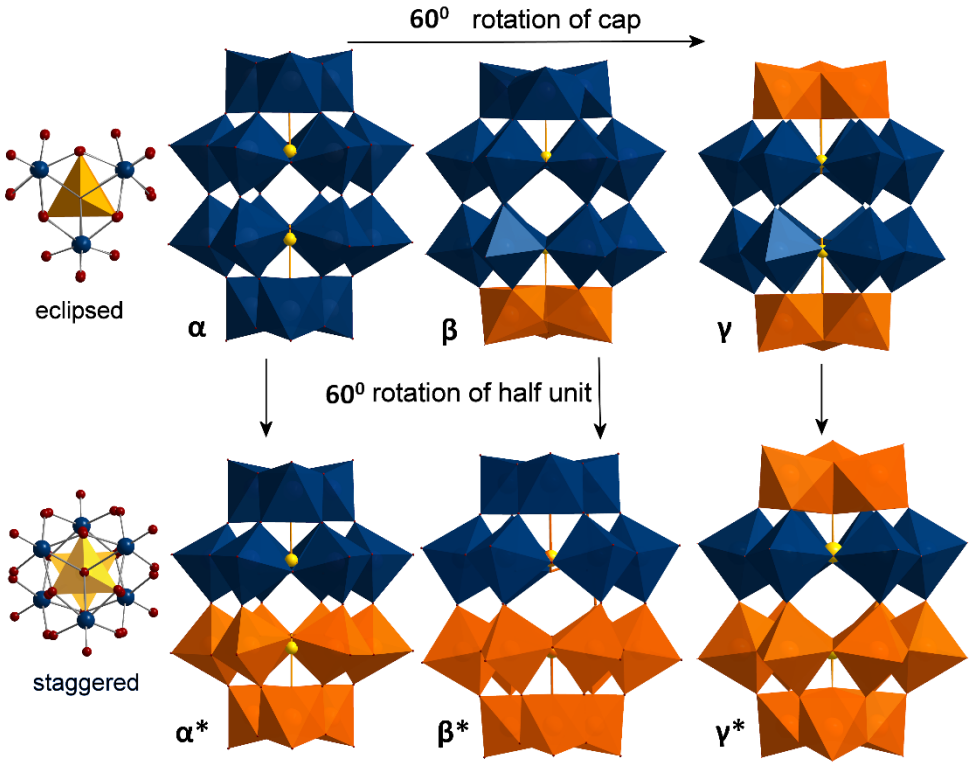

Figure 1.8: Polyhedra representation of the six isomers of Dawson structure which can be obtained by subsequent rotation of either the {M3} capping triads (top row) or further rotation of an entire $\{XM_9\}$ half-unit (bottom row). The eclipsed and staggered conformations which are possible between two tetrahedral $\{XO_4\}$ units in each isomer type is also shown for comparison. Colour code: MO_6: dark teal, XO_4: yellow sphere, rotated $\{MO_6\}$: orange, O: red.

1.5 Synthesis of Polyoxometalates

Polyoxometalates represent a unique family of compounds derived from a huge parameter space. The most common procedure to produce POM-based clusters is the 'one-pot' synthetic approach. This involves the acidification of a solution containing a metallic salt, usually molybdates, tungstates or vanadates, followed by the interaction of building block libraries leading to a formation of a variety of POM compounds. Hydro- or solvothermal is often used by researcher as a part of conventional synthesis as it has proved to give a variety of polyoxometalates. The use of flow reactors has been recently attracted the interest of the researchers, not only to study the formation mechanism of already known compounds but also to isolate new clusters and expand the family of polyoxometalates.

1.5.1 Classic Synthetic Approaches

1.5.1.1 'One-pot' Synthesis

The majority of the POM clusters are isolated *via* the acidification of an aqueous solution which contains the different metal oxide building units and heteroanions. [67] The acidification can be achieved by addition of common mineral acids. The isolation of the polyanion of the solution can be achieved by the addition of a counter-ion, such as alkali-metals, ammonium or tetraalkylammonium. There are numerous synthetic variables that can be employed in order to influence the self-assembly processes of the formation of the final product. The most common of these synthetic variables include: concentration of reaction reagents, type of metal oxide precursor, pH, type of hetero-atom, ionic strength, the presence of additional ligands, the presence of reducing agents, the sequence of the reagents addition and the temperature of the reaction mixture (Figure 1.9). This technique is simple and avoids complex and time consuming separation processes and thus it is much desired by chemists.

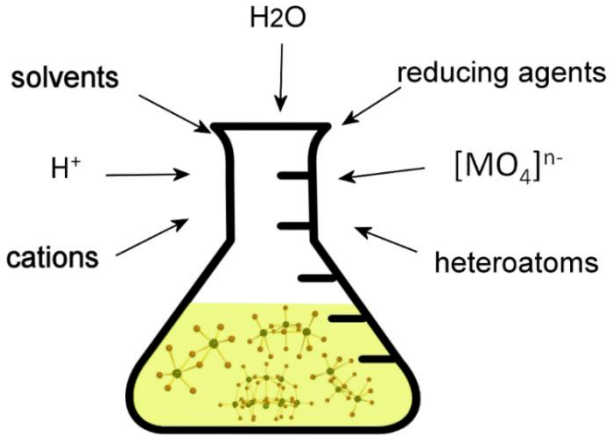

Figure 1.9: Factors that affect the synthesis/isolation of POMs during a "one-pot" reaction.

Another method in POM synthesis is the 'step-wise' method, where building blocks are first produced, followed by the coordination of addenda metal ions to form the final POM clusters. [68] The one-pot and step-wise approaches may be carried out by various reaction operations such as, microwave, hydrothermal/solvothermal or refluxing conditions.

1.5.1.2 Hydrothermal Synthesis

The hydrothermal technique is a synthesis method where *reactions occurring under the conditions of high temperature, high pressure (>100 °C, >1 atm) in aqueous solutions in a closed system* (autoclave bombs). [69] Over the past 20 years hydrothermal processing has become popular among scientists since it has proven to result in unusual polyoxometalates, especially in the transition-metal-substituted polyoxometalates chemistry. [70] The method is based on the ability of water and aqueous solutions to dissolve at high temperature and pressure substances practically insoluble under normal conditions: some oxides, silicates, sulphides. The use of water or organic solvents (e.g. acetonitrile, methanol and pyridine) limits the reaction temperature during the course of conventional synthesis. Due to the above limitations, the use of Teflon autoclaves during the solvothermal process gives the opportunity to reach higher temperatures at higher pressures for the same reaction mixture; typically such as reactions is carried out between 120 and 260 ^{o}C. Under these conditions, metastable or intermediate phases can be formed which normally lead to kinetically controlled products, such as the ''basket-shaped'' cluster $\{P_6Mo_{18}O_{73}\}$. [71] The main parameters of hydrothermal synthesis, which define both the processes kinetics and the properties of resulting products, are the initial pH of the medium, the duration and temperature of synthesis, and the pressure in the system. The ability to synthesize crystals of high quality and compounds which are unstable near the melting point, are some of the advantages of the hydrothermal technique. The limitations of the reaction temperature, due to safety concerns and the general reproducibility of the reactions are some of the weaknesses of this technique.

1.5.2 New Synthetic Approach

1.5.2.1 Flow Chemistry and Polyoxometalates

The flow reactor system approach has been extensively used in organic syntheses. [72-74] Many scientists have been focused at the fundamental differences between batch and flow systems with respect to stoichiometry and reaction time. [73, 74] Several advantages have been recognised such as facile automation, secured reproducibility, improved safety and process

reliability. With continuous flow processes constant reaction parameters (temperature, time, amount of reagents and solvents, efficient mixing, etc.) can easily be assured.

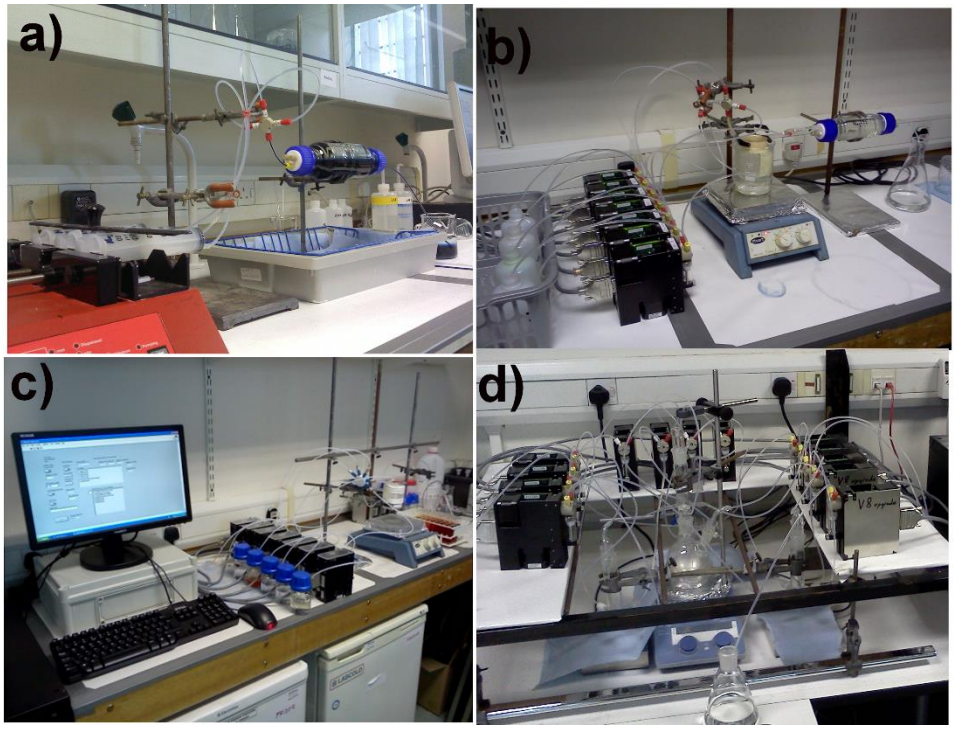

Figure 1.10 The development of the flow system (a) One simple pump controls the flow rate of the whole system; (b) Multiple electronic pumps control the individual flow rates of each starting materials; (c) Computer programmed linear flow reactions with varied flowing rate; (d) Multi-batched networked flow system.

The flow reactor systems approach (Figure 1.10) has attracted the interest of polyoxometalates chemists and has been used to both explore the synthesis of novel polyoxometalates clusters and the mechanism of their formation. Cronin *et al.* demonstrated how by using a flow system that enabled real-time control of the input variables (pH, concentration of molybdate and reducing agent), it has been possible to generate a static kinetic state of the 'intermediate' molybdenum-blue wheel [75] (Figure 1.11). Carrying out the reaction under controlled continuous flow conditions enabled selection for the generation of $\{Mo_{36}\}\subset\{Mo_{150}\}$ as the major product, and allowed the reproducible isolation of this host–guest complex in good yield, as opposed to the traditional ''one-pot'' batch synthesis which typically leads to crystallization of the $\{Mo_{154-x}\}$ species.

Figure 1.11 Representation of the flow system from which the blue reduction gradient formed within the vessel during the assembly of $\{Mo_{186}\}$.

The flow reactor systems have also been used for the discovery of Polyoxometalate clusters. Utilizing the Network Reaction System (NRS). Cronin *et al.* reported the synthesis of a gigantic isopolyoxotungstate (iso-POT) cluster, $\{W_{200}Co_8\}$ in the presence of templating transition metals such as Co^{2+} (Figure 1.12) by screening networks of one-pot reactions. [76] The gigantic isopolyanion $\{W_{200}Co_8\}$ cluster has been synthesized by the precise control of the recycling tungstate fragments, it contains unusual pentagonal-based units, and crystallizes as a hydrated sodium and dimethylammonium salt of the $[H_{16}Co_8W_{200}O_{660}(H_2O)_{40}]^{88-}$ anion cluster (Figure 1.12).

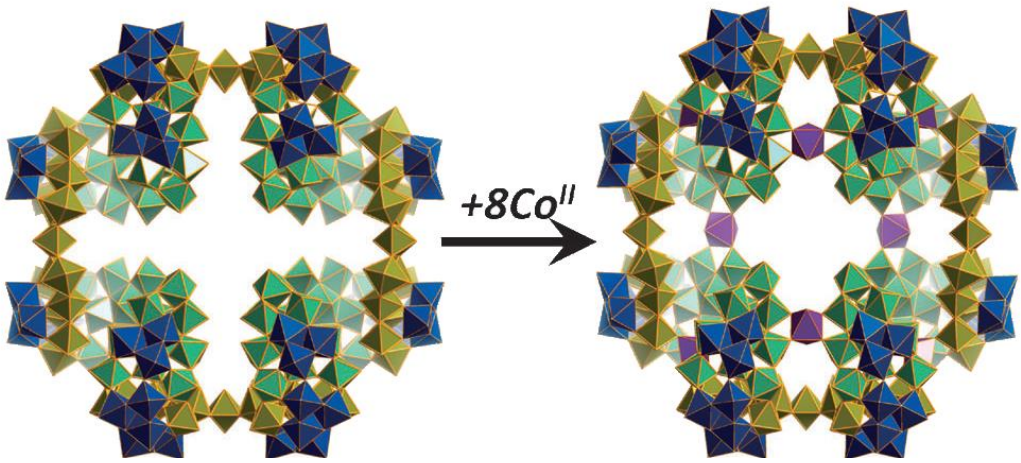

Figure 1.12: Polyhedra representation of the $[H_{16}Co_8W_{200}O_{660}(H_2O)_{40}]^{88-}$ anion cluster discovered utilizing the network system approach. Cobalt ions in purple polyhedra. [76]

1.6 Isopolyoxometalates

Isopolyoxometalates consist only of oxygen bridged addenda atoms without the participation of any hereto groups in the assembly process. This category of metal oxide cluster species is typically composed of $Mo^{V/VI}$, $W^{V/VI}$ and $V^{IV/V}$ metal ions. Their general formula is $[MxOy]^{n-}$, consisting of x addenda metal ions connected into a cluster by y oxygens to give an ion with a charge of n-. It is worth mentioning that these clusters contain no heteroatoms, and hence the formation of larger clusters and the number of geometries that can be formed are limited. Some of the common polyoxometalates of this category will be discussed in the following sections.

1.6.1 Isopolyoxovanadates

Isopolyoxovanadates (IsoPOVs) have attracted the attention of many research groups during the last 25 years, due to their interesting electronic and magnetic properties[77-79] and the flexibility of the vanadium metal atom to adapt equally the tetrahedral $\{VO_4\}$, square pyramidal $\{O=VO_4\}$ and octahedral coordination geometry $\{VO_6\}$. The isopolyoxovanadate anions can be constructed either by fully oxidized V^V and V^{IV} or mixed valent $V^{V/IV}$ and rarely V^{III} (usually observed in polyoxo(alkoxo)vanadates), [80, 81] making these clusters perfect candidates for redox chemistry investigation. This ability to adopt different oxidation states along with different coordination modes, leads to the formation of a wide range of structures. Even though the most thermodynamically favourable isopolyoxovanadate cluster is the $\{V_{10}\}=[V_{10}O_{28}]^{6-}$ decavanadate anion, [82] structures with different nuclearities, reduced/oxidized metal centres and shapes have been reported: $[V_4O_{12}]^{4-}$, [83] $[V_5O_{14}]^{3-}$, [84] $[V_{12}O_{32}]^{4-}$, [85] $[V_{13}O_{34}]^{3-}$, [86] $[V_{16}O_{38}]^{7-}$, [87] $[V_{17}O_{42}]^{4-}$, [88] and $[V_{19}O_{49}]^{9-}$. [89] The small nuclearity clusters are composed of tetrahedral building blocks, whilst the common $\{V_{10}\}$ cluster can be considered as being analogous to two fused Lindqvist moieties, [82, 90] containing thirteen edge-shared VO_6 octahedra and four square pyramids. The condensation of VO_5 units $\{O=VO_4\}$, which confer flexibility to the cluster, results in the formation of highly symmetrical archetypes which can act as hosts and encapsulate negatively charged ions that influence the shape and size of the cluster shell (e.g. $[V_{15}O_{36}(Cl)]^{6-}$, $[V_{18}O_{42}(SO_4)]^{11-}$ and $[V_{22}O_{54}(ClO_4)]^{5-}$). [91-93] To date, the cage-like $[V_{34}O_{82}]^{10-}$ cluster is the largest isoPOV with an approximate D_{2d} symmetry, and consists of thirty tetragonal VO_5 pyramids and a $\{V_4O_4\}$ cubane-like unit at the centre. [94]

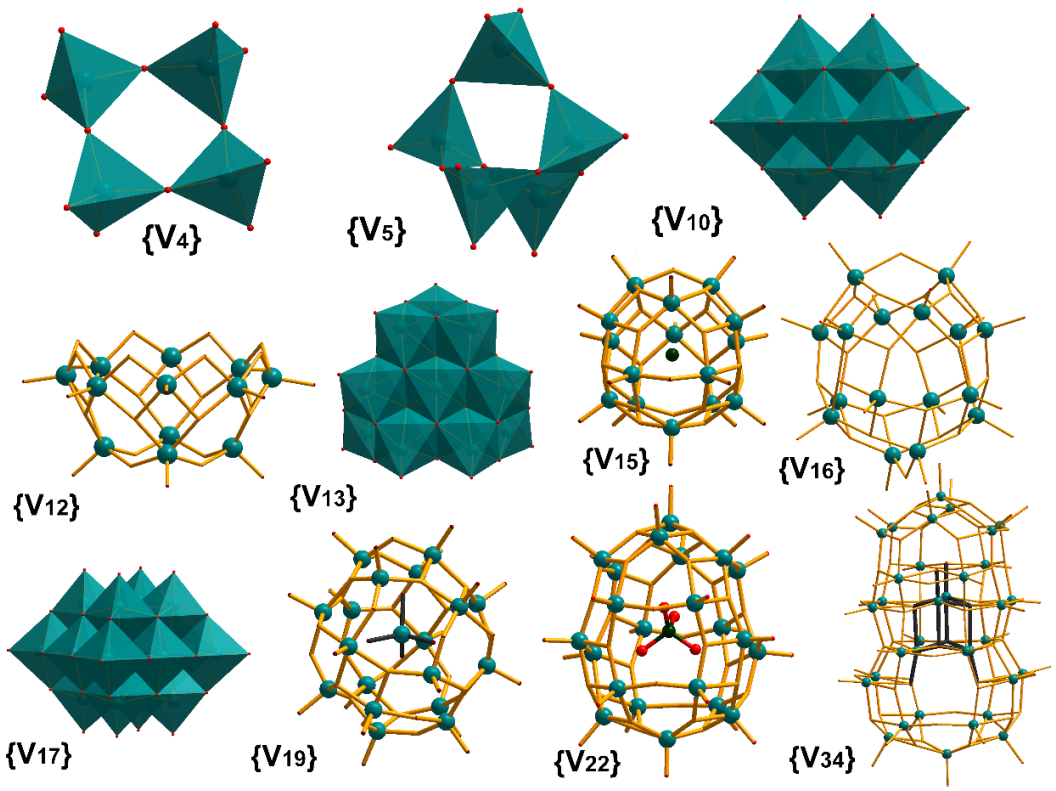

Figure 1.13 Polyhedra and ball and stick representation of different isopolyoxovanadates: $\{V_4\}$ and $\{V_5\}$ built up from $\{VO_4\}$ tetrahedral, $\{V_{10}\}$, $\{V_{13}\}$ and $\{V_{17}\}$ built up from $\{VO_6\}$ octahedral, whilst $\{V_{12}\}$ is built up from $\{VO_5\}$ square pyramids. In the case of the $\{V_{15}\}$, $\{V_{19}\}$ and $\{V_{22}\}$ species the guest is electrostatically incorporated in the IPOV shell, however the neutral $\{[V_4O_4]O_4\}$ moiety in $\{V_{34}\}$ is directly bonded to the cluster unit itself. Colour code: V: teal polyhedra and balls, Cl: dark green, O: red spheres.

1.6.2 Isopolyoxotungstates

Isopolyoxotungstates (IsoPOTs), compared to the other isopolyoxometalates, have limited structural motifs due to the W^{VI} ion's strong preference for adapting an octahedral coordination mode. The isolation of big polyoxotungstate compounds often requires the use of heteroatoms such as P, Se, Te or transition metal ions[24]. They can be produced by acidification of aqueous solutions of $[WO_4]^{2-}$. The pH and the nature of cation present play a significant role in the type of the final product. Examples of IsoPOTs include the dodecatungstates $[H_2W_{12}O_{40}]^{6-}$ (meta-tungstate) [95] and $[H_2W_{12}O_{42}]^{10-}$ (paratungstate-Z), [96] the heptatungstate $[W_7O_{24}]^{6-}$, [97] and the hexatungstate $[W_6O_{19}]^{2-}$, [98] as well as fragments of these anions, which act as isolated units or as components of high molecular aggregates. The $[H_{12}W_{36}O_{120}]^{12-}$ or the so called 'Celtic Ring' anion, is to date the largest IsoPOT and it has been studied as an inorganic 18-Crown-6 analogue for binding K^+ ions. [99] It consists of three

{W_{11}} units which are connected by three {WO_6} units into a triangular shape. The first {$W_{11}O_{38}$} fragment was first reported by Lehmann and Fuchs in 1988. [100] Cronin *et al.* [101] have developed a family (including the 'Celtic Ring') of {W_{11}} containing clusters, namely {W_{22}}=$[H_4W_{22}O_{74}]^{12-}$ and {W_{34}}=$[H_{10}W_{34}O_{116}]^{18-}$ with a double S-shaped architecture. The first cluster contains two {W_{11}} species which are connected by corner sharing of oxo ligands, whilst the second contains two {W_{11}} units and one central {W_{12}} unit. The first isoPOT, the ring-like $[W_{24}O_{86}]^{28-}$, displaying rare trigonal bipyramidal {WO_5} units, was first reported by Palm *et al.* [102] The structure synthesized from an aqueous solution of Cs_2WO_4 and $WO_3 \cdot H_2O$ stirred under argon conditions and contains an inner ring of six corner sharing {WO_6} units, which is expanded by addition of six {W_3O_{13}} units on the surface.

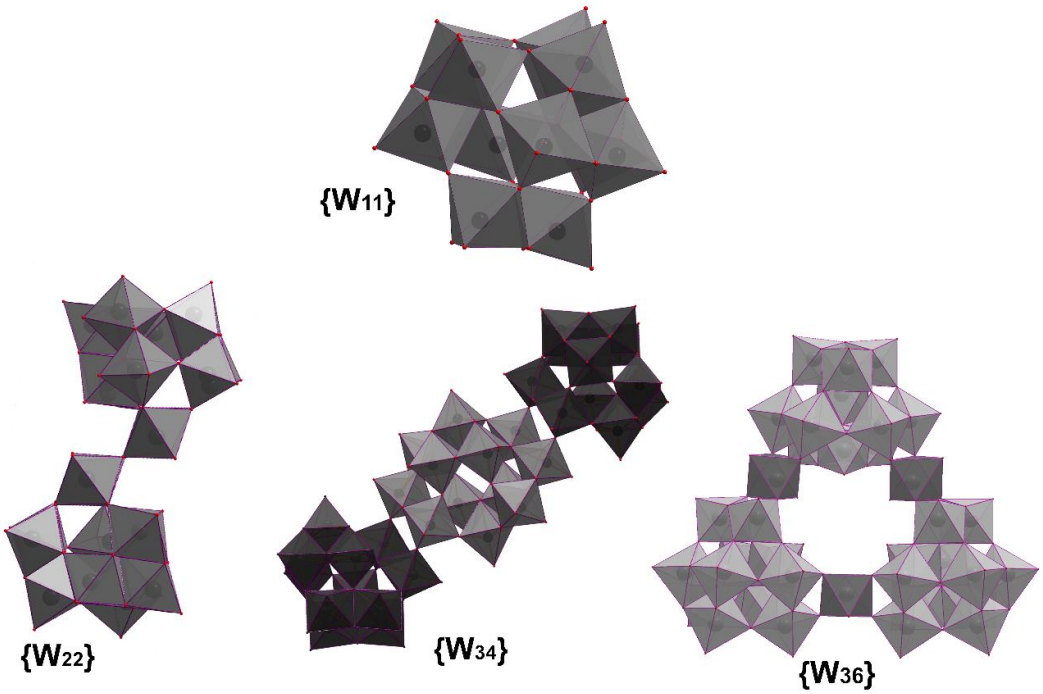

Figure 1.14: Polyhedral representation of the structures of the {W_{22}} cluster, which is built up from two {W_{11}}, the {W_{34}} cluster which consists of two {W_{11}} subunits and a {W_{12}} unit and the (W_{36}} cluster which is built up from 3 *cis* edge-shared {W_{11}} units linked by 3 {W_1} groups (dark grey polyhedral).

1.6.3 Isopolyoxomolybdates

The polymerization of the tetrahedral $[MoO_4]^{2-}$ anion under acidic conditions leads to the isolation of several isopolyoxomolybdates (IsoPOMos) with diverse nuclearities and shapes. The more flexible coordination chemistry of the molybdate ion has resulted to the isolation of a wider range of structures compared to IsoPOTs. Classical structures are the Lindqvist $[Mo_6O_{19}]^{2-}$, [103] the $[Mo_7O_{24}]^{6-}$, [104] and the $[Mo_8O_{26}]^{6-}$, [105] which are now used as starting materials for synthesizing organic derived POM materials, [106] and inorganic-organic hybrid materials. [107] IsoPOMos with fully oxidized Mo (VI) species include $\{Mo_{10}\}$, [108] $\{Mo_{28}\}$, [109] and $\{Mo_{36}\}$, first reported by Krebs and Paulat-Böschen. [110] The cluster can be viewed as a dimer of two 18-molybdate species, each of which contains two pentagonal $\{Mo(Mo_5)\}$ cores centred around a pentagonal bipyramidal $[MoO_7]$ unit and it is, to date, the largest cluster with all Mo metal ions in fully oxidized state. In a second category of IsoPOMos the clusters consist of partially reduced Mo (V/VI) species, such as $\{Mo_{12}\}$, [111] $\{Mo_{18}\}$, [112] and $\{Mo_{54}\}$, which was discovered by Lu *et al.*[113] in 2000. Cronin *et al*. [114] employed the 'shrink-wrapping' strategy to obtain a $\{Mo_{16}\}$ cluster which consists of four Mo^V species and twelve Mo^{VI} atoms $[H_2Mo^V_4Mo^{VI}_{12}O_{52}]^{10-}$.

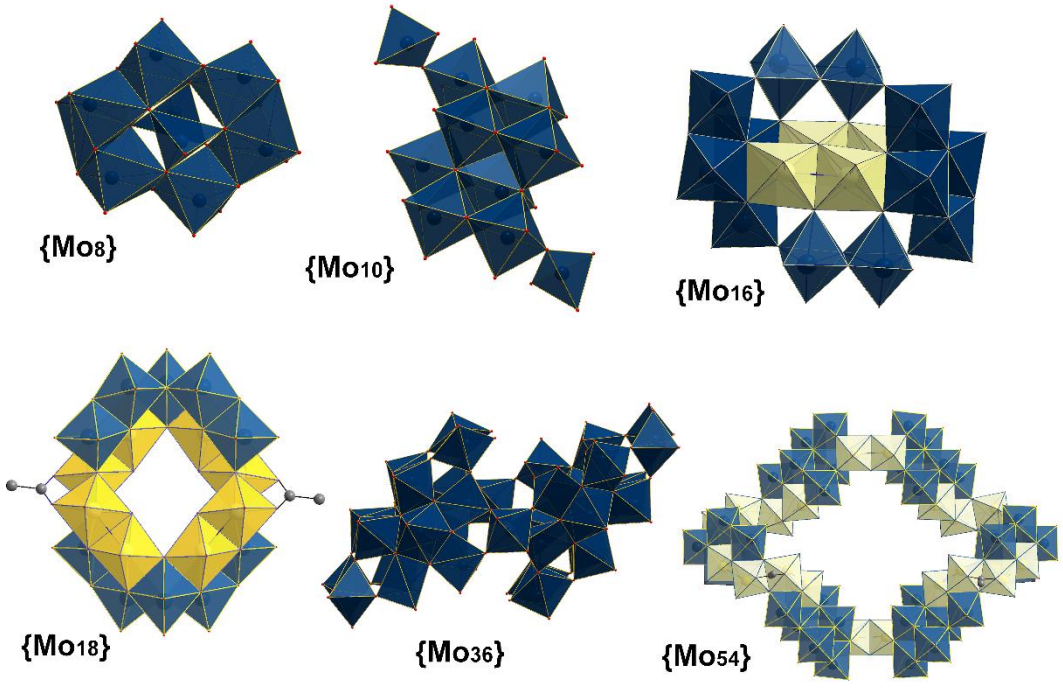

Figure 1.15: Selected polyhedral presentation of isopolyoxomolybdates. Mo^{VI}: blue polyhedral, Mo^V: yellow polyhedral, O: red spheres

1.7 Heteropolyoxometalates: Effects on Structures and Properties

Contrary to IsoPOMs, in which an inorganic framework built up from the condensation of only metal oxide building blocks, heteropolyoxometalates (HPOMs) are polyanions where an additional templating heteroatom (X), which is commonly described as heteroanion, $[XO_y]^{n-}$, has been incorporated in the centre of the inorganic cage. [17-19] Compounds with elements from almost the entire periodic table acting as heteroatoms have been reported, though it is the p-block elements which remain the most frequently employed. It is worth mentioning that the nature of the heteroatom, thus the geometry and the coordination number, are important variables that affect the self-assembly process and the properties of the final product. The majority of compounds reported in the literature are templated by the classical tetrahedral heteroanions (e.g. PO_4^{3-}, SO_4^{2-}, SiO_4^{4-}, SnO_4^{4-} etc.), [115] adopting mainly the Keggin, Dawson or Lindqvist- based structure (they have already been discussed in section 1.4). In the following section, compounds with non-classical heteroatoms will be discussed.

1.7.1 Unconventional heteroatoms

1.7.1.1 Trigonal Pyramidal Heteroatom

The trigonal pyramidal heteroatoms, with the general formula $\{XO_3\}$, consist of a central atom connected to three oxygen atoms which define the base of the trigonal pyramid, whilst the fourth vertex of is now occupied by a lone pair of electrons. These moieties adopt a trigonal pyramidal geometry, which is commonly found in the group 15 (As^{III}, Sb^{III} and Bi^{III}) and 16 elements (S^{IV}, Se^{IV} and Te^{IV}). In contrary to the conventional tetrahedral heteroatoms, in which the fourth oxo-ligand prevents the direct assembly of lacunary structures, the pyramidal heteroatoms can be used in order to build lacunary fragments which can be used as secondary building block for the isolation of large architectures. [116] (see Figure 1.16).

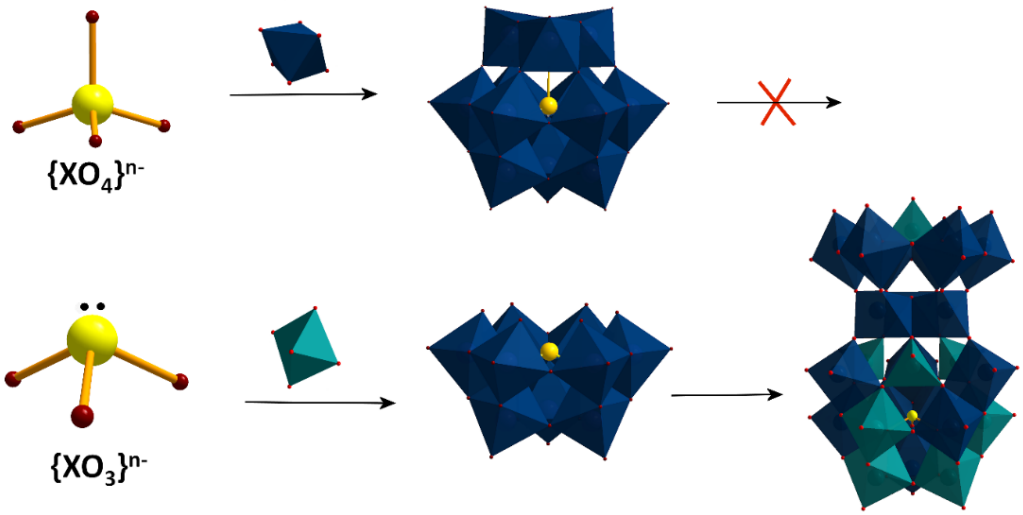

Figure 1.16 Schematic representation of different assembly processes utilizing conventional (top) and pyramidal (bottom) heteroatoms. The lone pair of the latter favours the formation of reactive lacunary species, allowing for the continued assembly of new products in solution, such as the $\{TeM_{25}\}$ species shown above. [132]

The first crystal structure of a POM templated by $\{XO_3\}$ moieties, was reported in 1976 by Sasaki and co-workers, [117] as the ammonium salt of the $[S^{IV}_2Mo_5O_{21}]^{4-}$ anion, which consists of a pentagonal Mo_5O_{21} ring capped by two SO_3^{2-} heteroanions. Pope *et al*. were among the first to report $\{AsO_3\}$-templated POM structures. The $\{Ce_{20}As_{12}W_{148}\}$ cluster, [118] which could be synthesized as an ammonium salt by straightforward self-assembly process in aqueous solution, consists of twelve $\{AsW_9\}$ fragments and it has a diameter of approximately 4 nm. This fragment has been extensively exploited by research groups resulting to the expansion of the $As^{III}O_3$-based POM family; [119] for example: $[As^{III}_6W_{65}O_{217}(H_2O)_7]^{26-}$ cluster was synthesized as a potassium salt using $K_{14}[As_2W_{19}O_{67}(H_2O)]$ as precursor, $[Fe_4(H_2O)_{10}(AsW_9O_{33})_2]^{6-}$ cluster consisting of $2\{AsW_9\}$ fragments and was synthesized as sodium salt and the large POM-embedded polynuclear lanthanoid complex, $[Gd_6As_6W_{65}O_{229}(OH)_4(H_2O)_{12}(OAc)_2]^{38-}$. Jeannin and Martin-Frère first reported in 1979 [120] an As^{III} containing Dawson-like $[H_2AsW_{18}O_{60}]^{7-}$ species. This crystal structure was synthesized as an ammonium salt and is built up with two $\{XW_9O_{33}\}$ units sharing six oxygen atoms and has a distorted "peanut-like" topology. In these species, the As^{III} ion which is located inside one $\{XW_9O_{33}\}$ unit, has its lone pair electron directed towards the other unit. Recently, Niu *et al*. reported a new unconventional Dawson-like cluster incorporating two pyramidal AsO_3^{3-} heteroanions within a β-$\{W_{18}O_{54}\}$ skeleton, which exhibits interesting short intramolecular As···As interaction between the two anions; *ca* 3.09(3) Å, which is much shorter than the sum of the van der Waals radii of two

arsenic atoms (ca. 3.70 Å). [121] The above mentioned work has been reported as an extension of the work of Long *et al*. in 2004 [122], when the unusual properties of such peanut-shaped clusters were reported. The structures with the general formula $[S^{IV}_2Mo_{18}O_{60}]^{n-}$ (n = 4, 6), exhibit a notably short S···S interaction (ca. 3.3 Å - the Van der Waals radius of S is ca. 1.8 Å) and interesting thermochromic (the tetrabutylammonium salts change colour from pale green to dark red upon heating) and redox properties. This discovery quickly led to the synthesis of a new Dawson-like polyoxotungstate, $[S^{IV}_2W_{18}O_{62}(H_2O)_2]^{8-}$ [123] ("Trojan Horse"), in which the two $[SO_3]^{2-}$ groups are no longer aligned along the central axis of the anion and four of the eighteen tungsten atoms have two terminal ligands (2 oxo and 2 aqua) on the $\{W_{18}\}$ cell. Interestingly, in this case the cluster upon heating releases four electrons from the encapsulated S^{IV} into the W^{VI} metal centres, resulting to a structural re-arrangement and thus the formation of the classical sulfate-based, mixed-valence Dawson cluster $[S^{VI}_2W^{V}_4W^{VI}_{14}O_{62}]^{8-}$ (figure 1.17). The mechanism of this transformation of reactive templates within a polyoxometalate cage was recently proposed by Cronin *et al*. [124] by using NMR spectroscopy and mass spectroscopy.

Sulfite heteroanions can act as ligand, such as in the first sulfite-based polyoxomolybdate cluster, $[(Mo^{V}_2O_4)_6(\mu_2\text{-}SO_3)_{12}(\mu_3\text{-}SO_3)_4]^{20-}$, where the incorporation of the sulfite anions results in an unpresented archetype; the sixteen $[SO_3]^{2-}$ heteroanions connect the six $[Mo^{V}_2O_4]^{2+}$ units with different coordination modes. [125] A new structure type related to the Dawson archetype, the "egg-shaped" cluster $[Mo^{VI}_{11}V^{V}_5V^{IV}_2O_{52}(\mu_9\text{-}SO_3)]^{7-}$ [126]. The compounds consists of molybdenum and mixed-valent (IV and V) vanadium metal centres. This new structural archetype differs from the classical Dawson-like structures since in only contains one templating $\{SO_3\}$ heteroatom.

A series of high nuclearity polyoxotungstate clusters have been synthesised using the $[SeO_3]^{2-}$ anion as a heteroatom and linker. Some examples are the clusters $[H_2W_{43}Se_3O_{148}]^{24-}$ $[H_2W_{43}Se_3O_{148}]^{24-}$, $[H_4W_{77}Se_5O_{265}]^{44-}$ and the gigantic nanosized cluster $[(H_8W_{100}Se_{16}O_{364})WO(H_2O)_2]^{52-}$, which is the first family of polyoxotungstate clusters that incorporates building blocks with pentagonal geometry. [127] Moreover, Yan *et al*. reported in a 2010 the pentagonal $\{WO_7\}$-based $[H_{34}W_{119}Se_8Fe_2O_{420}]^{54-}$ cluster in which $[SeO_3]^{2-}$ was acting as both a template and linker in order to generate this giant cluster based on the assembly of $\{SeW_9\}$ species. [128] The mixed-metal Mo/V lacunary type templated by the $[SeO_3]^{2-}$ heteroatom, reported by Corella-Ochoa *et al.*: the "egg-like" and isostructural to the $\{SO_3\}$-based cluster $[Mo^{VI}_{11}V^{V}_5V^{IV}_2O_{52}(\mu_9\text{-}SeO_3)]^{7-}$ and the "crowned" Dawson-like $[Mo^{VI}_{11}V^{V}_5V^{IV}_2O_{52}(\mu_9\text{-}SeO_3)(Mo^{V}_6V^{V}O_{22})]^{10-}$. [129]

Further studies on the pyramidal-base POMs using $[TeO_3]^{2-}$ heteroatoms, has resulted to the isolation of high nuclearity clusters. The new class of tungsten based structures, $[W_{28}Te_8O_{112}]^{24-}$, $[W_{28}Te_9O_{115}]^{26-}$ and $[W_{28}Te_{10}O_{118}]^{28-}$ have been reported, where the heteroanions act both as templates and as bridges within and between the building units respectively. [130] The ability of the Te-based pyramidal heteroatoms to direct the assembly of new POM architectures has further been demonstrated by Gao *et al*., with the discovery of a series of macrocycle-like clusters based on seldom observed heptatungstate $\{TeW_7\}$ units and a new, "pagoda-shaped" $\{Te_3W_{21}\}$. [131] The structure of $[Mo^{VI}_{11}V^{V}_{5}V^{IV}_{2}O_{52}(\mu_9\text{-}TeO_3)(Mo^{V}_{6}V^{V}O_{22})]^{10-}$ was added in the family of mixed-metal, mixed-valence polyoxomolybdenum/vanadium-tellurite clusters. It the "crowned"- Dawson motif, and it is isostructural to the selenite-based $\{M_{25}Se\}$ capsule. [132]

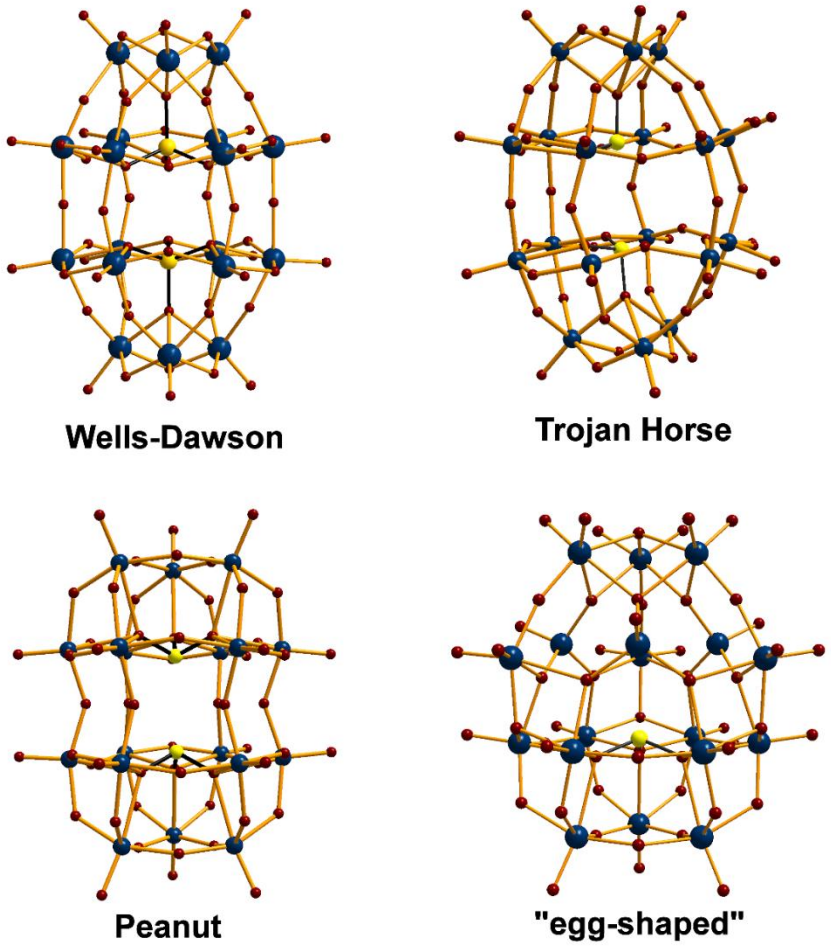

Figure 1.17 Comparison of the ball and stick models of unconventional Dawson-type cluster architectures showing: the 'classical' Wells-Dawson anion for reference, the 'Trojan Horse'-type Dawson cluster, the 'peanut'-type Dawson cluster and the 'non-conventional' or 'egg-like' Dawson-type cluster. Colour code: addenda: blue spheres, O: res spheres, heteroatom: yellow spheres.

1.7.1.2 Octahedral heteroatoms

The majority of structures with the non-tetrahedral, $\{XO_6\}$ heteroanions reported so far are based on the Anderson archetype (discussed in section 1.4.2). [133] Several examples of the Anderson archetype templated by octahedral heteroatoms and octahedral metal addenda in a wide range of oxidation states, have been reported to date. Some examples are $[Ni^{II}(OH)_6W_6O_{18}]^{4-}$,[134] $[Cr^{III}(OH)_6Mo_6O_{18}]^{3-}$ [135] and $[Mn^{IV}O_6W_6O_{18}]^{8-}$. [136] The first example of non-classical Dawson POM, $[H_4W_{19}O_{62}]^{6-}$, was reported by Long *et al*. [137] The structure consists of the typical $\{W_{18}O_{54}\}$ cage framework and an octahedral or a trigonal-prismatic $[WO_6]^{6-}$ anion encapsulated in the cage.

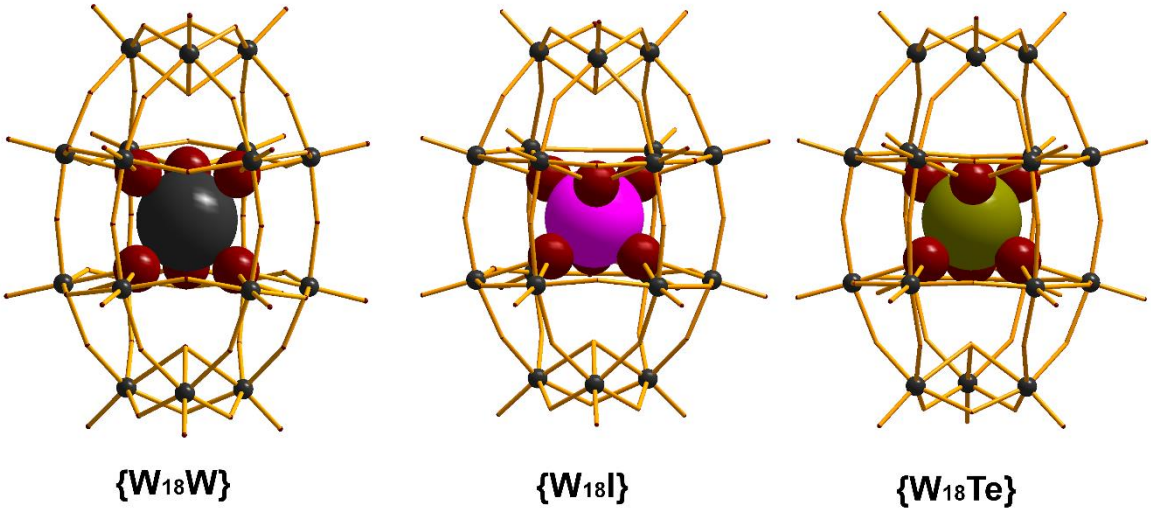

Figure 1.18 Representation of the non-classical Wells-Dawson $\{W_{18}X\}$ type POMs. The {W18} cages are shown in ball and sticks representation and the central $\{XO_6\}$ group is represented in space-filling mode. Left: α-$[W_{18}O_{56}(WO_6)]^{10-}$; Middle: β*-$[W_{18}O_{56}(IO_6)]^{9-}$; Right: γ*-$[W_{18}O_{56}(XO_6)]^{10-}$ X = W^{VI} and Te^{VI}. Colour code: W, grey; O, red; Te, dark yello; I, pink.

This work followed by the discovery of two Dawson capsules which incorporate either $Te^{VI}O_6$ [138] or the high-valent $I^{VII}O_6$; [139] for the tellurate based cage the anion adopts a γ*-configuration whereas for the iodate based cage it has a β*-configuration. Recent results by Vilà-Nadal *et al.* [140] have shown that these octahedrally templated non-classical Dawson clusters have markedly different electrochemical properties from conventional Dawson anions and that they are capable of 'trapping' an electron on the heteroatom, rather than delocalised across the surface of the POM, upon reduction.

1.8 Molybdenum Blues and Browns

The reduction of an acidified solution of molybdates results to a plethora of well-defined building blocks, which can be connected to form a wide variety of sophisticated nanostructures. This family of anions known widely as the 'molybdenum blues/browns', was first described by Scheele [10] in 1793, but was synthesized and crystallographically determined not earlier than 1995 when Müller and co-workers reported the $\{Mo_{154}\}$ 'big wheel'. [22] They represent the largest size of non-iological molecular POM clusters with some equalling the size of proteins (the $\{Mo_{368}\}$ "blue lemon" is ~6nm in diameter). [8] Molybdenum Blues contain mixed valence Mo^{V}/Mo^{VI} addenda and have delocalised electrons capable of intervalence charge transfer from Mo^{V} to Mo^{VI} facilitated by the π-orbitals of the bridging oxo ligands and it is this electronic interaction that gives the clusters their signature intense blue colour. Molybdenum Browns are further reduced relative to Mo Blues and have electrons localised between reduced Mo^{V} centres as Mo-Mo bonds which contribute to the brown colour of these clusters. The most well-known Molybdenum Blue structures are the giant wheels, $\{Mo_{154}\}$, [22] $\{Mo_{176}\}$, [141] and the $\{Mo_{132}\}$[142] Keplerate cluster, which are all constructed from the same pentagonal building block, $\{MoMo_5\}$. The wheels are formed by reducing a solution of $NaMoO_4{\cdot}2H_2O$ at low pH. If other elements are introduced into the reaction system then they can disrupt the symmetry of the wheel by substituting into some of the sites normally occupied by $\{Mo_2\}$ groups. The list of species that can substitute for the $\{Mo_2\}$ unit includes Cu^{2+}, [143] Pr^{3+}, [144] and Eu^{3+}. [145] A mentioned in section 1.5.2.1, Miras *et al.* [75] explored the synthesis of Mo blue wheels in flow and they were able to isolate the complex $Na_{22}[Mo^{VI}_{36}O_{112}(H_2O)_{16}]\subset [Mo^{VI}_{130}Mo^{V}_{20}O_{442}(OH)_{10}(H_2O)_{61}]{\cdot}180H_2O$ which is composed of a $\{Mo_{150}\}$ wheel and a central $\{Mo_{36}\}$ component which contains $\{Mo_6\}$ pentagonal building units and fits inside the elliptical cavity of the wheel.

When the pH of these systems is increased slightly, the self-assembly tends towards the formation of a second series of remarkable spherical anions, since colloquially referred to as 'Keplerate' clusters (after Johannes Kepler's early model of the cosmos). [141] The general formula can always be summarised as $\{(\mathit{Mo_6})_{12}(\mathit{linker})_{30}\}$, the linker units can be mono or dinuclear groups such as $\{Fe(H_2O)\}^{3+}$, $\{Mo^{V}O(H_2O)\}^{3+}$ and $\{Mo_2{}^{V}O_4(CH_3COO)\}^{+}$. [146] The $\{Mo_{132}\}$ ball was the first Keplerate reported and consists of $12\{Mo_{11}\}$ fragments [142] (Figure 1.19). In addition to that, Müller and co-workers reported the largest purely inorganic cluster known to date, built up from a $\{Mo_{288}\}$ ball capped by two $\{Mo_{40}\}$ units.

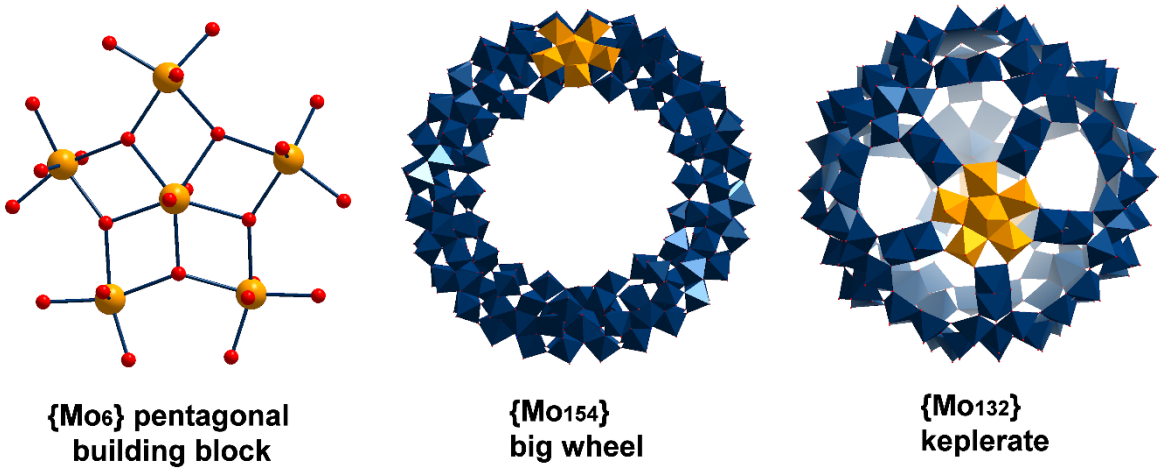

Figure 1.19 Ball-and-stick representation of the $\{Mo_6\}$ pentagonal bipyramidal building block integral to Molybdenum Blue and Brown architectures beside polyhedral and polydedral representations of how the pentagonal units are arranged within the $\{Mo_{154}\}$ wheel and $\{Mo_{132}\}$ Keplerate. Pentagonal building block in orange polyhedra.

The lemon-shaped cluster $\{Mo_{368}\}$ is obtained from a special type of molybdenum blue solution where only H_2SO_4 is used to control the pH of the reaction. This fact is related to the stability that the SO_4^{2-} ligands provide to the intermediates and the final cluster; whereas the presence of weaker coordinating ligands such as Cl^- or ClO_4^- ions leads to the formation of the wheel-shaped $\{Mo_{154}\}$ or $\{Mo_{176}\}$ instead. These giant, inorganic capsules with well-defined pores embedded in their surface have been studied for their encapsulation and host-guest properties amongst other interesting features. [147]

1.9 Applications

The unique versatility in terms of size, thermal stability, conductivity, photochemical response redox and magnetic properties, are some of the physical and chemical properties that make POMs promising candidates for a wide range of applications [148] (figure 1.20).

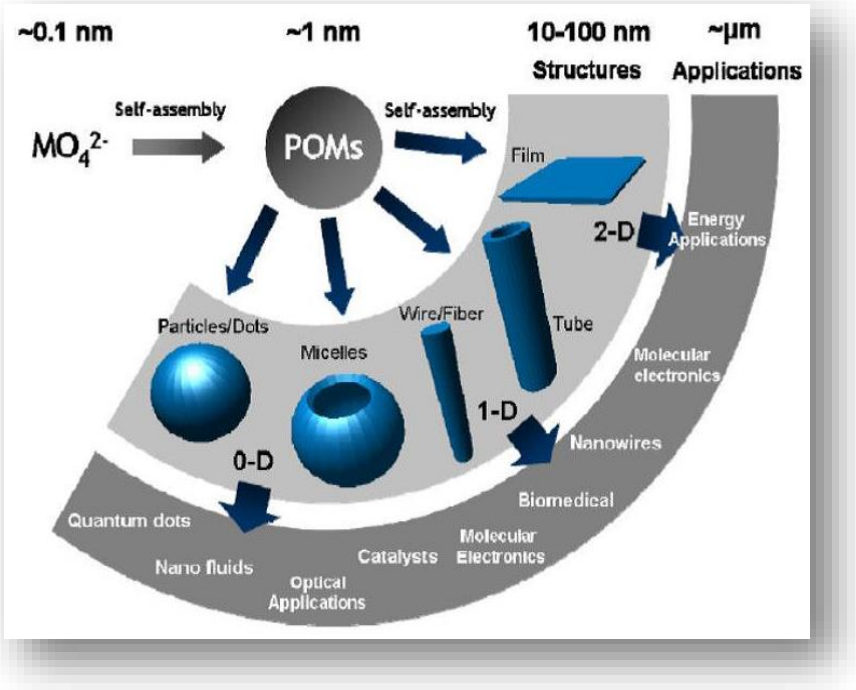

Figure 1.20 Structures and potential applications of Polyoxometalates. [149]

1.9.1 Catalysis

Characteristics such as the acidity, the solubility, the ability to release and accept electron, have made Polyoxometalates attractive candidates in catalysis. [150] Furthermore, POMs are discrete molecules consisting of polyanions and counter cations, giving them structural mobility when compared with network structures such as zeolites. The remarkable catalytic activity has a close relationship with the structure and composition of the POMs. Keggin-type clusters, Dawson lacunary anions and their transition metal complexes are used as catalysts. [151] Especially Keggin-based catalysts can be used in different catalytic processes [152] such as oxidation catalysis for alkanes and alkenes, due to their thermal stability and availability. Transition metals have been extensively used to enhance the redox properties of POMs-based catalysts. In 2003, Hill *et al.* reported the electrostatic immobilization of an iron-based polyoxometalate, which exhibits efficient catalytic activity towards the aerobic oxidation of sulphides and aldehydes. [153] Mizumo *et al*., [154] recently reported the vanadium-substituted γ-phosphotungstate, $TBA_4[\gamma\text{-}HPV_2W_{10}O_{40}]$, acting as an effective homogeneous catalyst for the H_2O_2-based oxidative bromination of alkenes, alkynes and aromatic

compounds. The hydration of various nitriles, including aromatic aliphatic and double bond-containing species, was catalysed by the palladium derivative, $TBA_4[\gamma\text{-}H_2SiW_{10}O_{36}Pd_2(OAc)_2]$, [155] while the $TBA_8H_2[(SiYW_{10}O_{36})_2]$ dimer (synthesized by the reaction of $TBA_4H_4[\gamma\text{-}SiW_{10}O_{36}]$ and $Y(acac)_3$) was shown to be catalytically active for the cyanosilylation of ketones and aldehydes. [156]

1.9.2 Molecular Magnets

The ability of POMs to form reduced species resulting in a wide range of electronic properties, makes them good candidates as ligands in magnetic materials. The flexibility in design and assembly of POMs along with their ability to act as multidentate ligands trapping paramagnetic cores, has led to the development of novel paramagnetic polyoxometalates. [157] To date, there have been several reports about the magnetic species being incorporated into POM clusters. Most examples include vanadium-substituted POM compounds such as, the $K_6[V^{IV}_{15}As_6\ O_{42}(H_2O)]$ [158] which consists of three discrete layers in each of which the magnetization shows a distinct temperature dependence, the $\{V_6(SO_3)_4\}$, [159] which represents the first example the $\{M_4O_4\}$ cubane core connection to two other metals. Also, $[PMo_{12}O_{40}(VO)_2]^{5-}$ cluster which comprises a redox active core capped at opposite ends by V=O units with localised s = ½ and it has been described as a potential spin qubit. [160] The family of 3d-substituted POM-based compounds have been revealed to be promising group a compounds that exhibit SMM behaviour. [161] For example, $[(XW_9O_{34})_2(Mn_6O_4(H_2O)_4)]^{12-}$ cluster (where X = Si, Ge), reported by Cronin *et al*. [162] is the first Mn^{II}/Mn^{III} SMM material consisting of two trivacant lacunary $[B\text{-}a\text{-}X^{IV}W^{VI}_9O_{34}]^{10-}$ polyanions which ‘‘trap’’ a novel mixed-valence double cubane hexanuclear {Mn6}= $[Mn^{III}_4(H_2O)_2Mn^{II}_2O_4(H_2O)_2]^{8+}$ magnetic core. In 2011, the synthesis and characterization of the tetrameric $[\{Co_4(OH)_3PO_4\}_4(PW_9O_{34})_4]^{28-}$ cluster which encapsulates a $\{Co_{16}\}$ magnetic core, was reported by Kortz and co-workers, [163] whilst the first hybrid bisphosphonate POM cluster containing seven Co^{II} metal cores sandwiched by two lacunary $\{PW_9\}$ units, was reported by Mialane et *al*. [164] The investigation of the 3d-substituted POM-based compounds as potential magnetic materials was followed by the studies on the interaction between POMs and lanthanides. The first series of Ln-based POM clusters exhibiting SMM behaviour with the general formula $[Ln(W_5O_{18})_2]^{9-}$ (Ln^{III} = Tb, Dy, Ho, and Er) and $[Ln(SiW_{11}O_{39})_2]^{13-}$ (Ln^{III} = Tb, Dy, Ho, Er, Tm, and Yb), were reported in 2008 by Coronado *et al*. [165] The first Ln-based single-molecule magnets with the general formula $[Ln_4As_5W_{40}O_{144}(H_2O)_{10}(gly)_2]$ (Ln = Gd, Tb, Dy, Ho and Y) were discovered by Boskovic *et al*. [166] in 2011. In conclusion, Kögerler *et al*. reported in 2009 the $\{Mo_{72}Fe_{30}\}$ Keplerate species with partially reduced

{(Mo)Mo_5} building units demonstrating how the 4d electron density on the still diamagnetic POM fragments strongly influences the magnetic exchange. [167]

1.9.3 Energy and Storage

The increase of the global energy consumption and the need for a more environmental friendly and ideally renewable energy source, has led to the investigation of alternative energy sources. The unique combination of properties of polyoxometalate systems, such as acidity, structural stability and diversity, redox properties, etc. make them promising candidates for the design of POM based materials for energy related applications. Many research groups are working towards the discovery of new clusters or the development of previous reported compounds which could be active in the water splitting/oxidation process. In 2004 Shannon *et al.* reported the first example of catalytically active species: the di-Ru-substituted $[WZnRu_2(OH)(H_2O)(ZnW_9O_{34})_2]^{11-}$ cluster. [168] Moreover, in 2011, Fukuzumi and co-workers, [169] reported that the mono-Ru Keggin clusters, $[Ru^{III}(H_2O)SiW_{11}O_{39}]^{5-}$ and $[Ru^{III}(H_2O)GeW_{11}O_{39}]^{5-}$, are catalytically active over a wide range of pH values and under the presence of $(NH_4)_2[Ce^{IV}(NO_3)_6]$ (CAN) as a one-electron oxidant in water. Additionally, in 2010 Bonchio *et al.* reported the functionalized water-oxidation electrodes, which were combined the tetra-Ru oxygen-evolving polyoxometalate cluster with a conducting bed of multi-walled carbon nanotubes (MWCNTs). [170] Awaga *et al*. reported a system in which the Keggin cluster, ($TBA_3[PMo_{12}O_{40}]$), can be adsorbed onto the surfaces of Single-Wall Carbon Nanotubes (SWNTs) without chemical decomposition. The large surface areas, the specific electrical conductivity and significant mechanical strength are some properties that make SWNTs promising materials for nanoelectronics. The authors showed that nanohybridization of molecular clusters with SWNTs is a promising method for improving smooth electron transport and lithium ion dispersion in battery reactions. [171] In conclusion, a step forward to the design and engineer of new types of data storage devices utilizing POM compounds, was conducted by Cronin and co-workers in 2013. [172] Authors demonstrated how the well-known Dawson structure $\{M_{18}{}^{VI}O_{54}\}$ (M=W, Mo), incorporating either sulfate, $[S^{VI}O_4]^{2-}$ or sulfite, $[S^{IV}O_3]^{2-}$ heteroanions can act as nanoscale molecular memory elements.

2. Aims

For the past 20 years polyoxometalates have attracted the interest of scientific groups due to their ability to display a wide range of structural archetypes and properties. It is well-known that the formation of the metal oxides involves the self-assembly process of the building blocks in the reaction mixtures, however the understanding of this formation remains a challenge within this class of inorganic materials. The investigation redox-driven self-assembly of mixed metal polyoxometalates has been the general aim of the work presented here.

It is well-established that the majority of the polyoxometalate clusters incorporate tetrahedral (traditional) heteroatoms such as sulphates and phosphates. The integration of non-conventional heteroatoms has only attracted the attention for the past few years with examples reported mainly from our group. [123, 126, 129] Following these examples, we tried to direct the self-assembly of mixed-metal polyoxometalates which incorporate pyramidal heteroanions, namely selenite (SeO_3^{2-}), tellurite (TeO_3^{2-}) and the psebdopyramidal phosphite heteroanions (HPO_3^{2-}) and investigate the effect of the different atomic radius in combination with a wide range of experimental variables (pH, temperature, concentration, etc.) on the self-assembly process and consequently on the final archetype. These types of triangular pyramidal anions have proven to be ideal templates in POM chemistry. This is because they contain a lone pair of electrons which could prevent the aggregation of POM fragments from forming closed Keggin clusters and promote the assembly of novel building blocks and consequently new clusters. In order to achieve the isolation of new mixed-metal polyoxometalate compounds, the traditional "one-pot" synthetic approach was mainly used.

Apart from the conventional synthetic approach, we decided to utilize different synthetic methods for the investigation of the polyoxometalate systems. For this purpose, hydrothermal synthetic conditions and the continuous processing of an automated flow system were used. With the first method, we intended to utilize more hard conditions (high temperature and pressure) for the isolation of possibly the most thermodynamically stable compound, whilst with the latter method we have been able to combine a large number of initial reagents in a systematic and automated fashion. Moreover, utilizing programmable multi-pumps reactor system, we aimed to a better control of the self-assembly processes by screening large parameter spaces and therefore to generate different building block libraries leading to the stabilization of different intermediates.

A third part of this present work has been the investigation of the periodicity of a reported from our group redox-controlled driven oscillatory template exchange between phosphate (P) and vanadate (V) anions enclosed in an Wells-Dawson cluster, utilizing UV-vis spectroscopy. As it has been reported, the phenomenon of the exchange of the heteroanions is observed under specific experimental conditions, such as high temperature and the presence of reducing agent. In an effort to investigate the role of the experimental variables in this phenomenon, various experimental conditions were also applied, revealing the sensitivity of the oscillatory system. Therefore, we aimed to explore the formation mechanism and the susceptibility of the system to experimental changes and investigate the potential of POM cluster capsules for the design of responsive materials.

3. Results and Discussion

Polyoxometalates are a family of anionic metal oxide clusters with a wide range of structural properties and applications. Many research groups have increased their interest in isolating novel POM compounds and on the investigation of their properties utilizing different synthetic approaches. Nevertheless, the 'one-pot' reaction approach is being characterized as an unpredictable approach, it has been the most popular technique for the formation of this type of clusters. It is well known that the final POM structure can be influenced by a variaty of experimental parameters such as, the ionic strength, the pH of the solution mixture, the temperature, the concentration of the reagents, etc. In an effort to gain control and if possible to direct the self-assembly processes, POM chemists have introduced different techniques, such as the structure directing properties of "shrink-wrapping" organic cations, [65, 76, 135] control of the ionic strength, [35] reaction and crystallisation under continuous flow conditions.

The synthesis of POMs utilizing tetrahedral heteroatoms, $\{XO_y\}$ (X = S, P, Si, Ge), is well known and it has been shown to play a crucial role in the self-assembly process, as they can stabilize reactive intermediates and consequently affect the final architecture of the cluster. [117, 173-175] The compounds which have these heteroatoms incorporated in the final product are called Heteropolyoxometalates (HPOMs). The nature of the heteroatoms can highly influence the final archetype of the HPOM. For example, the isolated cluster could be the Keggin $\{XM_{12}O_{40}\}$ with one $\{XO_4\}$ tetrahedral heteroanion within the central cavity [176, 177] the Anderson $\{XM_6O_{24}\}$ with an octahedrally coordinated heteroatom $\{XO_6\}$ in the centre of a cyclic polyanion, [178, 179] and the Wells-Dawson $\{X_2M_{18}O_{62}\}$ with two $\{XO_4\}$ tetrahedrally coordinated heteroanions inside the inorganic metal cage. The interest in investigating HPOMs templated by non-conventional heteroanions has been recently increased, as it has been shown that the use of unconventional heteroanions as templates yield new materials with interesting redox properties and unknown archetypes. [129]

In this work, we explored the assembly of novel POMs utilizing trigonal pyramidal heteroanions. Specifically, we present and discuss the incorporation of pyramidal heteroanions (HPO_3^{2-}, SeO_3^{2-} and TeO_3^{2-}) within mixed metal and mixed-valence systems, and how the atomic radius of the heteroanions along with its geometry impacts the self-assembly process of the building units involved in the reaction mixture and the archetype of the final products.

From the current work two novel structures with the HPO_3^{2-} anion have been isolated under one pot conditions. In addition two isostructural to the already known egg-shaped Dawson-like compounds incorporating TeO_3^{2-} and HPO_3^{2-} anions as heteroatoms and the first δ-isomer of the Keggin structure have been isolated also under one-pot conditions. The isolation of two novel molybdovanadate-based compounds has been achieved utilizing flow and hydrothermal conditions. Finally, the redox driven oscillations utilizing molybdenum based capsules, based on a previous Cronin's group work [180] was further explored in order understand the mechanism of the oscillations observed.

3.1 Phosphite-based Polyoxometalates

The first effort to explore the effects of the heteroatoms in the structure was by using the phosphite, HPO_3^{2-}, anion as template. The sequential addition of $Na_2MoO_4{\cdot}2H_2O$, $VOSO_4{\cdot}xH_2O$, $Na_2HPO_3{\cdot}5H_2O$ and DMA·HCl (dimethylamine hydrochloride) to a warm (~ 70 ^oC) solvent mixture of deionized H_2O and MeOH resulted in the formation of a dark purple solution. This reaction mixture was left to cool down to room temperature and then the pH was adjusted to 2.9 by drop-wise addition of concentrated aqueous HCl resulting to a dark green solution which was left to crystallize. Dark green needles of **1** formed after a week. The compound **1** can be synthesized within the pH range 2.5-3.5, although the highest yield and purity have been observed at the pH range 2.8-3.0. It is worth mentioning that crystals of compound **1** were first isolated by the technique of solvent diffusion with methanol. In this method a small vial with mother liquor is placed inside a bigger flask containing solvent with lower boiling point that the solution of the compound **1**, in this case methanol. However, it was observed that with that method a considerable amount of organic impurities was precipitated. On the other hand, the solvent mixture of H_2O and CH_3OH, resulted in the isolation of more pure and in higher yield product. In addition, any effort to isolate the compound **1** without adding solvent methanol was unsuccessful. Instead, the Keggin structure of $\{Mo_{12}(VO_4)DMA\}$, was isolated under slow evaporation.

Crystallographic studies revealed that **1** can be formulated as $(C_2H_8N)_5Na_2[Mo_{11}V^V_5V^{IV}_2O_{52}(HPO_3)(CH_3OH)]{\cdot}5H_2O$ and adopts a Dawson-like structure where seven of the molybdenum metal centres have been replaced by two reduced and five fully oxidized vanadium atoms. The structure consists of two hemispheres; the upper one is formed by three edge-sharing $\{MoO_6\}$ octahedra connected to the upper belt of the distorted egg-shape cluster through three $\{V^VO_4\}$ tetrahedra. The remaining four V positions (2 V^V

and 2 V^{IV}) are crystallographically disordered over the nine {MO_6} octahedra positions, formed the lower hemisphere of the cluster. According to BVS calculations, two electrons (one for each V^{IV}) have been found disordered between four positions (BVS_{av}= 4.4). Finally, the cavity is occupied by a μ_9-HPO_3^{2-} ion (Figure 3.1 right). The identification of the oxidation states of the metal centres was made on basis of change balance considerations of the entire compound, combined with bond valence sum calculations (BVS), [181] elemental analysis and atomic absorption spectroscopy. All Mo atoms have the oxidation state VI (BVS_{av}=6.05), the V atoms in the upper hemisphere are in the oxidation state V (BVS_{av}=5.09) and the P atom in the μ_9-HPO_3^{2-} is in the oxidation state III. The V atoms in the VO_4 tetrahedra are coordinated by three μ_3-O^{2-} moieties, with the V-O bonds in the range of 1.716(4)-1.768(4) Å and one terminal oxo group with a V=O bond in the range of 1.614(4)-1.627(5) Å. The Mo atoms in the same hemisphere exhibit two terminal oxo groups in cis position, with the Mo=O group bond lengths in the range of 1.698(4)-1.718(4) Å, one μ-O^{2-} and three μ_3-O^{2-} bridges with Mo-O bonds between 1.855(4)-1.884(4) Å and 2.048(4)-2.267(4) Å, respectively. Finally a CH_3OH molecule is coordinated to a Na atom in unit cell as a result of the crystallization procedure with the mixture of H_2O/CH_3OH solvents.

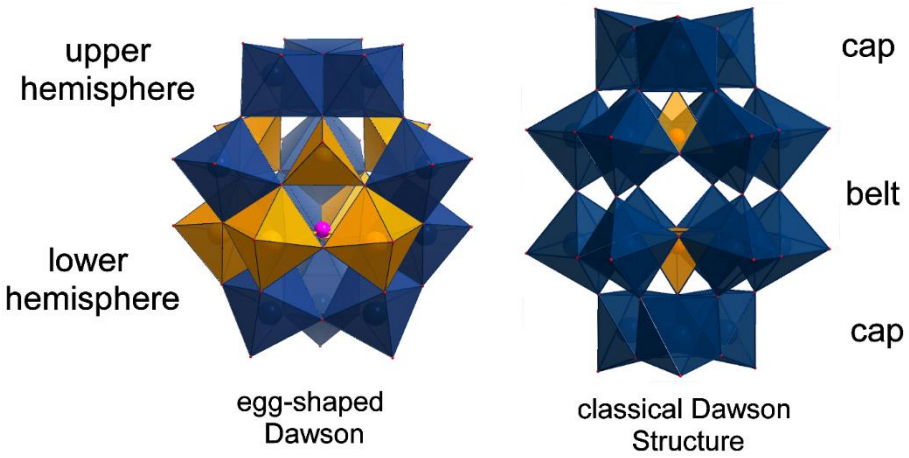

Figure 3.1 Polyhedral representation of the egg-shaped $[Mo_{11}V^{V}_5V^{IV}_2O_{52}(HPO_3)(CH_3OH)]^{7-}$ anion and the anion of the classical Dawson $[Mo_{18}O_{54}(XO_4)]^{n-}$. Colour code: Mo: blue polyhedral, V: orange polyhedral, P: pink sphere and O: red spheres.

It is worth noting that within the egg-shaped cluster different geometries can be observed from different metal centres, namely octahedral for Mo^{VI} and tetrahedral for pure V^{IV} metal ions. Moreover, V^{V} metal centres are present in the final structure even though the fully oxidized vanadium has been rapidly reduced in the presence of DMA·HCl. The cluster is only templated by one pyramidal HPO_3^{2-} anion, in contrast with the classical Dawson

structure which is templated by two tetrahedral heteroanions. Finally, the coordination sphere of the Mo^{VI} centres located at the upper hemisphere exhibit two terminal oxo groups, while in the conventional Dawson structure exhibit only one.

The addition of $Na_2S_2O_4$ in a clear aqueous solution of $Na_2MoO_4{\cdot}2H_2O$, resulted in a light brown solution with pH 6.78. The reaction mixture was stirred for about 5 minutes and then H_3PO_4 and DMA·HCl were added resulted to a dark green solution with pH 6.2. The reaction mixture was stirred for more 5 minutes and after filtration was left undisturbed at 5 ^oC to crystallize. Orange rod-like crystals of **2** were obtained after about a month. It is worth noting that the initial dark green solution gave black rod-like crystals of the well-known phosphotungstate Keggin within two days. Compound **2** can be isolated only after the removal of the Keggin compound by filtration.

After the filtration of this reaction mixture, the colour of the filtrate turned to light brown giving the desirable crystals of compound **2**. The formula of the compound **2**, as has been revealed from the crystallographic studies, is $(C_2H_8N)_3Na[Mo_{12}O_{30}(HPO_3)_8](H_2O)_{10}$ (Figure. 3.2a). The structure consists of a pair of six edge-sharing MoO_6 octahedra. All Mo atoms are coplanar and have the oxidation state VI (BVS_{av}=5.98). Finally, the resulting hexanuclear ring encapsulates a central μ_6-HPO_3^{2-} ion. The three peripheral HPO_3^{2-} ions act as bidentate ligands in a η^1: η^1: μ coordination mode. The central phosphite ion has distance of 1.5 Å from the same side of the planar defined by the six molybdenum atoms (Figure 3.2b). Each Mo atom exhibits one terminal oxo group, with the Mo=O group bond lengths in the range of 1.668(5)-1.681(5) Å, four μ-O^{2-} and one μ_3-O^{2-} bridges with Mo–O bonds between 1.928(5)-2.130(5) Å and 2.320(5)-2.341(5) Å, respectively. Each P atom of the three phosphite ligands exhibit one terminal oxo group, with the P=O group bond lengths in the range of 1.445(2)-1.448(2) Å and two μ-O^{2-} bridges with P-O bonds between 1.492(7)-1.608(2) Å. The structure of **2** crystallizes in monoclinic system in *C2/c* space group and has a 2-fold axis. The hexamer Mo_6P_4 units are bonded together with one sodium atom *via* six μ-O^{2-} bridges with average Na-O distance of 2.293(2) Å.

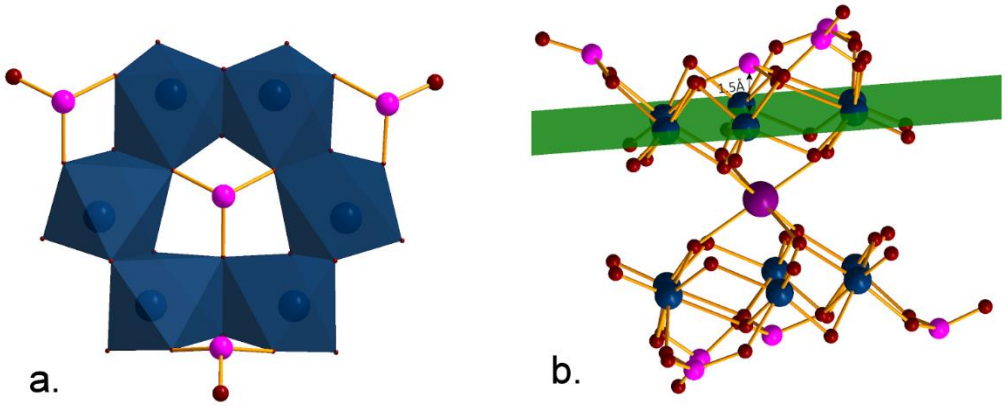

Figure 3.2 (a) Polyhedral representation of the asymmetric unit of $[Mo_{12}O_{30}(HPO_3)_8]^{4-}$ and (b) ball and stick representation of the anion highlighted that the Mo centres are in the same plane. Colour code: Mo: blue polyhedral and blue spheres, P: pink spheres, Na: violet sphere and O: red spheres.

Continuing to explore the effect of the HPO_3^{2-} ions in the Mo/V- based Polyoxometalates chemistry, compound **3** was isolated when $Na_2MoO_4{\cdot}2H_2O$, $VOSO_4{\cdot}4H_2O$ and TEA·HCl (triethanolamine hydrochloride) were sequentially added with a molar ratio 2:0.025:0.25:0.25, resulting to a dark purple solution with pH=6.70. Then H_3PO_3 was added with no significant change of the reaction mixture. After stirring for about 20 minutes, the pH was adjusted to 5.50 using concentrated hydrochloric acid and then the reaction mixture was filtrated giving clear dark purple solution. The filtrate was kept at 18 ^oC for 10 days, when orange needles of compound **3** were obtained. Crystallographic studies revealed that **3** can be formulated as $(C_6H_{16}NO_3)_6Na_8H[Mo_6O_{18}(\mu_6\text{-}HPO_3)(C_6H_{13}NO_3)]_2[(PV_4Mo_8O_{40})](H_2O)_{32}$.

The structure consists of a mixed metal α-Keggin Mo/V-based cluster with heteroanion the $\mu_6\text{-}HPO_4^{3-}$ and with the positions of the metal centres to be crystallographically disordered and a hexanuclear Molybdenum-based cluster that co-crystallizes in the unit cell. The later structure consists of six edge-sharing MoO_6 octahedra (Figure 3.3a). All Mo atoms that are crystallographically in the same plane, have the oxidation state VI (BVS_{av}=5.95). The cavity of the cluster is occupied by a $\mu_6\text{-}HPO_3^{2-}$ ion, while a deprotonated triethanolamine ion is coordinated to the compound in a η^2: η^2: μ_3 coordination mode, completing the octahedral geometry of the Mo atoms. Each Mo atom exhibits one terminal oxo group, with the Mo=O group bond lengths in the range of 1.707(4)-1.721(4) Å, four $\mu\text{-}O^{2-}$ and one $\mu_3\text{-}O^{2-}$ bridges with Mo–O bonds between 1.721(4)-2.224(4) Å and 2.316(5)-2.352(4) Å, respectively. The

presence of the Vanadium reagent plays an important role in the formation of final product, as the same reaction conditions in the absence of the vanadium reagent resulted to the formation of only the known hexanuclear compound with the formula $\{Mo_6O_{18}(HPO_3)Na_3(TEA)\}$. The compound **3** crystallizes in triclinic system in *P-1* space group and every $\{V_4Mo_8P\}$ unit is connected to each other *via* sodium cations forming a 2D chain (Figure 3.3b and 3.3c). The hexamer and the Keggin moieties are connected to each other *via* the triethanolamine ions.

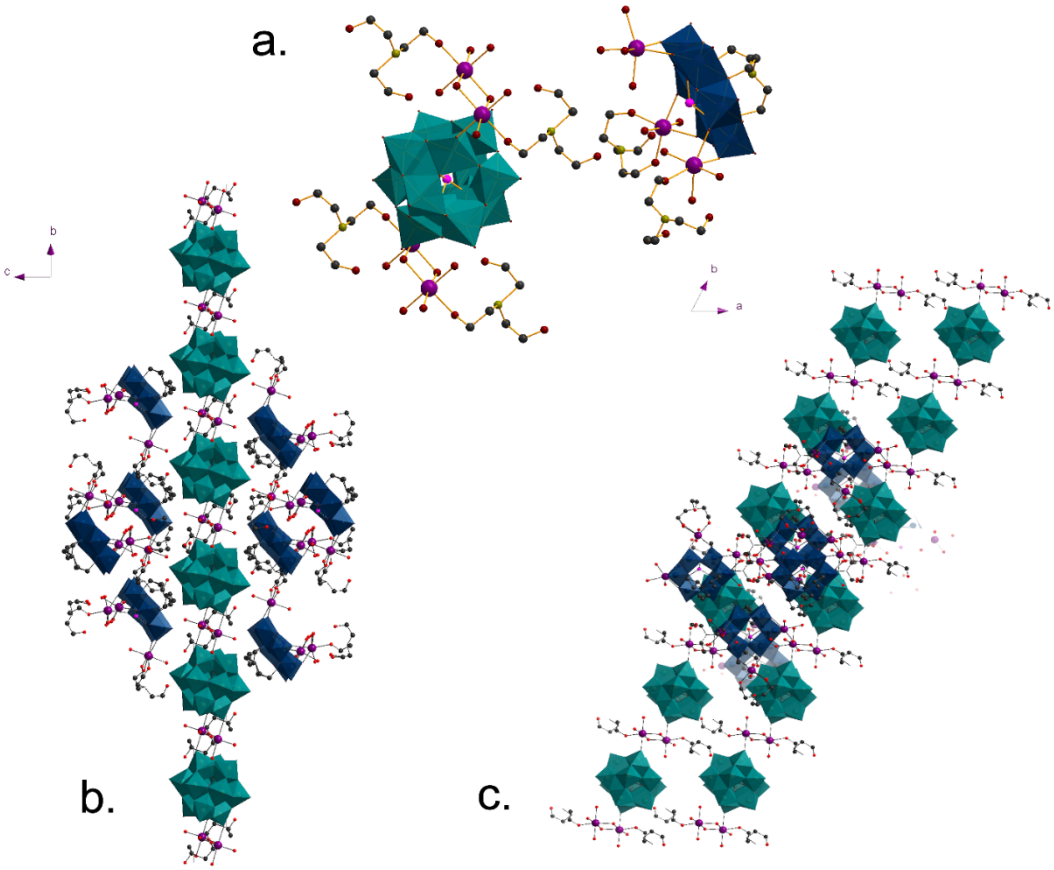

Figure 3.3 Polyhedral representation of compound **3**: a) co-crystallization of the hexamer and the keggin structures in the unit cell; b) and c) packing mode of compound **3** along *a* axis and *c* axis showing the 2D chain formed by the kegging structure. Colour code: Mo: dark teal polyhedra, Mo/V: Teal polyhedra, C: black spheres, N: dark yellow spheres, Na: violet spheres, O: red spheres. Hydrogen atoms have been omitted for clarity.

3.2 Tellurite -based Mixed Metal Polyoxometalates

In an effort to further investigate the effect of the geometry and size of the incorporated heteroanions from Group XVI, we studied the implication of the pyramidal selenite heteroanion within the molybdenum and vanadium mixed-metal systems. Herein we report the synthesis, solid state and solution characterization of a new family of selenite-based mixed-metal and mixed-valence polyoxometalates namely: {$Mo_{11}V_7Te$} = $(C_2H_8N)_6Na[Mo^{VI}_{11}V^{V}_5V^{IV}_2O_{52}(TeO_3)]\cdot 15H_2O$ **4**, $K_4(C_2H_8N)_3[Mo^{VI}_{12}V^{V}_3O_{39}(\mu_6\text{-}TeO_4)_3(\mu_6\text{-}TeO_3)_2]\cdot 14(H_2O)$ **5** and $Na_3(C_2H_8N)_4[Mo^{VI}_{12}V^{V}_3O_{39}(\mu_6\text{-}TeO_4)_3(\mu_6\text{-}TeO_3)_2]\cdot 15(H_2O)$ **6**.

3.2.1 "One-pot" Synthesis

Compound **4** was synthesized by the addition of $Na_2MoO_4{\cdot}2H_2O$, $NaVO_3$, Na_2TeO_3 and DMA·HCl to deionized H_2O. Because of the limited solubility of the vanadate salt in water, the cloudy yellow mixture was heated at 90°C until the complete dissolving of the $NaVO_3$, resulting in clear yellowish solution. The reaction mixture was left to cool down at room temperature under magnetic stirring and then solid $N_2H_4{\cdot}HCl$ was added to give a dark green solution. The pH adjusted to 2.5 by drop-wise addition of concentrated $_{aq.}$HCl giving a dark purple solution. Dark green needles of **4** were formed under gas diffusion with MeOH after one week. It is worth mentioning that the use of reduced V as a reagent led to the formation of the well-known "crowned" Dawson-like structure, [132] $K_{10}[Mo^{VI}_{11}V^{V}_5V^{IV}_2O_{52}(Te^{VI}O_3)(Mo^{VI}_6V^{V}O_{22})]\cdot 15H_2O$, even after changing the experimental conditions (e.g. temperature, concentration, pH). Finally, the use of solvent methanol seems to be crucial for the crystallization of the compounds **4**, otherwise only already known compounds could be isolated, such as α-Keggin and α-Dawson clusters.

Compound **4** adapts the same distorted egg-shaped cage with selenite- , sulfite- and phosphite-based heteropolyoxometalates, with the formula of the compound **4** to be $(C_2H_8N)_6Na[Mo^{VI}_{11}V^{V}_5V^{IV}_2O_{52}(TeO_3)]$, figure 3.4a. The cluster has been found by the crystallographic studies to be isostructural with all the other three molybdovanadates, with the difference that the cavity is occupied by a $\mu_9\text{-}TeO_3^{2-}$ ion (Figure 3.4b), instead. In the upper hemisphere the Mo atoms have the oxidation state VI (BVSav=6.01), the V atoms are in the oxidation state V (BVSav=5.04) and the Te atom is in the oxidation state IV. The Vanadium atoms in the VO_4 tetrahedra are coordinated by three $\mu_3\text{-}O^{2-}$ moieties, with the V-O bonds in the range of 1.727(9)-1.777(6) Å and one terminal oxo group with a V=O bond in the range of 1.603(10)-1.615(7) Å. The Mo atoms in the same hemisphere exhibit two

terminal oxo groups in cis position, with the Mo=O group bond lengths in the range of 1.697(7)-1.708(7) Å, one μ-O^{2-} and three μ_3-O^{2-} bridges with Mo-O bonds between 1.876(7)-1.896(7) Å and 1.889(7)-2.044(9) Å, respectively. It is worth mentioning that the cluster can be isolated only in the presence of MeOH solvent. It seems that MeOH molecules help towards the formation of the cluster, but they do not participate in the final formula of the compound.

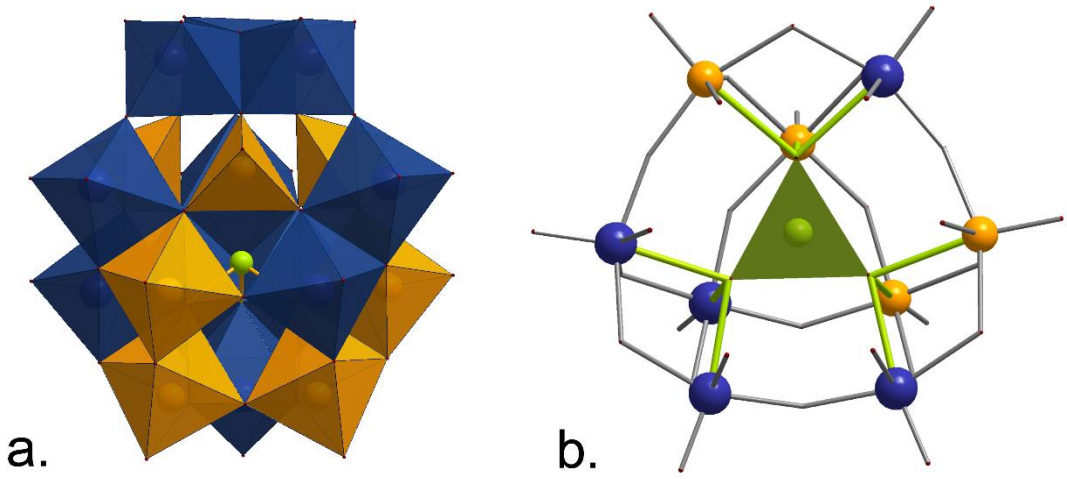

Figure 3.4 (a) Polyhedral representation of {$Mo_{11}V_7Te$}, (b) Ball-and-stick representation of the lower hemisphere where it is shown the coordination mode of the μ_9-TeO_3 heteroanion (dark yellow pyramid). Color code: Mo: dark teal polyhedral and spheres, V: orange polyhedral and spheres, Te: lime spheres and O: red spheres.

3.2.1.1 Comparing the four isostructural egg-like Dawson structures

As it has already been reported, the isolation of the {$Mo_{11}V_7Se$} [129] and the {$Mo_{11}V_7S$} [126] compounds was held by the addition of the potassium- and the ammonium-based reagents with the in situ reduction of the V^V species, respectively. Any attempts to isolate the isostructural Te-based cluster in a same manner were unsuccessful. Only with the use of different cations, namely sodium and dimethylamine salt, the isolation of this cluster was successful. The compounds {$Mo_{11}V_7Se$} and {$Mo_{11}V_7S$} have been described in detail in our group's reported work. However, it is worth noting the differences in the bond lengths of the heteroatoms could be pointed out. The X-O bond lengths (X= P, Te, Se, S) increase proportional to the electronic density of the atoms, thus the (P-O)av. bond is 1.53(1) Å, similar to the (S-O)av. bond which is 1.53(8) Å. Likewise, longer bond lengths have been observed for the Se-based cluster with (Se-O)av. to be 1.70(3) Å and finally, the Te-based compound exhibits the longest bond lengths, namely (Te-O)av.=1.86(9) Å (see Table 2) with

bond lengths/angles). Utilization of different counter ions resulted in the crystallization of all four compounds in different space groups and therefore in diverse packing configurations (Figure 3.5). When sodium and DMAH are used as cations, the {$Mo_{11}V_7P$} cluster is crystallized in the *P-1* space group, whilst the different amount of the same cations results in the crystallization of the {$Mo_{11}V_7Te$} cluster in the *Pnma* space group. Consequently, the use of potassium or ammonium counter ions resulted in the crystallization of the {$Mo_{11}V_7Se$} and {$Mo_{11}V_7S$} compounds in the *P*-4b_2 and *P*2$_1$/*m* space groups respectively (for details see Table 8.2 of the appendices).

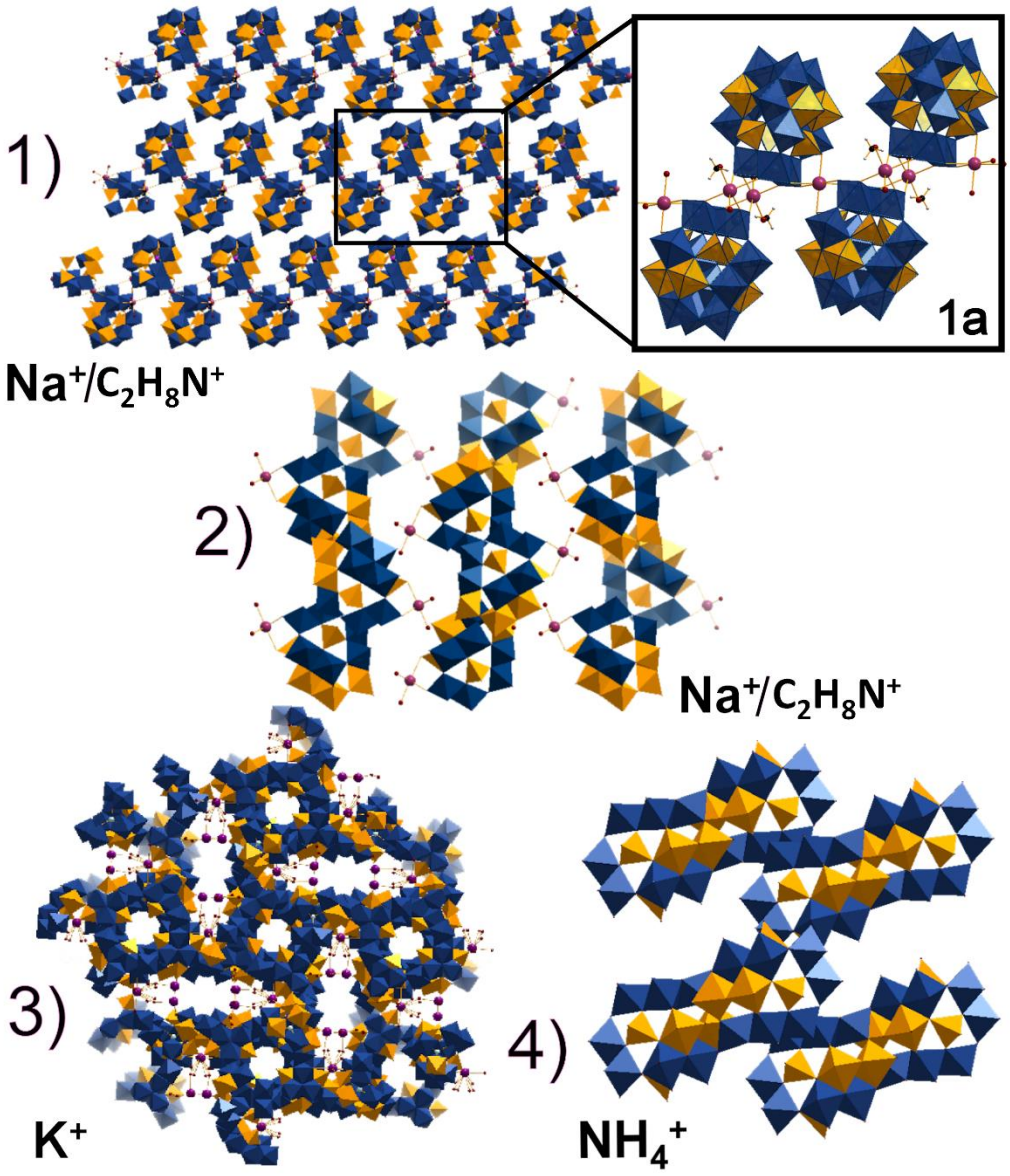

Figure 3.5 Polyhedral representation of the packing mode of the compounds along *b* axis: 1) {$Mo_{11}V_7P$}, 1a) zooming in the packing mode of {$Mo_{11}V_7P$}, 2) {$Mo_{11}V_7Te$}, 3) {$Mo_{11}V_7Se$} and 4) {$Mo_{11}V_7S$} compounds. Colour code: Mo: blue, V: light orange, K: violet, Na: plum. DMA cations have been omitted for clarity.

The {$Mo_{11}V_7P$} compound packs in a 2D planar configuration which consists of pairs of clusters. Each cluster of the phosphate-based molecule connects with its pair *via* two sodium cations, while each pair connects with its adjacent one *via* one sodium cation. In addition, these pairs of cluster form arrays which are connected to each other via DMAH cations forming all together the 2D planar packing configuration of the P-based compound (**1** and **1a** in figure 3.5). It is worth mentioning that one MeOH is connected to each of the two sodium atoms which link the pair of the clusters. The different amount of sodium and DMAH cation added in the reaction mixture of the Te-based compound resulted in a different packing configuration. The {$Mo_{11}V_7Te$} clusters are connected to each other *via* one sodium cation in an antiparallel mode. The {$Mo_{11}V_7Se$} clusters pack in a herringbone configuration of alternating rectangular and circular cavities with dimensions of about 20x4.4 Å and 3.2 Å, respectively, while the clusters of {$Mo_{11}V_7S$} are connected to each other through *via* ammonium cations forming a zig-zag configuration.

Table 2: Bond distances and angles of the four heteroanions.

bond lengths (Å)			
P(1)-O(36)	1.528(4)	Se(1)-O(1)	1.703(15)
P(1)-O(42)	1.532(4)	Se(1)-O(11)	1.706(15)
P(1)-O(37)	1.533(4)	Se(1)-O(4)	1.707(16)
Te(1)-O(20)	1.868(8)	S(1)-O(7)	1.547(5)
Te(1)-O(23)	1.871(6)	S(1)-O(31)	1.550(3)
angles [°]			
O(36)-P(1)-O(42)	110.8(2)	O(1)-Se(1)-O(11)	99.6(7)
O(36)-P(1)-O(37)	110.9(2)	O(1)-Se(1)-O(4)	100.3(7)
O(42)-P(1)-O(37)	110.9(2)	O(11)-Se(1)-O(4)	99.0(7)
O(20)-Te(1)-O(23)	95.3(3)	O(7)-S(1)-O(31)	103.87(17)
O(23)#1-Te(1)-O(23)	94.9(4)	O(31)-S(1)-O(31)#1	102.9(3)

The stability of the four compounds has also been investigated in aqueous solution by using UV-Vis spectroscopy. For this purpose the selenite and sulphite derivatives of the compound were reproduced according to the reported reaction procedures. Figure 3.6 represents the four spectra of the Dawson-like products. From the results we could say that {$M_{17}P$} slightly decomposes after two hours, whilst {$M_{17}Te$} retains its integrity for at least one day. It is well known that in POM chemistry several species may be in equilibrium, depending on the pH. The {$M_{17}Se$} cluster seems to start decomposing slightly after two hours in aqueous solution whilst in the case of the {$M_{17}S$} cage we can appreciate the stability of the cluster over at least three hours.

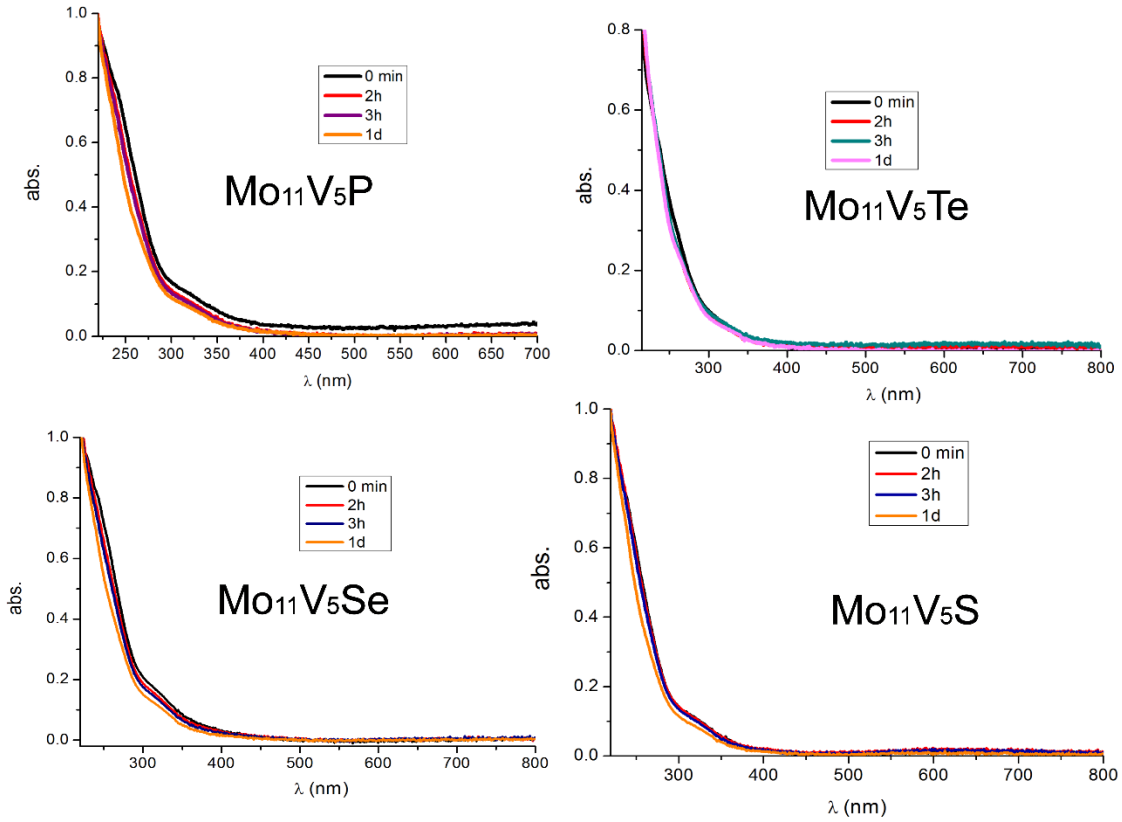

Figure 3.6 Time-dependent UV-vis spectrum of the four compounds in aqueous solution at a concentration of $7.3x10^{-6}$ mol·L^{-1} for {$M_{17}P$}, $9.3x10^{-6}$ mol·L^{-1} for {$M_{17}Te$}, $7.8x10^{-6}$ mol·L^{-1} for {$M_{17}Se$} and $8.3x10^{-6}$ mol·L^{-1} for {$M_{17}S$} clusters.

The next step, having isolated the four isostructural clusters, was to investigate the effect of the heteroanions in the structure. Cyclic Voltammetry of the compounds was performed in a 0.1 M acetate buffer solution of 0.1 M acetic acid and 0.1 M sodium acetate, using Na_2SO_4 as electrolyte. [182] The measurements were performed over the potential window ranging from +1400 to -1200 mV at a scan rate in the range of 50-400 mV s^{-1} towards the positive direction. The measurements revealed that the oxidation peak of the compounds has been shifted proportional to the electronic density of the heteroanion. Thus, as it is expected, the Te-based molybdovanadate compound has been oxidized (first oxidation of V^{IV} metal centres) more quickly that the other compounds with an oxidation peak at 0.544 V. The Se-based compound follows with a peak at 0.660 V, quicker that the S-based polyoxometalate with an oxidation peak at 0.824 V. Finally, the compound consisted of the heteroatom with less electronic density, namely HPO_3^{2-}, displays the oxidation peak at 0.828 V. The values for peak-to-peak separations ($\Delta_{Ep} = E_{pred}-E_{pox}$) obtained for these processes were 413 mV, 96 mV, 69 mV and 70 mV, respectively at a scan rate of 50 mV s^{-1} (Figure 3.7). These values

are higher than the theoretical value for reversible electron transfer, which is about 56 mV, indicating quasi-reversible processes. A clear shift to the left (lower potential) in the oxidation peak of each compound can be observed during the first oxidation. However, this phenomenon could not be clearly observed during the second oxidation, due to the electron existence in the cell that is more influential in the redox process than the electronic density of the heteroatom in each of the compounds.

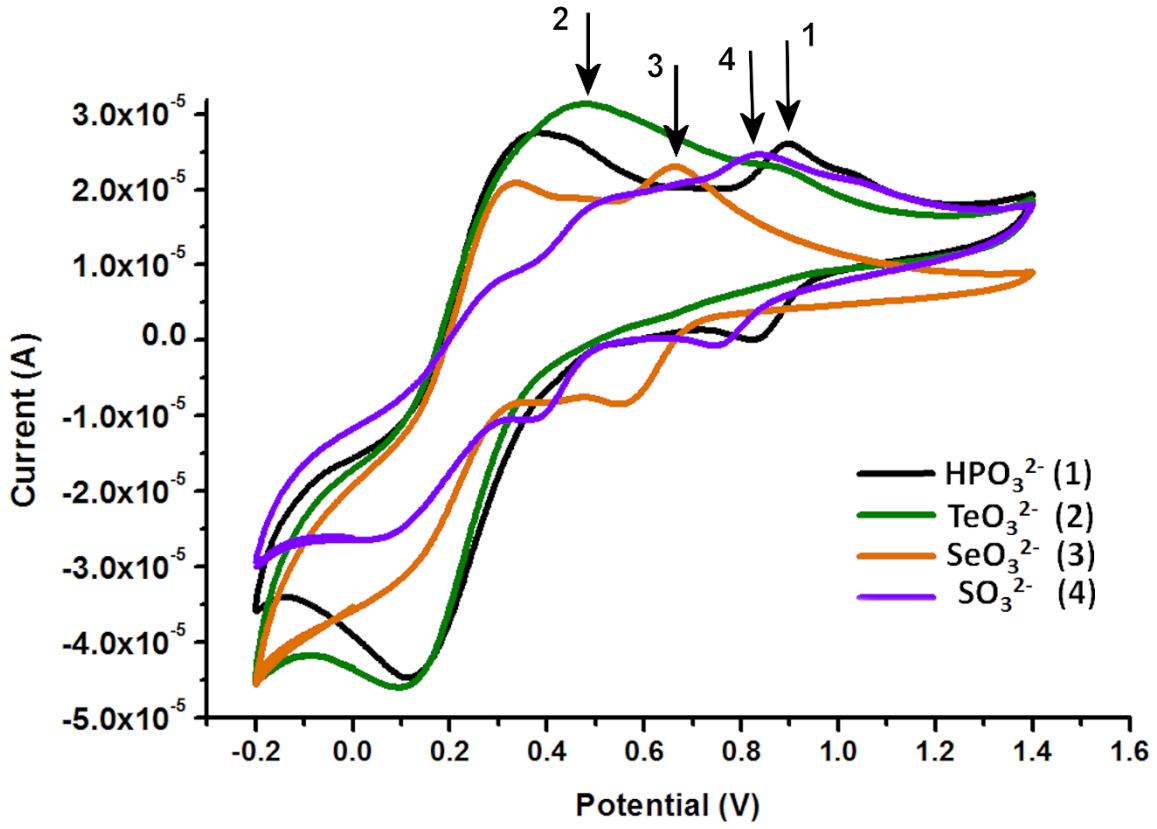

Figure 3.7 Cyclic Voltammograms of the compounds at a scan rate of 50 mV/s. The first oxidation peak of each compound is shown with arrows. Compound **4** exhibits a broad peak of both first and second oxidation peaks.

In order to understand the assembly process of the POMs systems, Electrospray Mass Spectrometry has been used as a complementary technique to X-Ray crystallography studies. The composition as well as the structural integrity of the $\{Mo_{11}V_7P\}$ and $\{Mo_{11}V_7Te\}$ clusters in solution have been investigated. The ESI-MS studies were performed by dissolving a small amount of the compounds in solvent mixture of H_2O/CH_3CN. An overlap of the peaks has been observed in the case of the $\{Mo_{11}V_7P\}$ anion (Figure 3.8), giving envelopes centered between *m/z* 1384.9 and 1478.9. The peaks can be assigned to the general formula $\{[Mo_{11}V_7O_{52}(HPO_3)]_r(CH_3OH)H_xNa_y(C_2NH_8)_z(H_2O)_m\}^{n-}$, with r=1 or 2, x=2-6, y=1-2, z= 2-7, m=14-25 and n=2 or 4. Similar results have been observed in the case of the

{$Mo_{11}V_7Te$} anion (Figure 3.9). The overlapped envelopes centered between *m/z* 964.2 and 1640.4 can be assigned to the above general formula with r=1 or 2, x=0-5, y=1-4, z= 4-8, m=7-22 and n=2 and 3. Tables 3 and 4 describe in details the molecular formula that could be assigned for the most significant peaks. The change of the oxidation state of the metals that has been observed is due to the high voltage used in the mass spectrometry ion-transfer process. [123]

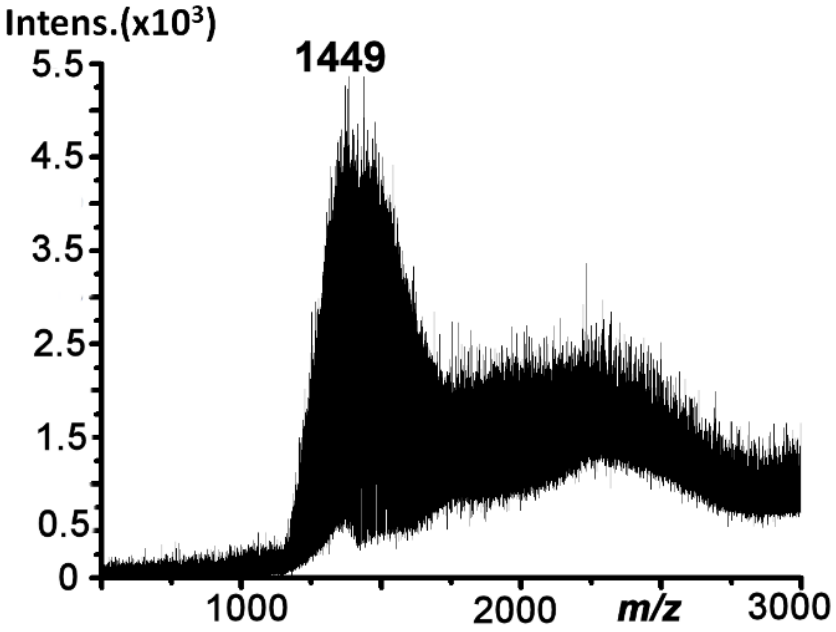

Figure 3.8: Negative ion mass spectrum of **1a** in solvent mixture H_2O/CH_3CN showing the main species, $\{Mo_{11}V^{V}_{2}V^{IV}_{5}O_{52}(HPO_3)(CH_3OH)H_2Na(C_2H_8N)_5(H_2O)_{16}\}^{2-}$.

Table 3: Selected *m/z* range of the ESI-MS of {$Mo_{11}V_7P$}.

***m/z* found**	***m/z* calc.**	**z**	**Molecular formula**
1356.46	1356.25	2-	$Mo^{V}_{4}Mo^{VI}_{4}V^{V}_{2}V^{IV}_{5}O_{52}(HPO_3)(CH_3OH)H_5Na_5(C_2H_8N)_2(H_2O)_8$
1384.9	1384.8	2-	$Mo_{11}V^{V}V^{IV}_{6}O_{52}(HPO_3)(CH_3OH)H_5Na_2(C_2H_8N)_2(H_2O)_{15}$
1426.98	1426.83	4-	$[Mo_{11}V^{V}_{3}V^{IV}_{4}O_{52}(HPO_3)]_2(CH_3OH)_6\ H_2Na_6(C_2H_8N)_6(H_2O)_{25}$
1449.98	1449.9	2-	$Mo_{11}V^{V}_{2}V^{IV}_{5}O_{52}(HPO_3)(CH_3OH)H_2Na(C_2H_8N)_5(H_2O)_{16}$
1474.99	1474.95	2-	$Mo^{V}_{3}Mo^{VI}_{8}V^{IV}_{7}O_{52}(HPO_3)(CH_3OH)H_6Na(C_2H_8N)_6(H_2O)_{16}$
1478.99	1478.96	2-	$Mo^{V}_{2}Mo^{VI}_{9}V^{IV}_{7}O_{52}(HPO_3)(CH_3OH)H_4Na(C_2H_8N)_7(H2O)_{14}$

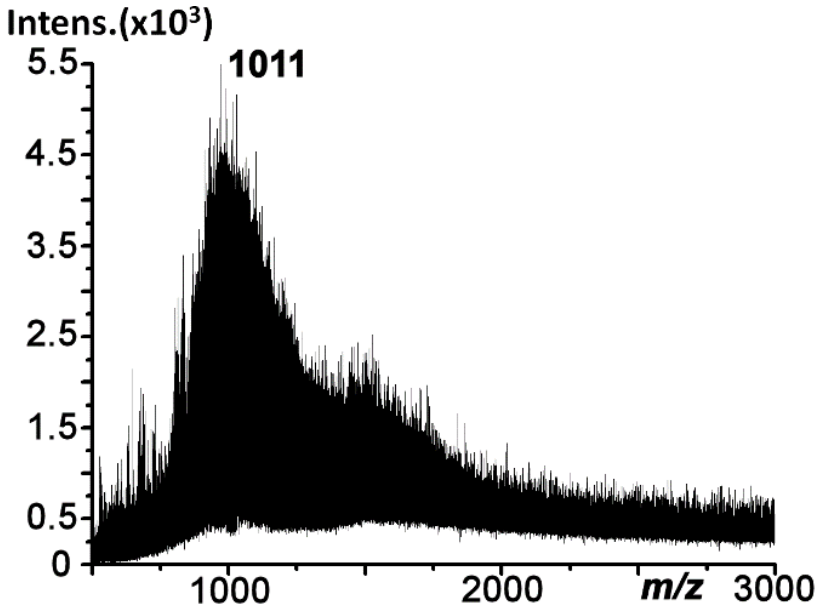

Figure 3.9: Negative ion mass spectrum of **4a** in solvent mixture H_2O/CH_3CN showing the main species, $\{Mo^{V}_{3}Mo^{VI}_{8}V^{V}V^{IV}_{6}O_{52}(TeO_3)(C_2H_8N)_6H_3Na_2(H_2O)_{16}\}^{3-}$.

Table 4: Selected *m/z* range of the ESI-MS of $\{Mo_{11}V_7Te\}$.

***m/z* found**	***m/z* calc.**	**z**	**Molecular formula**
964.25	964.2	3-	$Mo_{11}V^{IV}_{7}O_{52}(TeO_3)(C_2H_8N)_3H_5Na(H_2O)_{16}$
972.25	972.22	3-	$Mo^{V}_{4}Mo^{VI}_{7}V^{V}_{2}V^{IV}_{5}O_{52}(TeO_3)(C_2H_8N)_5H_4Na_2(H_2O)_{12}$
991.26	991.22	3-	$Mo^{V}_{3}Mo^{VI}_{8}V^{V}_{2}V^{IV}_{5}O_{52}(TeO_3)(C_2H_8N)_5H_2Na_3(H_2O)_{14}$
1011.26	1011.25	3-	$Mo^{V}_{3}Mo^{VI}_{8}V^{V}V^{IV}_{6}O_{52}(TeO_3)(C_2H_8N)_6H_3Na_2(H_2O)_{16}$
1024.26	1024.24	3-	$Mo^{V}_{3}Mo^{VI}_{8}V^{V}_{2}V^{IV}_{5}O_{52}(TeO_3)(C_2H_8N)_6HNa_3(H_2O)_{17}$
1031.26	1031.26	3-	$Mo^{V}_{4}Mo^{VI}_{7}V^{IV}_{7}O_{52}(TeO_3)(C_2H_8N)_6H_4Na_3(H_2O)_{18}$
1051.27	1051.27	3-	$Mo^{V}_{3}Mo^{VI}_{8}V^{V}_{2}V^{IV}_{5}O_{52}(TeO_3)(C_2H_8N)_7Na_3(H_2O)_{19}$
1091.95	1091.95	3-	$Mo^{V}_{8}Mo^{VI}_{3}V^{IV}_{7}O_{52}(TeO_3)(C_2H_8N)_8H_2Na_7(H_2O)_{18}$
1131.28	1131.3	3-	$Mo^{V}_{8}Mo^{VI}_{3}V^{IV}_{7}O_{52}(TeO_3)(C_2H_8N)_{10}H_2Na_5(H_2O)_{22}$
1390.3	1390.27	2-	$Mo^{V}_{2}Mo^{VI}_{9}V^{V}_{2}V^{IV}_{5}O_{52}(TeO_3)(C_2H_8N)_4H_4Na_2(H_2O)_7$
1505.4	1505.37	2-	$Mo^{V}_{3}Mo^{VI}_{8}V^{V}_{2}V^{IV}_{5}O_{52}(TeO_3)(C_2H_8N)_7HNa_3(H_2O)_{11}$
1640.4	1640.4	2-	$Mo^{V}_{6}Mo^{VI}_{5}V^{IV}_{7}O_{52}(TeO_3)(C_2H_8N)_8H_4Na_4(H_2O)_{22}$

3.2.2 Flow systems overview

The automated systems for the synthesis of polyoxometalate clusters have been extensively reported by our group. [76, 183]As an attempt to optimize the batch approaches, the reaction conditions were adjusted in an automated system. For this purpose, reactor platforms based on syringe pumps were prepared, followed by a simple and programmable methodical language. The synthesis of POM clusters has limitations regarding predictability and control over the self-assembly process due to the fast kinetic states that the building block are involved in. The control over the self-assembly of primary building blocks is a key step to understand the formation of such inorganic clusters. This kind of automated systems allow us to explore the large number of combinations of the initial reagents and thus to understand better the fundamental rules which guide the formation of complex POM-based clusters. In this work, using specifically the linear flow system (Figure 3.10), we tried to investigate the redox modulated assembly of the Vanadium-based Polyoxometalate system. For this purpose, several vanadium and molybdenum reagents have been combined with different inorganic/organic salts (NaCl, KCl, DMA·HCl, etc.) and reducing agents, under various experimental conditions.

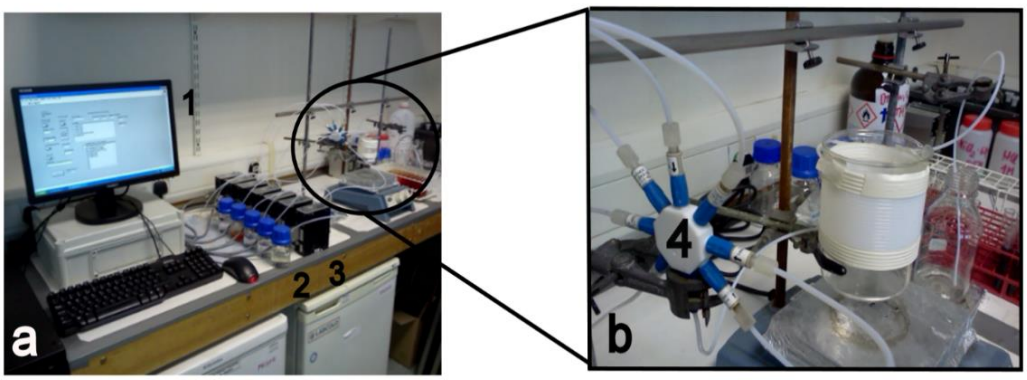

Figure 3.10 a) Picture of the linear flow (continuous processing) system showing the computer-control equipment (1), the stock solutions used for the reaction (2), the pumps (3) and b) Picture of the tube reactor (4) composed by an 8-way manifold (seven reagent inputs and one reaction output) and a plastic tubing coil to conduct the reaction with precise residence times.

The use of flow systems firstly requires careful experimental design by programming flow rate values for the pumping devices according to the reagent compositions and the features of the flow system device. Secondly, the flow system design requires accurate preparation by connecting with plastic tubing the pumping device with the stock solutions, check valves, glass reactors and any other desired equipment attached to the flow system. In this work, TriContinent™ pumps provided by TriContinent Scientific, Inc. [184] were used (Figure 3.11). These pumps are a PC-controlled programmable module equipped with a glass syringe allowing precise liquid handling. By simply programming code and preparing reagent stock solutions, the operator can run multiple chemical reactions and collect the output product.

Figure 3.11 Front and back picture views of TriContinent™ syringe pumps.

In order to perform automated chemical reactions using TriContinent pumps, the experiment variables need to be translated in to programmable parameters (residence times, flow rates, volume, etc). The TriContinent pumps use a specific command language (created by TriContinent Scientific, Inc.), see Experimental Section 7 for further details, allowing to conduct systematic pumping sequences. Hence, the LabVIEW software, provided by National Instruments Corp., [185] was used in order to facilitate the automation of the chemical reactions. The command scripts were programmed manually and sent to the pumps by using a LabVIEW graphical user interface (GUI) which is able to read and send the commands to the pumps. Following the concept of the one-pot approach for POM synthesis presented in the introduction, the flow systems become a synthetic alternative to perform multi-step POM reactions and crystallization. This approach is a useful method to line up distinct one-pot conditions in an automated fashion, rather via segmented or parameter-controlled reactions by single-stream reactors. By assembling such electronic and pumping components, the aim is to design flow devices capable of performing highly complex reaction sequences. Also, distinct processing operations (crystallization chamber, filtration, etc.) could be attached to

the flow device and in-line analytics (IR, NMR, UV, etc.) [186] are fundamental parts of the flow system in order to monitor the evolution of the chemical reactions.

3.2.3 Synthesis under flow

Utilizing the flow systems approach, a novel $\{Mo_{12}V_3Te_5\}$ compound has been isolated from the V/Mo-based system with the formula $K_4(C_2H_8N)_3[Mo^{VI}_{12}V^{V}_{3}O_{39}(\mu_6\text{-}TeO_4)_3(\mu_6\text{-}TeO_3)_2]\cdot 14(H_2O)$ **5**. The matrix has been designed so it is possible to perform 50 different reactions just by changing the dilution or the ratio of the reagents (see figure 7.1 of the experimental section for details). The mixture of $Na_2MoO4\cdot 2H_2O$, $VOSO_4.xH_2O$, $K_2TeO_3\cdot xH_2O$ and DMA·HCl, resulted in a clear, dark green solution (Figure 3.12a) in a pH range of 5.69-6.7 and was left stable to crystallize at 18 ^{0}C. Two days later the colour of the solution changed to light green (Figure 3.12b) and light green thin needles suitable for X-Ray Crystallography were obtained within a month. The formula of the anion of the compound **5**, as has been revealed from the crystallographic studies, is $[Mo^{VI}_{12}V^{V}_{3}O_{39}(\mu_6\text{-}TeO_4)_3(\mu_6\text{-}TeO_3)_2]^{7-}$ (**5a**) (Figure 3.12). The compound consists of twelve MoO_6 octahedra that form two layers of 6 Mo atoms each. These two layers are connected with three VO_5 units and three TeO_4 units forming a distorted cylinder. Finally the cavity in each layer is occupied by one TeO_3 unit. The coordination number of all the Mo atoms is 6 (CN 6) and have the oxidation state VI (BVSav=5.99). Each of them exhibits two terminal oxo groups, with the Mo=O group bond lengths at 1.711(3) Å and 1.722(3) Å, two $\mu\text{-}O^{2-}$ and two $\mu_3\text{-}O^{2-}$ bridges with Mo-O bonds at 1.909(7) Å, 1.949(2) Å and 2.241(3), 2.286(3) Å, respectively. Each of the V atoms in the VO_5 trigonal pyramids are coordinated by one terminal oxo group with the V=O bond length at 1.609(7) Å and four $\mu_3\text{-}O^{2-}$ moieties, with all the V-O bonds at 1.953(3) Å. The coordination number of all the V atoms is 5 exhibiting trigonal pyramidal geometry and the oxidation state is V (BVSav=4.97). The three Te atoms that compile the "belt" of the compound exhibit a distorted square planar geometry (CN 4). Each atom is coordinated by four $\mu_3\text{-}O^{2-}$ moieties, with all the Te-O bond lengths at 1.979(3) Å. Finally, the Te atoms in the $\mu_6\text{-}TeO_3^{2-}$ are in the oxidation state IV (BVS=3.97) with three Te-O bond lengths at 1.882(5) Å (see Table 5 for examples).

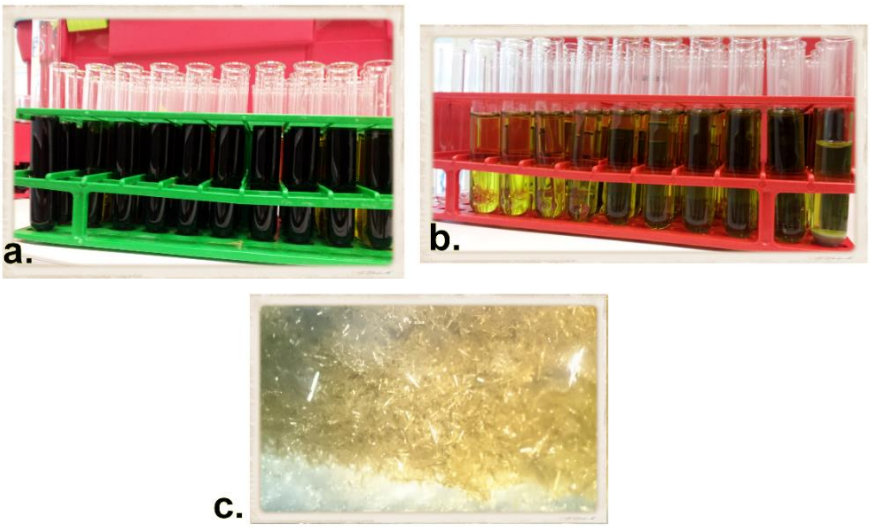

Figure 3.12 The reaction mixture during the experiment in flow system: a) initial reaction mixture, b) two days later and c) the isolated crystals.

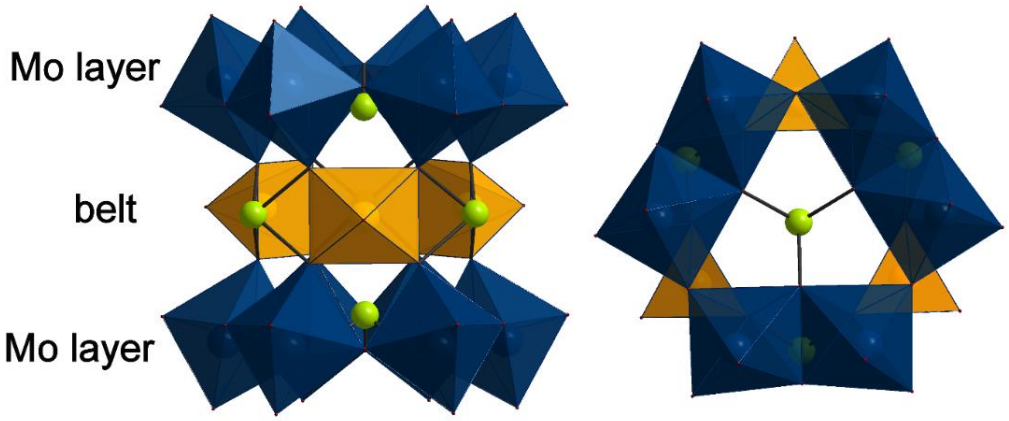

Figure 3.13 Polyhedral representation of the compound **5a** from the frond (right) and the top (left) view. The "belt" of the structure consist of three vanadium atoms and three tellurite anions. Colour code: Mo: dark teal polydedra; V: orange polyhedra; Te: lime spheres; O: red spheres.

The compound **5** crystallizes in hexagonal system in *P6/mmm* space group and every $\{Mo_{12}V_3Te_5\}$ unit is connected to each other *via* potassium cations forming a 2D honeycomb arrangement. The packing configuration of the structure reveals a plane net consisting of circular cavities with dimension of 1.7 nm (Figure 3.14). Each cavity is formed by 6 $\{Mo_{12}V_3Te_5\}$ clusters connected with *via* 6 potassium cations. A 3-fold axis passes through the tellurite anions which are located in the centre of the cluster. Also, the structures displays seven mirror planes of which one is perpendicular to the 6-fold axis, three are containing this axis and are passing though opposite daces and three more that are passing through opposite edges.

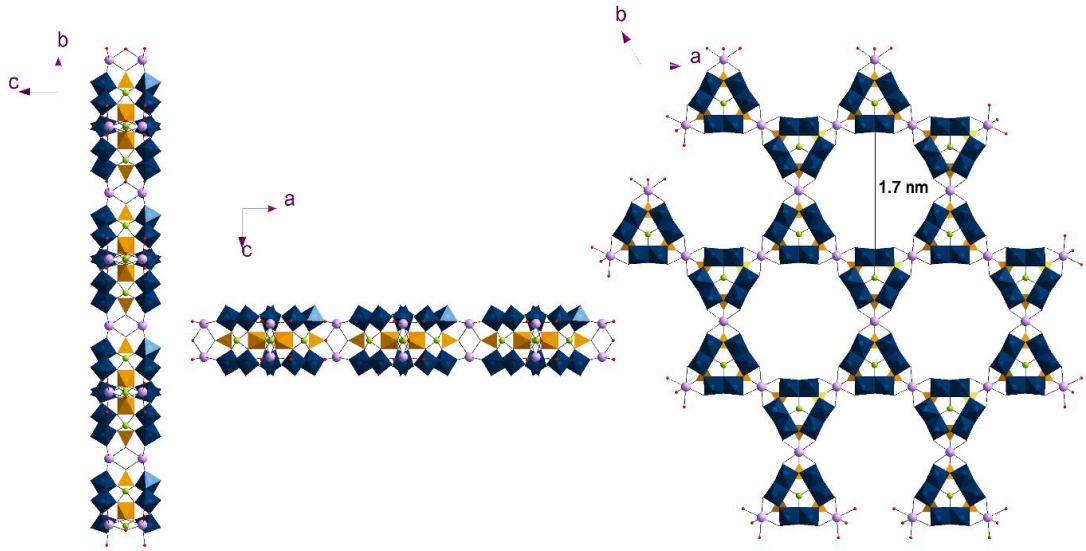

Figure 3.14 Polyhedral representation of the packing mode from **5a** in the space group *P6/mmm*. From right to left: view along *a, b* and *c axis* respectively. The structure forms a characteristic honeycomb arrangement with an empty space of 17Å. Colour code: Mo: dark teal polydedra; V: orange polyhedra; Te: lime spheres; K: light pink spheres; O: red spheres.

Table 5 Selected bond distances and angles of compound **5**.

bond lengths (Å)			
Mo(1)-O(1)	2.286(3)	V(1)-O(3)#2	1.953(3)
Mo(1)-O(2)	1.949(2)	Te(1)-O(1)	1.882(5)
Mo(1)-O(3)	2.241(3)	Te(2)-O(3)#7	1.979(3)
Mo(1)-O(4)	1.711(3)	K(1)-O(7)	2.774(4)
V(1)-O(7)	1.609(7)	K(2)-O(6)	2.796(4)

angles [°]			
O(4)-Mo(1)-O(6)	103.93(16)	O(1)#3-Te(1)-O(1)#1	94.87(18)
O(4)-Mo(1)-O(5)	99.36(18)	O(3)#7-Te(2)-O(3)	74.70(17)
O(7)-V(1)-O(3)#3	111.08(10)	O(3)-Te(2)-O(3)#4	82.51(18)
O(3)#2-V(1)-O(3)#3	75.86(18)	O(3)#5-Te(2)-O(3)#4	74.70(17)

3.2.4 Hydrothermal Synthesis

The synthesis of new polyoxometalates under hydrothermal conditions was also investigated. Compound **6** was synthesized by the sequential addition of $Na_2MoO_4{\cdot}2H_2O$, NH_4VO_3, Na_2TeO_3 and DMA·HCl were added in 10 ml of distilled water giving a colourless solution with pH=9.21. The pH was adjusted to 6.09 with 37% HCl resulting to a cloudy yellow solution. The mixture then was sealed in a 20-ml autoclave reactor and remained at 140 ^{0}C for three days. After cooling the autoclave to room temperature, dark green solution and light green needles suitable for X-Ray crystallography were obtained. Crystallography studies revealed the isostructural compound to cluster **5** with the general formula $Na_3(C_2H_8N)_2[Mo^{VI}_{12}V^{V}_{3}O_{39}(\mu_6\text{-}TeO_4)_3(\mu_6\text{-}TeO_3)_2]{\cdot}15(H_2O)$ **6**. Each of the Mo metal centres exhibits two terminal oxo groups, with the Mo=O bond lengths at the range of 1.702(4) Å-1.725(3) Å, two $\mu\text{-}O^{2-}$ and two $\mu_3\text{-}O^{2-}$ bridges with Mo-O bonds at the range of 1.896(4) Å-1.967(4) Å and 2.214(4)- 2.301(4) Å, respectively. Each of the three V atoms in the VO_5 trigonal pyramids are coordinated by one terminal oxo group with the V=O bond length at the range of 1.604(4) Å-1.610(4) Å and four $\mu_3\text{-}O^{2-}$ moieties, with V-O bonds at the range of 1.946(4) Å-1.959(4) Å. The coordination number of all the V atoms is 5 exhibiting square pyramidal geometry, while the oxidation state is IV (BVSav=4.13). The three Te atoms that compile the "belt" of the compound exhibit a distorted square planar geometry (CN 4) and are in the oxidation state IV. Each atom is coordinated by four $\mu_3\text{-}O^{2-}$ moieties, with the Te-O bond lengths at the range of 1.975(4) Å-1.996(4) Å. Finally, the two $\mu_6\text{-}TeO_3^{2-}$ inions which are located in the centre of each Mo_6 unit, are in the oxidation state IV (BVS=3.97) with three Te-O bond lengths at the range of 1.885(4) Å-1.892(4) Å (see Table 6 for examples). The compound **6** crystallizes in monoclinic system in *P21/c* space group and every $\{Mo_{12}V_5Te_5\}$ unit is connected to each other *via* sodium cations (Figure 3.15) forming a pattern of rectangular cavities with dimensions of about (18 x 5) Å .

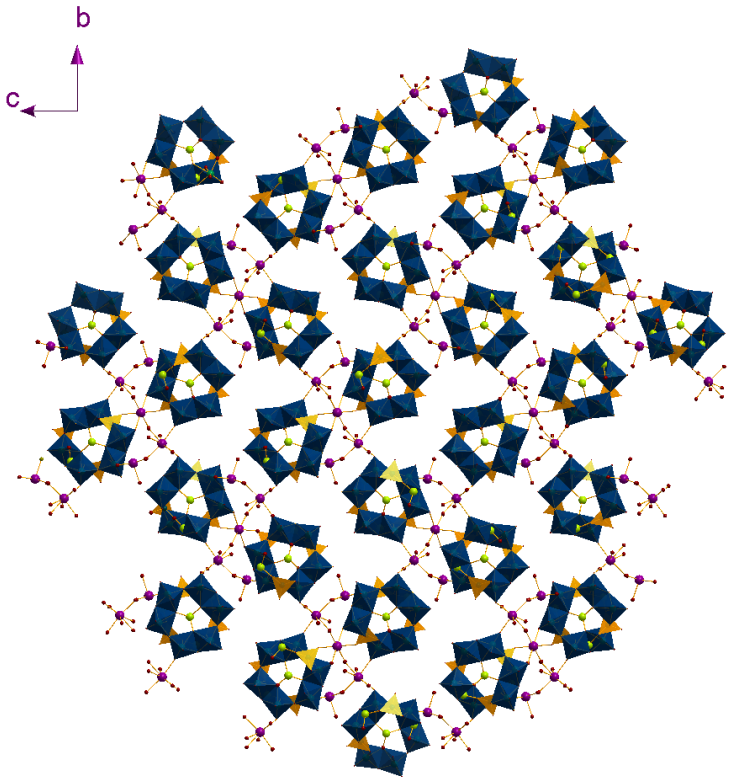

Figure 3.15 Polyhedral presentation of the compound **6a** showing the differences in the packing of compound **5a**. Colour code: Mo: dark teal polydedra; V: orange polyhedra; Te: lime spheres; Na: violet spheres; O: red spheres. The DMAH cations have been omitted for clarity.

Utilizing the continuous processing approach (flow system), we were able to possibly isolate the most kinetically favourable product, whilst utilizing the hydrothermal technique (harder technique compared to the flow approach), were able to possibly isolate the most thermodynamically favourable product. It is worth mentioning that in the first case the sodium cations from the $Na_2MoO_4 \cdot 2H_2O$ reagent do not participate in the formation of the final product. Moreover, both reaction procedures were performed with both hydrothermal and flow system methods, but unfortunately no product was able to be formed apart from vanadium oxides and colourless crystals of organic compounds. Utilizing the continuous processing, a variety of experimental variables were screened under mild experimental conditions. We were also able to investigate 50 different concentrations of the reaction mixture per experiment by using programmable pump systems. Under these conditions, compound **5** was isolated displaying a honeycomb packing configuration, with the potassium ions to stabilize the final product, whilst the sodium ions do not participate in the formation of the structure. On the other hand, utilizing the hydrothermal process and therefore harder

experimental conditions (high temperature and pressure), compound **6** was isolated. Under these conditions the sodium cations directed the packing configuration in a different way than in the case of compound **5**. Even if the two compounds are isostructural (indicating the stability of this archetype), the symmetry of the structures has changed and the big circular cavities have been replaced by smaller rectangular cavities.

Table 6 Selected bond distances and angles of compound **6**.

bond lengths (Å)			
Mo(1)-O(1)	1.713(4)	V(1)-O(29)	1.610(4)
Mo(1)-O(8)	1.899(4)	V(2)-O(30)	1.606(4)
Mo(2)-O(9)	1.717(4	V(3)-O(22)	1.959(4)
Mo(2)-O(23)	2.217(4)	Te(1)-O(19)	1.886(4)
Mo(4)-O(25)	1.609(7)	Te(2)-O(33)	1.981(4)
angles [°]			
O(1)-Mo(1)-O(7)	103.7(2)	O(36)-V(2)-O(26)	137.16(18)
O(1)-Mo(1)-O(22)	164.19(18)	O(31)-V(3)-O(22)	76.06(17)
O(18)-Mo(1)-O(19)	75.31(16)	O(19)-Te(1)-O(20)	93.87(18)
O(29)-V(1)-O(33)	110.7(2)	O(32)-Te(2)-O(24)	127.48(17)

3.3 Selenite-based Mixed Metal Polyoxometalates

In the previous chapter (Section 3.2) we have reported the characterization of tellurite-based polyoxometalates with mixed-metal/valence archetypes. In an effort to further investigate the effect of the geometry and size of the incorporated heteroanions from Group XVI, we studied the implication of the pyramidal selenite heteroanion within the molybdenum and vanadium mixed-metal systems. Herein we report the synthesis and characterization of two new selenite-based mixed-metal and mixed-valence polyoxometalates namely: $\{Mo_{16}V_{11}Se_5\}$ = $Na_{15}(C_2H_8N)_6K_6(Mo_{11}V_7SeO_{55})(Mo_5V_4Se_4O_{36})_3(H_2O)_{36}$ **7** and $\{Mo_6V_{16}Se_8\}$ = $K_8Na_6[Mo_6V_{16}Se_8O_{79}](H_2O)_{25}$ **8**.

The sequential addition of $Na_2MoO_4{\cdot}2H_2O$, $VOSO_4$, K_2SeO_3 and DMA·HCl in 10 ml of warm distilled water resulted to a purple solution with pH=7. The pH then was adjusted to 5.68 with 2M HCl resulting to a dark purple solution. The mixture then stirred for 5 more minutes and then was filtrated and remained undisturbed at 18 ^oC. Around 1 week later, dark green solution and green rhombic crystals suitable for X-Ray crystallography were obtained

and air-dried. Crystallographic studies revealed that compound **7** can crystallize in a trigonal system in *R-3m* space group and can be formulated as $Na_{15}(C_2H_8N)_6K_6[(Mo_{11}V_7SeO_{55})(Mo_5V_4Se_4O_{36})_3](H_2O)_{36}$. The cluster has been found to consist of three $\{Mo_5V_4Se_4O_{36}\}$ moieties connected to an egg-like Dawson structure *via* potassium and sodium cations forming an isosceles triangle (Figure 3.16). Each $\{Mo_5V_4Se_4O_{36}\}$ subunit consists of 5 MoO_6 octahedra with fully oxidized Mo metal centers and four VO_6 octahedra with the V metal centers in theirs +5 oxidation state. Finally, one μ_9-SeO_3 bridging anion occupies the central part of the units, whilst three (η, μ)-SeO_3 bridging anions on the top of each moiety, complete the final structure of the subunits. The Dawson subunit, $\{Mo_{11}V_7SeO_{55}\}$, consists of 11 MoO_6 octahedra with fully oxidized Mo metal centers, three VO_4 tetrahedra with the V metal centers in theirs +5 oxidation state and four VO_6 octahedra with the V metal centers in theirs +4 oxidation state. Finally, the cavity of the Dawson cluster is occupied by one μ_9-SeO_3 bridging anion (Figure 3.17). The octahedral Mo and V metal centers have been found crystallographically distorted, making the clear identification of the position of each metal fairly difficult. Selected bond distances and angles of compound **7** can be found on Table 8.3 of the Appendices. The Vanadium atoms in the VO_4 tetrahedra are coordinated by three μ_3-O^{2-} moieties, with the V-O bonds in the range of 1.731(9)-1.763(7) Å and one terminal oxo group with a V=O bond length at 1.602(11) Å. The Se-O bond lengths of the four $\{SeO_3\}$ heteroanions are at the range of 1.656(8) Å-1.725(8) Å.

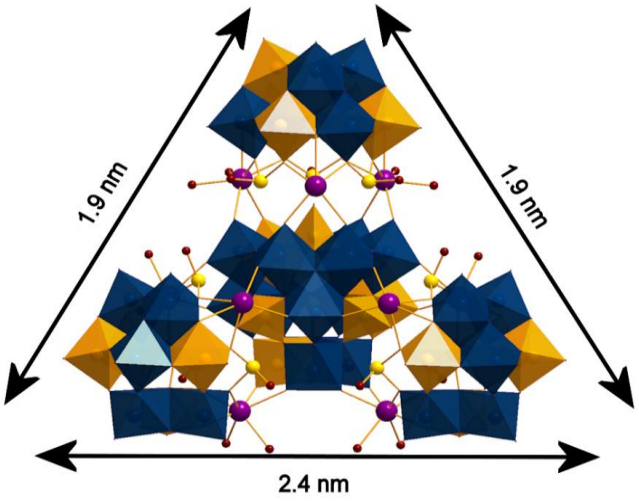

Figure 3.16 Polyhedral representation of the compound **7**. The three $\{Mo_5V_4Se_4O_{36}\}$ units are connected directly to the $\{Mo_{11}V_7SeO_{55}\}$ egg-shaped Dawson structure *via* K cations. The two different moieties are also connected each other through Na cations *via* the selenite heteroanions. Colour code: Mo: dark teal polydedra; V: orange polyhedra; Se: yellow spheres; Na: violet spheres; O: red spheres. The K and DMAH counterions have been omitted for clarity.

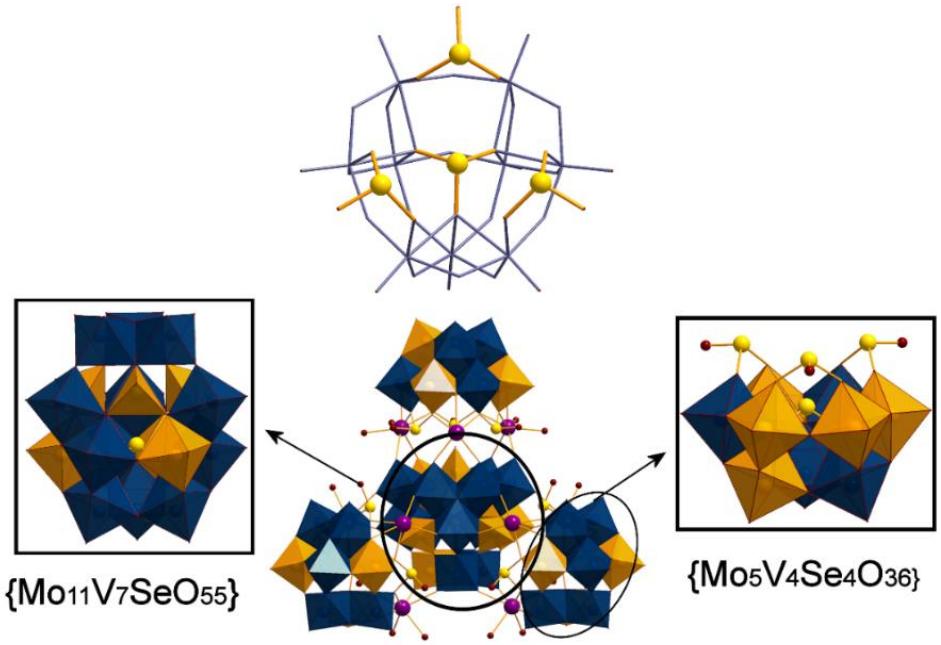

Figure 3.17 Bottom: Polyhedra representation of the compound **7** highlighting the $\{Mo_5V_4Se_4O_{36}\}$ unit are and the $\{Mo_{11}V_7SeO_{55}\}$ egg-shaped Dawson structure of the cluster. Top: Ball-and-stick representation of the $\{Mo_5V_4Se_4O_{36}\}$ subunit where it is shown the coordination mode of the SeO_3 heteroanions. Colour code: Mo: dark teal polydedra; V: orange polyhedra; Se: yellow spheres; Na: violet spheres; O: red spheres. The K and DMAH counterions have been omitted for clarity.

The cluster with the general formula $K_8Na_6[Mo_6V_{16}Se_8O_{79}](H_2O)_{25}$ (**8)** was isolated from the same reaction procedure as the one followed for compound **7** but this time using two equivalents of the selenite reagent. All the reaction reagents were added in 10 ml of warm distilled water giving a purple solution with pH=7.7. The pH was adjusted to 5.63 with 2M HCl resulting to a dark purple solution. The mixture then was filtrated and remained at 5^0C and after around 10 days, dark green solution and big green cubic crystals suitable for X-Ray crystallography were separated and air-dried. Crystallographic studies revealed that compound **8** can crystallizes in a trigonal system in *P3221* space group and can be formulated as $[Mo_6V_{16}Se_8O_{79}]^{14-}$ **8a**. Each $\{Mo_3V_8(SeO_3)_4O_{40}\}$ "basket"-like subunits consist of $3\{M_3O_{13}\}$ triads, where M=Mo or V. These triads are connected to each other *via* corner-sharing MO_6 octahedra, whilst one capping VO_5 square pyramidal is attached to the square "window" of the M_6Se anion. Twelve Vanadium metal centers are in the oxidation state V and four Vanadium cations are in the oxidation state VI. Finally, one μ_9-SeO_3 bridging anion occupies the central part of the units, whilst three (η, μ)-SeO_3 bridging anions are on the top of each moiety. The two moieties are connected with each other *via* two edge-

sharing MoO_6 octahedra and *via* Na cations. Notably, the presence of the K^+ ions has been proven crucial for the formation of the compound, as these cations connect the $\{Mo_6V_{16}Se_8O_{79}\}$ with each other. The resulted packing configuration (view from c axis) reveals crown cavities with size of about 10 Å (Figure 3.18 and 3.19). These cavities, as it happens in the case of the crown ether structures, have ion recognition properties and they can function as sensors for various applications. Each of the ten MO_6 octahedra exhibits one terminal oxo group, with the M=O bond lengths at a range of 1.586(2) Å-1.638 (2) Å, four μ_2-O^{2-} and one μ_3-O^{2-} bridges with M-O bonds at a range of 1.758(7) Å-1.981(2) Å and 2.024(3)- 2.403(2) Å, respectively. Each of the V atoms in the VO_5 square pyramids are coordinated by one terminal oxo group with the V=O bond length at 1.609(7) Å and four μ_3-O^{2-} moieties, with the V-O bonds at the range of 1640(2)-1.935(2) Å. The two MoO_6 octahedra exhibit two terminal oxo groups with the Mo=O bond lengths at the range of 1.680(2) Å-1.700(3) Å, two μ-O^{2-} and two μ_2-O^{2-} bridges with Mo-O bonds at the range of 1.844(2) Å-1.952(3) Å and 1.981(2)-2.359(2) Å, respectively. The three Se atoms that are located on the top of the basket exhibit pyramidal geometry and the Se-O bond lengths are at range of 1.642(2) Å-1.784(2) Å. Finally, the Te atoms in the μ_6-SeO_3^{2-} are in the oxidation state IV with three Se-O bond lengths at the range of 1.693(2) Å-1.727(2) Å.

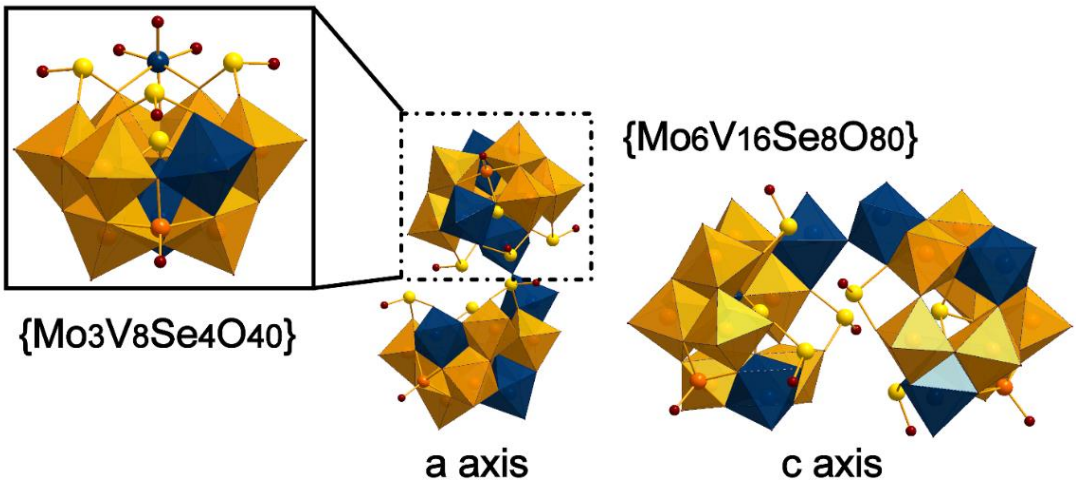

Figure 3.18 Polyhedral representation of the anion $[Mo_6V_{16}Se_8O_{79}]^{14-}$ of compound **8** along the a and c axis, highlighting the $\{Mo_3V_8Se_4O_{40}\}$ units templating by four selenite anions. The vanadium metal centre of the square pyramidal is in ball and stick representation. Colour code: Mo: dark teal polydedra and spheres; V: orange polyhedral and spheres; Se: yellow spheres; O: red spheres. The K and Na counter-ions have been omitted for clarity.

It is important to mention that the two Se-based compounds **7** and **8,** could be isolated in a pH range of 5-6 and by the sequential addition of the reaction reagents as mentioned above. A reaction mixture with pH greater than 6 or less than 5 or any change in the order of the reagents could not result in the desirable products. It has been observed that any change in the variables mentioned above could led to the precipitation of organic salts as colourless crystals or to the isolation of the known S-shaped $\{Mo_{12}V_{10}Se_8\}$ cluster (Figure 3.20) as red needles.

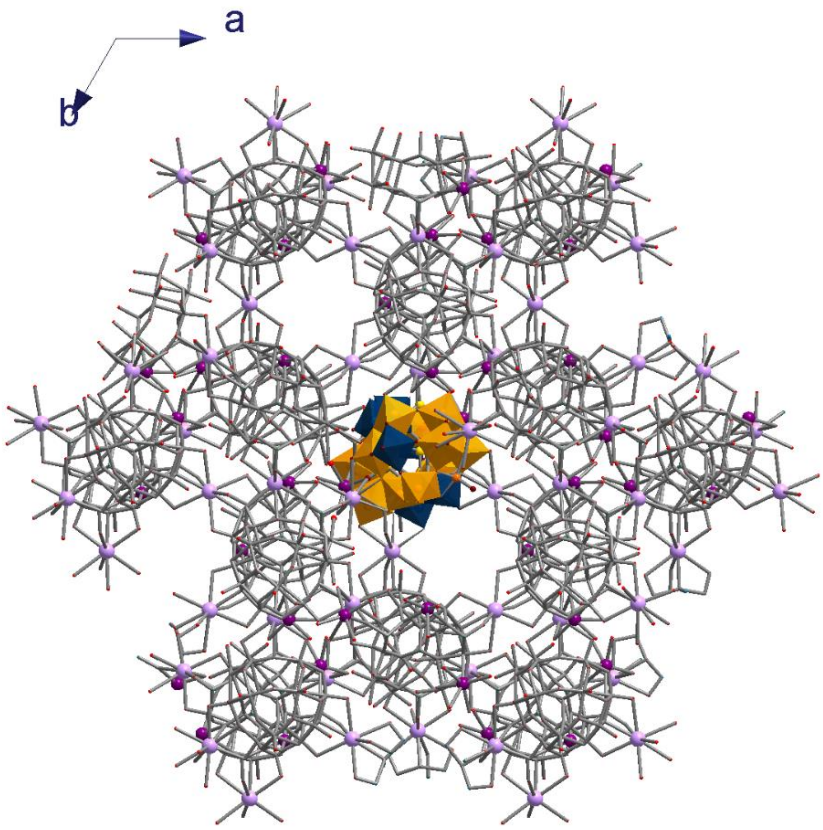

Figure 3.19 Wires and ball representation of the packing mode for $\{Mo_6V_{16}Se_8\}$ in in *P3₂21* along c axis, highlighting with polyhedral representation the position of the cluster. Na (violet) cations connect the two $\{Mo_3V_8Se_4\}$ subunits, while K (light pink) cations connect the clusters forming cavities with "crown ether" configuration.

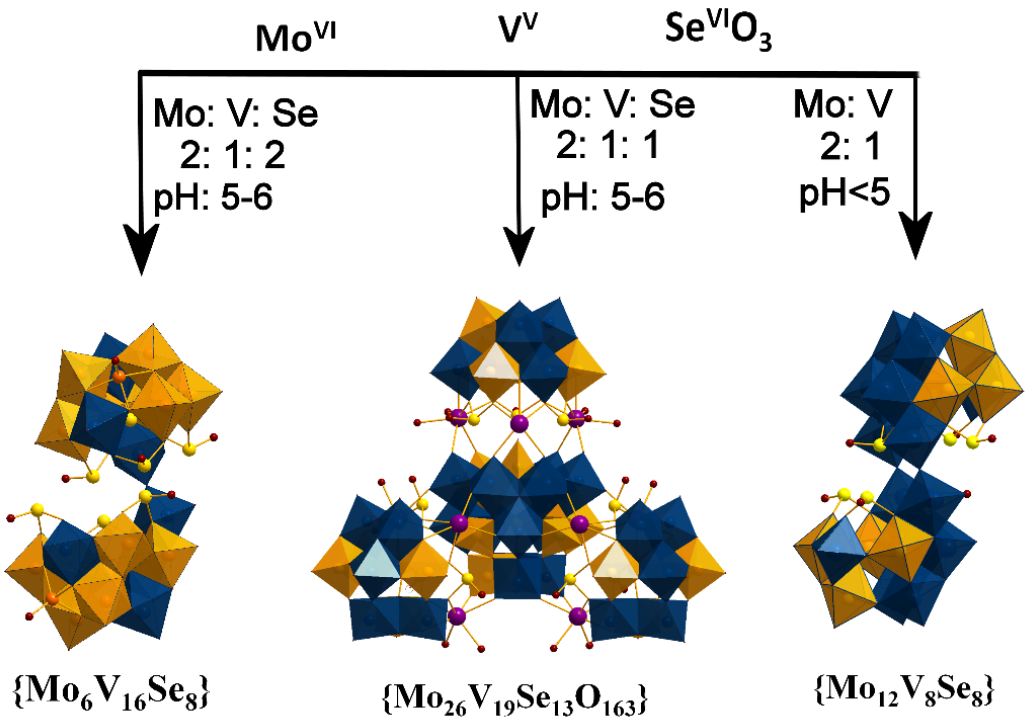

Figure 3.20 Synthetic procedure for the isolation of the three selenite-based mixed-metal polyoxometalates **7**, **8** and the S-shaped cluster (from left to right). The effect of the pH and the {Mo:V} ratios are highlighted. Colour code: Mo: dark teal polydedra; V: orange polyhedral and spheres; Se: yellow spheres.

3.4 Synthesis of the elusive δ-Keggin isomer

In an effort to synthesize new mixed-metal POM compounds, we managed to isolate and characterize the first members of the δ-Keggin polyoxometalate isomer, compounds **9** and **10**, with the general formula: $TEAH_pNa_q[H_2M_{12}(XO_4)O_{33}(TEA)]\cdot rH_2O$ where p, q, r = [2,3,8] for **9** and [4,1,4] for **10** (TEAH: $C_6H_{16}NO_3$; M: $W^{VI}_4V^V_8$; X: V^V; TEA: $C_6H_{13}NO_3$: deprotonated triethanolamine), respectively. Crystallographic studies revealed that **9** crystallizes in the monoclinic system in $P2_1/c$ space group and the anion can be formulated as $[H_2W_4V_8(VO_4)O_{33}(C_6H_{13}NO_3)]^{5-}$ (**9a**). The anions exhibit a δ-Keggin structural motif and is derived from the α-Keggin isomer by 60° rotation of the three $\{M_3O_{13}\}$ subunits that are directly bonded to the top TEA tripodal ligand and edge-shared to each other (Figure 3.21). The fourth $\{M_3O_{13}\}$ subunit remains at its original position and is located at the bottom cap opposite to the coordinated TEA ligand coinciding a C_3 axis and is corner-shared with the three neighbouring $\{M_3O_{13}\}$ subunits. Structure refinements revealed that the central XO_4 template and six metal centres that are directly bonded to the TEA tripodal ligand are fully occupied by vanadium atoms whilst the remaining bottom $\{M_3O_{13}\}$ and the three belt sites

are occupied by four tungsten and two vanadium atoms disordered over the six positions. Crystallographic studies and BVS [181] calculations have been carried out to establish the oxidation states of the metal centres. The tungsten atoms are found to be in the oxidation state VI (BVS_{av}=6.02) while all the vanadium atoms found to be in the oxidation state V (BVS_{av}=5.04). The 'capping' triethanolamine ligand adopts a $\eta^2:\eta^2:\mu^3$ coordination mode, completes the octahedral coordination sphere of the upper "cap" vanadium centres and appears to stabilize the δ-Keggin structure according to experimental evidence obtained from our control experiments (see experimental discussion below). The vanadium atom in the VO_4 tetrahedron is coordinated to four μ_3-O^{2-} bridges, with the V–O bonds within the range of 1.679(9)-1.752(1) Å. Each V atom in the VO_6 octahedra exhibits one terminal oxo group, with a V=O bond length of 1.585(6)-1.690(6) Å, four μ-O^{2-} and one μ_4-O^{2-} bridges with V–O bonds spanning the range 1.785(5)-2.050(5) Å and 2.269(5)-2.372(5) Å, respectively. The remaining W atoms in the WO_6 octahedra support one terminal oxo group, with the W=O bond length in the range of 1.630(5)-1.679(6) Å, four μ-O^{2-} and one μ_4-O^{2-} bridges with W-O bond lengths in the range of 1.861(5)-1.938(5) Å and 2.305(5)-2.382(5) Å, respectively.

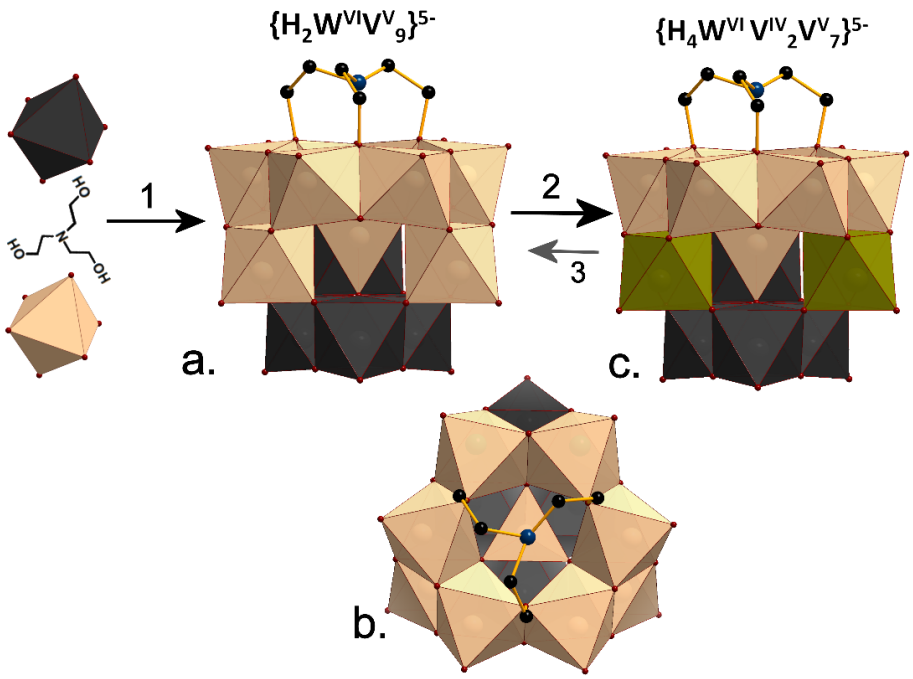

Figure 3.21 Polyhedral representations of the structure of the δ Keggin found in compounds **9** and **10**. (a) and (c) the positions of the V^V (cream), W^{VI} (dark gray) centres and the V^{IV} (green) produced upon reduction resulting on irradiation. The coordinated tripodal ligand TEA is shown. (b) The structure as it is shown from the top view. Counterions have been omitted for clarity. Process 1 is the assembly of the cluster; process 2 when the cluster is irradiated; 3 when the cluster is left to stand in the dark. Colour scheme: W^{VI}: blue, V^V: green, V^{IV}: dark yellow, C: black, N: blue;

Compound **9** was prepared under "one-pot" conditions from a warm aqueous solution of $NaVO_3$, $Na_2WO_4{\cdot}2H_2O$, TEA·HCl and NaCl, where $Na_2S_2O_4$ was subsequently added, followed by the adjustment of the pH of the reaction mixture with HCl. Yellow needles of suitable quality for X-Ray diffraction analysis were isolated 2-3 weeks later, but both the purity and crystallisation time improved to under 5 days when excess TEA·HCl was used (see experimental section). However, structural analysis revealed an isostructural species to compound **9** with the formula $(C_6H_{16}NO_3)_4Na[H_2W^{VI}_4V^{V}_8(V^{V}O_4)O_{33}(C_6H_{13}NO_3)]{\cdot}4H_2O$ **10**. The structure crystallises in space group $P2_1/m$ with a crystallographic mirror plane passing through the centre of the cluster with the main difference being the $TEAH^+$: Na^+ ratio. In order to determine the role and the impact of the reducing agent, $Na_2S_2O_4$, on the formation of the final product, the same experimental procedure was carried out in the absence of $Na_2S_2O_4$. Orange needles of **9** were isolated from an orange solution along with unidentified green precipitate after one week, indicating the presence of the $Na_2S_2O_4$ is important for the purity and increased yield of the isolated product. It is worth noting that the crystallization time can also be reduced from 2-3 weeks to 1 week. Also, attempts to synthesize the δ-Keggin isomer in the absence of the TEAH ions have been unsuccessful, suggesting the crucial role of the tripodal ligand in the formation and stabilization of the final product (see figure 8.3-Appendices). When **9** and **10** were left illuminated under a 150 W Xe lamp, the crystals underwent a colour change from yellow to green; observed at room temperature after 2 and 12 hours, respectively, under these conditions a single-crystal-to-single-crystal transformation occurs, whereby compounds **9** and **10** become dark green to give compounds **9'** and **10'** (Figures 3.22 and 3.23). X-ray studies showed that the structure of compound **9'** and **10'** are isostractural to **9** and **10**, but a BVS analysis indicates the δ-Keggin shell is two electrons reduced and two additional oxygen atoms are now protonated (the source of the electrons appears to be the TEA and the water content in the crystal lattice of **9** and **10**) while the M-O (M = W, V) distances of compounds **9'** and **10'** have changed, as expected for the reduced species (see Table 8.4 of the Appendices). If the compounds are left in air they slowly return back to the fully oxidized state (yellow coloured crystals) if kept under dark. In the presence of atmospheric oxygen **9'** converted back to **9** (8-9 months) and **10'** to **10** (4 months), respectively. Additionally, X-ray diffraction data of the single crystal samples were collected before and after the irradiation, confirming further the structural integrity and composition of the cluster [21]. Further studies have been carried out in order to unambiguously identify the reduction state of the cluster. By conducting ^1H NMR studies exploiting the Evans Method [187] (see Figures 8.4 and 8.5 of the Appendices) it was possible to deduce that the compounds have been reduced by 2 electrons (μ_{eff} = 2.4 μB and S=1.6). A second peak could be observed after the ^1H NMR measurements of the reduced compound

(Figure 8.5 of the Appendices). The shift difference (compared to the spectrum of the oxidized compound, Figure 8.4) was used for the calculation of μ_{eff} and consequently of the number of electrons. The small discrepancy between the theoretical numbers and the calculation should probably be due to experimental errors. The calculations were performed according to the literature. [187] Also, in compounds **9'** and **10'**, V4 and V5 are likely to be in oxidation state V^{4+}, BVS_{av}=4.3 and 4.2, respectively (see Figure 3.22).

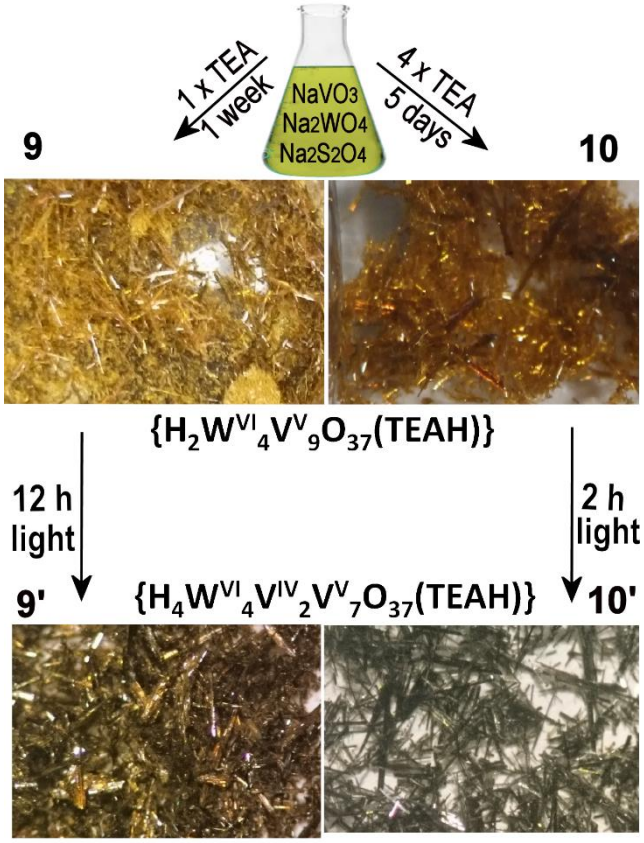

Figure 3.22 Colour change of compounds **9** and **10** during time and under Xe UV-vis lamp along with the structures **9-10** and **9'-10'**. The compound with more $TEAH^+$ ions needs notably less time to switch colour than the one with less amount of ions.

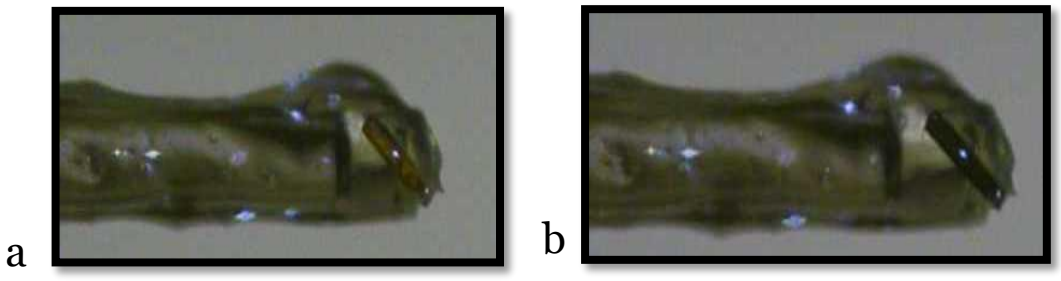

Figure 3.23 Real-time monitoring of the colour change. A crystal of compound **10** was exposed in UV-vis light. a: before and b: after the exposure. The colour change was clearly observed after two hours of light exposure. X-ray diffraction analysis confirmed the integrity of the architecture upon irradiation.

The composition of **9** was verified further using high resolution electrospray ionization mass spectrometry (ESI-MS). The studies were performed by dissolving a small amount (~0.010g) of compound **9** in a mixture of H_2O/CH_3CN (3:1) solvents. At the *m/z* range of 1364-2110, the observed distribution envelopes could be assigned to the anionic fragment of compound **9**, with the formula $[W_4V^{V}_5V^{IV}_4O_{37}H_9(C_6H_{13}NO_3)(C_6H_{16}NO_3)(H_2O])]^{1-}$ or even the anionic dimer and trimer of **9** species, formulated as $\{[W_4V_5{}^{V}V_4{}^{IV}O_{37}H_9(C_6H_{13}NO_3)]_2(C_6H_{16}NO_3)(H_2O)_2\}^{3-}$ and $\{[W_4V^{V}_6V^{IV}_3O_{37}H_7(C_6H_{13}NO_3)]_3Na_4(C_6H_{16}NO_3)(H_2O)_9\}^{4-}$, respectively. Moreover, the peak located at *m/z* = 969.2 corresponds to the fragment $\{[V^{V}_5V_2{}^{IV}O_{25}H_7Na_5(C_6H_{13}NO_3)](C_6H_{16}NO_3)_5(H_2O)_9\}^{2-}$, whilst the peak centred at *m/z* = 835.7 could be assigned to the cluster fragment $\{[V^{V}_4V^{IV}_3O_{25}H_7Na_8(C_6H_{13}NO_3)](C_6H_{16}NO_3)_3(H_2O)_7\}^{2-}$. Finally, peaks in the region *m/*z 1054-1209, correspond to the $\{[WV^{V}V^{IV}_6O_{25}H_8Na(C_6H_{13}NO_3)](C_6H_{16}NO_3)_6(H_2O)_5\}^{2-}$ and $\{[WV^{V}V^{IV}_7O_{25}H_{11}(C_6H_{13}NO_3)Na](H_2O)_2\}^{1-}$ species (Figure 3.24 and Table 7).

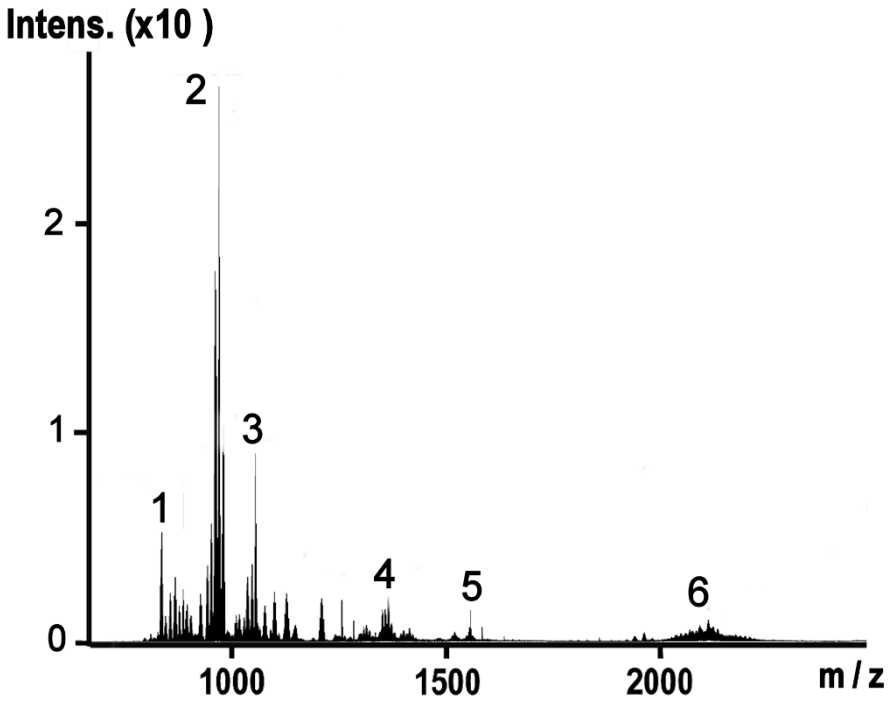

Figure 3.24 ESI mass spectrum in negative-mode of **9a** in the m/z range of 800-2500 showing the major peaks of charged fragments.

Table 7 Selected *m/z* range of the ESI-MS of **9a**

Peaks	m/z	Cluster shell	Counter ions	charge
1	835.7	$\{M_6O_{18}(XO_4)H_7(TEA)\}$	$Na_8(TEAH)_3$	2-
2	969.2	$\{M_6O_{21}(XO_4)H_7(TEA)\}$	$Na_5(TEAH)_5$	2-
3	1054.8	$\{M_7O_{21}(XO_4)H_8(TEA)\}$	$Na(TEAH)_6$	2-
4	1356.9	$\{M_{12}O_{33}(XO_4)H_9(TEA)\}_2$	(TEAH)	3-
5	1556.2	$\{M_{12}O_{33}(XO_4)H_7(TEA)\}_3$	$Na_4(TEAH)$	4-
6	2110.7	$\{M_{12}O_{33}(XO_4)H_9(TEA)\}$	(TEAH)	1-

To understand the electronic structure of the clusters we performed a density functional theory (DFT) analysis to elucidate the most favourable positions of two vanadium (V^{IV}) atoms in the geometry, since they found to be crystallographically disordered over 6 positions. Figure 3.25 shows the relative energies with respect to the most stable positional isomer for the parent compound, $[W^{VI}_4V^{V}_8(V^{V}O_4)\ O_{33}(C_6H_{13}NO_3)]^{7-}$ and the two electron reduced species, $[W^{VI}_2V^{IV}_2V^{V}_6(V^{V}O_4)O_{33}(C_6H_{13}NO_3)]^{9-}$. Note that we have omitted the protons in the $\{M_{12}\}$ cage, therefore the negative charge of the cluster increased accordingly. For the parent compound the relatively most stable geometries are δK-1, with one vanadium in the bottom cap and the second one in the belt, and δK-2 with two vanadium atoms in the bottom cap (where 1= compound **9** and 2= compound **10**). Nevertheless, the small energy difference (3.5 kcal mol^{-1}) with respect to geometries δK-3 and 4 means that these are both plausible since the average method error is around 1–2 kcal mol^{-1} (<5 %). [188] Fortunately, a theoretical analysis of the two electron reduced species gives a much more definitive energy difference within isomers. In this case, the most stable isomer is δK-3, being 4 kcal mol^{-1} relatively more favourable compared δK-1, 2 and 4. In δK-3 both V(IV) atoms are in the belt region and three, of the four tungsten atoms, form a triad $[M_3O_{13}]$. Previous knowledge of the mechanism of formation of POM clusters has shown that triads can be considered as structural building blocks. Therefore our preliminary results allows us to propose that the ideal isomer is δK-3, however further theoretical and experimental analysis will be necessary to validate this hypothesis (Figure 3.25).

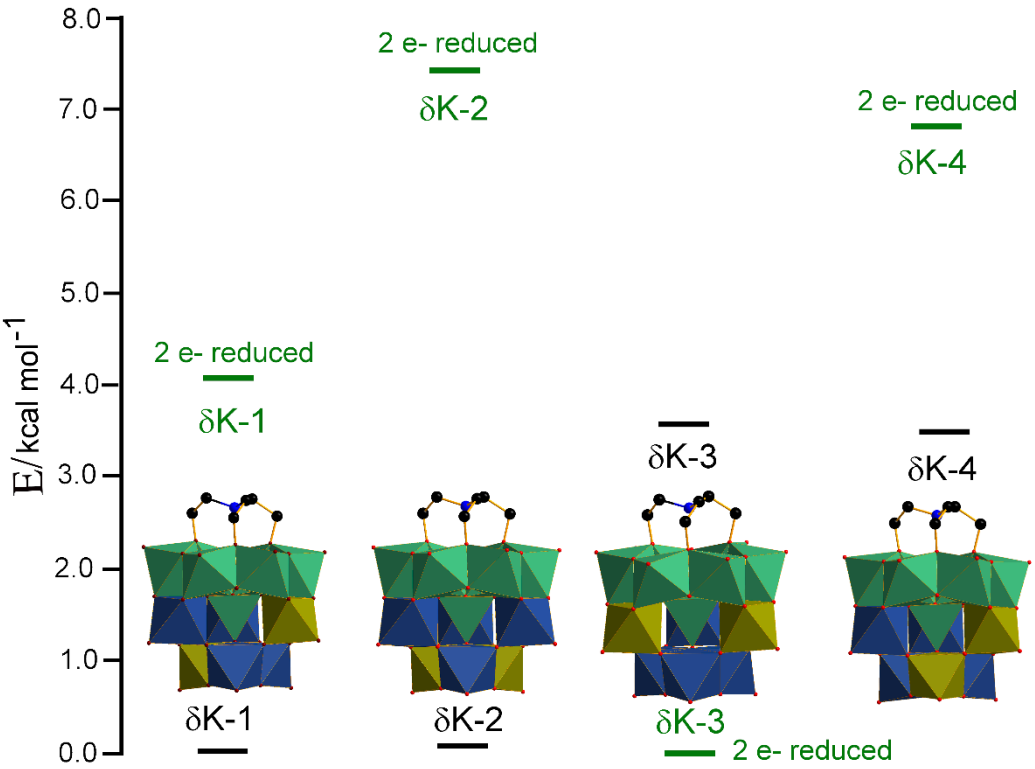

Figure 3.25 Theoretical relative energies with respect to the most stable positional isomer (δK-1 to δK-4), with the formula $[W^{VI}_4V^{V}_8(V^{V}O_4)O_{33}(C_6H_{13}NO_3)]^{7-}$, black lines and its two electron reduced analogues, $[W^{VI}_4V_2{}^{IV}V^{V}_6(V^{V}O_4)O_{33}(C_6H_{13}NO_3)]^{9-}$ green lines. These results helped us to determine the more favourable positions of the two V^{IV} atoms. W: Indigo, V^{V}: green, V^{IV}: dark green, C: black, N: blue; Counter ions have been omitted for clarity.

3.5 Redox oscillation

The redox driven oscillations utilizing molybdenum based capsules, based on a previous work reported by our group, [180] was further explored in order understand the mechanism of the oscillations observed. In particular, this work describes a redox-driven oscillatory template exchange that causes the exchange of the two XO_4^{3-} heteroatom guests (X = P^{V} and V^{V}, respectively) contained within the $\{M_{18}O_{54}(XO_4)_2\}^{6-}$ capsule for two complete oscillation cycles (P2 → V2 → P2 → V2 → P2), Figure 3.26. The reaction mixture has been carried out according to the procedure reported by Miras [180] *et al.* The sequential addition of $(NH_4)_6P_2Mo_{18}O_{62}{\cdot}12H_2O$, triethanolamine hydrochloride (TEA·HCl) and NH_4VO_3 in 50 ml of warm water, resulted to a yellow solution. The pH of the solution was adjusted to 1 by addition of concentrated HCl (37%). After the adjustment of the pH the solution was heated at 90 ^{0}C. Additional TEAH (0.5 g) were added to reaction mixture after

around 6-8 hours. It is worth noting that the oscillations can be restarted by "resetting" the process, allowing further complete cycles. The "resetting" process involves pH adjustment at the value of 8 by addition of concentrated NH_3. The reaction mixture was then kept stable for 5 minutes at pH 8, before the pH was adjusted to 1 again by addition of concentrated HCl. Finally, 0.5 g of triethanolamine hydrochloride were added upon vigorous stirring. The oscillating process was followed by UV-vis and the experimental procedure was repeated several times (Figure 3.28). After about 22 hours of collecting data, the oscillatory system has been restarted by addition of concentrated ammonia, concentrated hydrochloric acid and reducing agent (see experimental data for details). A UV-vis probe was used to follow the yellow ↔ green (low ↔ high absorbance at 650 nm) oscillation associated with the switch between the P_2 and V_2 clusters. It is noticeable that the system oscillates for more than four cycles, revealing a redox-powered oscillating host-guest system.

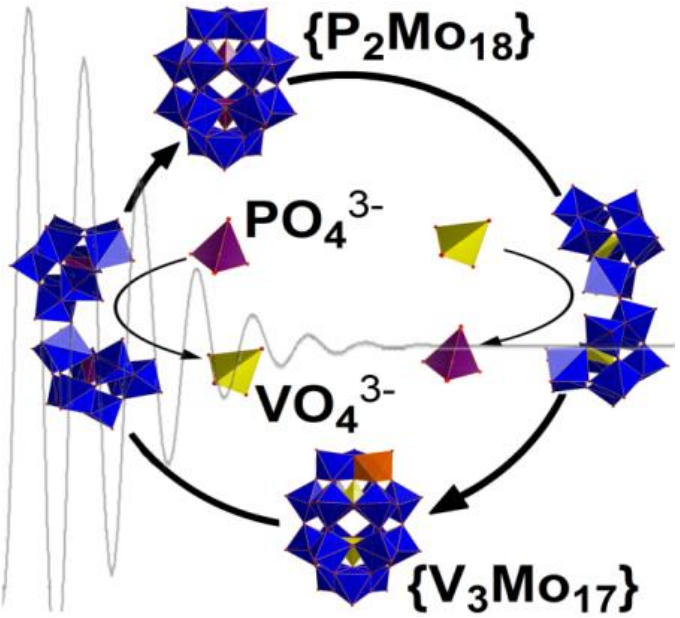

Figure 3.26 Description of the redox-driven guest exchange reaction. Colour scheme: PO_4^{3-} templated cluster, grey; VO_4^{3-} templated cluster, blue; PO_4^{3-} purple; VO_4^{3-} template, yellow; reduced V, orange. [180]

The oscillatory guest exchange process was also monitoring in real time utilizing ESI-MS. Samples of the reaction mixture were collected at specific time intervals. The studies were performed at the *m/z* range of 1450-1900 in CH_3CN solvent and aliquots were treated by ion exchange (precipitated as TBA salt). At the beginning of the reaction, as it was expected, only $\{P_2Mo_{18}\}$ species formulated as $\{P_2Mo_{18}O_{62}(TBA)_4\}^{2-}$ were observed. At the *m/z* range of around 1590, the observed envelopes could be assigned to the anionic fragment of the

{V_3Mo_{18}} species, with the formula [$V^{IV}Mo^{VI}_{13}Mo^{V}_4(VO_4)_2O_{54}(TBA)_7(TEA)_2]^{3-}$ after three hours. A full oscillating cycle can be observed the first 8-10 hours of the reaction, as very small peaks for the phosphate-based Dawson compound could be detected. At this time {V_2Mo_{18}} species with the formula [$Mo^{VI}_{14}Mo^{V}_4(VO_4)_2O_{54}(TBA)_7(H_2O)]^{3-}$ could also be assigned at the *m/z* range of around 1515, the along with the {V_3Mo_{17}} species. Finally, a second cycle of the oscillatory process starts after 15 hours, where all three species appear in the solution (Figure 3.27).

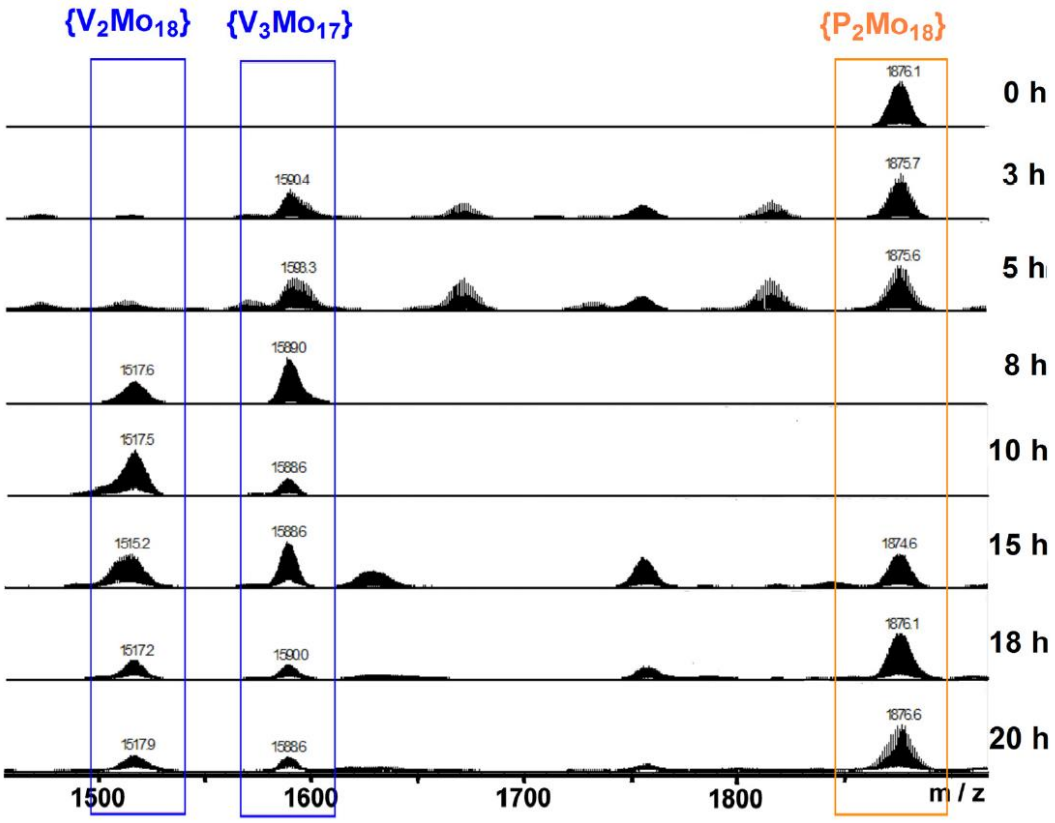

Figure 3.27 ESI-MS spectra of the {P_2Mo_{18}}/{V_2Mo_{18}}/{V_3Mo_{17}} reaction mixture at different time intervals in negative mode. [$Mo^{VI}_{14}Mo^{V}_4(VO_4)_2O_{54}(TBA)_7(H_2O)]^{3-}$, {$V_2Mo_{18}$} /[$V^{IV}Mo^{VI}_{13}Mo^{V}_4(VO_4)_2O_{54}(TBA)_7(TEA)_2]^{3-}$, {V_3Mo_{17}} / {$P_2Mo_{18}O_{62}(TBA)_4$}$^{2-}$, {P_2Mo_{18}}at m/z = 1511.96, 1591.04 and 1875.53. Note that the intensity is so high for the V_2 and V_3 peaks compared to any residual P_2 for the 8 and 10 hrs the baseline shows nothing at this zoom although there are some very small residual peaks.

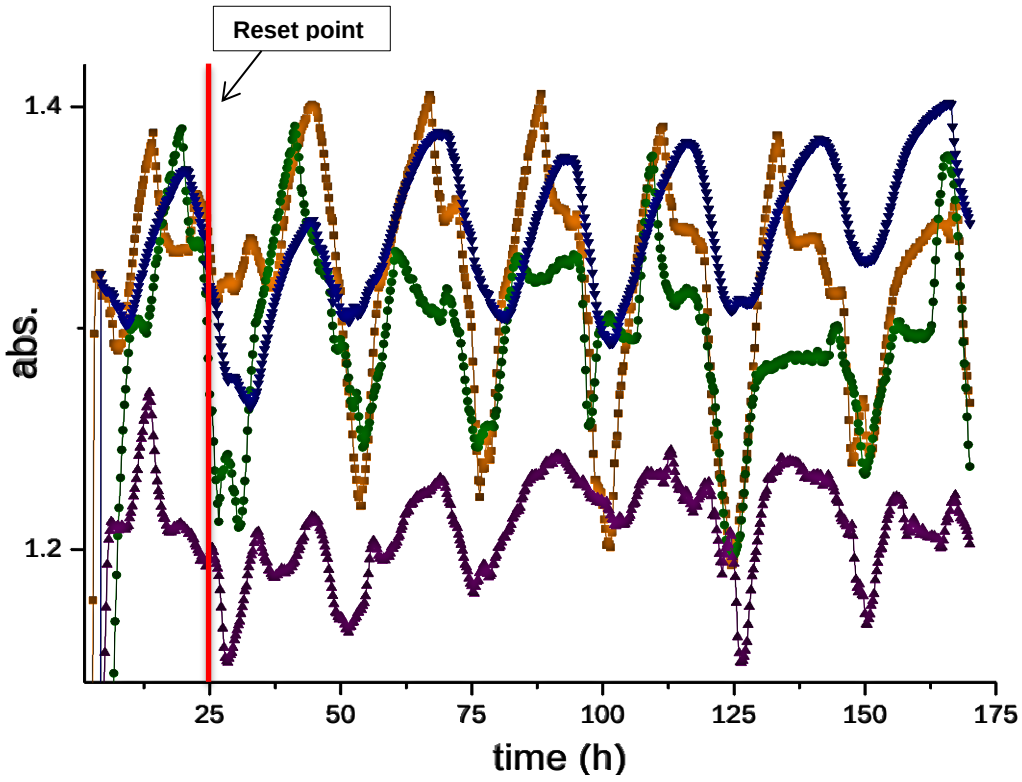

Figure 3.28 Time-dependent UV−vis monitoring at 170 hours, showing a periodicity of the oscillations. Each of the spectrum represents different experiments. The red line represents the reset point of the reaction system (24 hours after the beginning of the reaction).

The repeated UV-vis measurements (Figure 3.28) revealed that this exchange of the heteroanions follows a similar pattern, however we cannot be confident about the periodicity of the system. The number of cycles as well as the period of each cycle were calculated (Table 8). As it could be observed, each UV-vis measurement reveals a different number of cycles with different time periods at range of 9-25 hours, which is not allow us to safely conclude about the periodicity of the oscillating system.

Table 8 Number of cycles and the period of each cycle observed during 170 h of UV-vis studies.

Oscillations	N_o of cycles	Period of each cycle (hrs)
orange	10	10.5/9.5/9.5/12/22/21/23/22.5/16.25/17.5
green	8	21.5/20/23/17/16/27.5/12/9.25
purple	9	11/15.75/11/24.5/22/21.5/21/21.5/11.5
blue	7	16.75/24/25/24.25/23.5/25.24.5

Furthermore, we tried to find out how long could the oscillations last and finally the expiration time of the oscillatory system. For this purpose, the reaction mixture was followed by UV-vis for more than one week (170 h). Surprisingly, the system continued oscillating for more than 500 hours, although the intensity of the peaks seems to decrease with the time (3 weeks, Figure 3.29). We believe that the huge amount of TEA·HCl (12 times more than the amount of NH_4VO_3, helps the oscillations and prevents the damage of the system. At this point, a series of control experimental procedures were followed in order to investigate the reasons that the system was still oscillating and preventing the damage of the oscillations. The total amount of TEA·HCl added in the reaction was significantly reduced, showing a totally different UV-vis spectrum. In the same way, three more reactions in the presence of N_2, without any addition of TEA·HCl and at room temperature were carried out, revealing UV-vis spectra with no oscillations observed (Figure 3.31). These four experimental procedures indicated the significant role of the O_2 (oxidizing agent), the organic compound (reducing agent) and the heating (helps the reaction procedure) in the reaction system, respectively. It is also worth mentioning that in all these alternative experimental procedures, the first two oscillations (before the reset point, figure 3.30, orange circle) were not observed as they were in a normal reaction procedure (Figure 3.28, red line), showing the sensitivity of the system.

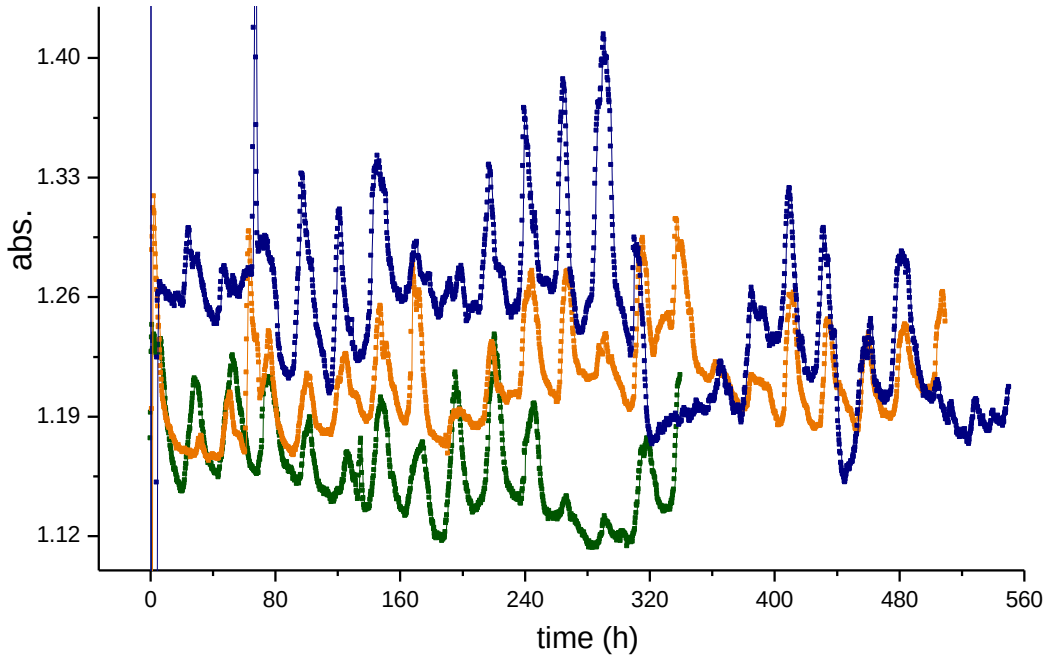

Figure 3.29 Time-dependent UV−vis monitoring at 650 nm for 340 hr (green), 510 hr (orange) and 551 hours (blue). It can be observed that the system is oscillating after three weeks of continuous measurements.

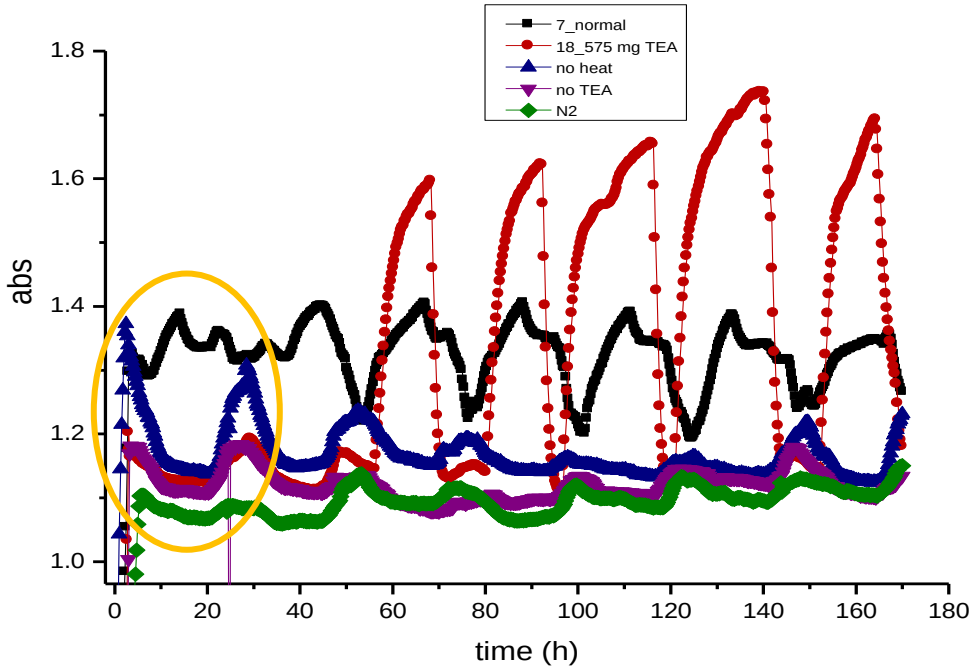

Figure 3.30 Time-dependent UV−vis monitoring at 650 nm for 170 hours. In black line the normal experimental procedure showing the oscillations. In red line the reaction with less amount of TEA·HCl, showing different behaviour of the system. The rest of the spectra follow the same pattern showing no oscillations. The orange circle is indicating the two oscillations occurring before the reset of the experiment.

According to the current results (Figure 3.28), we could agree that this phenomenon of the successive exchange of the heteroanions follows a similar pattern. Even if the experimental procedure has been repeated multiple times, we have not been able to arrive at a safe conclusion regarding this oscillating reaction system.

4. Conclusions

Within the scope of this work we explored alternative routes to control the self-assembly of new mixed-metal polyoxometalate clusters. We have also demonstrated that the incorporation of non-traditional heteroanions within mixed-valence molybdovanadate cages results in the isolation of a new family of materials. It has been shown that molybdenum and vanadium metal centres can exhibit a wide variety of coordination modes and geometries, while the pyramidal heteroanions (HPO_3^{2-}, SeO_3^{2-}, $SO_3^{2-}$and TeO_3^{2-}), which incorporate a lone pair of electrons, can act as bridging ligands exhibiting multiple coordination modes and direct the self-assembly process. In contrast to the rigid tetrahedral heteroatoms, the pyramidal heteroatoms containing a lone pair of electrons could direct the assembly process in a different way, prevent the aggregation of POM fragments from forming closed Keggin clusters and promote the assembly of novel building blocks and consequently new clusters. The combination of molybdenum and vanadium metal centres with pyramidal heteroanions can therefore lead to the formation of novel inorganic frameworks considerably different from the analogous structures templated by tetrahedral heteroanions. The control of the pH and cation involved in the formation mechanism, as well as the ratio of the starting materials, have been crucial to the successful isolation of such material. In this work, the study of the interaction of the pyramidal anions on the self-assembly of POMs indicates that the atomic radius of the heteroatom could not affect the final archetype. Specifically, the careful selection of the experimental procedures resulted to the isolation of the isostructural clusters incorporating different pyramidal heteroatoms.

The electronic effect taking place on the cage of the egg-shaped structure was studied by conducting CV measurements. The measurements revealed that the oxidation peak of the compounds has been shifted proportional to the electronic density of the heteroanions, meaning the greater the electronic density the easier the compound is being oxidized. Thus, as it is expected, the Te-based molybdovanadate compound has been oxidized (first oxidation of V^{IV} metal centres) more quickly that the other compounds. The Se-based compound follows, quicker that the S-based polyoxometalate and the oxidation peak of the compound consists of the heteroatom with less electronic density, namely HPO_3^{2-}, was finally observed. A clear shift to the left in the oxidation peak of each compound can be observed during the first oxidation. However, this phenomenon could not be clearly observed during the second oxidation, due to the electron existence in the cell that is more influential in the redox process that the electronic density of the heteroatom in each of the compounds.

We also introduced the use of the pyramidal HPO_3^{2-} heteroanion within the molybdovanadate system, which has led to the isolation of three compounds, namely $[Mo^{VI}_{11}V^{V}_{5}V^{IV}_{2}O_{52}(HPO_3)(CH_3OH)]^{7-}$ **1**, $[Mo_{12}O_{30}(HPO_3)_8]^{4-}$ **2** and $\{[Mo_6O_{18}(HPO_3)(C_6H_{13}NO_3)]_2(PV_4Mo_8O_{40})\}^{15-}$ **3**. Compound **1** is related to the $M_{18}(XO_4)_2$ Wells-Dawson anion but exhibit different structural features as a consequence of the presence of the phosphite heteroatom with its lone pair of electrons, and the participation of molybdenum and vanadium metal centres with different oxidation states and coordination modes. This compound is isostructural to the sulfite- and selenite-based egg-shaped Dawson clusters, previously reported from our group. Compound **2** and **3** consist of a hexanuclear molybdenum-based compound and indicate the important role of the vanadium centres in the formation of the Keggin moiety in compound **3**.

In general, the use of phosphite ions in polyoxometalate chemistry could be the following: Phosphite ion could be characterized as a challenging heteroatom for polyoxometalates synthetic chemists. As can be observed by the literature reports, polyoxometalate compound with HPO_3^{2-} ions are limited and mainly hexanuclear ring compounds. In terms of the experimental conditions, most of the final products found to be common Keggin clusters incorporating the oxidized phosphate ion, PO_4^{3-}. Moreover, the careful addition of the phosphite reagents in the reaction mixture has been proved to be necessary in order to avoid the precipitation of vanadium oxides.

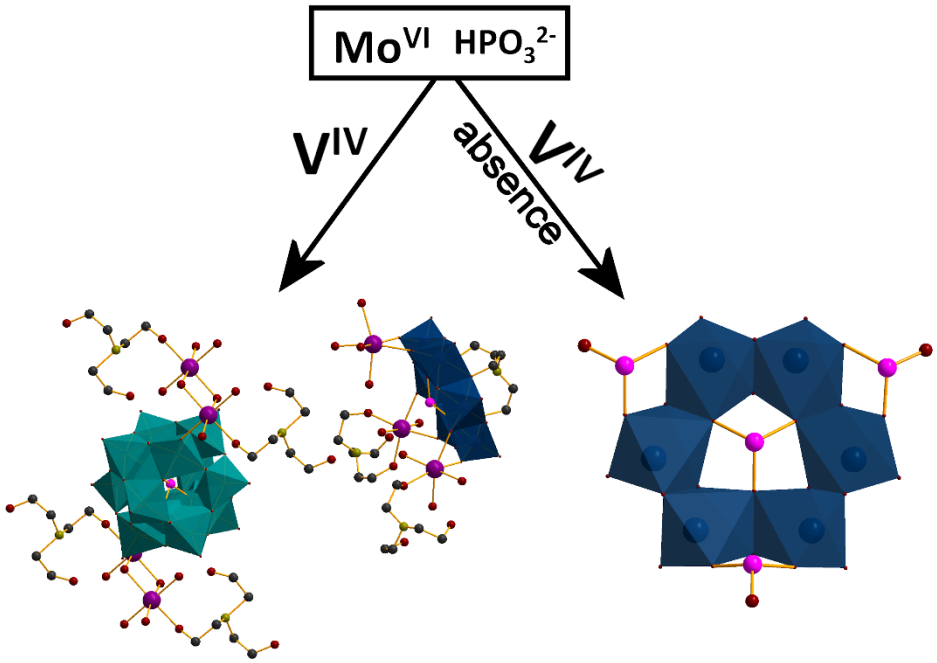

Figure 4.1 Schematic presentation of the formation of the phosphite-based compounds **2** and **3**.

The incorporation of the pyramidal TeO_3^{2-} heteroanion within the molybdovanadate system led to the isolation of three compounds, namely $[Mo^{VI}_{11}V^{V}_{5}V^{IV}_{2}O_{52}(TeO_3)]^{7-}$ **4**, $[Mo^{VI}_{12}V^{V}_{3}O_{39}(\mu_6\text{-}TeO_4)_3(\mu_6\text{-}TeO_3)_2]^{4-}$ **5** and the isostructural to the latter, compound **6**. The syntheses of these tellurite-based compounds was conducted by utilizing three different synthetic approaches. Compound **4**, which was synthesised under traditional "one-pot" conditions, is isostructural to compound **1**, with the phosphite heteroanion being replaced by one tellurite anion. With this compound **4** isolated, a family of 4 egg-shaped structures utilizing pyramidal heteroanions has been created. The Se- and S-based molybdovanadates have already been reported. We have managed to synthesize and characterize the P- and Te-based compounds, while Cyclic Voltammetry studies were performed for all four compounds. According to the experimental procedure followed, the use of reducing agents ($N_2H_4{\cdot}2HCl$, DMAH, etc.) played a significant role in the isolation of the final product. In the case of the compound **1** (phosphite-based), $VOSO_4$, was used, whilst the remaining 3 compounds were isolated by using reagents with fully oxidized vanadium metal centres. It is worth mentioning that in all compounds the vanadium ions are in both +4 and +5 oxidation states, even though the fully oxidized vanadium has been rapidly reduced in the presence of reducing agent, or the reduced vanadium centres have been used. Compound **1** could not be isolated in the absence of MeOH, while the purity of compound **4** is improved in the presence of solvent MeOH. Finally, the compounds can be crystallized from solutions with initial pH at the range of 2.5-5.

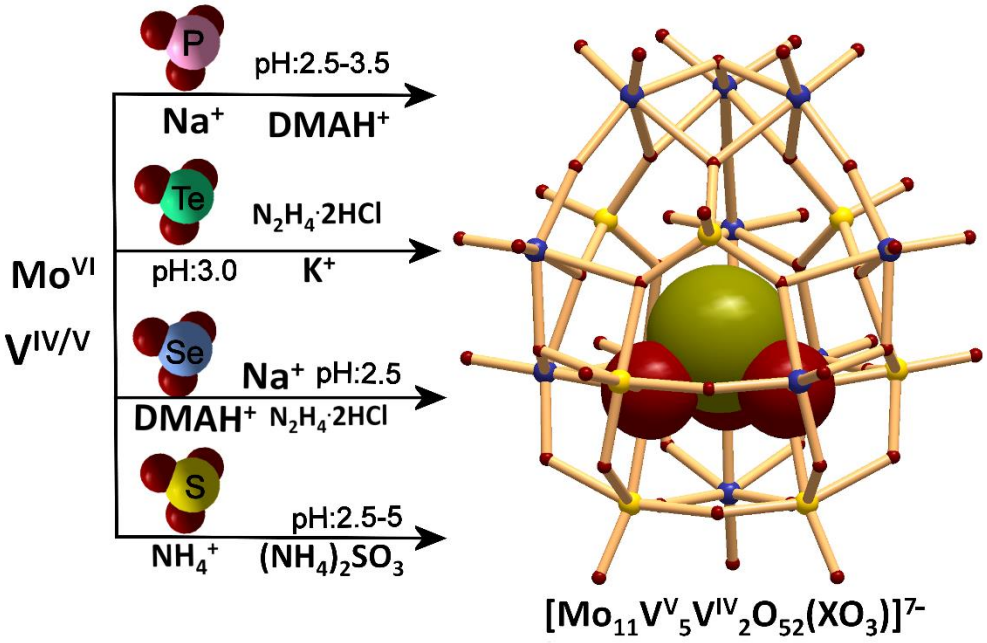

Figure 4.2 Schematic representation of the formation of the four egg-shaped Dawson structures.

Compounds **5** and **6** have been found to be isostructural and they have been isolated with two different techniques. Every $\{Mo_{12}V_3Te_5\}$ unit of compound **5** is connected to each other *via* potassium cations forming a 2D honeycomb arrangement of circular cavities with dimension of 1.7 nm. Each cavity is formed by 6 $\{Mo_{12}V_3Te_5\}$ clusters connected with 6 potassium cations. On the other hand, every $\{Mo_{12}V_5Te_5\}$ unit of compound **6** is connected to each other *via* sodium cations forming a pattern of rectangular cavities with dimensions of about (18 x 5) Å. Utilizing continuous flow processes, we were able to scan a variety of experimental variables at the same time and consequently to identify the most favourable conditions in order to achieve crystallization. Under these conditions, compound **5** was isolated displaying a honeycomb packing configuration, with the potassium ions to stabilize the final product, whilst the sodium ions do not participate in the formation of the structure. On the other hand, the harder conditions applied with the hydrothermal process resulted to the rearrangement of the cluster in the crystal lattice. Under these conditions the sodium cations directed the packing configuration in a different way than in the case of compound **5**. Even if the two compounds are isostructural (indicating the stability of this archetype), the symmetry of the structures has changed and the big circular cavities have been replaced by smaller rectangular cavities.

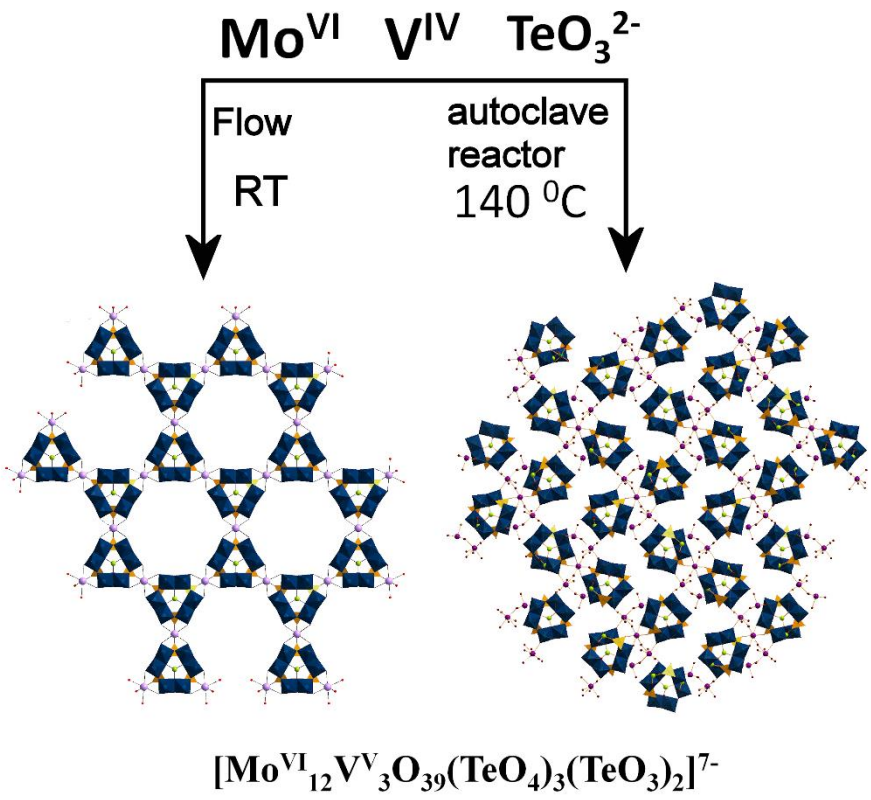

Figure 4.3 Representation of two different modes of compounds **5** (left) and **6** (right) in the crystal lattice.

We have also successfully isolated compounds **7** and **8** utilizing SeO_3^{2-} heteroanion within the molybdovanadate system, showing how a simple change in the ratio of the reaction reagents can lead to the isolation of new archetypes. Compound **7** has been found to consist of three $\{Mo_5V_4Se_4O_{36}\}$ moieties connected to an egg-like Dawson structure *via* potassium and sodium cations forming an isosceles triangle. Compound **8** consists of two $\{Mo_3V_8Se_4O_{40}\}$ moieties which are connected with each other *via* two edge-sharing MoO_6 octahedra and *via* Na cations. Notably, the presence of the K^+ ions has been proven crucial for the formation of the compound, as these cations connect the $\{Mo_6V_{16}Se_8O_{79}\}$ with each other. The resulted packing configuration reveals crown cavities with size of about 10 Å which as it happens in the case of the crown ether structures, have ion recognition properties and they can function as sensors for various applications. It is worth noting that this reaction system has a lot of space left for investigation and thus for discovery of novel clusters. The free selenite ions capping the Mo/V-basket like moieties also allow the use of compound **8** as a starting material.

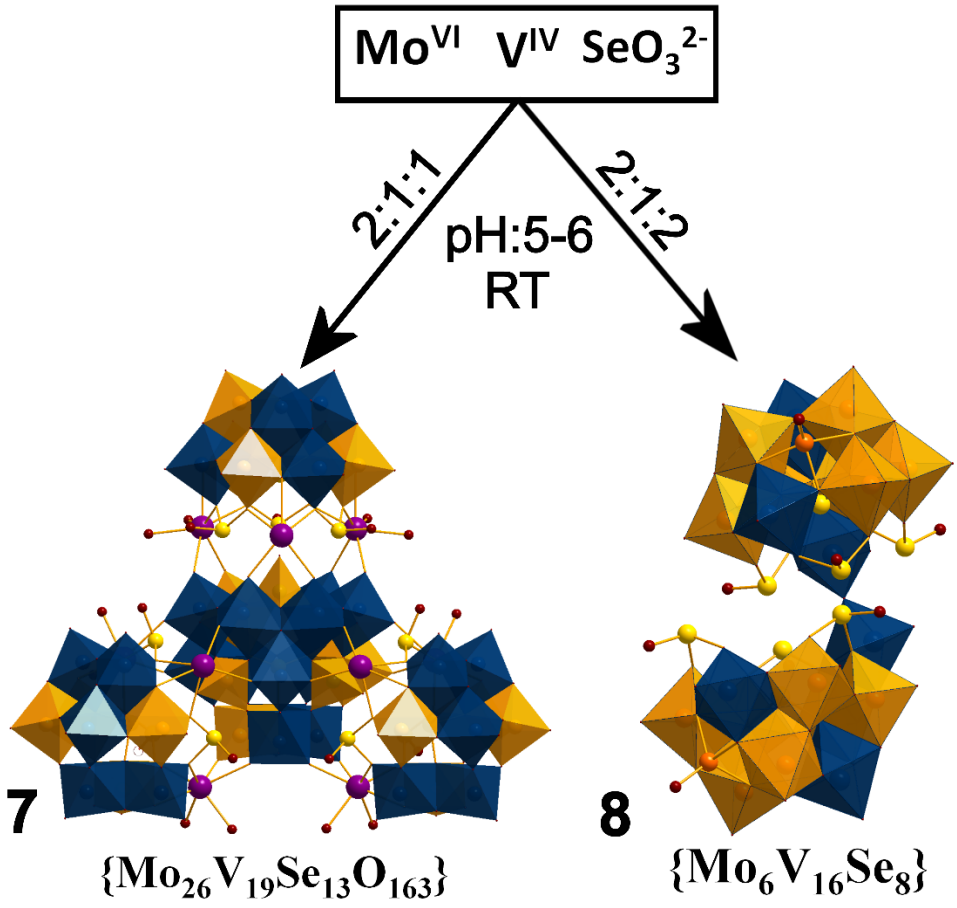

Figure 4.4 Schematic representation of the formation of the two Se-based molybdovanadate clusters.

The theoretically predicted, but experimentally elusive δ-isomer of the Keggin polyoxometalate cluster has been isolated, $[H_2W^{VI}{}_4V^V{}_8(V^VO_4)O_{33}(C_6H_{13}NO_3)]^{5-}$, indicating that the combination of mixed addenda with the "right" organic salt under simple reaction conditions can lead to the discovery of novel molecular structures. The crucial role of the tripodal organic ligand has been determined by performing control experiments. In the absence of the ligand, the classical α-Keggin isomer could only be isolated. Also, attempts to replace the TEAH compound with other organic ligands have so far been unsuccessful. The structural motif of the TEAH reagent has been proven to be the key to the formation of the isomer, as it locks and stabilizes the three rotated triads of the δ-Keggin structure. We have also demonstrated that the change of the molecular ratio of only one of the reagent can affect the properties of the final product. Interestingly, a redox-driven single-crystal-to-single-crystal transformation occurred when the compound was left illuminated under a Xe lamp, as the crystals underwent a colour change from yellow to green. The amount of the TEAH cation is proportional to the time needed for the colour change. The structure containing more cations, requires less time for the colour to change from yellow to green. It has also been observed that the green crystals return back to the fully oxidized state if kept dark. The crystals with less amount of TEAH require more time to return into the initial state. In contrast with the molybdenum and vanadium metal centres as starting materials, the combination of tungsten and vanadium metal centres with the pyramidal heteroanions was proved to be challenging. Under mild "one-pot" conditions, the combination of W and V reagents could lead to either colourless crystals of organic salts or the well-known α-Keggin isomer incorporating the conventional tetrahedral heteroanions. Future work will focus on investigating further the electronic properties as well as attempting to tune the variables and the effect of the isomerism that controls the solid state electron transfer processes in polyoxometalate systems.

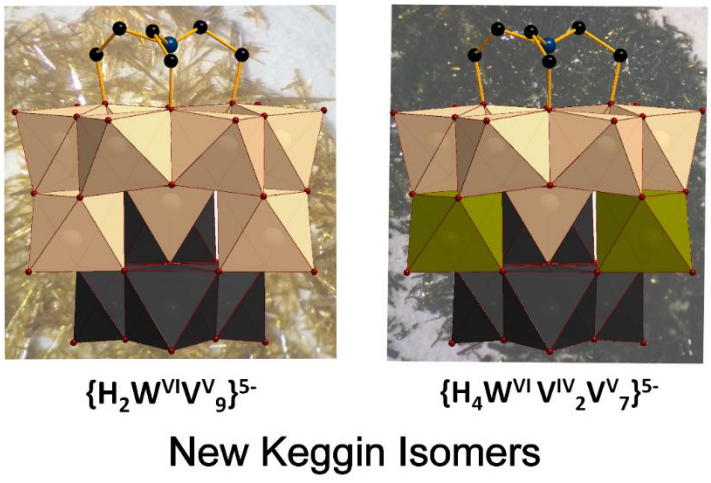

Figure 4.3 The structure of the two new Keggin isomers: left, the oxidized species and right, the reduced species. The colour of the crystals is shown in the background.

The redox-driven oscillatory template exchange that causes the exchange of the two XO_4^{3-} heteroatom guests, namely P^VO_4 and V^VO_4, contained within the $\{M_{18}O_{54}(XO_4)_2\}^{6-}$ has been investigated utilizing UV-vis spectroscopy. This oscillatory guest exchange process was also monitoring in real time utilizing ESI-MS, indicating the presence of the $\{V_3Mo_{17}\}$ species after about 3 hours of the reaction. We have explored the periodicity of this phenomenon by time-dependent UV-vis monitoring for 1 week to 3 weeks. We have observed that the oscillations follow a similar pattern, however we have not been able to arrive at a safe conclusion regarding the periodicity of the oscillatory system. A series of control experimental procedures were followed in order to investigate the reasons that the system was kept alive and prevent the damage of the oscillations. The total amount of TEA·HCl added in the reaction was significantly reduced, showing a totally different UV-vis spectrum. In the same way, three more reactions in the presence of N_2, without any addition of TEA·HCl and at room temperature were carried out, revealing UV-vis spectra with no oscillations observed. These four experimental procedures indicated the significant role of the O_2 (oxidizing agent), the organic compound (reducing agent) and the heating (helps the reaction procedure) in the reaction system, respectively. It is also worth mentioning that in all these alternative experimental procedures, the first two oscillations were not observed as they were in a normal reaction procedure. Thus, the system has been proven to be highly sensitive, as any changes to the experimental conditions resulted to the damage of the oscillations. This system offers space for further investigation. It could be worth investigating and comparing the behaviour of different Dawson-like polyoxometalates, such as $\{Mo_{18}Si_2\}$, $\{W_{18}P_2\}$ and $\{W_{18}Si_2\}$. Also an automated system (pumps) could be used in order to ensure the accurate and consistent addition of the reaction reagents.

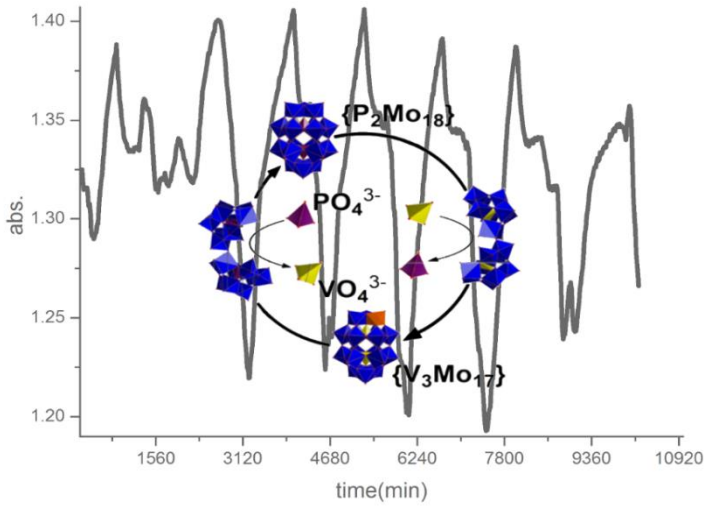

Figure 4.4 Schematic representation of the redox-driven exchange reaction and the UV-spectrum after one week of monitoring.

5. Experimental Data

5.1 Materials

All reagents and chemicals were supplied by Sigma Aldrich Chemical Company Ltd., Alfa Aesar and Fisher Scientific. Solvents were supplied by Fisher Chemicals. Unless stated otherwise, the materials were used without further purification.

5.2 Instrumentation and Techniques

Data processing and software: The pump control panel was programmed by using LabVIEW 2011 and the command scripts were written by using MicrosoftTM Excel software. The 2D and 3D plots were prepared by using OriginPro 8.5 data analysis and graphing software. Representations of crystal and molecular structures were prepared by using Diamond 3.1 crystal visualisation software on single crystal diffraction datasets.

Single Crystal X-ray Diffraction: Single crystal datasets and units cells were collected at 150(2) K on the following instruments: Oxford Diffraction Gemini Ultra S equipped with a graphite monochromator (λ (MoKα) = 0.7107 Å or λ (CuKα) = 1.5405 Å) and ATLAS CCD detector or a Bruker Apex II Quasar diffractometer equipped with a graphite monochromator (λ (MoKα) = 0.7107 Å). Structure solution and refinement were carried out with SHELXS-97/2013[189] and SHELXL-97/2013[190] *via* WinGX. [191] Corrections for incident and diffracted beam absorption effects were applied using either analytical [192] or empirical[193] methods. All non-hydrogen atoms were refined anisotropically unless otherwise stated.

pH measurements: Hanna Instruments H I 9025 C microcomputer pH meter.

UV-Vis spectroscopy: UV-Vis spectra were collected using a JASCO V-670 spectrometer and TIDAS II, 100 Diode Array fibre optic spectrometer (Z&M Company).

Thermogravimetric analysis (TGA): Thermogravimetric analysis was performed on a TA Instruments Q 500 Thermogravimetric Analyzer under nitrogen at a typical heating rate of 10 °C min^{-1} in platinum pan.

Fourier-transform infrared (FT-IR) spectroscopy: Materials were dried in a desiccator prior to use and were prepared as a KBr pellet. Data was collected using a *Shimadzu FTIR 8400S* Fourier Transform Infrared Spectrophotometer. Wavenumbers (ν) are given in cm-1; intensities are denoted as w = weak, sh = sharp, m = medium, b = broad, s = strong.

Microanalysis: Carbon, nitrogen and hydrogen content were determined by the microanalysis services within the School of Chemistry, University of Glasgow using an EA 1110 CHNS, CE- 440 Elemental Analyzer.

UV-vis irradiation: Power Supply, Xe, Hg and Hg (Xe) DC Arc Lamps, 50 to 200 Watts, Model: 69907 with a Q Series Lamp Housing, Holds Adjustable Reflectors.

Flame Atomic Absorption Spectroscopy Analysis: FAAS analysis was performed at the Environmental Chemistry Section, Department of Chemistry, The University of Glasgow on a Perkin-Elmer 1100B Atomic Absorption Spectrophotometer. The calibration was carried out from known stock solutions of 10, 30 and 50 ppm. All analytes were dissolved to an appropriate concentration in deionised water prior to analysis and metal concentration was calculated from the appropriate calibration curve.

Flame Photometry: FP was conducted to determine alkali metal content was performed on a *Sherwood Scientific M410 INDUSTRIAL Flame Photometer*, calibrated to a detection range of 0 - 5 ppm from known stock solutions. All analytes were dissolved to an appropriate concentration in deionised water prior to analysis and metal concentration was calculated from the appropriate calibration curve.

Inductively Coupled Plasma Optical Emission Spectroscopy: (ICP-OES) was conducted on a *TJA-IRIS-Advantage* spectrometer with thanks to the Zentralabteilung für Chemische Analysen, Forschungszentrum Jülich and Prof. Paul Kögerler (*RWTH Aachen University*). A minimum of 15 mg solid sample was submitted for analysis and these were subsequently prepared for ICP-OES analysis by digestion in a 1:1 mixture of H2O2 (30%) and conc. HNO3.

Cyclic Voltammetry: Cyclic Voltammograms were obtained using a CHI 730D Electrochemical Workstation. The standard three-electrode arrangement was employed with a Pt mesh auxiliary electrode, glassy carbon working electrode, and Ag/AgCl reference electrode. All potentials are quoted relative to the Ag/AgCl reference electrode. The glassy carbon working electrodes (diameter 1.5 mm) were polished with alumina (3 μm) on polishing pads and then rinsed with distilled water and sonicated in H_2O and then acetone solution before each experiment. The cell was purged with Ar for at least 10 min before each experiment. All experiments were performed at the room temperature, and the scan rate was 50 mV/s. The supporting electrolyte was 0.1 M NaAc-HAc buffer solution containing 0.2 M Na_2SO_4.

^{1}H-Nuclear magnetic resonance spectroscopy (^{1}H-NMR): 500 MHz Bruker Avance III

Magnetic Susceptibility Balance: Sherwood Scientific ltd. The number of unpaired electrons have been calculated according to the equation $\mu_s = \sqrt{n\,(n+2)}$, where μ_{so}= spin-only value in B.M. and n=numbers of unpaired electrons. The value (R_0) of an empty glass tube was recorded. The tube was filled with sample weighting **m** and with filling level (l) around 2.5-3.5 cm. The value (R) for the sample was then recorded. The magnetic susceptibility μ_{eff} was calculated according to the equation $\mu_{eff} = 2.828 * \sqrt{\chi M * T}$, where $\chi_M = \chi_g * M$, the Molar Susceptibility, $\chi_g = C*l*(R-R_0)/m*10^9$, the Gram Susceptibility, m= sample mass, M=molecular weight, C=balance calibration constant and T= Temperature. In case of the first row transition metals, $\mu_s = \mu_{eff,}$ as the orbital contribution is largely quenched. The variables for compound **9'** are as follows: C=1.576, l=1.7 cm, R=79, R_0=-49.5, T=291.15 K and m=0.065 g.

ESI-MS: Electrospray-ionisation mass spectrometry (ESI-MS) and coldspray-ionisation mass spectrometry (CS-MS) were performed using a Bruker micrOTOF-Q quadrupole time-of -flight mass spectrometer. Samples were dissolved in water and MeCN introduced into the MS at a dry gas temperature of 180 °C. The ion polarity for all MS scans recorded was negative, with the voltage of the capillary tip set at 4500 V, end plate offset at -500 V, funnel 1 RF at 400 Vpp and funnel 2 RF at 400 Vpp, hexapole RF at 200 Vpp, ion energy 5.0 eV, collision energy at 10 eV, collision cell RF at 2000 Vpp, transfer time at 120.0µs, and the pre-pulse storage time at 20.0µs.

Density Functional Theory (DFT) Analyses: All quantum chemical calculations were performed at the density functional theory (DFT) level. Geometry optimizations performed using B3LYP method as implemented in TURBOMOLE V6.3.1 package. TZVP basis set was used on all atoms. To allow for solvation effects, the conductor-like screening model (COSMO) method was used with ionic radii of the atoms, which define the dimensions of the cavity surrounding the molecule, are chosen to be (in Å) 2.23 for W and V, 2.0 for C, 1.8 for N, 1.72 for O, 1.3 for H.

Features of TriContinent™ pumps: The C3000 OEM Syringe Pump modules are designed for automated instrumentation with high resolution options available up to 192,000 steps/full-stroke. All normal aspiration and dispensing operations expected from an OEM syringe pump modules can be accomplished with this unit. The stepper motor driven syringe accurately and precisely handles fluids from a few micro-liters to 12.5 millilitres. The

syringe drive arm can be easily back driven, making syringe installation or replacement extremely quick and easy. [184]

5.3 Method of Crystal Growth

Regardless the approach used for the synthesis of the POM compounds, two methods of crystal growth were mainly applied: Slow evaporation and gas diffusion. The technique of slow evaporation involves filtering the mother solutions into a beaker or a conical flask and then the solutions were left undisturbed in a controlled temperature environment (18 ^{o}C or 5 ^{0}C) to allow for evaporation. In gas diffusion a small vail with the solution of the compound is placed inside a larger vial that contains a solvent with a lower boiling point than the compound's solvent. The large container is then sealed well and left for crystallization. The best containers to use for gas diffusion are test or centrifuge tubes. The rate of evaporation can be controlled by using Parafilm^{TM}.

5.4 Synthesis of the Compounds

5.4.1 Synthesis of $(C_2H_8N)_5Na_2[Mo^{VI}_{11}V^{V}_{5}V^{IV}_{2}O_{52}(HPO_3)(CH_3OH)]\cdot 5H_2O$ (1)

$Na_2MoO_4\cdot 2H_2O$ (0.714 g, 2.9 mmol), $VOSO_4\cdot xH_2O$ (0.163 g, 1 mmol), $Na_2HPO_3\cdot 5H_2O$ (0.108 g, 0.5 mmol) and dimethylamine hydrochloride (0.244 g, 3 mmol) were dissolved in a warm mixture of deionised water (10 mL) and methanol (5 mL) under vigorous stirring, resulting to a dark purple solution. The mixture was left to cool down to room temperature under magnetic stirring and then the pH was adjusted carefully to 2.9 by the addition of concentrated HCl. At this point the solution was turned dark green and the reaction mixture was stirred for 5 more min. The dark green solution was filtered and the filtrate was left to crystalize for a week. Dark green needles were filtered and were left to dry in air. Yield: 50 mg (30% based on V). MW: 2722.14 g·mol^{-1}. IR (cm^{-1}) in KBr pellets: 3450.9 (b), 3130.8 (b) 1617.9 (m), 1462.7 (s), 1057.7 (m), 950.7 (s), 853.3 (s), 805.1 (s), 774.4 (m), 583.4 (s). Elemental analysis calcd for $C_{11}H_{55}N_5Na_2O_{61}PMo_{11}V_7$: C 4.85, H 2.04, N: 2.57, Na 1.69, V 13.10, P 1.14, Mo 38.77%. Found: C 4.87, H 2.85, N 1.89, Na 1.70, V 14.4, P 1.17, Mo 38.3%.

5.4.2 Synthesis of $(C_2H_8N)_3Na[Mo_{12}O_{30}(HPO_3)_8](H_2O)10$ (2)

$Na_2MoO_4 \cdot 2H_2O$ (4.839 g, 20 mmol), $Na_2S_2O_4$ (0.522 g, 3 mmol) and DMA·HCl (2 g, 24.6 mmol) were dissolved in deionised water (30 ml) under vigorous stirring, resulting to a light brown solution with pH=6.78. Then, H_3PO_3 (0.820 g, 10 mmol) was added in the reaction mixture giving clear, dark green solution with pH=6.2. After about 10 minutes of stirring the mixture was filtrated and the filtrate was left to crystallize at 5 ^{0}C and after a month period, orange rod-like crystals of (**2**) suitable for X-Ray crystallography were obtained. Yield: 145 mg (3% based on Mo). MW: 2826.93 g·mol^{-1}. IR (cm^{-1}) in KBr pellets: 3426.9 (b), 1632.5(m), 1467.6 (m), 1128.1 (m), 1078 (s), 1009.6 (m), 904.2 (s), 731.9 (m), 547.7 (m). Elemental analysis calcd for $C_{14}H_{91}N_7Na_2O_{64}P_8Mo_{12}$: C 5.95, H 2.49, N: 3.61, Na 1.63, P 8.77, Mo 40.73%. Found: C 5.7, H 2.4, N 3.4, Na 1.7, P 9.1, Mo 42.3%.

5.4.3 Synthesis of $(C_6H_{16}NO_3)_6Na_8H[Mo_6O_{18}(HPO_3)(C_6H_{13}NO_3)]_2(PV_4Mo_8O_{40})(H_2O)_{32}$ (3)

$Na_2MoO_4 \cdot 2H_2O$ (5.080 g, 21 mmol), and $VOSO_4 \cdot xH_2O$ (4 ml, 0.5 M) were dissolved in deionised water (30 ml) containing NaCl (0.400 g, 6.85 mmol) under stirring, resulting to a dark purple solution with pH=6.7. TEA·HCl (0.928 g, 3 mmol) and H_3PO_3 (0.410 g, 5 mmol) were then added with no significant change. After 20 minutes of stirring the pH was adjusted to 5.50 by the addition of concentrated HCl and the mixture was filtrated giving clear dark purple solution. The filtrate was kept at 18 ^{0}C for 10 days, when orange needles of compound (**3**) were obtained. Yield: 70 mg (22% based on V). MW: 5524.53 g·mol^{-1}. IR (cm^{-1}) in KBr pellets: 3215.7 (b), 3117.4 (b), 1633.4(m), 1446.4 (m), 1088.6 (m), 1056.8 (s), 940.12 (s), 855.3 (s), 783.9 (s), 518.8 (m). Elemental analysis calcd for $C_{48}H_{189}N_8Na_8O_{138}P_3Mo_{20}V_4$: C 10.51, H 3.47, N: 2.04, Na 3.35, P 1.69, Mo 34.97, V 3.71%. Found: C 10.3, H 2.58, N 1.99, Na 3.09, P 1.52, Mo 34.8, V 4.01%.

5.4.4 Synthesis of $(C_2H_8N)_6Na[Mo_{11}V_7O_{52}(TeO_3)]\cdot 15H_2O$ (4)

$Na_2MoO_4 \cdot 2H_2O$ (2 g, 8.5 mmol), $NaVO_3$ (0.518 g, 4.25 mmol), Na_2TeO_3 (0.465 g, 2.1 mmol) and dimethylamine hydrochloride (2 g, 24.5mmol) were dissolved in deionised water (20 mL) under vigorous stirring resulting to a cloudy yellow solution. The mixture was heated at 90 °C for about 10 min resulting to a clear yellowish solution. The reaction mixture was allowed to cool down at room temperature under magnetic stirring and then solid $N_2H_4 \cdot 2HCl$ (0.067 g, 0.64 mmol) was added resulting to a dark brown slurry. The mixture was stirred for more 5 min and the pH was adjusted to 2.5 by addition of concentrated HCl.

The resulting dark purple solution was then filtrated and the filtrate was left to crystallise under gas diffusion with MeOH for a week when green needles suitable for X-ray crystallography came out. Yield: 34 mg (7% based on V). MW: 2989.02 g·mol^{-1}. IR (cm^{-1}, in KBr pellets): 3432.6 (b), 3167.5 (b) 1625.7 (m), 1463.7 (s), 1015.3 (m), 982.5 (s), 846.6 (s), 773.3 (m), 669.2 (m), 517.7 (m). Elemental analysis calcd for $C_{12}H_{78}N_6NaO_{70}TeMo_{11}V_7$: C 4.82, H 2.63, N 2.81, Na 0.77, V 11.93, Te 4.27, Mo 35.31%. Found C 5.00, H 2.91, N 1.84, Na 0.79, V 11.72, Te 4.19, Mo 34.68%.

5.4.5 Synthesis of $K_4(C_2H_8N)_3[Mo_{12}V_3O_{39}(\mu_6\text{-}TeO_4)_3(\mu_6\text{-}TeO_3)_2]\cdot 14(H_2O)$ (5)

The aqueous stock solutions were prepared as follows: A) 1 M $Na_2MoO_4{\cdot}2H_2O$ (100 ml, 24.2 g), B) 0.5 M $VOSO_4{\cdot}xH_2O$ (100ml, 8.15 g), C) 0.25 M $K_2TeO_3{\cdot}xH_2O$ (100ml, 6.35 g), D) 1 M DMA·HCl (100ml, 4.51 g) and E) 2M HCl (100 ml). These solutions of reagents were connected to the inlets for the assigned pumps. For this experiment, 7 pumps were active. Six pumps for the solutions of the reagents (including distilled H_2O) and one pump for the space required between each reaction (spacer). The matrix commands, which have already been written, were executed to initiate the infusion of the reagent solution (7 ml) into the reactor. The 50 individual reactions were collected in test tubes, which were changed manually at each programmed refill point. The collected samples were left at 18 ^{0}C to crystalize. One month later, light green needles suitable for X-ray crystallography came out. Yield: 280 mg (3.4% based on V). MW: 3435.14 g·mol^{-1}. IR (cm^{-1}, in KBr pellets): 3426.9 (b), 1621.8 (m), 1483.7 (m), 989 (s), 890.9 (s), 830.2 (s), 707.7 (s), 628.6 (s), 593 (m). Elemental analysis calcd for $C_6H_{52}N_3O_{71}K_4Te_5V_3Mo_{12}$: C 2.12, H 1.54, N 1.24, K 4.6, V 4.49, Te 18.96, Mo 33.85%. Found C 2.6, H 1.15, N 1.3, K 3.5, V 5.1, Te 21.2, Mo 32%.

5.4.6 Synthesis of $Na_3(C_2H_8N)_4[Mo_{12}V_3(\mu_6\text{-}TeO_4)_3(\mu_6\text{-}TeO_3)_2O_{39}]\cdot 15(H_2O)$ (6)

$Na_2MoO_4{\cdot}2H_2O$ (0.968 g, 4 mmol), NH_4VO_3 (0.141 g, 1.2 mmol), Na_2TeO_3 (0.266 g, 1.2 mmol) and DMA·HCl (0.978 g, 12 mmol) were added in 10 ml of distilled water giving a colourless solution with pH=9.21. The pH was adjusted to 6.09 with 37% HCl resulting to a cloudy yellow solution. The mixture then was sealed in a 20-ml autoclave reactor and remained at 140 ^{0}C for three days. After cooling the autoclave to room temperature, dark green solution and light green needles suitable for X-Ray crystallography were separated and air-dried. Yield: 250 mg (26% based on Mo). MW: 3412.33 g·mol^{-1}. IR (cm^{-1}, in KBr pellets): 3417.9 (b), 1597 (m), 1411.9 (m), 964.4 (s), 871.8 (s), 794.7 (s), 671.2 (m), 578 (m). Elemental analysis calcd for $C_8H_{64}N_4O_{72}Na_3Te_5V_3Mo_{12}$: C 2.84, H 1.85, N 1.66, Na

2.04, V 4.52, Te 18.89, Mo 34.09%. Found C 3.67, H 1.9, N 2.55, Na 1.95, V 4.32, Te 18.6, Mo 33.85%.

5.4.7 $Na_{15}(C_2H_8N)_6K_6(Mo_{11}V_7SeO_{55})(Mo_5V_4Se_4O_{36})_3(H_2O)_{36}$ (7)

$Na_2MoO_4{\cdot}2H_2O$ (1.694 g, 7 mmol), $VOSO_4$ (0.570 g, 3.5 mmol), K_2SeO_3 (0.718 g, 3.5 mmol) and DMA·HCl (0.570 g, 7 mmol) were added in 10 ml of warm distilled water giving a purple solution with pH=7. The pH was adjusted to 5.68 with 2M HCl resulting to a dark purple solution. The mixture then was filtrated and remained undisturbed at 18 ^{0}C and after around 1 week, dark green solution and green rhombic crystals suitable for X-Ray crystallography were obtained and air-dried. Yield: 52 mg (9.1% based on V). MW: 8601.25 g·mol^{-1}. IR (cm^{-1}, in KBr pellets): 3441.9 (b), 1635.6(m), 1384.9 (m), 948.9 (s), 759.9 (m), 594 (m). Elemental analysis calcd for $C_{12}H_{64}N_6O_{199}Na_{15}K_6Se_{13}V_{19}Mo_{26}$: C 1.68, H 1.41, N 0.98, Na 4.01, K 2.73, V 11.25, Se 11.93, Mo 29%. Found C 1.62, H 1.27, N 0.6, Na 3.85, K 2.65 V 11.5, Se 11.5, Mo 25.2%.

5.4.8 $K_8Na_6[Mo_6V_{16}Se_8O_{79}](H_2O)_{25}$ (8)

$Na_2MoO_4{\cdot}2H_2O$ (1.694 g, 7 mmol), $VOSO_4$ (0.570 g, 3.5 mmol), K_2SeO_3 (1.436 g, 7 mmol) and DMA·HCl (0.570 g, 7 mmol) were added in 10 ml of warm distilled water giving a purple solution with pH=7.7. The pH was adjusted to 5.63 with 2M HCl resulting to a dark purple solution. The mixture then was filtrated and remained at 5^{0}C and after around 10 days, dark green solution and big green cubic crystals suitable for X-Ray crystallography were separated and air-dried. Yield: 80 mg (14% based on V). MW: 4205.38 g·mol^{-1}. IR (cm^{-1}, in KBr pellets): 3439.9 (b), 1620.2 (m), 956.7 (s), 864.1 (m), 763.8 (m), 555.5 (m). Elemental analysis calcd for $H_{50}O_{104}K_8Na_6Se_8V_{16}Mo_6$: H 1.2, Na 3.29, K 7.47, V 19.46, Se 15.09, Mo 13.75%. Found H 1.06, Na 3.1, K 7.2, V 19.5, Se 15.04, Mo 12.9%.

5.4.9 Synthesis of $(C_6H_{16}NO_3)_2Na_3[H_2W^{VI}_4V^V_8(V^VO_4)O_{33}(C_6H_{13}NO_3)]{\cdot}8H_2O$ (9)

Method A: $NaVO_3$ (0.854 g, 7 mmol), $Na_2WO_4{\cdot}2H_2O$ (0.990 g, 3 mmol), TEA·HCl (0.464 g, 2.5 mmol) and NaCl (0.117 g, 2 mmol) were dissolved in deionised water (10 ml) giving a cloudy yellow solution. The reaction mixture was heated at 80-90 °C for 1 hour, during which time the cloudy yellow solution changed to clear orange. After cooling the reaction mixture down to room temperature, $Na_2S_2O_4$ (0.087 g, 0.5 mmol) was added to the reaction mixture resulting to dark brown solution and the pH was adjusted to 2.0-2.5 by addition of 37% HCl followed by a colour change to dark green. The reaction mixture was filtered and

the filtrate was left undisturbed to crystallize at 18 ^{0}C. Orange needles suitable for X-ray diffraction analysis obtained after 2-3 weeks. Yield: 80 mg (8.1% based on W). MW: 2448.48 g·mol^{-1}. IR (cm^{-1}): 3410.2 (b), 1627.9 (m), 1384.9 (m), 1211.3 (m), 1064.7 (m), 975.9 (s), 891.1 (s), 833.25 (m), 775.4 (s), 636.5 (w), 551.6 (w). Elemental analysis calcd for $C_{18}H_{63}N_3Na_3O_{54}V_9W_4$: C 8.83, H 2.59, N: 1.72, Na 2.82, V 18.73, W 30.04%. Found: C 9.04, H 2.19, N 1.69, Na 3.00, V 19.66, W 28.24%.

Method B: The above synthetic procedure was repeated in the absence of $Na_2S_2O_4$. The reaction mixture was filtered and the filtrate was left undisturbed to crystallize at 18 ^{0}C. Orange needles suitable for X-ray diffraction analysis obtained after 1 week. Yield: 150 mg (15.2% based on W). The obtained spectroscopic and crystallographic data of the isolated compound are identical to **1**.

5.4.10 Synthesis of $(C_6H_{16}NO_3)_4Na[H_2W^{VI}_4V^V_8(V^VO_4)O_{33}(C_6H_{13}NO_3)]\cdot 4H_2O$ (10)

The compound **2** was synthesized as compound **1** (method A) using an increased amount of TEA·HCl (1.857g, 10 mmol) instead. Orange needles suitable for X-ray diffraction analysis obtained after 5 days. Yield: 120 mg (12.1% based on W). MW: 2630.83 g·mol^{-1}. IR (cm^{-1}): 3354.2 (b), 1627.9 (m), 1384.9 (m), 1213.2 (w), 1066.6 (m), 970.2 (s), 891.1 (s), 831.3 (m), 777.3 (m), 624.9 (w), 547.8 (w). Elemental analysis calcd for $C_{30}H_{87}N_5NaO_{56}V_9W_4$: C 13.70, H 3.33, N: 2.66, Na 0.87, V 14.43, W 27.96%. Found: C 13.40, H 3.09, N 2.63, Na 0.67, V 17.06, W 25.45%.

5.4.11 Synthesis of Starting material $(NH_4)_6P_2Mo_{18}O_{62}\cdot 12H_2O$

The $(NH_4)_6P_2Mo_{18}O_{62}\cdot 12H_2O$ salt was synthesized according to the procedure reported by Miras [180, 194] *et. al.*

5.4.12 Synthesis of the oscillating reaction mixture

The oscillating mixture was prepared according to the procedure reported by Miras [180] *et. al.*: 8 g (2.5 mmol) of $(NH_4)_6P_2Mo_{18}O_{62}\cdot 12H_2O$, 1.3g (7.0 mmol) triethanolamine (TEA) and 0.18g (1.5mmol) NH_4VO_3 were dissolved in warm water (50 ml) under stirring resulting in a yellow solution. The pH was then adjusted to 1 by addition of concentrated HCl (37%). After the pH was adjusted the solution was heated at 90-100 °C during which time the cloudy solution changed from yellow to green indicating that the guest-template-exchange process had begun. After 7-8 h, additional amount of TEA was added (0.5 g, 2.7 mmol) to the

reaction mixtures before continuing the heating for longer period of times. After the observation of two cycles and the formation of Keggin precipitate (about 20 h from the beginning of the reaction), the pH was adjusted by the value of 8 with concentrated NH_3 and kept stable for 5 minutes. Then, the pH adjusted immediately to the value of 1 with concentrated HCl, followed by 0.5 g of TEA·HCl, while the UV-vis spectrum recorded in real time for additional time.

5.5 IR Spectroscopy

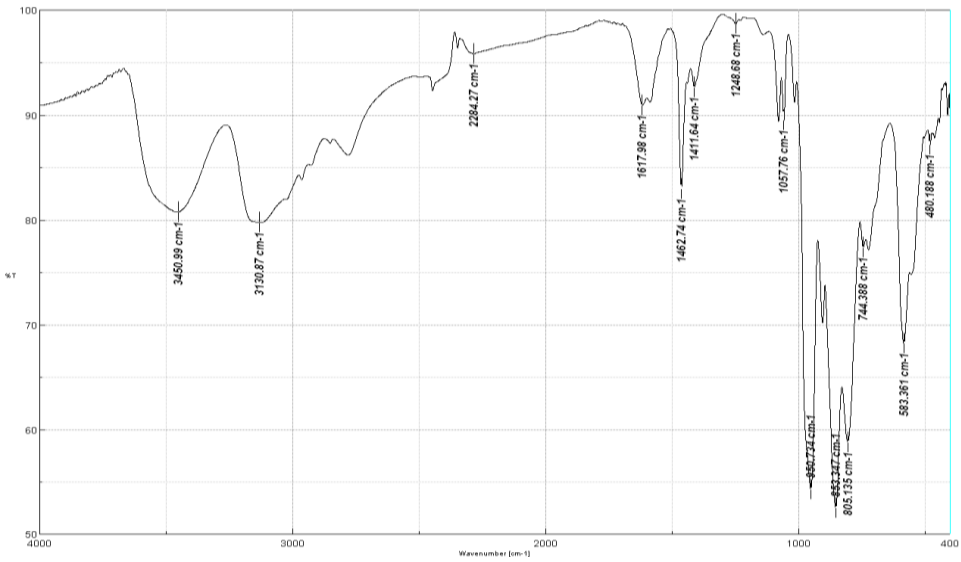

Figure 5.1 Infrared Spectrum of compound **1**. The strong bands observed at 951 cm^{-1}, 853 cm^{-1} and 805 cm-1 are characteristic of the terminal {V=O} and {Mo=O} vibrations, whilst the peaks at 792 cm^{-1}, 744 cm-1 and 583 cm^{-1} are characteristic of the bridging {M-O-M} vibrational modes of the POM cluster. Broad signals at 3450 cm^{-1} and 3130 cm^{-1} correspond to O-H stretches in water molecules.

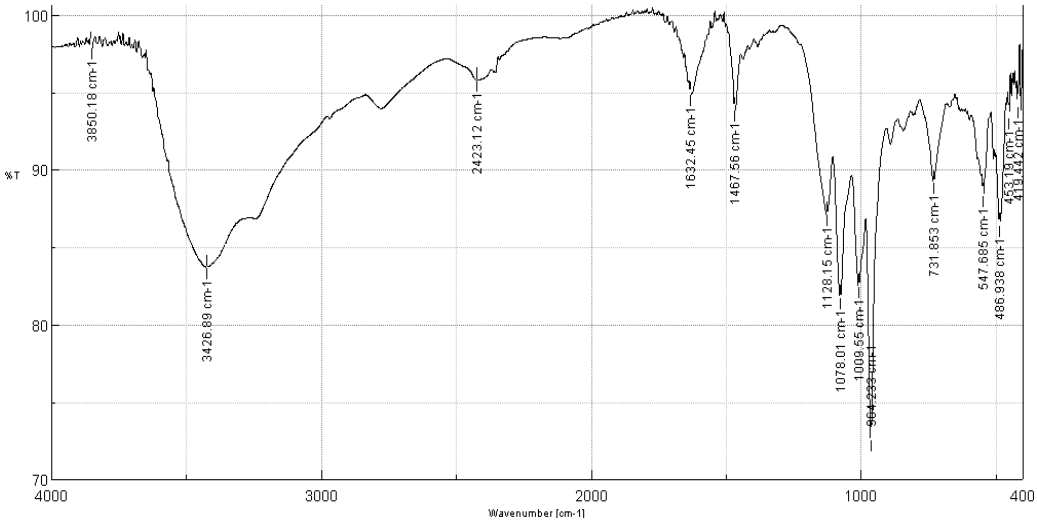

Figure 5.2 Infrared Spectrum of compound **2.** The strong bands observed at 904 cm^{-1} is characteristic of the terminal {Mo=O} vibrations, whilst the peaks at 731 cm^{-1} and 547 cm^{-1} is characteristic of the bridging {Mo-O-Mo} vibrational modes of the POM cluster. Broad signals around 3400 cm^{-1} correspond to O-H stretches in water molecules.

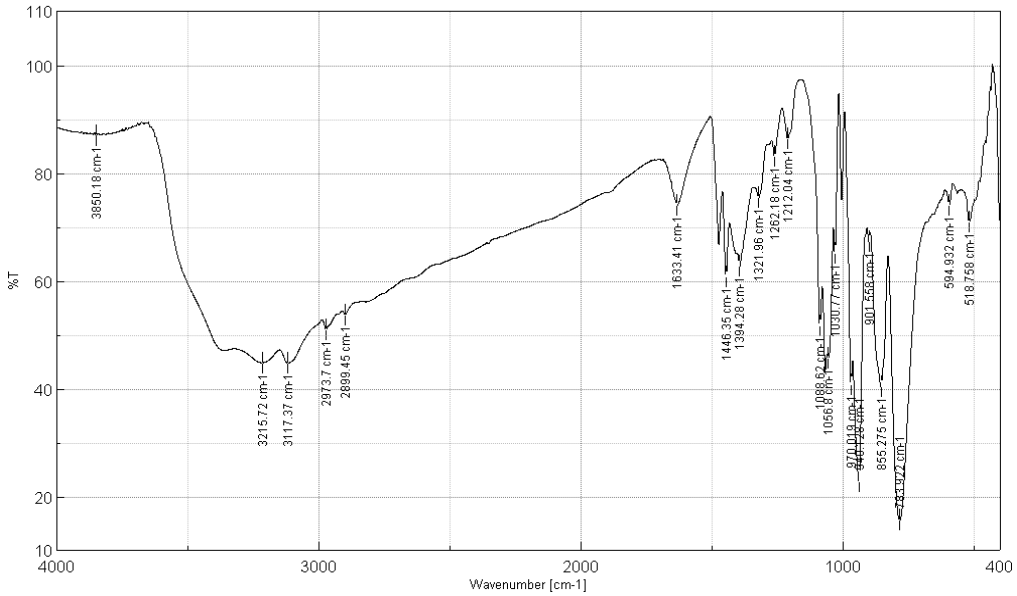

Figure 5.3 Infrared Spectrum of compound **3.** The strong bands observed at 970 cm^{-1}, 855 cm^{-1} are characteristic of the terminal {V=O} and {Mo=O} vibrations, whilst the peaks at 783 cm^{-1}, 744 cm^{-1} and 583 cm^{-1} are characteristic of the bridging {M-O-M} vibrational modes of the POM cluster. Broad signals at around 3000 cm^{-1} correspond to O-H stretches in the organic cations that encapsulate the cluster and water molecules.

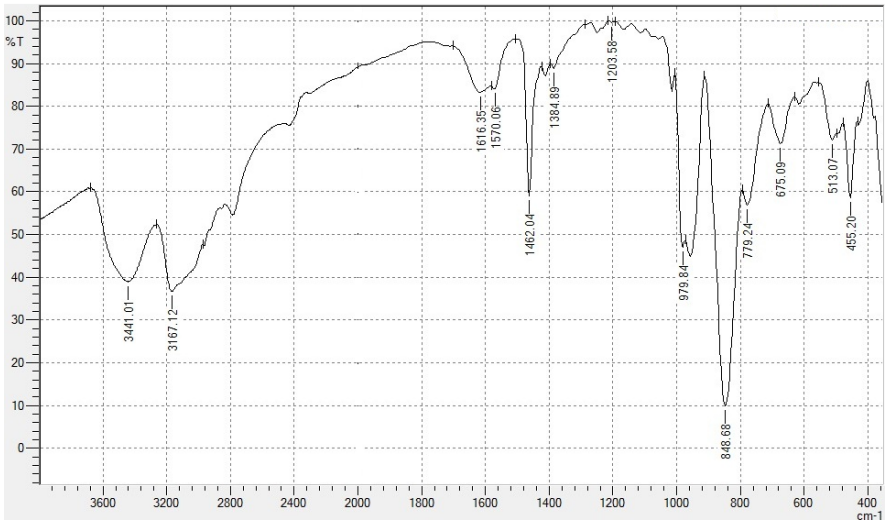

Figure 5.4 Infrared Spectrum of compound **4.** The strong bands observed at 979 cm^{-1} is characteristic of the terminal {V=O} and {Mo=O} vibrations, whilst the peaks at 779 cm^{-1} and 675 cm^{-1} are characteristic of the and bridging {V-O-V} vibrational modes of the POM cluster. Broad signals at 3441 cm^{-1} and 3167 cm^{-1} correspond to O-H stretches in H_2O molecules.

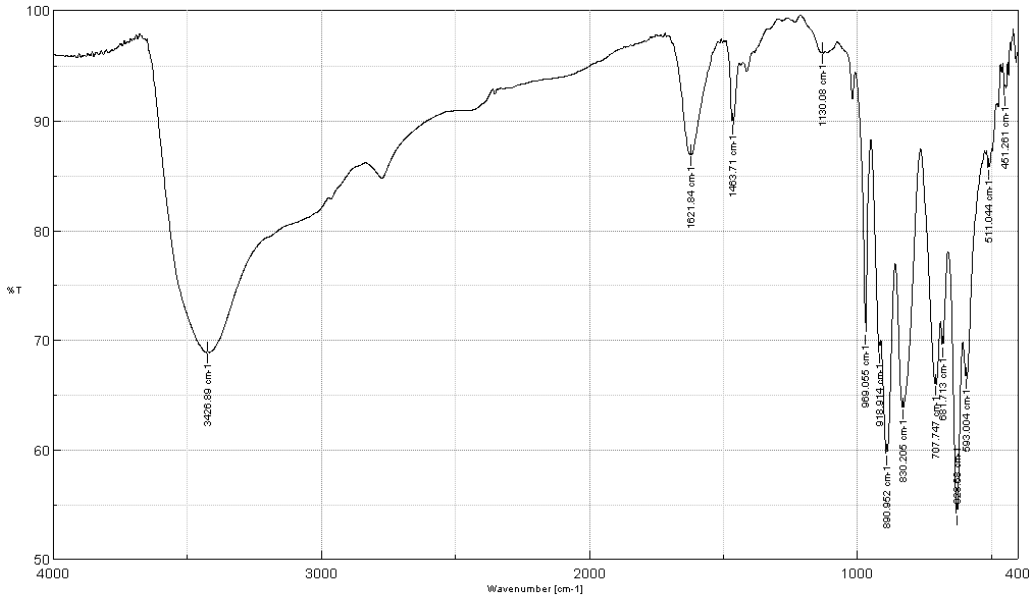

Figure 2.5 Infrared Spectrum of Compound **5.** The strong bands observed in the region between 970-830 cm^{-1} are characteristic of the terminal {V=O} and {Mo=O} and the strong peaks in the region between 707-593 are characteristic of the bridging {V-O-V} vibrational modes of the cluster. The broad peak at around 3000 cm^{-1} correspond to O-H stretches in water molecules.

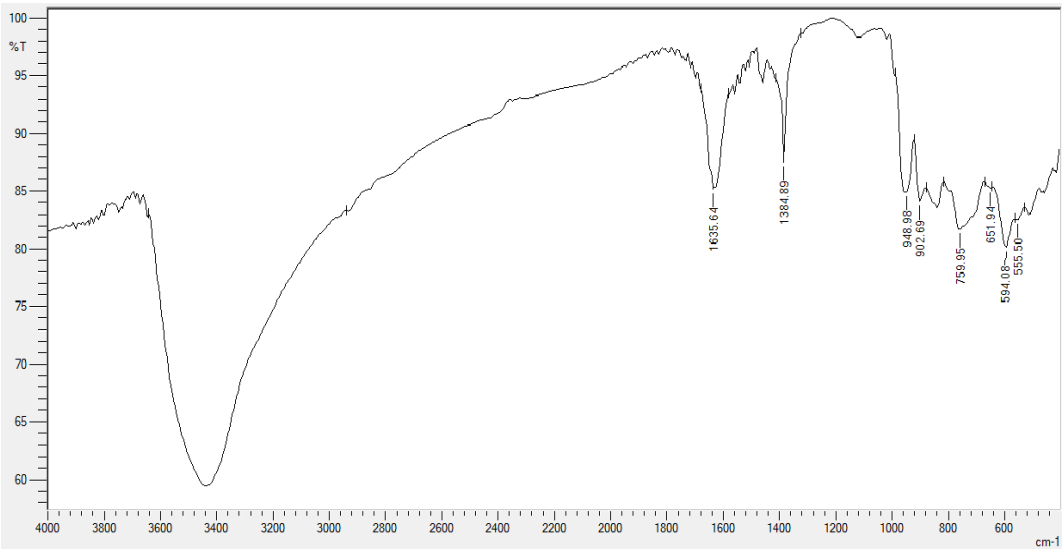

Figure 5.6 Infrared Spectrum of compound **6**. The peaks observed at 964 cm^{-1}, 871 cm^{-1} are characteristic of the terminal {V=O} and {Mo=O} and the signals at 794 cm^{-1} and 671 are characteristic of the bridging {M-O-M} vibrational modes of the POM cluster. The broad peak at around 3000 cm^{-1} correspond to O-H stretches in water molecules.

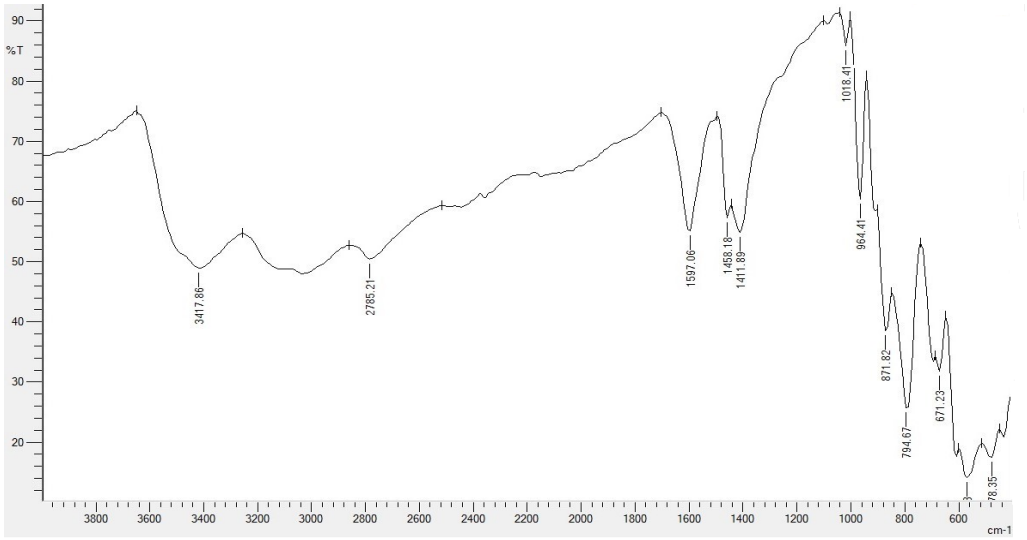

Figure 5.7 Infrared Spectrum of compound **7**. The peak observed at 948 cm^{-1} and at 902 cm^{-1} are characteristic of the terminal {V=O} and {Mo=O}. The peaks of the bridging {M-O-M} vibrational modes can be identified at 794 cm^{-1} and 671 cm^{-1}. The broad peak at around 3400 cm^{-1} correspond to O-H stretches in water molecules.

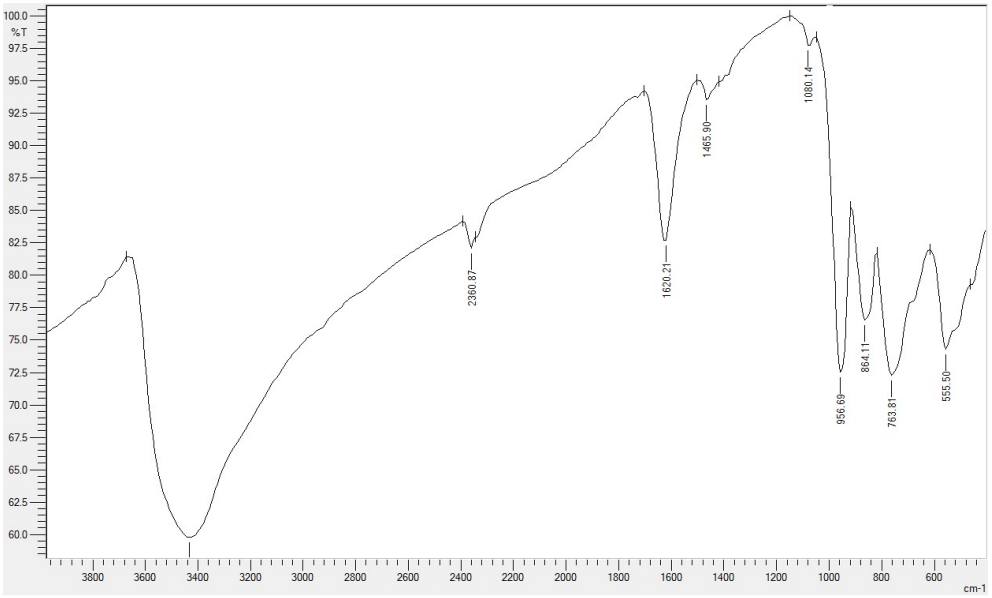

Figure 5.8 Infrared Spectrum of compound **8**. The signals observed at 956 cm^{-1} and at 864 cm^{-1} are characteristic of the terminal {V=O} and {Mo=O}. The peaks of the bridging {M-O-M} vibrational modes can be identified in the region between 794 cm^{-1} and 555 cm^{-1}. The broad peak at around 3400 cm^{-1} correspond to O-H stretches in water molecules.

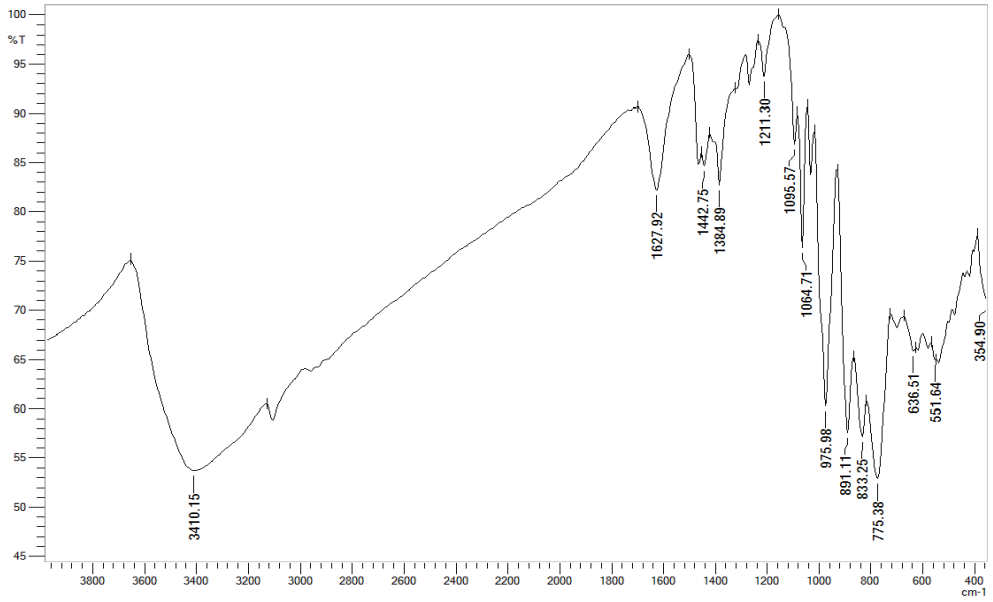

Figure 5.9 Infrared Spectrum of compound **9**. The strong bands observed in the region between 975 cm^{-1} and 833 cm^{-1} are characteristic of the terminal {V=O} and {Mo=O} vibrations, whilst the peaks at 775 cm^{-1}, 636 cm^{-1} and 551 cm^{-1} are characteristic of the bridging {M-O-M} vibrational modes of the cluster. Broad signals at around 3400 cm^{-1} correspond to O-H stretches in the organic cations that encapsulate the cluster and H_2O molecules.

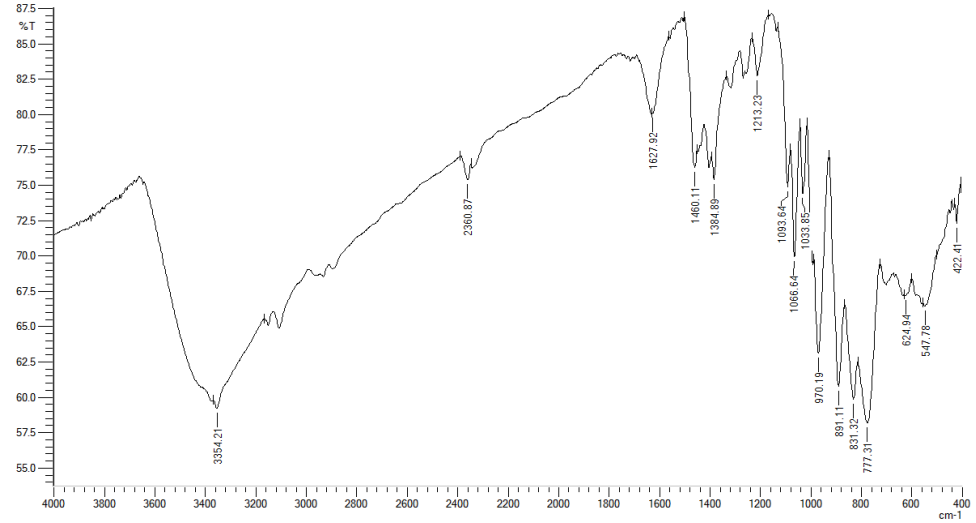

Figure 5.10 Infrared Spectrum of compound **10**. The strong bands observed at 970 cm^{-1}, 891 cm^{-1} and 831 cm^{-1} are characteristic of the terminal {V=O} and {Mo=O} vibrations, whilst the peaks at 777 cm^{-1}, 624 cm^{-1} and 547 cm^{-1} are characteristic of the bridging {M-O-M} vibrational modes. Broad signals at around 3300 cm^{-1} correspond to O-H stretches in the organic cations that encapsulate the cluster and water molecules.

5.6 UV-vis Spectroscopy

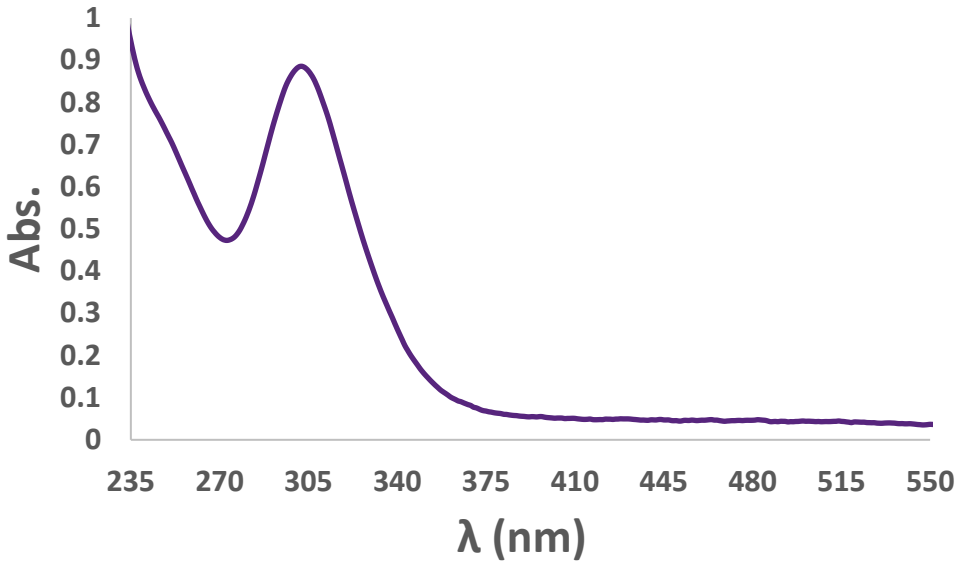

Figure 5.11 UV-vis spectrum of compound **1** in H_2O at a concentration of $2.94x10^{-5}$ mol·L^{-1}.

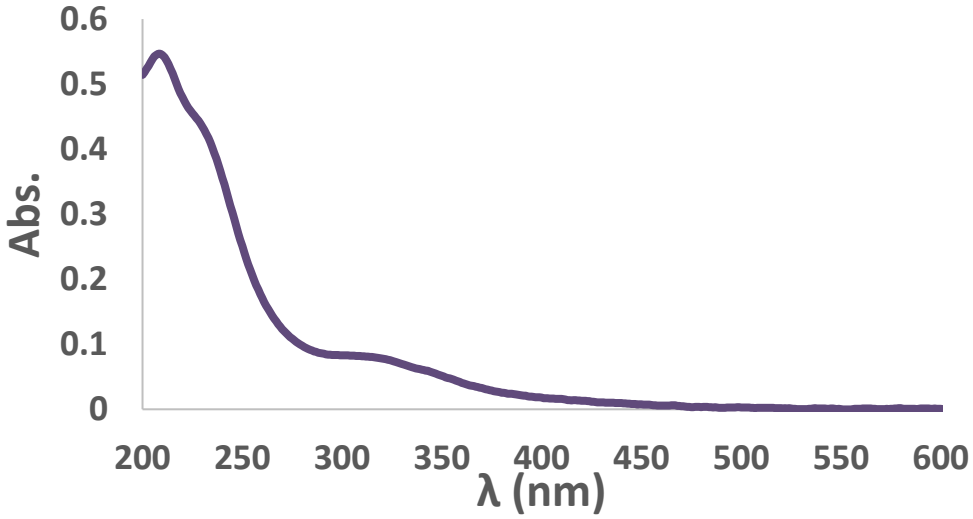

Figure 5.12 UV-vis spectrum of compound **2** in H_2O at a concentration of $1.77x10^{-4}$ mol·L^{-1}.

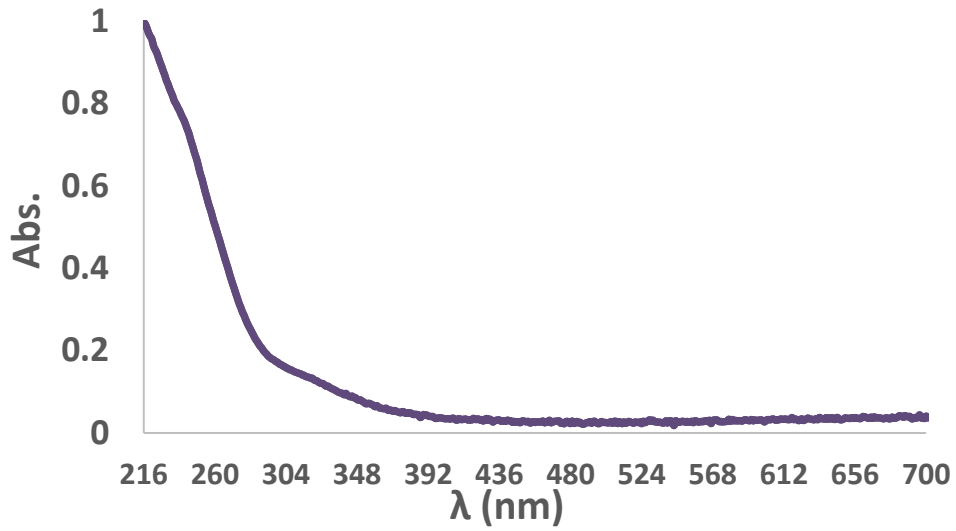

Figure 5.13 UV-vis spectrum of compound **3** in H_2O at a concentration of $5x10^{-6}$ mol·L^{-1}.

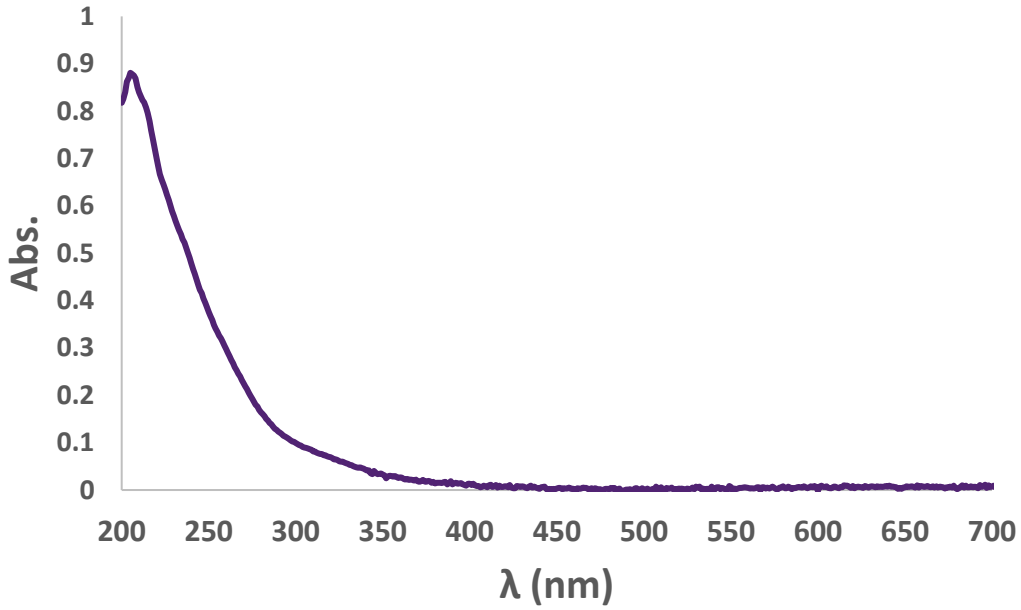

Figure 5.14 UV-vis spectrum of compound **4** in H_2O at a concentration of $2x10^{-6}$ mol·L^{-1}.

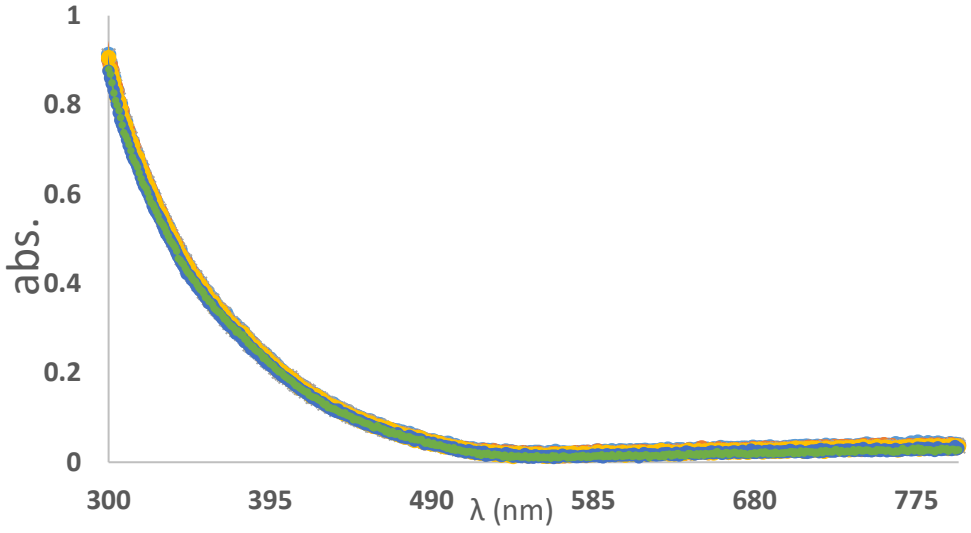

Figure 5.15 Time-dependent UV-vis spectrum of compound **4** in solvent mixture CH_3COOH-CHCOONa at a concentration of $0.53x10^{-4}$ $mol{\cdot}L^{-1}$. The measurement was contacted every 30 min for 3 hours. The compound remains stable for at least this time.

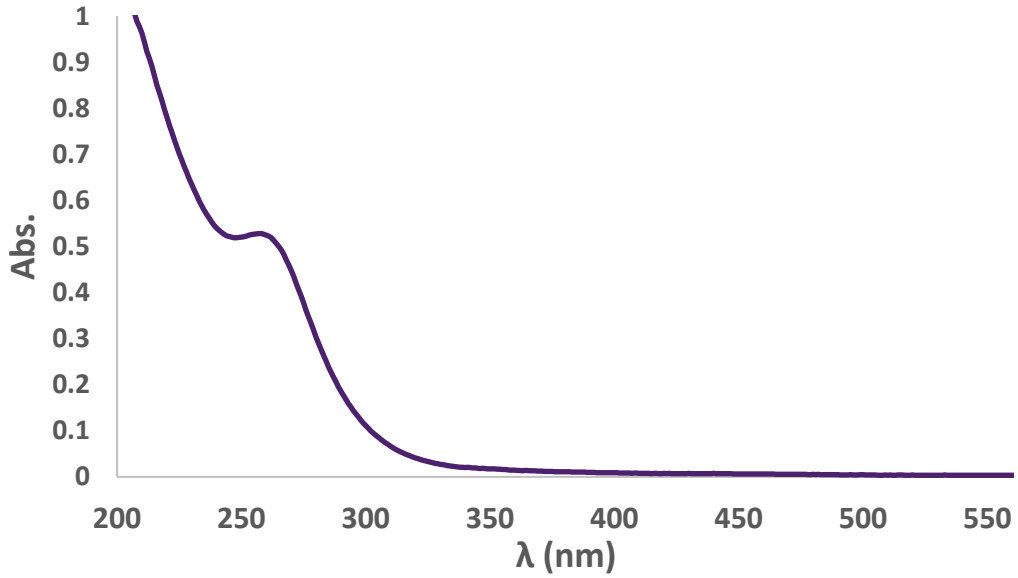

Figure 5.16 UV-vis spectrum of compound **5** in H_2O at a concentration of $6.29x10^{-5}$ $mol{\cdot}L^{-1}$.

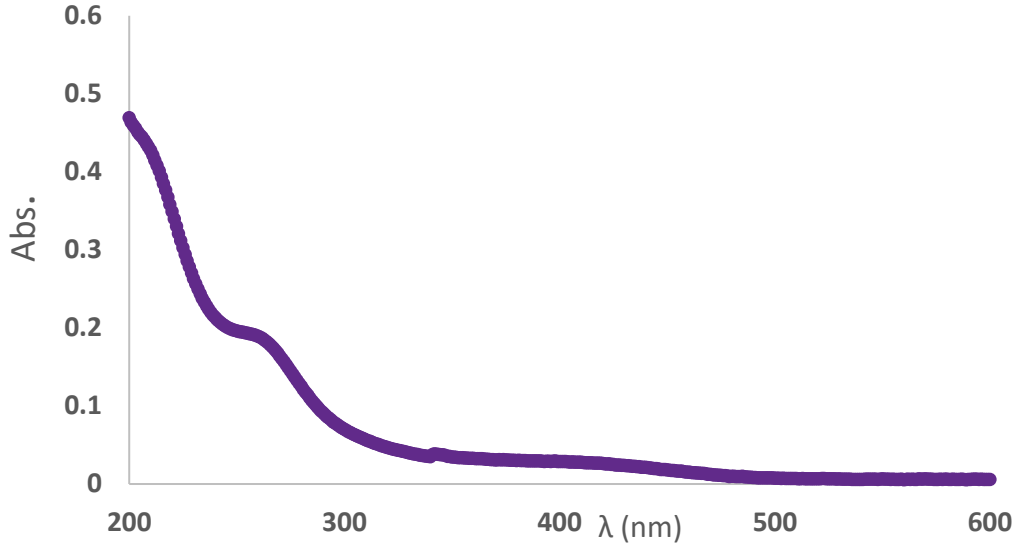

Figure 5.17 UV-vis spectrum of compound **6** in H_2O at a concentration of $6.34x10^{-5}$ $mol \cdot L^{-1}$.

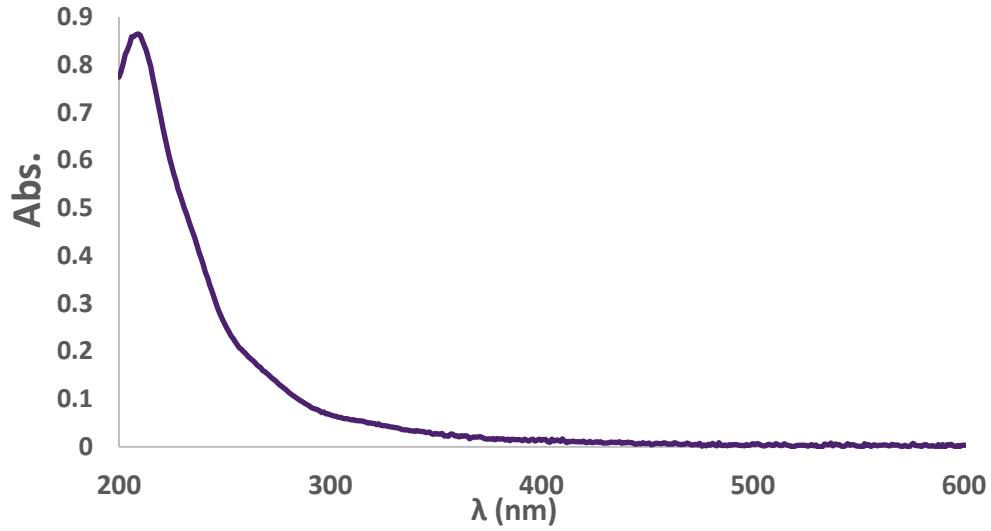

Figure 5.18 UV-vis spectrum of compound **7** in H_2O at a concentration of $3.3x10^{-6}$ $mol \cdot L^{-1}$.

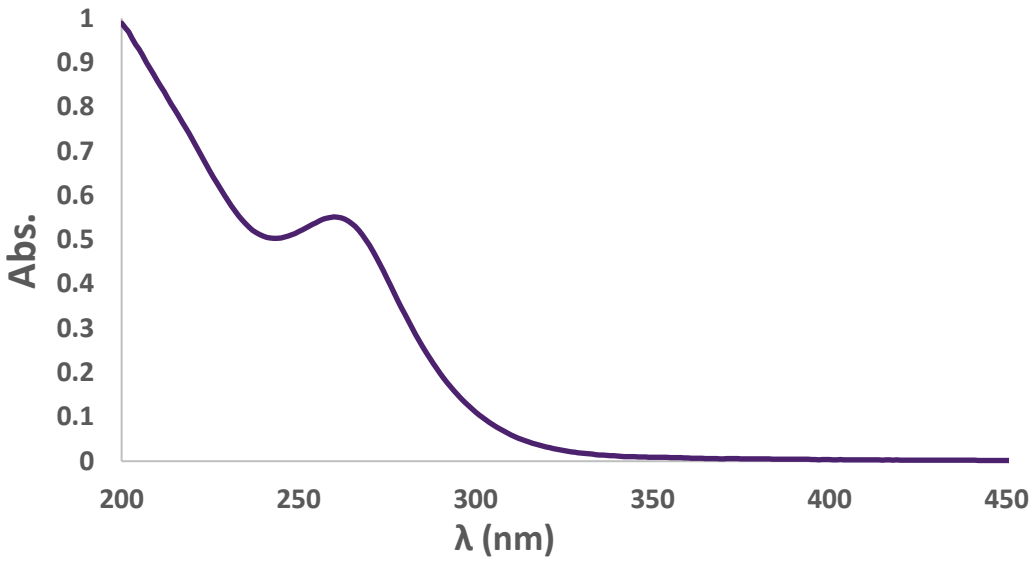

Figure 5.19 UV-vis spectrum of compound **8** in H_2O at a concentration of $5.97x10^{-5}$ mol·L^{-1}.

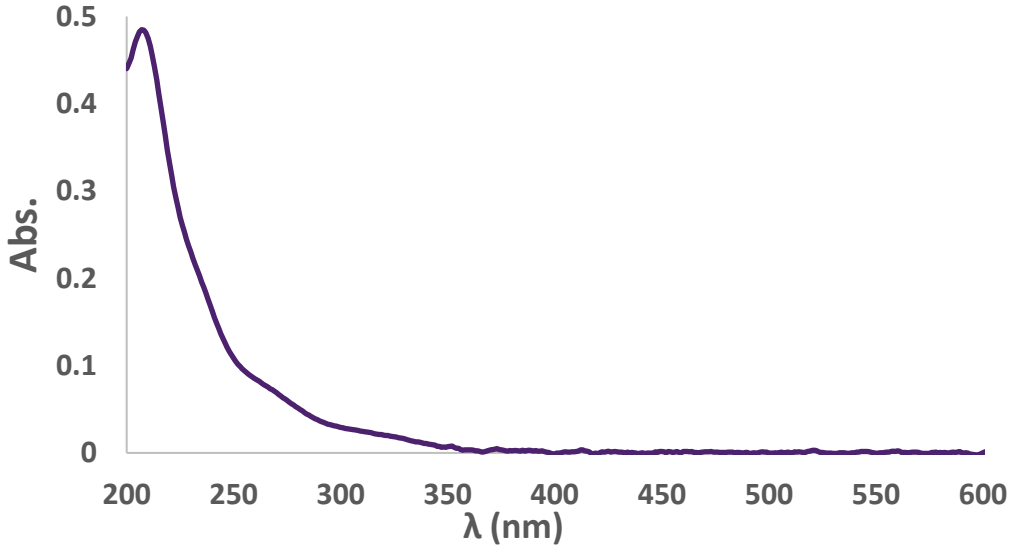

Figure 5.20 UV-vis spectrum of compound **9** in H_2O at a concentration of $2.49x10^{-5}$ mol·L^{-1}.

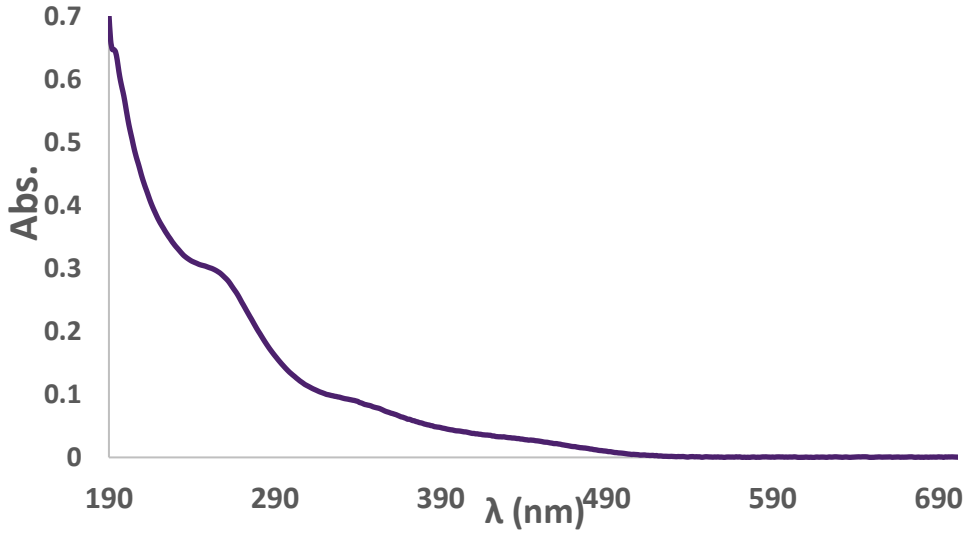

Figure 5.21 UV-vis spectrum of compound **10** in H_2O at a concentration of 2.8x10-5 mol·L-1.

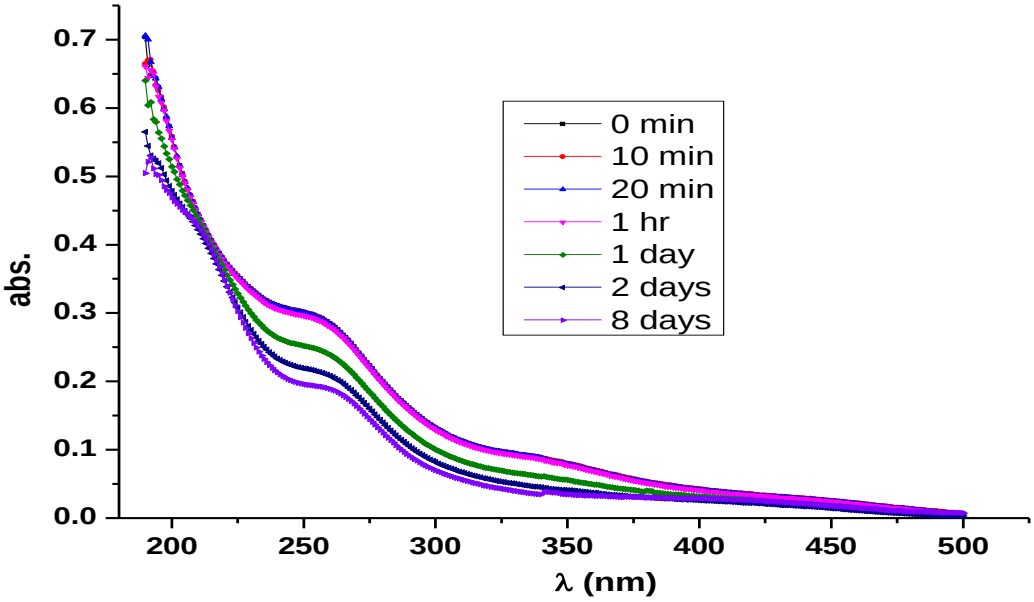

Figure 5.22 Time-dependent UV-vis spectrum of compound **10** in H_2O at a concentration of $2.8x10^{-5}$ mol·L^{-1}. The structure remains stable for at least one hour.

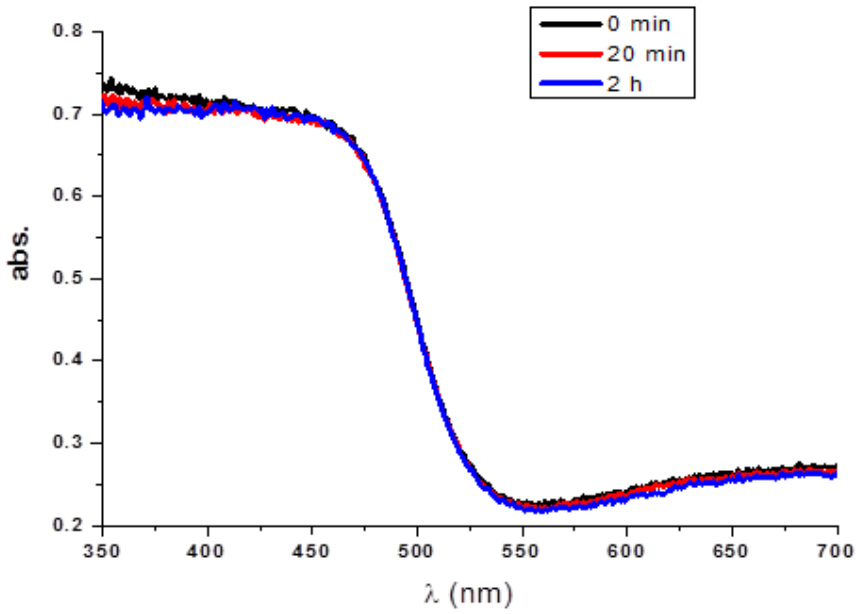

Figure 5.23 Time-dependent UV-vis spectrum of compound **10'** in D_2O/*tert*-Butanol at a concentration of $1.1x10^{-3}$ mol·L^{-1}.

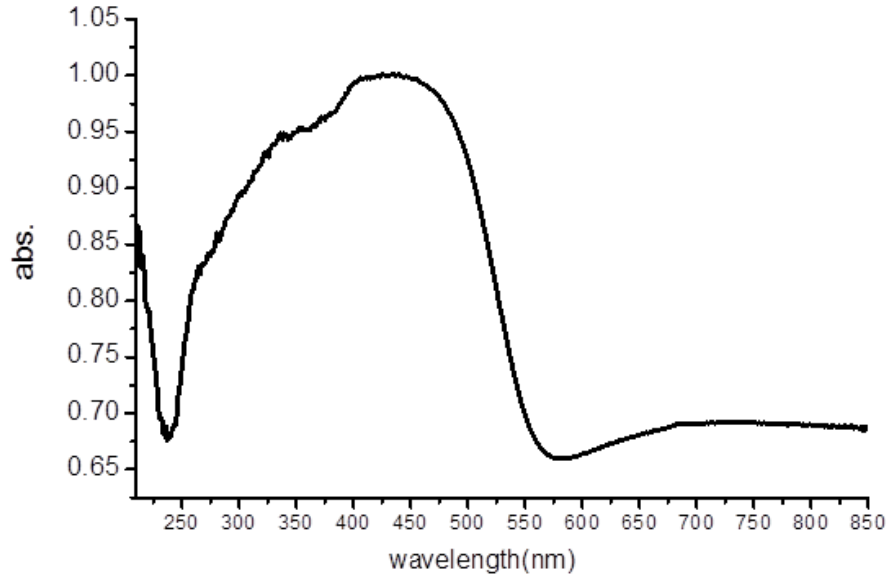

Figure 5.24 Solid state Uv-vis of compound **9** and compound **10**.

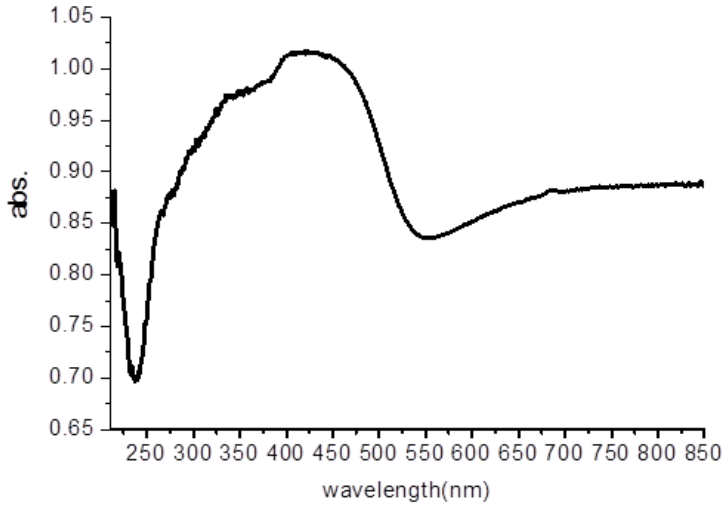

Figure 5.25 Solid state Uv-vis of compound **9'** and compound **10'**.

5.7 Thermogravimetric Analysis

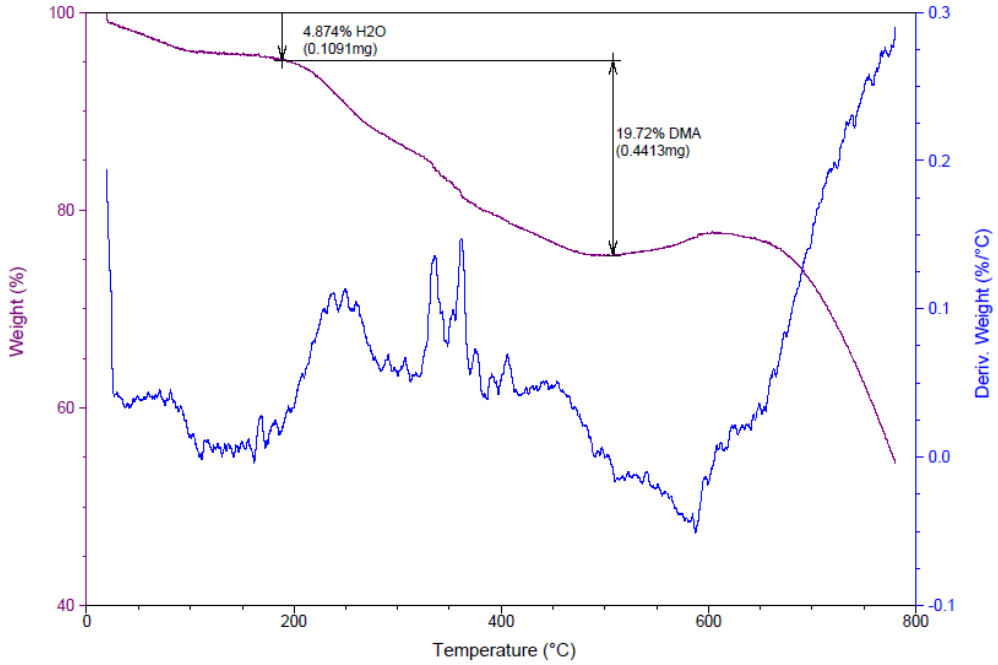

Figure 5.26 Thermal gravimetric analysis of **1**, showing the loss of ca. 5 H_2O molecules (RT – 150 °C) as well as the loss of ca. 5 DMAH cations between 150 – 500 °C.

We have not been able to perform thermogravimetric analysis of **2** due to high impurity of the compound (co-crystallization with α-Keggin).

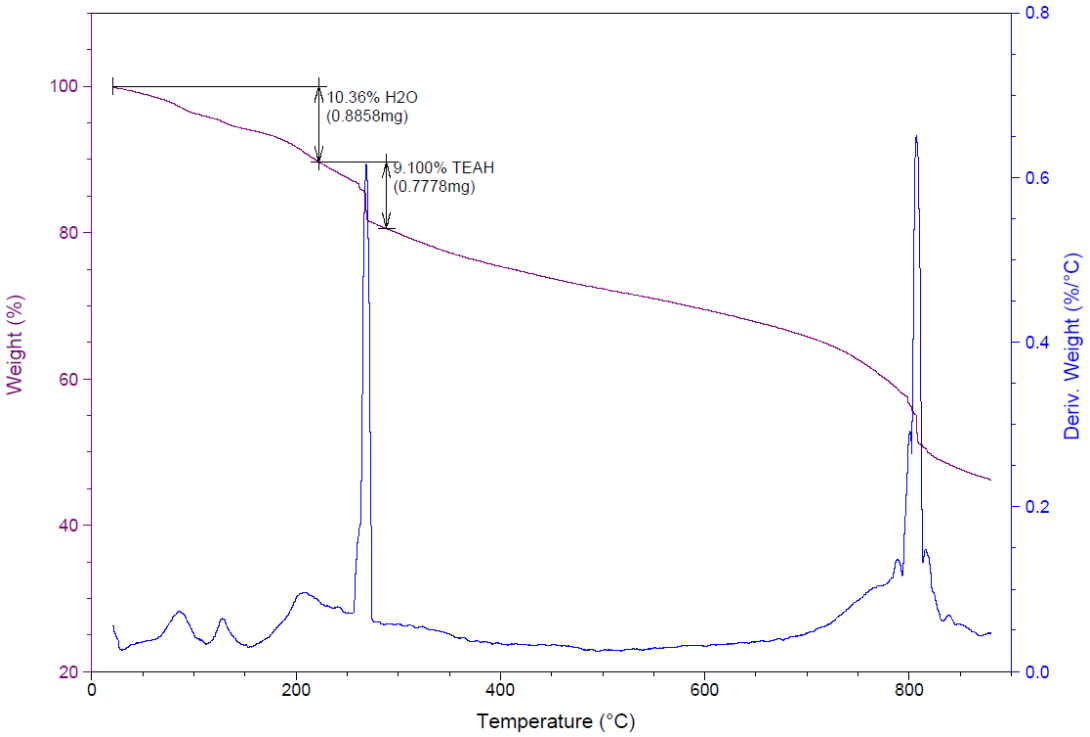

Figure 5.27 Thermal gravimetric analysis of **3**, showing the loss of ca. 16 H_2O molecules (RT – 250 ˚C) as well as the loss of ca. 6 TEAH cations between 250 – 450 °C.

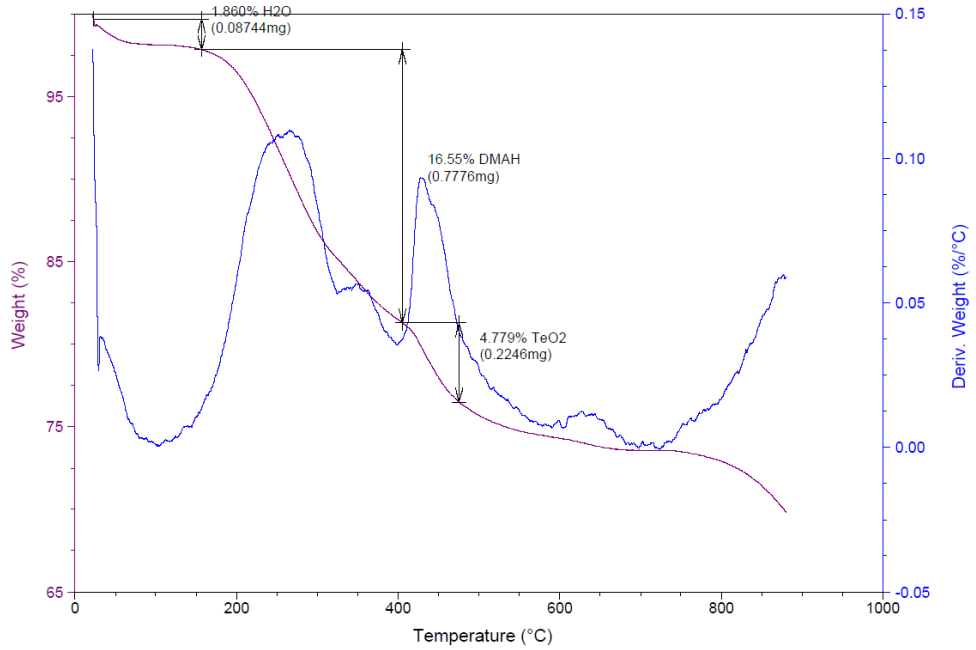

Figure 5.28 Thermal gravimetric analysis of **4**, showing the loss of ca. 14 H_2O molecules (RT – 180 ˚C), the loss of ca. 4 DMAH cations between 180 – 400 °C, as well as of the TeO_3^{2-} as TeO_2.

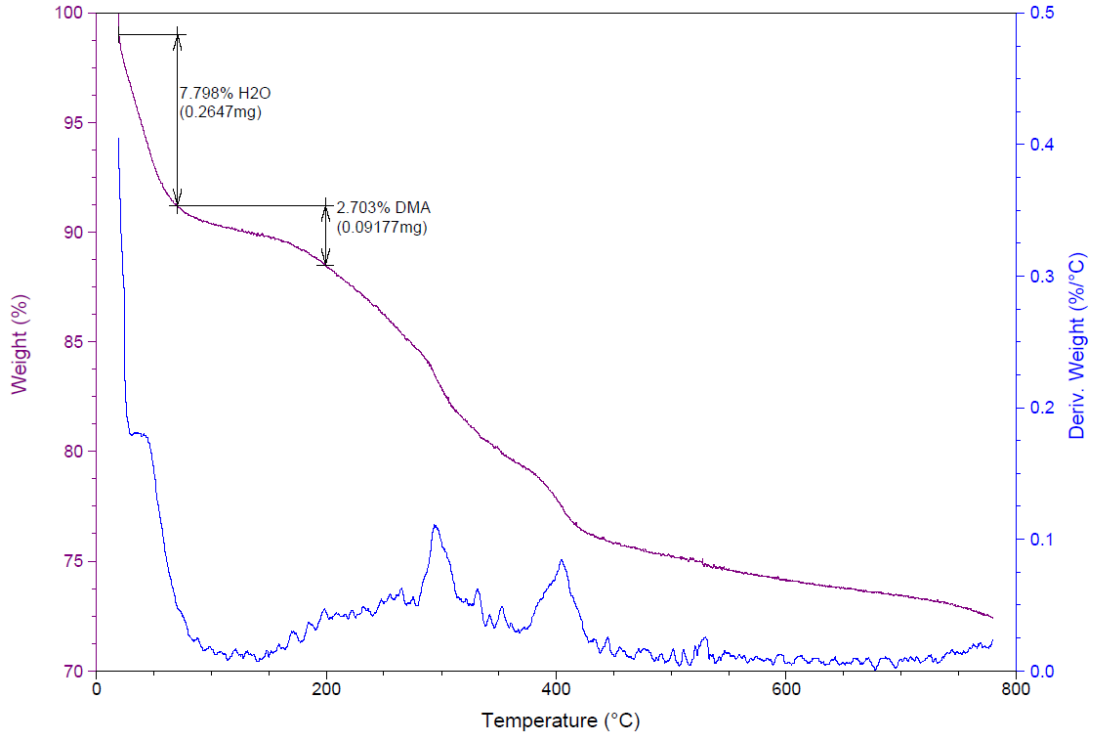

Figure 5.29 Thermal gravimetric analysis of **5**, showing the loss of ca. 15 H_2O molecules (RT – 180 ˚C) as well as the loss of ca. 3 DMAH cations between 180 – 300 °C.

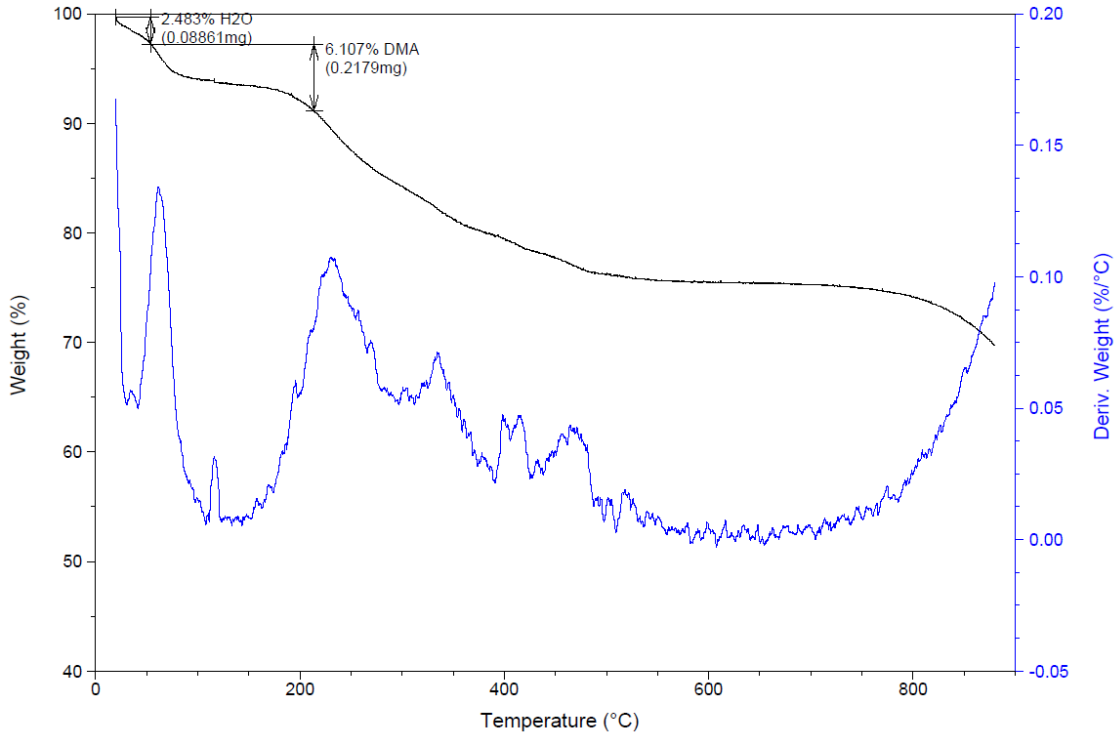

Figure 5.30 Thermal gravimetric analysis of **6**, showing the loss of ca. 13 H_2O molecules (RT – 170 ˚C) as well as the loss of ca. 4 DMAH cations between 170 – 300 °C.

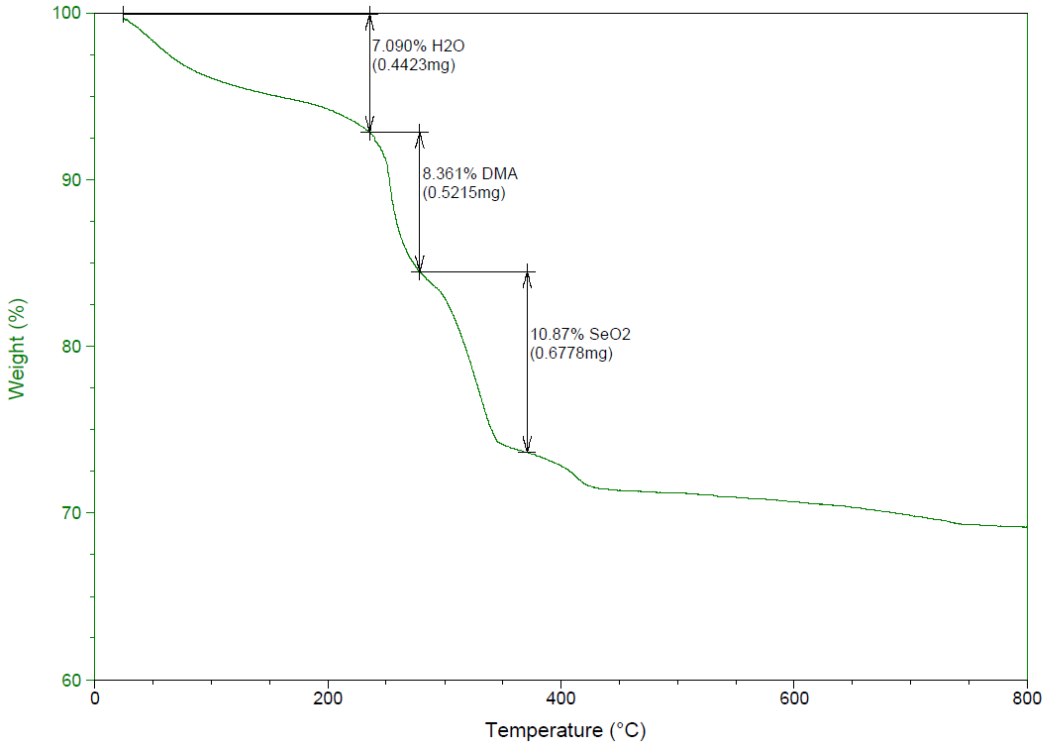

Figure 5.31 Thermal gravimetric analysis of **7**, showing the loss of ca. 34 H_2O molecules (RT – 250 °C), the loss of ca. 4 DMAH cations between 250 – 300 °C, as well as of the SeO_3^{2-}as SeO_2.

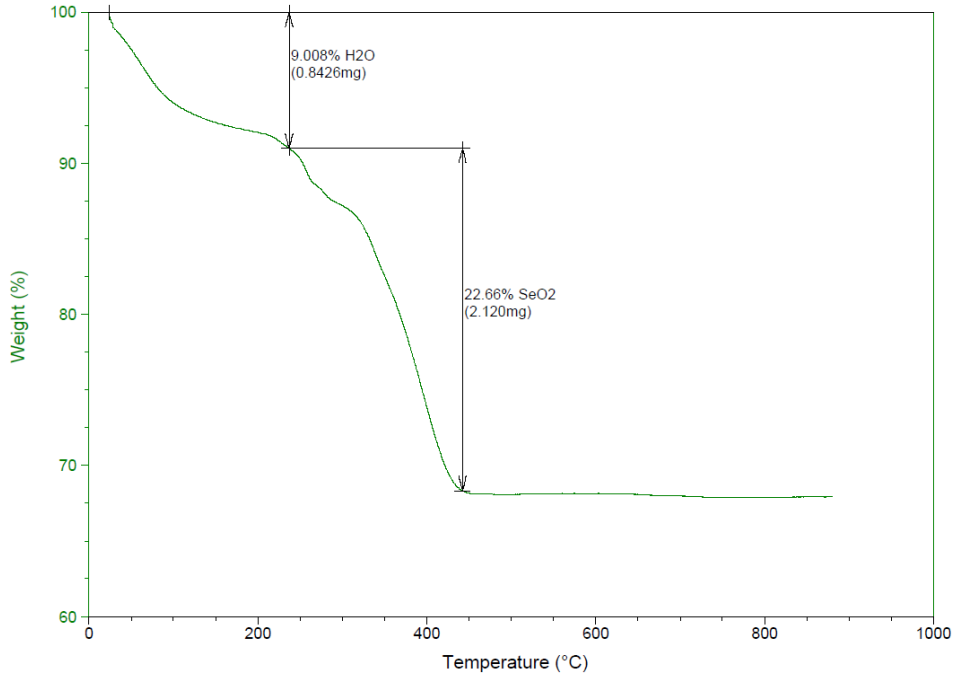

Figure 5.32 Thermal gravimetric analysis of **8**, showing the loss of ca. 23 H_2O molecules (RT – 250 °C), as well as of the SeO_3^{2-}as SeO_2 (250-400 °C).

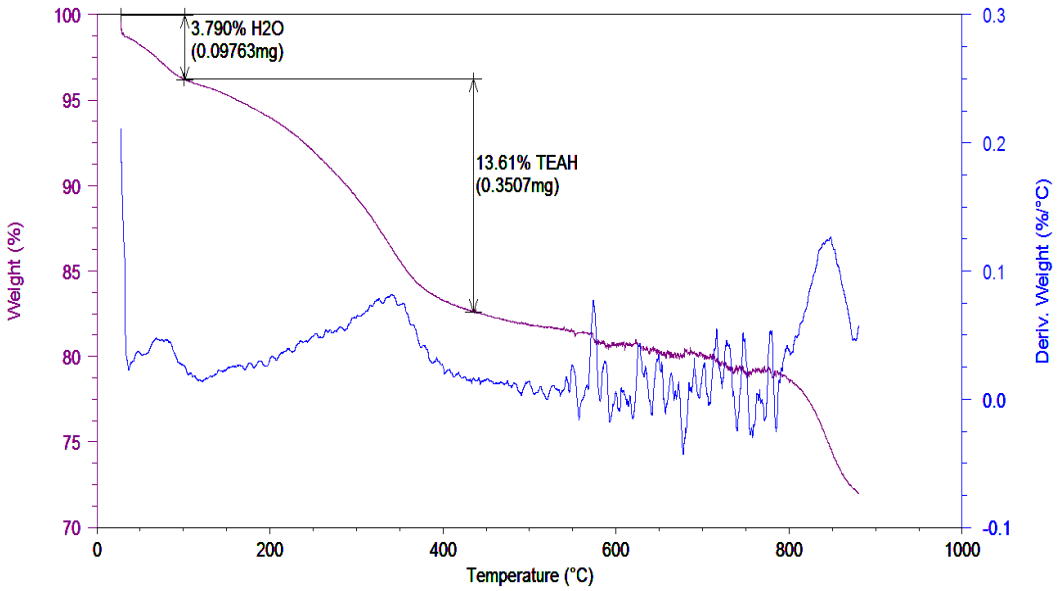

Figure 5.33 Thermal gravimetric analysis of **9**, showing the loss of ca. 5 H_2O molecules (RT – 100 °C) as well as the loss of ca. 2 TEAH cations between 100 – 450 °C.

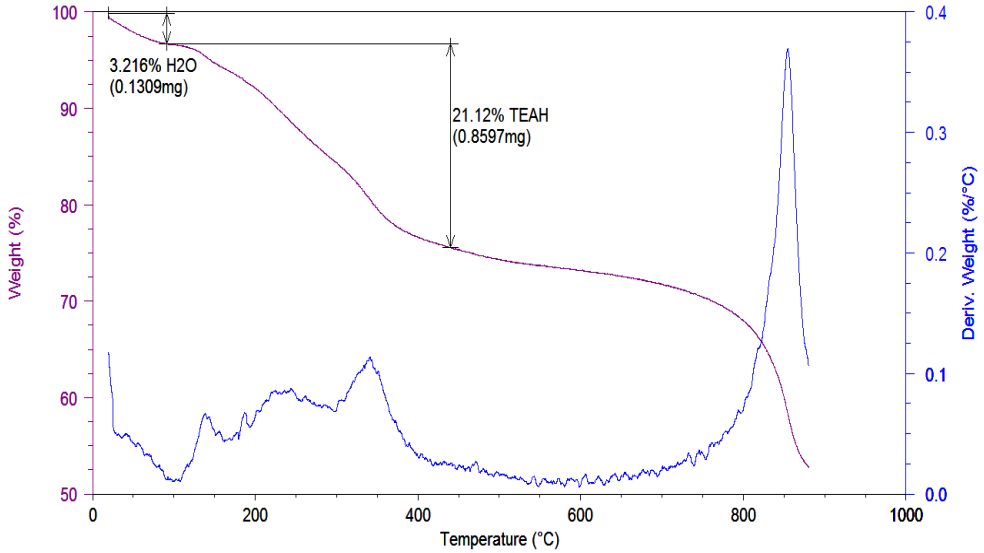

Figure 5.34 Thermal gravimetric analysis of **10**, showing the loss of ca. 4 H_2O molecules (RT – 100 °C) as well as the loss of ca. 4 TEAH cations between 100 – 450 °C.

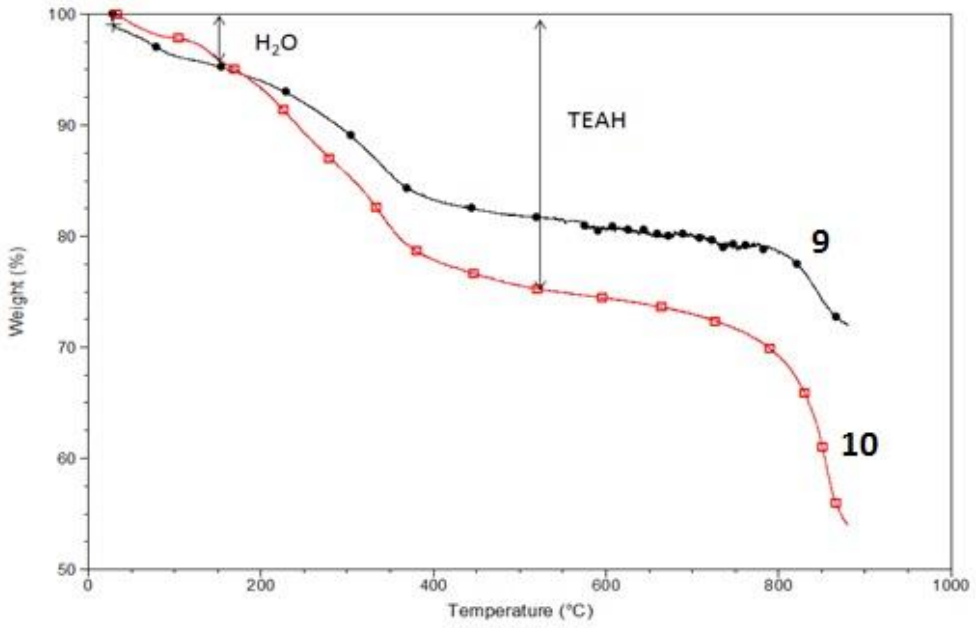

Figure 5.35 Thermogravimetric analysis of compound **9** and **10**, showing the different amount of H_2O and TEAH molecules in the crystal lattice. Percentage analysis of shown 5.33 and 5.34.

6. Crystallographic Data

This section contains only the refinement details of each structure. For full bonding distances and angles the reader is referred to the supplementary data which is deposited with this thesis and can be obtained from the University of Glasgow. Structures were solved using Patterson or Direct methods with SHELXS-97227 using WinGX routines. Refinement was accomplished by full matrix least-squares on *F2 via* SHELXL-97.3 Analytical absorption corrections were done using a multi-faced crystal model based on expressions derived by R. C. Clark and J. S. Reid; [192] whereas empirical absorption corrections were done using SADABS program on expression derived by R. H. Blessing. [193] All non-hydrogen atoms were refined anisotropically unless stated otherwise. Hydrogen positions were calculated using standard geometric criteria and refined using riding model. All data manipulation and presentation steps were performed using WinGX. Details about the structure refinement are given in tables. The following quantities are given in the information for each structure and were calculated as follows:

Equations employed:

$$\text{Goodness-of-fit (GooF)} = \left(\sqrt{\sum \frac{w(F_0^2 - F_c^2)^2}{(n-p)}} \right)$$

$$\text{Weighting scheme } w = \frac{1}{[\sigma^2(\mathrm{F}_0)^2 + (\mathrm{A}\,\mathrm{P})^2 + (\mathrm{BP})]}$$

$$\text{With } P = \frac{[\max(I_{obs,O}) + 2F_c^2]}{3}$$

p: number of parameters; *n*: number of data; A, B: weighting scheme parameters

$$\mathrm{R1} = \frac{\Sigma \,||\, \mathrm{F}_0 \,| - |\, \mathrm{F}_c \,||}{\Sigma \,|\, \mathrm{F}_o \,|}$$

$$\mathrm{wR2} = \sqrt{\frac{\Sigma[\mathrm{w}(\mathrm{F}_0^2 - \mathrm{F}_c^2)^2]}{\Sigma \mathrm{w}(\mathrm{F}_0^2)^2}}$$

$$\mathrm{R(int)} = \frac{\Sigma \left| F_0^2 - F_c^2(mean) \right|}{\Sigma \left| F_0^2 \right|}$$

Each summation involves reflections for which > 1 symmetry equivalent is averaged.

6.1 $(C_2H_8N)_5Na_2[Mo^{VI}_{11}V^{V}_{5}V^{IV}_{2}O_{52}(HPO_3)(CH_3OH)]\cdot 5H_2O$ (1)

Identification code	hst267a	
Empirical formula	C11 H55 Mo11 N5 Na2 O61 P V7	
Formula weight	2722.47	
Temperature	150(2) K	
Wavelength	0.71073 Å	
Crystal system	Triclinic	
Space group	P-1	
Unit cell dimensions	*a* = 13.2527(10) Å	α = 89.090(4)°
	b = 14.1147(11) Å	β = 83.599(4)°
	c = 19.1405(15) Å	γ = 89.054(4)°
Volume	3557.2(5) $Å^3$	
Z	2	
Density (calculated)	2.542 Mg/m^3	
Absorption coefficient	2.883 mm^{-1}	
F(000)	2608	
Crystal size	0.100 x 0.080 x 0.040 mm^3	
Theta range for data collection	1.443 to 26.000°.	
Index ranges	-16<=h<=15, -17<=k<=17, -23<=l<=23	
Reflections collected	49633	
Independent reflections	13963 [R(int) = 0.0372]	
Completeness to theta = 25.242°	99.9 %	
Refinement method	Full-matrix least-squares on F^2	
Data / restraints / parameters	13963 / 12 / 888	
Goodness-of-fit on F^2	1.048	
Final R indices [I>2sigma(I)]	R1 = 0.0388, wR2 = 0.1024	
R indices (all data)	R1 = 0.0519, wR2 = 0.1125	
Extinction coefficient	n/a	
Largest diff. peak and hole	1.775 and -1.177 $e \cdot Å^{-3}$	

6.2 $(C_2H_8N)_3Na[Mo_{12}O_{30}(HPO_3)_8]\cdot 10(H_2O)$ (2)

Identification code	hst257corange	
Empirical formula	C6 H84 Mo12 N3 Na O64 P8	
Formula weight	2826.95	
Temperature	150(2) K	
Wavelength	0.71073 Å	
Crystal system	Monoclinic	
Space group	C2/c	
Unit cell dimensions	*a* = 30.4995(11) Å	α = 90°
	b = 21.9412(11) Å	β = 108.369(3)°
	c = 13.4367(5) Å	γ = 90°
Volume	8533.6(6) $Å^3$	
Z	4	
Density (calculated)	2.200 Mg/m^3	
Absorption coefficient	1.966 mm^{-1}	
F(000)	5528	
Crystal size	0.100 x 0.050 x 0.050 mm^3	
Theta range for data collection	1.165 to 25.999°.	
Index ranges	-37<=h<=37, -27<=k<=22, -15<=l<=16	
Reflections collected	55698	
Independent reflections	8373 [R(int) = 0.0475]	
Completeness to theta = 25.242°	99.8 %	
Absorption correction	Empirical	
Max. and min. transmission	0.747 and 0.591	
Refinement method	Full-matrix least-squares on F^2	
Data / restraints / parameters	8373 / 10 / 464	
Goodness-of-fit on F^2	1.093	
Final R indices [I>2sigma(I)]	R1 = 0.0443, wR2 = 0.1199	
R indices (all data)	R1 = 0.0590, wR2 = 0.1341	
Extinction coefficient	n/a	
Largest diff. peak and hole	1.93 and -0.91 $e\cdot Å^{-3}$	

6.3 $(C_6H_{16}NO_3)_6Na_8H[Mo_6O_{18}(HPO_3)(C_6H_{13}NO_3)]_2(PV_4Mo_8O_{40})\cdot 32(H_2O)$ (3)

Identification code	hst261b	
Empirical formula	C48 H189 Mo20 N8 Na8 O138 P3 V4	
Formula weight	5486.45	
Temperature	150(2) K	
Wavelength	0.71073 Å	
Crystal system	Triclinic	
Space group	P-1	
Unit cell dimensions	*a* = 13.6486(4) Å	α = 88.851(2)°
	b = 14.3630(3) Å	β = 87.794(2)°
	c = 22.2878(5) Å	γ = 64.454(2)°
Volume	3939.10(18) $Å^3$	
Z	1	
Density (calculated)	2.313 Mg/m^3	
Absorption coefficient	1.936 mm^{-1}	
F(000)	2702	
Crystal size	0.265 x 0.091 x 0.054 mm^3	
Theta range for data collection	2.853 to 26.000°.	
Index ranges	-16<=h<=16, -17<=k<=17, -27<=l<=27	
Reflections collected	63848	
Independent reflections	15494 [R(int) = 0.0487]	
Completeness to theta = 25.242°	99.9 %	
Absorption correction	Analytical	
Max. and min. transmission	0.845 and 0.488	
Refinement method	Full-matrix least-squares on F^2	
Data / restraints / parameters	15494 / 18 / 1026	
Goodness-of-fit on F^2	1.059	
Final R indices [I>2sigma(I)]	R1 = 0.0440, wR2 = 0.1006	
R indices (all data)	R1 = 0.0597, wR2 = 0.1082	
Extinction coefficient	n/a	
Largest diff. peak and hole	1.31 and -1.11 $e\cdot Å^{-3}$	

6.4 $(C_2H_8N)_6Na[Mo^{VI}_{11}V^{V}_{5}V^{IV}_{2}O_{52}(TeO_3)]\cdot 15H_2O$ (4)

Identification code	hst373	
Empirical formula	C12 H78 Mo11 N6 Na O70 Te V7	
Formula weight	2989.31	
Temperature	150(2) K	
Wavelength	0.71073 Å	
Crystal system	Orthorhombic	
Space group	Pnma	
Unit cell dimensions	*a* = 28.1994(10) Å	α = 90°
	b = 20.6903(7) Å	β = 90°
	c = 14.6394(5) Å	γ = 90°
Volume	8541.4(5) $Å^3$	
Z	4	
Density (calculated)	2.325 Mg/m^3	
Absorption coefficient	2.728 mm^{-1}	
F(000)	5752	
Crystal size	0.100 x 0.050 x 0.040 mm^3	
Theta range for data collection	1.969 to 26.000°.	
Index ranges	-33<=h<=34, -25<=k<=25, -18<=l<=13	
Reflections collected	64752	
Independent reflections	8623 [R(int) = 0.0500]	
Completeness to theta = 25.242°	99.9 %	
Refinement method	Full-matrix least-squares on F^2	
Data / restraints / parameters	8623 / 7 / 458	
Goodness-of-fit on F^2	1.175	
Final R indices [I>2sigma(I)]	R1 = 0.0558, wR2 = 0.1525	
R indices (all data)	R1 = 0.0738, wR2 = 0.1746	
Extinction coefficient	n/a	
Largest diff. peak and hole	1.894 and -1.736 $e \cdot Å^{-3}$	

6.5 $K_4(C_2H_8N)_3[Mo^{VI}_{12}V^{V}_3O_{39}(\mu_6\text{-}TeO_4)_3(\mu_6\text{-}TeO_3)_2]\cdot 14(H_2O)$ (5)

Identification code	hst4310a_lfs	
Empirical formula	C6 H52 K4 Mo12 N3 O71 Te5 V3	
Formula weight	3401.00	
Temperature	150(2) K	
Wavelength	0.71073 Å	
Crystal system	Hexagonal	
Space group	P6/mmm	
Unit cell dimensions	*a* = 21.2945(4) Å	α = 90°
	b = 21.2945(4) Å	β = 90°
	c = 13.2491(2) Å	γ = 120°
Volume	5203.0(2) $Å^3$	
Z	2	
Density (calculated)	2.171 Mg/m^3	
Absorption coefficient	3.270 mm^{-1}	
F(000)	3172	
Crystal size	0.349 x 0.134 x 0.120 mm^3	
Theta range for data collection	2.922 to 25.998°.	
Index ranges	-26<=h<=26, -26<=k<=25, -16<=l<=16	
Reflections collected	44141	
Independent reflections	2016 [R(int) = 0.0384]	
Completeness to theta = 25.242°	99.4 %	
Refinement method	Full-matrix least-squares on F^2	
Data / restraints / parameters	2016 / 2 / 113	
Goodness-of-fit on F^2	1.140	
Final R indices [I>2sigma(I)]	R1 = 0.0309, wR2 = 0.1038	
R indices (all data)	R1 = 0.0327, wR2 = 0.1054	
Extinction coefficient	n/a	
Largest diff. peak and hole	2.043 and -0.684 $e \cdot Å^{-3}$	

6.6 $Na_3(C_2H_8N)_4[Mo^{VI}_{12}V^{V}_3(\mu_6\text{-}TeO_4)_3(\mu_6\text{-}TeO_3)_2O_{39}]\cdot 15(H_2O)$ (6)

Identification code	hst380b1	
Empirical formula	C8 H62 Mo12 N4 Na3 O72 Te5 V3	
Formula weight	3377.68	
Temperature	150(2) K	
Wavelength	0.71073 Å	
Crystal system	Monoclinic	
Space group	P21/c	
Unit cell dimensions	*a* = 13.075(2) Å	α = 90°.
	b = 26.169(4) Å	β = 120.125(8)°
	c = 25.458(3) Å	γ = 90°.
Volume	7534(2) $Å^3$	
Z	4	
Density (calculated)	2.978 Mg/m^3	
Absorption coefficient	4.316 mm^{-1}	
F(000)	6320	
Crystal size	0.100 x 0.070 x 0.040 mm^3	
Theta range for data collection	1.209 to 26.000°.	
Index ranges	-16<=h<=16, -32<=k<=32, -31<=l<=31	
Reflections collected	104263	
Independent reflections	14794 [R(int) = 0.0505]	
Completeness to theta = 25.242°	100.0 %	
Absorption correction	Empirical	
Max. and min. transmission	0.7454 and 0.6075	
Refinement method	Full-matrix least-squares on F^2	
Data / restraints / parameters	14794 / 8 / 970	
Goodness-of-fit on F^2	1.068	
Final R indices [I>2sigma(I)]	R1 = 0.0310, wR2 = 0.0718	
R indices (all data)	R1 = 0.0404, wR2 = 0.0784	
Extinction coefficient	n/a	
Largest diff. peak and hole	1.80 and -0.81 $e \cdot Å^{-3}$	

6.7 $Na_{15}(C_2H_8N)_6[K_6(Mo_{11}V_7SeO_{55})(Mo_5V_4Se_4O_{36})_3]\cdot 36(H_2O)$ (7)

Identification code	hst478b1	
Empirical formula	C12 H120 K6 Mo26 N6 Na15 O199 Se13 V19	
Formula weight	8601.36	
Temperature	150(2) K	
Wavelength	0.71073 Å	
Crystal system	Trigonal	
Space group	R-3m	
Unit cell dimensions	*a* = 33.1149(11) Å	α = 90°
	b = 33.1149(16) Å	β = 90°
	c = 39.786(3) Å	γ = 120.000(15)°
Volume	37784(4) $Å^3$	
Z	6	
Density (calculated)	2.268 Mg/m^3	
Absorption coefficient	4.019 mm^{-1}	
F(000)	24456	
Crystal size	0.100 x 0.050 x 0.050 mm^3	
Theta range for data collection	1.947 to 26.000°.	
Index ranges	-40<=h<=40, -40<=k<=31, -49<=l<=48	
Reflections collected	126070	
Independent reflections	8719 [R(int) = 0.0657]	
Completeness to theta = 25.242°	99.9 %	
Absorption correction	Empirical	
Max. and min. transmission	0.746 and 0.570	
Refinement method	Full-matrix least-squares on F^2	
Data / restraints / parameters	8719 / 0 / 469	
Goodness-of-fit on F^2	1.077	
Final R indices [I>2sigma(I)]	R1 = 0.0669, wR2 = 0.1920	
R indices (all data)	R1 = 0.0908, wR2 = 0.2264	
Extinction coefficient	n/a	
Largest diff. peak and hole	4.07 and -1.72 $e\cdot Å^{-3}$	

6.8 $K_8Na_6[Mo_6V_{16}Se_8O_{79}]\cdot 25(H_2O)$ (8)

Identification code	hst483c	
Empirical formula	H50 K8 Mo6 Na6 O104 Se8 V16	
Formula weight	4750.06	
Temperature	293(2) K	
Wavelength	0.71073 Å	
Crystal system	Trigonal	
Space group	P3221	
Unit cell dimensions	*a* = 21.0146(10) Å	α = 90°
	b = 21.0146(10) Å	β = 90°
	c = 22.0171(16) Å	γ = 120°
Volume	8420.4(10) $Å^3$	
Z	2	
Density (calculated)	1.873 Mg/m^3	
Absorption coefficient	3.021 mm^{-1}	
F(000)	4550	
Theta range for data collection	1.119 to 30.228°.	
Index ranges	-29<=h<=29, -29<=k<=29, -29<=l<=31	
Reflections collected	81006	
Independent reflections	15950 [R(int) = 0.0776]	
Completeness to theta = 25.242°	92.4 %	
Refinement method	Full-matrix least-squares on F^2	
Data / restraints / parameters	15950 / 0 / 322	
Goodness-of-fit on F^2	1.038	
Final R indices [I>2sigma(I)]	R1 = 0.0710, wR2 = 0.2243	
R indices (all data)	R1 = 0.1023, wR2 = 0.2397	
Absolute structure parameter	0.186(4)	
Extinction coefficient	n/a	
Largest diff. peak and hole	4.612 and -2.614 $e \cdot Å^{-3}$	

6.9 $(C_6H_{16}NO_3)_2Na_3[H_2W^{VI}_4V^{V}_8(V^{V}O_4)O_{33}(C_6H_{13}NO_3)]\cdot 8H_2O$ (9)

Identification code	hst154cy	
Empirical formula	C18 H63 N3 Na3 O54 V9 W4	
Formula weight	2448.54	
Temperature	150(2) K	
Wavelength	0.71073 Å	
Crystal system	Monoclinic	
Space group	P21/c	
Unit cell dimensions	*a* = 12.2670(9) Å	α = 90°
	b = 16.6290(14) Å	β = 95.886(3)°
	c = 29.488(2) Å	γ = 90°
Volume	5983.4(8) $Å^3$	
Z	4	
Density (calculated)	2.718 Mg/m^3	
Absorption coefficient	9.132 mm^{-1}	
F(000)	4640	
Crystal size	0.110 x 0.070 x 0.040 mm^3	
Theta range for data collection	1.408 to 25.999°.	
Index ranges	-13<=h<=15, -12<=k<=20, -30<=l<=35	
Reflections collected	44468	
Independent reflections	11527 [R(int) = 0.0484]	
Completeness to theta = 25.242°	98.3 %	
Absorption correction	Empirical	
Max. and min. transmission	0.746 and 0.516	
Refinement method	Full-matrix least-squares on F^2	
Data / restraints / parameters	11527 / 4 / 814	
Goodness-of-fit on F^2	1.021	
Final R indices [I>2sigma(I)]	R1 = 0.0436, wR2 = 0.1024	
R indices (all data)	R1 = 0.0646, wR2 = 0.1129	
Extinction coefficient	n/a	
Largest diff. peak and hole	2.11 and -2.07 $e\cdot Å^{-3}$	

6.10 $(C_6H_{16}NO_3)_2Na_3[H_4W^{VI}_4V_2^{IV}V^V_6(V^VO_4)O_{33}(C_6H_{13}NO_3)]\cdot 8H_2O$ (9')

Identification code	hst154cc	
Empirical formula	C18 H65 N3 Na3 O54 V9 W4	
Formula weight	2450.56	
Temperature	150(2) K	
Wavelength	0.71073 Å	
Crystal system	Monoclinic	
Space group	P21/c	
Unit cell dimensions	*a* = 12.3297(11) Å	α = 90°
	b = 16.8007(15) Å	β = 95.831(5)°
	c = 29.241(3) Å	γ = 90°
Volume	6025.9(10) Å^3	
Z	4	
Density (calculated)	2.701 Mg/m^3	
Absorption coefficient	9.068 mm^{-1}	
F(000)	4648	
Crystal size	0.100 x 0.060 x 0.050 mm^3	
Theta range for data collection	1.400 to 26.000°.	
Index ranges	-15<=h<=12, -20<=k<=19, -36<=l<=36	
Reflections collected	53964	
Independent reflections	11841 [R(int) = 0.0618]	
Completeness to theta = 25.242°	100.0 %	
Absorption correction	Empirical	
Max. and min. transmission	0.746 and 0.579	
Refinement method	Full-matrix least-squares on F^2	
Data / restraints / parameters	11841 / 8 / 817	
Goodness-of-fit on F^2	1.132	
Final R indices [I>2sigma(I)]	R1 = 0.0537, wR2 = 0.1120	
R indices (all data)	R1 = 0.0752, wR2 = 0.1203	
Extinction coefficient	n/a	
Largest diff. peak and hole	1.62 and -1.46 e·Å^{-3}	

6.11 $(C_6H_{16}NO_3)_4Na[H_2W^{VI}_4V^{V}_8(V^{V}O_4)O_{33}(C_6H_{13}NO_3)]\cdot 4H_2O$ (10)

Identification code	hst154cb	
Empirical formula	C30 H87 N5 Na O56 V9 W4	
Formula weight	2630.89	
Temperature	150(2) K	
Wavelength	0.71073 Å	
Crystal system	Monoclinic	
Space group	P21/m	
Unit cell dimensions	*a* = 17.3940(12) Å	α= 90°
	b = 12.2133(9) Å	β= 107.620(3)°
	c = 17.7973(11) Å	γ = 90°
Volume	3603.4(4) $Å^3$	
Z	2	
Density (calculated)	2.425Mg/m^3	
Absorption coefficient	7.583 mm^{-1}	
F(000)	2528	
Crystal size	0.110 x 0.050 x 0.040 mm	
Theta range for data collection	1.200 to 25.999°.	
Index ranges	-21<=h<=21, -15<=k<=15, -21<=l<=21	
Reflections collected	50491	
Independent reflections	7423 [R(int) = 0.0414]	
Completeness to theta = 25.242°	99.9 %	
Absorption correction	Empirical	
Max. and min. transmission	0.747 and 0.445	
Refinement method	Full-matrix least-squares on F^2	
Data / restraints / parameters	7423 / 14 / 375	
Goodness-of-fit on F^2	1.161	
Final R indices [I>2sigma(I)]	R1 = 0.0630, wR2 = 0.1846	
R indices (all data)	R1 = 0.0860, wR2 = 0.2317	
Extinction coefficient	n/a	
Largest diff. peak and hole	2.62 and -2.01 e·$Å^{-3}$	

6.12 $(C_6H_{16}NO_3)_4Na[H_4W^{VI}_4V_2^{IV}V^V_6(V^VO_4)O_{33}(C_6H_{13}NO_3)]\cdot 4H_2O$ (10‘)

Identification code	hst154cbg	
Empirical formula	C30 H89 N5 Na O56 V9 W4	
Formula weight	2632.91	
Temperature	150(2) K	
Wavelength	0.71073 Å	
Crystal system	Monoclinic	
Space group	P 21/m	
Unit cell dimensions	*a* = 17.4595(14) Å	α= 90°.
	b = 12.2435(9) Å	β= 107.843(4)°.
	c = 17.8245(13) Å	γ = 90°.
Volume	3627.0(5) $Å^3$	
Z	2	
Density (calculated)	2.411 Mg/m^3	
Absorption coefficient	7.534 mm^{-1}	
F(000)	2532	
Crystal size	0.204 x 0.066 x 0.056 mm^3	
Theta range for data collection	1.960 to 25.998°.	
Index ranges	-21<=h<=21, -14<=k<=15, -20<=l<=21	
Reflections collected	62363	
Independent reflections	7490 [R(int) = 0.0598]	
Completeness to theta = 25.242°	99.9 %	
Absorption correction	Empirical	
Max. and min. transmission	0.801 and 0.403	
Refinement method	Full-matrix least-squares on F^2	
Data / restraints / parameters	7490 / 14 / 375	
Goodness-of-fit on F^2	1.130	
Final R indices [I>2sigma(I)]	R1 = 0.0701, wR2 = 0.1816	
R indices (all data)	R1 = 0.1005, wR2 = 0.2319	
Extinction coefficient	n/a	
Largest diff. peak and hole	2.74 and -2.27 $e\cdot Å^{-3}$	

7. Experimental Operations

7.1 Command Scripts

In order to communicate the PC and the Tricontinent pumps a language created by the pump manufacturer was used. The command scripts are lineal stream codes and edited by using main command functions, such as IP (Input Pulse), OD (Output Dispense) and V (Velocity). Specific examples of "bracket" command scripts for Pump number 1, are shown below, to operate three 5 mL injections at 10 mL/min (1), to re-start/initialize the pump (2) and to transform to normal mode (3).

(1) /**1**gV3000IP3000V3000ODG3**R**

(2) /**1**Z**R**

(3) /**1**N0**R**

The 1-to-14 pumps are named as: /1-/9, /:, /;, /<, /= and />, respectively.

7.2 General steps to operate the Linear Flow System

The procedure to operate the device is as follows:
(1) Plan the experiment and sequence of operations.
(2) Create the .txt file using the language based on unit operations (see section 7.3).
(3) Check the system is well-connected, the pumps and the tubing are clean.
(4) Set the LabVIEW .vi file (see section 7.4).
(5) Check that the glass reactors and tubing are dry and flush some of each reagent through each syringe pump.
(6) Import the .txt file into the LabVIEW front panel and execute it.
(7) Run the sequence of experiments and wait for collection.

7.3 How to create the *.txt* file

The experimental conditions need to be added as .txt file. This file can be created either using text editors or Excel worksheets, see figure 7.1.

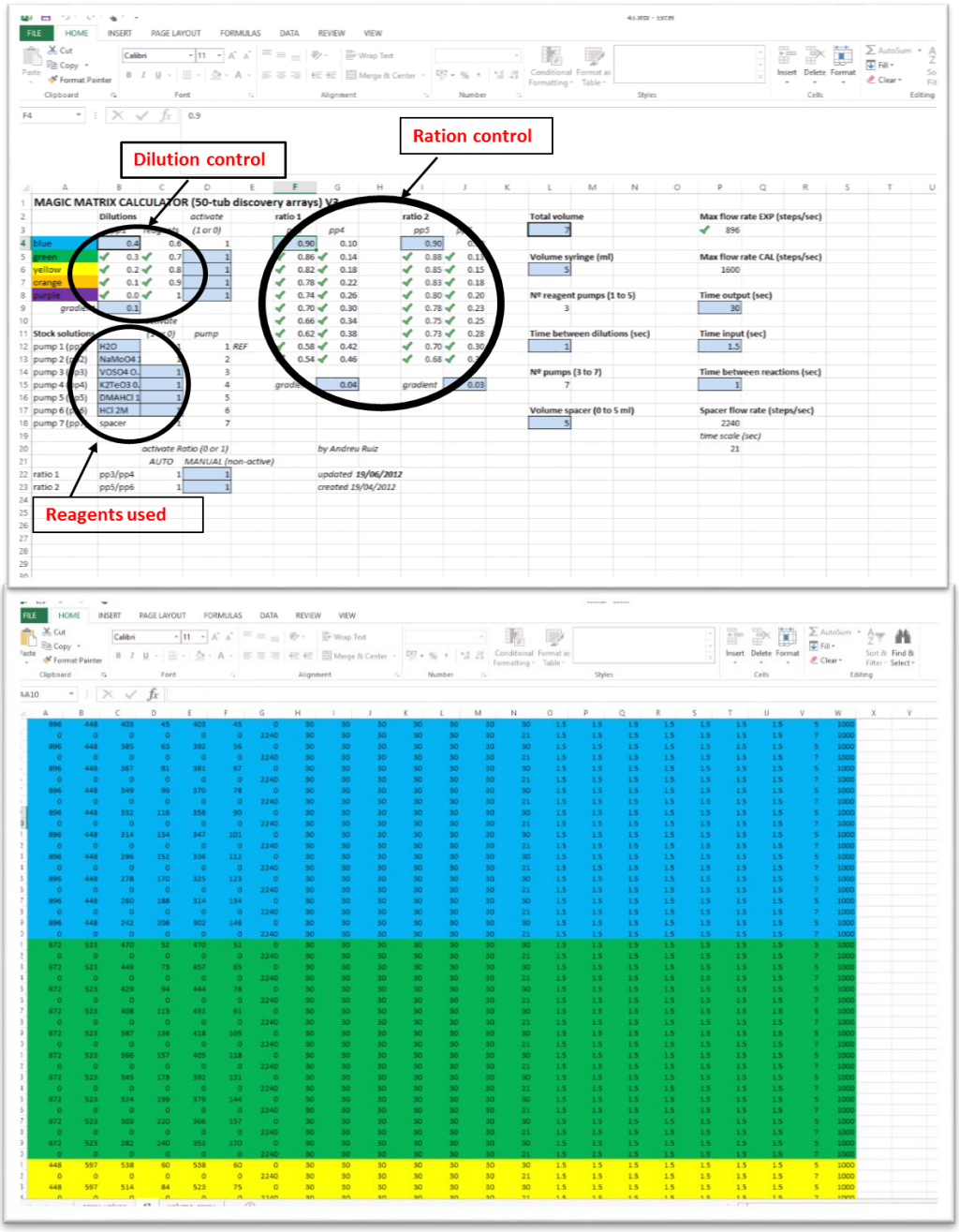

Figure 7.1 An Excel based front panel (top) and an example of *.txt* file (bottom), are shown above.

The .txt file must contain the X x Y table (X, number of rows and Y, number of columns), where Y = 3i+2, where i is the number of pumps. Each row corresponds to a set of pumping operations (input S, output O and transfer P), according to the configuration of the networked system. The table has always the same inner column structure; however the size of the array may vary depending on the features of the reactor and the synthesis protocol chosen. The X x Y table must have five sections:

i. A first set of columns contains the pumping rates for each pump, in steps/second (where 1600 plunger steps mean 5 mL, in 30 sec).

ii. The second set of columns is related to the expel/dispense time (to) for each pump, in seconds.

iii. The third set of columns is related to the filling time (ti) for each pump, in seconds.

iv. The RP single column refers to the "reference pump" in each set of operations; this column is required for the LabVIEW processing.

v. The Δt single column has the delay time (in micro-seconds) at the end of each reagent mixture.

7.4 .vi files in LabVIEW

The Figure 7.2 shows a snapshot of the plain view of the control panel from the PC screen. The procedure is described below:

(1) Press "Initialize Pumps to micro mode" button.

(2) Select the number of pumps used in the experiment sequence.

(3) Select the VISA resource name (COM-USB connection).

(4) Browse the .txt file.

(5) Press "Go" button to initiate the experiment sequence.

Each set of autonomously generated commands is displayed in the viewer panel (6) and the number of rows, n, is also displayed on the right of the front panel (7).

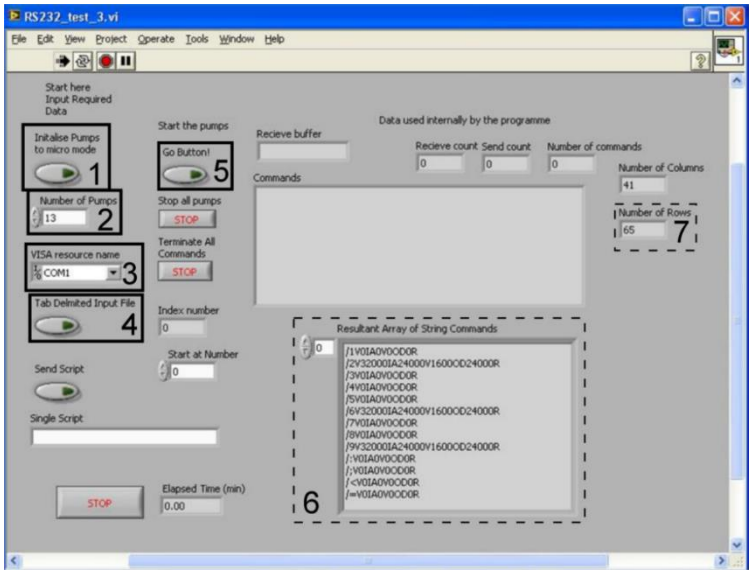

Figure 7.2 Scheme of the work-flow and the LabVIEW front panel is shown above.

7.5 Volume arrays

Table 7.1 The volumes of starting stock solutions for the synthesis of compound **5**.

H_2O	$NaMoO_4 \cdot 2H_2O$	$VOSO_4 \cdot xH_2O$	K_2TeO_3	DMA·HCl	HCl	
2.80	1.40	1.26	0.14	1.26	0.14	1a
2.80	1.40	1.20	0.20	1.23	0.18	2a
2.80	1.40	1.15	0.25	1.19	0.21	3a
2.80	1.40	1.09	0.31	1.16	0.25	4a
2.80	1.40	1.04	0.36	1.12	0.28	5a
2.80	1.40	0.98	0.42	1.09	0.32	6a
2.80	1.40	0.92	0.48	1.05	0.35	7a
2.80	1.40	0.87	0.53	1.02	0.39	8a
2.80	1.40	0.81	0.59	0.98	0.42	9a
2.80	1.40	0.76	0.64	0.95	0.46	10a
2.10	1.63	1.47	0.16	1.47	0.16	1a
2.10	1.63	1.40	0.23	1.43	0.20	2a
2.10	1.63	1.34	0.29	1.39	0.25	3a
2.10	1.63	1.27	0.36	1.35	0.29	4a
2.10	1.63	1.21	0.42	1.31	0.33	5a
2.10	1.63	1.14	0.49	1.27	0.37	6a
2.10	1.63	1.08	0.56	1.23	0.41	7a
2.10	1.63	1.01	0.62	1.18	0.45	8a
2.10	1.63	0.95	0.69	1.14	0.49	9a
2.10	1.63	0.88	0.75	1.10	0.53	10a
1.40	1.87	1.68	0.19	1.68	0.19	1a
1.40	1.87	1.61	0.26	1.63	0.23	2a
1.40	1.87	1.53	0.34	1.59	0.28	3a
1.40	1.87	1.46	0.41	1.54	0.33	4a
1.40	1.87	1.38	0.49	1.49	0.37	5a
1.40	1.87	1.31	0.56	1.45	0.42	6a
1.40	1.87	1.23	0.63	1.40	0.47	7a
1.40	1.87	1.16	0.71	1.35	0.51	8a
1.40	1.87	1.08	0.78	1.31	0.56	9a
1.40	1.87	1.01	0.86	1.26	0.61	10a
0.70	2.10	1.89	0.21	1.89	0.21	1a
0.70	2.10	1.81	0.29	1.84	0.26	2a
0.70	2.10	1.72	0.38	1.79	0.32	3a
0.70	2.10	1.64	0.46	1.73	0.37	4a
0.70	2.10	1.55	0.55	1.68	0.42	5a
0.70	2.10	1.47	0.63	1.63	0.47	6a
0.70	2.10	1.39	0.71	1.58	0.53	7a

0.70	2.10	1.30	0.80	1.52	0.58	8a
0.70	2.10	1.22	0.88	1.47	0.63	9a
0.70	2.10	1.13	0.97	1.42	0.68	10a
0.00	2.33	2.10	0.23	2.10	0.23	1a
0.00	2.33	2.01	0.33	2.04	0.29	2a
0.00	2.33	1.91	0.42	1.98	0.35	3a
0.00	2.33	1.82	0.51	1.93	0.41	4a
0.00	2.33	1.73	0.61	1.87	0.47	5a
0.00	2.33	1.63	0.70	1.81	0.53	6a
0.00	2.33	1.54	0.79	1.75	0.58	7a
0.00	2.33	1.45	0.89	1.69	0.64	8a
0.00	2.33	1.35	0.98	1.63	0.70	9a
0.00	2.33	1.26	1.07	1.58	0.76	10a
70	93.33	67.2	26.13	73.5	19.83	Total

8. Appendices

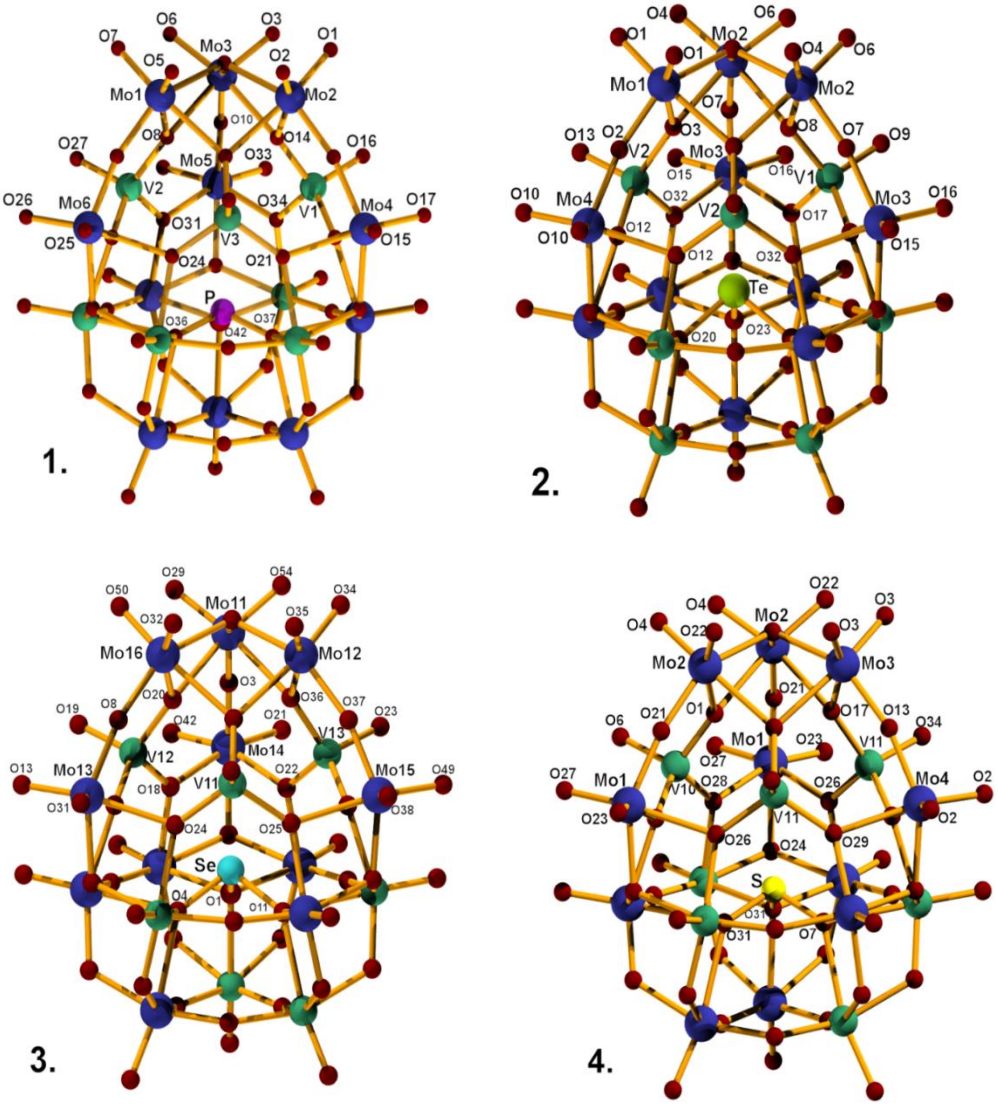

Figure 8.1 Balls and sticks representation of the 4 egg-shaped Dawson compounds: 1) $\{Mo_{11}V_7P\}$, 2) $\{Mo_{11}V_7Te\}$, 3) $\{Mo_{11}V_7Se\}$ and 4) $\{Mo_{11}V_7S\}$ showing the position of the metal centres in the clusters. Colour code: Mo: indigo, V: sea green, O: red, P: pink, Te: lime, Se: aqua, S: yellow

Table 8.1 Selected bond lengths and angles of the 4 egg-shaped compounds.

P	Å	Te	Å	Se	Å	S	Å
Mo(1)-O(7)	1.701(4)	Mo(1)-O(1)	1.698(7)	Mo(11)-O(29)	1.647(17)	Mo(1)-O(23)	1.705(4)
Mo(1)-O(5)	1.702(4)	Mo(1)-O(3)	2.262(6)	Mo(11)-O(54)	1.699(17)	Mo(1)-O(27)	1.715(3)
Mo(2)-O(1)	1.698(4)	Mo(2)-O(4)	1.698(7)	Mo(11)-O(3)	1.904(17)	Mo(1)-O(21	1.867(3)
Mo(2)-O(4)	1.718(4)	Mo(2)-O(6)	1.708(7)	Mo(11)-O(20)	2.257(14)	Mo(2)-O(22)	1.698(4)
Mo(3)-O(3)	1.695(4)	Mo(2)-O(7)	1.876(7	Mo(11)-O(36)	2.273(14)	Mo(2)-O(4)	1.715(4)
Mo(3)-O(6)	1.699(4)	Mo(3)-O(15)	1.697(7)	Mo(12)-O(34)	1.682(17)	Mo(2)-O(21)	1.896(3)
Mo(4)-O(17)	1.699(4)	Mo(3)-O(16)	1.704(7)	Mo(13)-O(13)	1.701(17)	Mo(2)-O(1)	2.290(3)
Mo(4)-O(15)	1.700(4)	Mo(3)-O(7)	1.896(7)	Mo(14)-O(21)	1.710(17)	Mo(3)-O(3)	1.706(4)
Mo(5)-O(33)	1.690(4)	Mo(4)-O(10)	1.703(6)	Mo(15)-O(37)	1.881(18)	Mo(3)-O(13)	1.883(5)
Mo(5)-O(32)	1.703(4)	Mo(4)-O(12)	2.277(6)	Mo(16)-O(8)	1.874(17)	Mo(3)-O(17)	2.256(3)
Mo(6)-O(26)	1.697(5)	Mo(4)-O(2)	1.889(9)	V(11)-O(24)	1.741(16)	Mo(4)-O(2	1.705(4)
Mo(6)-O(25)	1.710(4)	V(1)-O(9)	1.603(10)	V(12)-O(19)	1.619(16)	V(10)-O(6)	1.642(5)
V(1)-O(34)	1.767(4)	V(1)-O(17)	1.762(6)	V(12)-O(18)	1.771(15)	V(10)-O(1)	1.711(5)
V(2)-O(27)	1.627(5)	V(2)-O(13)	1.615(7)	V(13)-O(23)	1.600(17)	V(11)-O(34)	1.636(4)
V(2)-O(31)	1.753(4)	V(2)-O(12)	1.765(6)	V(13)-O(22)	1.758(15)	V(11)-O(29)	1.754(3)
P(1)-O(36)	1.528(4)	V(2)-O(32)	1.777(6)	Se(1)-O(1)	1.703(15)	V(11)-O(26)	1.764(3
P(1)-O(42)	1.532(4)	Te(1)-O(20)	1.868(8)	Se(1)-O(11)	1.706(15)	S(1)-O(7)	1.547(5)
P(1)-O(37)	1.533(4)	Te(1)-O(23)	1.871(6)	Se(1)-O(4)	1.707(16)	S(1)-O(31)	1.550(3)

Table 8.2 Comparison of the crystallographic data for the four egg-shaped compounds.

Formula	$C_{11}H_{55}Na_2Mo_{11}N_5O_{61}PV_7$	$C_{12}H_{78}NaMo_{11}N_6O_{70}TeV_7$	$H_{62}K_7Mo_{11}O_{86}SeV_7$	$H_{52}Mo_{11}N_7O_{67}SV_7$
M_r [g mol^{-1}]	2722.47	2989.31	3203.08	2666.47
symmetry	Triclinic	Orthorhombic	Tetragonal	Monoclinic
Space group	*P-1*	*Pnma*	*P-4b2*	*P2$_1$/m*
a [Å]	13.2527(10)	28.1994(10)	25.7061(2)	12.140(2)
b [Å]	14.1147(11)	20.6903(7)	25.7061(2)	19.148(3)
c [Å]	19.1405(15)	14.6394(5)	19.9182(4)	13.492(3)
α [°]	89.090(4)	90	90	90
β [°]	83.599(4)	90	90	105.650(4)
γ [°]	89.054(4)	90	90	90
ρ_{calcd} [μg m^{-3}]	2.542	2.325	3.233	2.932
V [Å^3]	3557.2(5)	8541.4(5)	13162.0(2)	3020.18(10)
Z	2	4	8	2
μ [mm^{-1}]	2.883	2.728	30.584	3.396
T [K]	150(2)	150(2)	150(2)	293(2)
rflns(collected)	49633	64752	50907	21908
rflns(unique)	13963	8623	11667	5765
R1	0.0388	0.0558	0.0685	0.0301
*w*R2	0.1024	0.1525	0.1882	0.0355
GooF, S	1.048	1.175	1.115	1.069

Table 8.3 Selected bond distances and angles of compound **7**.

bond lengths (Å)			
Mo(1)-O(1)	1.699(7)	V(1)-O(7)	1.602(11)
Mo(1)-O(3)	1.874(9)	Se(1)-O(9)	1.708(9)
Mo(2)-O(3)	1.876(9)	Se(2)-O(15)	1.707(9)
Mo(2)-O(5)	2.011(9)	Se(3)-O(16)	1.656(8)
Mo(3)-O(13)	1.644(10)	Se(4)-O(26)	1.725(7)
angles [°]			
O(1)-Mo(1)-O(3)	101.5(3)	O(7)-V(1)-O(6)	111.0(5)
O(5)-Mo(2)-O(8)	72.2(3)	O(6)-V(1)-O(8)	108.6(3)
O(13)-Mo(3)-O(12)	102.7(4)	O(14)-Se(2)-O(15)	98.9(3)
O(10)-Mo(4)-O(9)	86.5(3)	O(16)-Se(3)-O(18)	103.8(4)

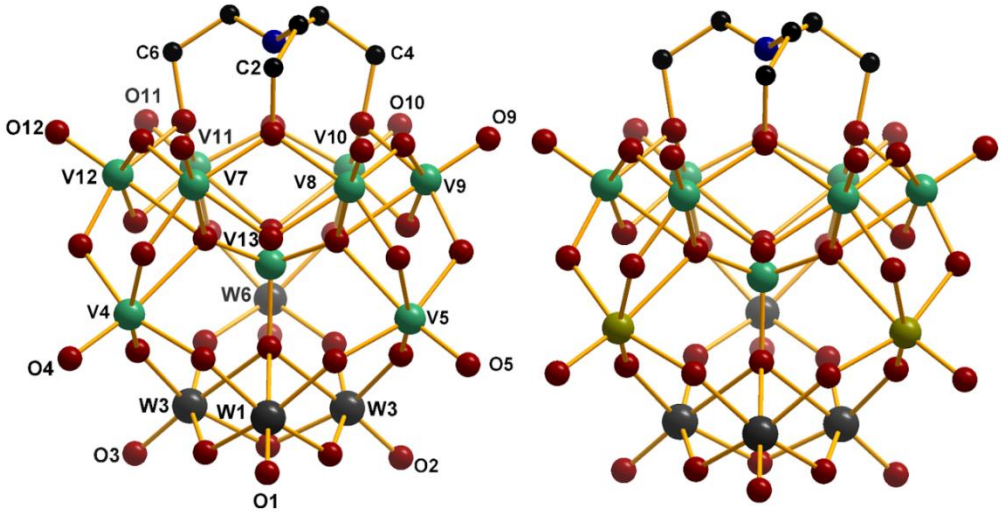

Figure 8.2 Left to right: Balls and sticks representation of compound **9** and **9'**, respectively, showing the position of the metal centres in the clusters. Compounds **10** and **10'** adapt the same configuration. The reduced V atoms (V4 and V5) are represented in dark green. C: black, N: blue

Table 8.4 Selected bond lengths (Å) and angles (°) for compounds **9** and **9**'.

9	**Å**	**9'**	**Å**
W(1)-O(1)	1.692(6)	W(1)-O(1)	1.681(7)
W(3)-O(2)	1.670(6)	W(3)-O(2)	1.669(7)
V(4)-O(4)	1.653(6)	V(4)-O(4)	1.669(6)
V(5)-O(5)	1.642(6)	V(5)-O(5)	1.641(8)
W(6)-O(6)	1.629(6)	W(6)-O(6)	1.653(7)
V(7)-O(7)	1.585(6)	V(7)-O(7)	1.593(7)
V(8)-O(8)	1.585(6)	V(8)-O(8)	1.595(7)
V(9)-O(9)	1.594(6)	V(9)-O(9)	1.602(7)
V(10)-O(10)	1.594(6)	V(10)-O(10)	1.596(7)
V(11)-O(11)	1.585(7)	V(11)-O(11)	1.591(8)
V(12)-O(12)	1.586(6)	V(12)-O(12)	1.578(7)
V(13)-O(38)	1.683(5)	V(13)-O(40)	1.689(7)
V(13)-O(37)	1.753(6)	V(13)-O(37)	1.761(6)
C(2)-O(32)	1.407(10)	C(2)-O(32)	1.420(12)
C(4)-O(34)	1.429(10)	C(4)-O(34)	1.434(12)
C(4)-O(36)	1.419(11)	C(6)-O(36)	1.427(12)

9	**°**	**9**	**°**
O(1)-W(1)-O(16)	102.1(3)	O(1)-W(1)-O(16)	101.8(3)
O(16)-W(1)-O(13)	156.2(3)	O(16)-W(1)-O(13)	156.6(3)
O(1)-W(1)-O(37)	174.7(2)	O(1)-W(1)-O(37)	174.5(3)
O(2)-W(3)-O(19)	101.7(3)	O(2)-W(3)-O(19)	101.0(3)
O(13)-W(3)-O(37)	76.1(2)	O(13)-W(3)-O(37)	76.4(2)
O(3)-W(3)-O(21)	102.9(3)	O(3)-W(3)-O(21)	102.9(3)
O(31)-V(7)-O(32)	90.0(2)	O(31)-V(7)-O(32)	90.1(3)
O(33)-V(9)-O(34)	91.2(2)	O(33)-V(9)-O(34)	91.7(3)
O(35)-V(10)-O(34)	94.4(3)	O(35)-V(10)-O(34)	92.8(3)
O(35)-V(11)-O(36)	90.2(3)	O(35)-V(11)-O(36)	89.8(3)
O(31)-V(12)-O(36)	93.8(2)	O(31)-V(12)-O(36)	94.2(3)

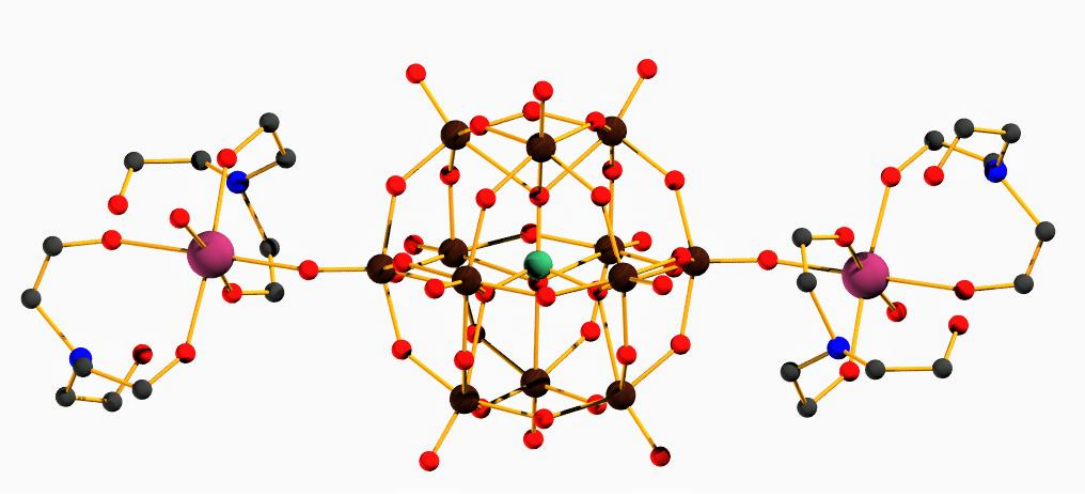

Figure 8.3 Ball and stick representation of the a-Keggin structure isolated in the absence of the reducing agent $Na_2S_2O_4$. Colour code: W/V: brown; V (heteroatom): green; Na: purple; N:blue; O:red spheres.

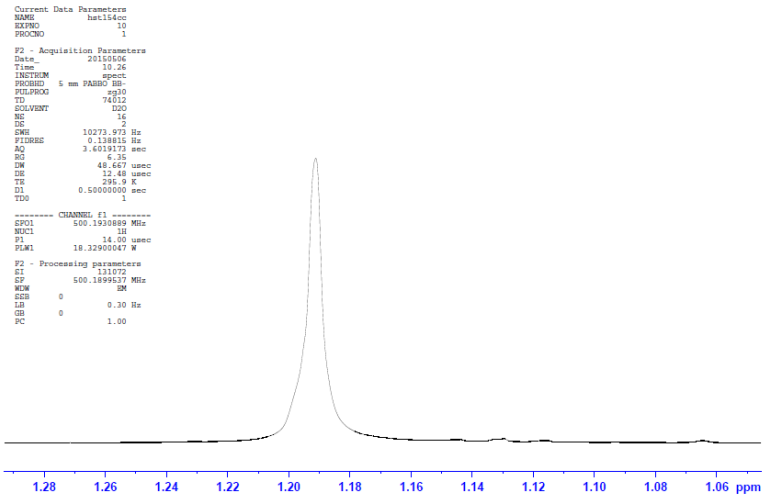

Figure 8.4 1HNMR spectrum for compound **9**.

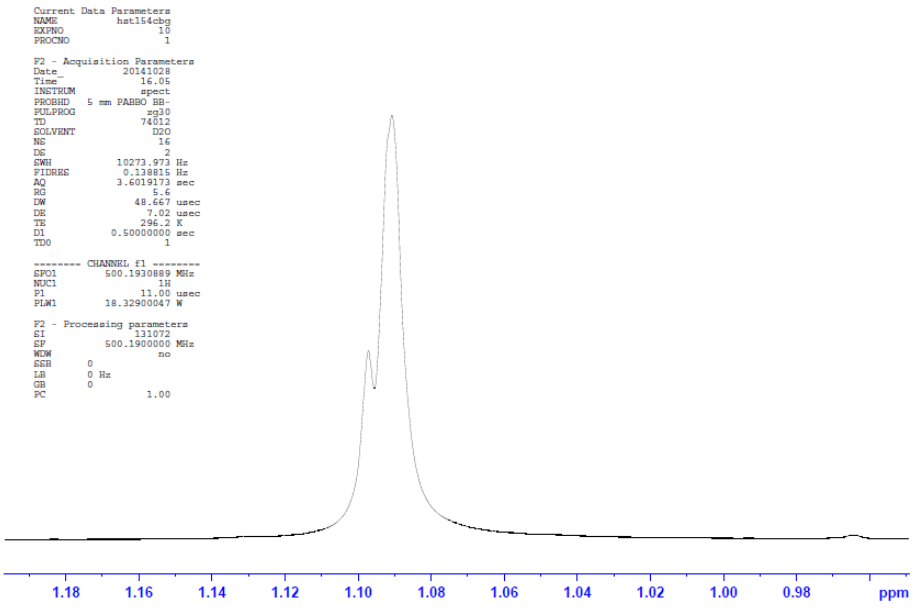

Figure 8.5 ^{1}HNMR spectrum for compound **9'** showing the peak separation and therefore the present of unpaired electrons. The ppm difference (shift difference) between the two peaks was used for the calculations.

9. References

1. (a) M. T. Pope, A. Müller, *Angew. Chem. Int. Ed.*, **1991**, *30*, 34-48; (b) C. L. Hill, Chem. Rev., **1998**, *98*, 1-2; (c) J. Forster, B. Rösner, R. H. Fink, L. C. Nye, I. Ivanovic-Burmazovic, K. Kastner, J. Tucher, C. Streb, *Chem. Sci.*, **2013**, *4*, 418-424; (c) A. Müller, M. Penk, E. Krickemeyer, H. Bögge, H.-J. Walberg, *Angew. Chem.*, **1988**, *100*, 1787-1789; (d) W. G. Klemperer, T. A. Marquart, O. M. Yaghi, *Mater. Chem. Phys.*, **1991**, *29*, 97-104.
2. (a) Y. Hou, L. N. Zakharov, M. Nyman, *J. Am. Chem. Soc.*, **2013**, *135*, 16651-16657; (b) M. Nyman, *Dalton Trans.*, **2011**, *40*, 8049-8058.
3. (a) W. H. Nelson, R. S. Tobias, *Inorg. Chem.* **1963**, *2*, 985-992; (b) S. Li, S. Liu, S. Liu, Y. Liu, Q. Tang, Z. Shi, S. Ouyang, J. Ye, *J. Am. Chem. Soc.* **2012**, *134*, 19716-19721.
4. N. V. Izarova, M. T. Pope, U. Kortz, *Angew. Chem. Int. Ed.* **2012**, *51*, 9492-9510.
5. L. C. W. Baker, D. C. Glick, *Chem. Rev.*, **1998**, *98*, 3-50.
6. (a) J. M. Clemente-Juan, E. Coronado, A. Gaita-Arino, *Chem. Soc. Rev.*, **2012**, *41*, 7464-7478; (b) M. Clemente-León, E. Coronado, C. Gómez-García, E. Martínez-Ferrero, *J. Cluster Sci.* **2002**, *13*, 381-407.
7. I. V. Kozhevnikov, *Chem. Rev.* **1998**, *98*, 171-198.
8. (a) T. Yamase, *J. Mater. Chem.* **2005**, *15*, 4773-4782; (b) H. Stephan, M. Kubeil, F. Emmerling, C. E. Müller, *Eur. J. Inorg. Chem.* **2013**, *2013*, 1585-1594; (c) C. Jasmin, J. C. Chermann, G. Herve, A. Teze, P. Souchay, C. Boy-Loustau, N. Raybaud, F. Sinoussi, M. Raynaud, *Journ. Nat. Can. Inst.*, **1974**, *53*, 469-474.
9. (a) E. Coronado, C. J. Gómez-García, *Chem. Rev.* **1998**, *98*, 273-296; (c) A. Proust, R. Thouvenot, P. Gouzerh, *Chem. Commun.* **2008**, 1837-1852.
10. C. W. Scheele, *ed. Martin Sändig, Niederwalluf/Wiesbaden (reprint: original 1793), Vol. 1*, **1971**.
11. J. J. Berzelius, *Poggend. Ann. Phys. Chem.* **1826**, *82*, 369-392.
12. (a) C. de Marignac, *C. R. Acad. Sci.*, **1862**, *55*, 888; (b) C. de Marignac, *Ann. Chim. Phys.* **1864**, *3*, 5.
13. A. Werner, *Ber. Dtsch. Chem. Ges.* **1907**, *40*, 15-69.
14. A. Miolati, R. Pizzighelli, *J. Prakt. Chem.* **1908**, *77*, 417-456.
15. A. Rosenheim, J. Jaenicke, *Z. Anorg. Allg. Chem.* **1917**, *101*, 215-224.
16. L. Pauling, *J. Am. Chem. Soc.* **1929**, *51*, 2868-2880.
17. (a) J. F. Keggin, *Nature* **1933**, *132*, 351-351; (b) J. F. Keggin, *P. Roy. Soc. Lond. A. Mat.* **1934**, *144*, 75-100.

18. J. S. Anderson, *Nature* **1937**, *140*, 850-850.
19. (a) H. T. Evans, *J. Am. Chem. Soc.* **1948**, *70*, 1291-1292; (b) H. T. Evans, *Acta Crystallogr. B* **1974**, *30*, 2095-2112.
20. B. Dawson, *Acta Crystallogr.* **1953**, *6*, 113-126.
21. G. M. Sheldrick, *Acta Crystallogr A* **2008**, *64*, 112-122.
22. A. Müller, E. Krickemeyer, J. Meyer, H. Bögge, F. Peters, W. Plass, E. Diemann, S. Dillinger, F. Nonnenbruch, M. Randerath, C. Menke, *Angew. Chem. Int. Ed.*, **1995**, *34*, 2122-2124.
23. (a) U. Kortz, *Eur. J. Inorg. Chem*, 2009, **2009**, 5055-5276; (b) L. Cronin, A. Müller, *Chem. Soc. Rev.* **2012**, *41*, 7333-7334.
24. D.-L. Long, E. Burkholder, L. Cronin, *Chem. Soc. Rev*., **2007**, *36*, 105-121.
25. A. Müller, P. Kögerler, *Coordin. Chem. Rev.* **1999**, *182*, 3-17.
26. L. Pauling, The Nature of the Chemical Bond, 3rd ed., *Cornell University Press, Ithaca,* **1960**.
27. A. J. Bridgeman, G. Cavigliasso, Faraday Discussions **2003**, *124*, 239-258.
28. J. H. Kennedy, *J. Inorg. Nucl. Chem.* **1961**, *20*, 53-57.
29. A. Dolbecq, E. Dumas, C. R. Mayer, P. Mialane, *Chem. Rev*. **2010**, 110, 6009-6048.
30. C. L. Hill, Special Issue, Chemical Reviews, **1998**, *98*, 1-390.
31. M. T. Pope, Heteropoly and Isopoly Oxometalates, Springer-Verlag, New York, 1983.
32. I. Lindqvist, *Arkiv Kemi*, **1950**, *2*, 349-355.
33. K. H. Tytko, Mehmke, J., Fischer, S., *Struct. Bond*, **1990**, *93*, 129.
34. (a) J. Fuchs, W. Freiwald, H. Hartl, *Acta Crystallogr. B* **1978**, *34*, 1764-1770.
35. (a) H. Hartl, *Z. Anorg. Allg. Chem.* **1997**, *623*, 1311-1316; (b) C. D. Garner, N. C. Howlader, F. E. Mabbs, A. T. McPhail, R. W. Miller, K. D. Onan, *J. Chem. Soc., Dalton Trans.* **1978**, 1582-1589.
36. M. Nyman, T. Alam, F. Bonhomme, M. Rodriguez, C. Frazer, M. Welk, *J. Clust. Sci.* **2006**, *17*, 197-219.
37. F. Ito, T. Ozeki, H. Ichida, H. Miyamae, Y. Sasaki, *Acta. Crystallogr., Sect. C: Cryst. Struct. Commun.*, **1989**, *45*, 946-947.
38. U. Lee and H.-C. Joo, *Acta Crystallogr., Sect. E: Struct. Rep. Online*, **2004**, *60*, i86-i88.
39. A. L. Nolan, C. C. Allen, R. C. Burns, D. C. Craig, G. A. Lawrance, *Aust. J. Chem.*, **1998**, *51*, 825-834.
40. A. Perloff, *Inorg. Chem.*, **1970**, *9*, 2228-2239.

41. V. S. Sergienko, V. N. Molchanov, M. A. P. Koshits, E. A. Torchenkova, *Koord. Khim.*, **1979**, *5*, 936.
42. H. Kondo, A. Kobayashi, Y. Sasaki, *Acta Crystallogr., Sect. B: Struct. Crystallogr. Cryst. Chem.*, **1980**, *36*, 661-664.
43. H. Y. Lee, K. M. Park, U. Lee, H. Ichida, *Acta Crystallogr., Sect. C: Cryst. Struct. Commun.*, **1991**, *47*, 1959-1961.
44. A. Ogawa, H. Yamato, U. Lee, H. Ichida, A. Kobayashi, Y. Sasaki, *Acta Crystallogr., Sect. C: Cryst. Struct. Commun.*, **1988**, *44*, 1879-1881.
45. K. J. Schmidt, G. J. Schrobilgen, J. F. Sawyer, *Acta Crystallogr., Sect. C: Cryst. Struct. Commun.*, **1986**, *42*, 1115-1118.
46. H. Naruke, T. Yamase, *Acta Crystallogr., Sect. C: Cryst. Struct. Commun.*, **1992**, *48*, 597-599.
47. (a) C. Rocchiccioli-Deltcheff, M. Fournier, R. Franck, R. Thouvenot, *Inorg. Chem.* **1983**, *22*, 207-216; (b) S. Himeno, M. Takamoto, M. Hoshiba, A. Higuchi, M. Hashimoto, *Bull. Chem. Soc. Jpn.* **2004**, *77*, 519-524.
48. L. C. W. Baker, T. P. McCutcheon, *J. Am. Chem. Soc.* **1956**, *78*, 4503-4510.
49. G. N. Newton, S. Yamashita, K. Hasumi, J. Matsuno, N. Yoshida, M. Nihei, T. Shiga, M. Nakano, H. Nojiri, W. Wernsdorfer, H. Oshio, *Angew. Chem. Inter. Ed.*, **2011**, *50*, 5716–5720.
50. L. C. W. Baker, J. S. Figgis, *J. Am. Chem. Soc.* **1970**, *92*, 3794-3797.
51. M. T. Pope, *Inorg. Chem.*, **1976**, *15*, 2008-2010.
52. (a) A. Kobayashi, Y. Sasaki, Bull. Chem. Soc. Jpn., **1975**, *48*, 885-888; (b) J. Fuchs, A. Thiele, R. Z. Palm, Naturforsch., **1981**, *36b*, 161-171; (c) F. Robert, A. Tézé, G. Hervé, Y. Jeannin, *Acta Crystallogr.*, **1980**, *B36*, 11-15; (d) J. N. Barrows, G. B. Jameson, M. T. Pope, J. Am. Chem. Soc., **1985**, *107*, 1771-1773.
53. (a) N. Shimizu, T. Ozeki, H. Shikama, T. Sano, M. Sadakane, J. Clust. Sci., **2013**, *25*, 755-770; (b) A. Ishii, T. Ozeki, Polyhedron, **2005**, *24*, 1949-1952.
54. (a) B. Botar, A. Ellern, P. Kögerler, Dalton Trans., **2009**, *29*, 5606-5608; (b) A. S. Assran, S. Sankar Mal, N. V. Izarova, A. Banerjee, A. Suchopar, M. Sadakane, U. Kortz, Dalton Trans., **2011**, *40*, 2920-2925; (c) E. Cadot, V. Béreau, B. Marg, S. Halut, F. Sécheresse, Inorg. Chem., **1996**, *35*, 3099-3106; (d) K. Uehara, T. Taketsugu, K. Yonehara, N. Mizuno, Inorg. Chem., **2013**, *52*, 1133−1140; (e) André Tézé, Emmanuel Cadot, V. Béreau, G. Hervé, Inorg. Chem., **2001**, *40*, 2000-2004.
55. (a) V. K. Day, W. G. Klemperer, D. E. Páez Loyo, Inorg. Chem., **1992**, *31*, 3187-3189.

56. M. I. Khan, A. Müller, S. Dillinger, H. Bögge, Q. Chen, J. Zubieta, Angew. Chem., **1993**, *105*, 1811-1814; Angew. Chem. Int. Ed. Engl., **1993**, *32*, 1780-1782.
57. (a) A. Müller, C. Beugholt, P. Kögerler, H. Bögge, S. Bud'ko, M. Luban, Inorg. Chem., **2000**, *39*, 5176-5177; (b) P. Mialane, A. Dolbercq, L. Lisnard, A. Mallard, J. Marrot, F. Sécheresse, Angew. Chem., **2002**, *114*, 2504-2507; Angew. Chem. Int. Ed., **2002**, *41*, 2398-2401.
58. J. Tucher, L. C. Nye, I. Ivanovic-Burmazovic, A. Notarnicola, C. Streb, Chem. Eur. J., **2012**, *18*, 10949–10953.
59. H. Sartzi, H. N. Miras, L. Vilà-Nadal, D.-L. Long, L. Cronin, *Angew. Chem. Inter. Ed.*, **2015**, *54*, 15488-15492.
60. W. H. Casey, Chem. Rev., **2006**, *106*, 1–16.
61. (a) V. Baskar, M. Shanmugam, M. Helliwell, S. J. Teat, R. E. P. Winpenny, *J. Am. Chem. Soc.*, **2007**, *129*, 3042–3043; b) B. K. Nicholson, C. J. Clark, S. G. Telfer, T. Groutso, *Dalton Trans.*, **2012**, *41*, 9964–9970.
62. (a) X. Lopez, C. Bo, J. M. Poblet, *Inorg. Chem.* **2003**, *42*, 2634-2638;
63. (a) H. Wu, *J. Biol. Chem.* **1920**, *43*, 189-220; (b) R. Acerete, C. F. Hammer, L. C. W. Baker, *Inorg. Chem.*, **1984**, *23*, 1478-1482;
64. R. Contant, R. Thouvenot, *Inorg. Chim. Acta* **1993**, *212*, 41-50.
65. P. J. S. Richardt, R. W. Gable, A. M. Bond, A. G. Wedd, *Inorg. Chem.* **2001**, *40*, 703-709.
66. F.-Q. Zhang, W. Guan, L.-K. Yan, Y.-T. Zhang, M.-T. Xu, E. Hayfron-Benjamin, Z.-M. Su, *Inorg. Chem.* **2011**, *50*, 4967-4977.
67. C.-H. Zhan, R. S. Winter, Q. Zheng, J. Yan, J. M. Cameron, D.-L. Long, L. Cronin, **2015**, *54*, 14308-14312.
68. J. Gao, J. Yan, S. Beeg, D.-L. Long, L. Cronin, *J. Am. Chem. Soc.* **2013**, *135*, (5), 1796-1805.
69. M. Yoshimura, H. Suda, Hydroxyapatite and Related Materials, (P. W. Brown and B. Constanz, eds.), **1994**, 45–72.
70. (a) M. I. Khan, Q. Chen, J. Zubieta, *Inorg. Chem.* **1993**, *32*, 2924-2928; (b) S. -T. Zheng, G. -Y. Yang, *Chem. Soc. Rev.*, **2012**, *41*, 7623-7646.
71. (a) D.-L. Long, P. Kögerler, L. J. Farrugia, L. Cronin, *Angew. Chem., Int. Ed.*, **2003**, *42*, 4180; (b) M. Ibrahim, Y. Lan, B. S. Bassil, Y. Xiang, A. Suchopar, A. K. Powell, U. Kortz, *Angew. Chem., Int. Ed.*, **2011**, *50*, 4708; (c) C. P. Pradeep, D.-L. Long, P. Kögerler, L. Cronin, *Chem. Commun.*, **2007**, 4254; (d) B. S. Bassil, M. Ibrahim, R. Al-Oweini, M. Asano, Z. Wang, J. van Tol, N. S. Dalal, K.-Y. Choi, R. Ngo Biboum, B. Keita, L. Nadjo, U. Kortz, *Angew. Chem., Int. Ed.*, **2011**, *50*,

5961; (s) S. G. Mitchell, P. I. Molina, S. Khanra, H. N. Miras, A. Prescimone, G. J. T. Cooper, R. S. Winter, E. K. Brechin, D.-L. Long, R. J. Cogdell, L. Cronin, *Angew. Chem., Int. Ed.*, **2011**, *50*, 9154.

72. D. Webb, T. F. Jamison, *Chem. Sci.*, **2010**, *1*, 675-680.
73. J. Wegner, S. Ceylan, A. Kirschning, *Chem. Commun.*, **2011**, *47*, 4583-4592.
74. J.-ichi Yoshida,Y. Takahashi, A. Nagaki, *Chem. Commun.*, **2013**, *49*, 9896-9904.
75. H. N. Miras, G. J. T. Cooper, D.-L. Long, H. Bögge, A. Müller, C. Streb, L. Cronin, *Science*, **2010**, *327*, 72-74.
76. A. Ruiz de la Oliva, V.Sans, H.N. Miras, J. Yan, H. Zang, C. J. Richmond, D.-L. Long, L. Cronin, *Angew. Chem. Int. Ed.*, **2012**, *51*, 12759 -12762.
77. A. Müller, F. Peters, M. T. Pope and D. Gatteschi, *Chem. Rev.*, **1998**, *98*, 239-272.
78. W. G. Klemperer, T. A. Marquart and O. M. Yaghi, *Angew. Chem. Int. Ed. Engl.*, **1992**, *31*, 49-51.
79. R. H. Laye, M. Murrie, S. Ochsenbein, A. R. Bell, S. J. Teat, J. Raftery, H. Güdel, E.
    McInnes, *Chem. Eur. J*. **2003**, 9, 6215-6220.
80. R. P. Bontchev, M. Nyman, *Angew. Chem. Int. Ed.*, **2006**, *45*, 6670-6672.
81. M. Maekawa, Y. Ozawa, A. Yagasaki, *Inorg. Chem.*, **2006**, *45*, 9608-9609.
82. H. T. Evans, *Inorg. Chem.*, **1966**, *5*, 967-977.
83. J. Fuchs, S. Mahjour, J. Pickardt, *Angew. Chem. Int. Ed. Engl.*, **1976**, *15*, 374-375.
84. V. W. Day, W. G. Klemperer, O. M. Yaghi, *J. Am. Chem. Soc.*, **1989**, *111*, 4518-4519.
85. V. W. Day, W. G. Klemperer, O. M. Yaghi, *J. Am. Chem. Soc.*, **1989**, *111*, 5959-5961.
86. D. Hou, K. S. Hagen, C. L. Hill, *J. Am. Chem. Soc.*, **1992**, *114*, 5864-5866.
87. D.-L. Long, D. Orr, G. Seeber, P. Kögerler, L. J. Farrugia, L. Cronin, *J. Cluster Sci.*, **2003**, *14*, 313-324.
88. Y. Hayashi, K. Fukuyama, T. Takatera, A. Uehara, *Chem. Lett.*, **2000**, *29*, 770-771.
89. A. Müller, M. Penk, E. Krickemeyer, H. Bögge, H.-J. Walberg, Angew. *Chem. Int. Ed. Engl.*, **1988**, *27*, 1719-1721.
90. A. G. Swallow, F. R. Ahmed, W. H. Barnes, *Acta Crystallogr.*, **1966**, *21*, 397-405.
91. A. Müller, M. Penk, R. Rohlfing, E. Krickemeyer, J. Döring, Angew. *Chem. Int. Ed. Engl.*, **1990**, *29*, 926-927.
92. A. Müller, E. Krickemeyer, M. Penk, R. Rohlfing, A. Armatage, H. Bögge, *Angew. Chem. Int. Ed. Engl.*, **1991**, *30*, 1674-1677.

93. B. Dong, C. J. Gómez-García, J. Peng, S. Benmansour, J. Ma, *Polyhedron*, **2007**, *26*, 1310-1316.

94. A. Müller, R. Rohlfing, J. Döring, M. Penk, *Angew. Chem. Int. Ed.*, **1991**, *30*, 588-590.

95. (a) J. F. Keggin, *Nature*, **1933**, *131*, 908-909; (b) J. F. Keggin, *Proc. R. Soc. A*, **1934**, *144*, 75-100.

96. (a) R. Allmann, *Acta Crystallogr. Sect. B*, **1971**, *27*, 1388-1393; (b) A. Chrissafidou, J. Fuchs, H. Hartl, R. Palm, *Z. Naturforsch. B*, **1995**, *50*, 217-222.

97. J. Fuchs, E. P. Flindt, *Z. Naturforsch. B*, **1979**, *34*, 1393-1404.

98. J. Fuchs,W. Freiwald, H. Hartl, *Acta Crystallogr. Sect. B*, **1978**, *34*, 1757-1764.

99. D.-L. Long, O. Brucher, C. Streb, L. Cronin, *Dalton Trans.*, **2006**, 2852-2860.

100. T. Lehmann, J. Fuchs, *Z. Naturforsch., B: J. Chem. Sci.*, **1988**, *43*, 89-93.

101. H. N. Miras, J. Yan, D.-L. Long, L. Cronin, *Angew. Chem. Int. Ed.*, **2008**, *47*, 8420-8423.

102. I. Bruedgam, J. Fuchs, H. Hartl, R. Palm, *Angew. Chem. Int. Ed.*, **1998**, 37, 2668-2671.

103. R. G. Bhattacharyya, S. Biswas, *Inorg. Chim. Acta*, **1991**, *181*, 213-216; (b) M. McCann, D. McDonnell, *Chem. Commun.*, **1993**, 1718-1719.

104. (a) H. Lü, W. Ren, P. Liu, S. Qi, W. Wang, Y. Feng, F. Sun, Y. Wang, *Appl. Catal. A.*

Gen., **2012**, *136*, 441-442; (b) H. T. Evans, B. M. Gatehouse, P. Leverett, *J. Chem. Soc. Dalton Trans*. **1975**, 505-514.

105. (a) D. Hagrman, C. Zubieta, D. J. Rose, J. Zubieta, R. C. Haushalter, *Angew. Chem. Int. Ed. Engl.*, **1997**, *36*, 873-876; (b) A. J. Bridgeman, *J. Phys. Chem. A*, **2002**, *106*, 12151-12160.

106. P. Wu, Q. Li, N. Ge, Y. Wei, Y. Wang, P. Wang, H. Guo, *Eur. J. Inorg. Chem.*, **2004**, *14*, 2819-2822.

107. (a) H. Y. Zang, K. Tan, W. Guan, S. L. Li, G. S. Yang, K. Z. Shao, L. K. Yan, Z. M. Su, *Cryst. Eng. Comm.*, **2010**, *12*, 3684-3690; (b) H. Y. Zang, Y. Q. Lan, S. L. Li, G. S. Yang, K. Z. Shao, X. L. Wang, L. K. Yan, Z. M. Su, *Dalton Trans.*, **2011**, *40*, 3176-3182.

108. A. Proust, F. Robert, P. Gouzerh, Q. Chen, J. Zubieta, *J. Am. Chem. Soc*., **1997**, *119*, 3523-3535.

109. U. Turpeinen, I. Mutikainen, M. Klinga, R. Hamalainen, Z. Kristallogr. *New Cryst. Struct*., **2001**, *216*, 515-520.

110. D.-L. Long, C.Streb, P. Kögerler, L.Cronin, *J. Cluster Sci.*, **2006**, *17*, 257-266.

111. T. Shibahara, M. Sasaki, G. Sakane, *Inorg. Chim. Acta*, **1995**, *237*, 1-3.

112. G. Liu, S.-W. Zhang, *Acta Cryst.* **2002**, *58*, 92-94.

113. W. Yang, C. Lu, X. Lin, H. Zhuang, *Chem. Commun.*, **2000**, *41*, 1623-1624.

114. D.-L. Long, P. Kögerler, L. J. Farrugia, L. Cronin, *Angew. Chem. Int. Ed.* **2003**, 42, 4180-4183.

115. (a) O. Kraus, *Z. Kristall.*, **1939**, *100*, 394-413; (b) S. W. Zhang, G. Q. Huang, Y. G. Wei, M. C. Shao, Y. Q. Tang, *Acta Crystallogr., Sect. C: Cryst. Struct. Commun.*, **1993**, *49*, 1446-1448; (c) T. Hori, S. Himeno, O. Tamada, *Dalton Trans.*, **1996**, 2083-2087; (d) B. Krebs, E. Droste, M. Piepenbrink, G. Vollmer, *C. R. Acad. Sci., Serie IIc: Chim.*, **2000**, *3*, 205-210.

116. M. Ibrahim, S. S. Mal, B. S. Bassil, A. Banerjee, U. Kortz, *Inorg. Chem.*, **2011**, *50*, 956-960.

117. K. Y. Matsumoto, M. Kato, Y. Sasaki, *Bull. Chem. Soc. Jpn.*, **1976**, *49*, 106-110.

118. K. Wassermann, M. H. Dickman, M. T. Pope, *Angew. Chem. Int. Ed.*, **1997**, *36*, 1445-1448.

119. (a) F. Hussain, R. W. Gable, M. Speldrich, P. Kogerler, C. Boskovic, *Chem. Commun.*, **2009**, 328-330; (b) C. Ritchie, V. Baslon, E. G. Moore, C. Reber, C. Boskovic, *Inorg. Chem.*, **2011**, *51*, 1142-1151; (c) U. Kortz, M. G. Savelieff, B. S. Bassil, M. H. Dickman, *Angew. Chem. Int. Ed.*, **2001**, *40*, 3384-3386; (d) U. Kortz, M. G. Savelieff, B. S. Bassil, B. Keita, L. Nadjo, *Inorg. Chem.*, **2002**, *41*, 783-789.

120. Y. Jeannin and J. Martin-Frère, *Inorg. Chem.*, **1979**, *18*, 3010-3014.

121. Q. Han, X. Sun, J. Li, P. Ma, J. Niu, *Inorg. Chem.*, **2014**, *53*, 2006-2011.

122. (a) D.-L. Long, P. Kögerler, L. Cronin, *Angew. Chem. Int. Ed.*, **2004**, *43*, 1817-1820; (b) C. Baffert, J. F. Boas, A. M. Bond, P. Kögerler, D.-L. Long, J. R. Pilbrow, L. Cronin, *Chem. Eur. J.*, **2006**, *12*, 8472-8483; (c) C. Fleming, D.-L. Long, N. McMillan, J. Johnston, N. Bovet, V. Dhanak, N. Gadegaard, P. Kogerler, L. Cronin, M. Kadodwala, *Nat. Nano*, **2008**, *3*, 229-233.

123. D.-L. Long, H. Abbas, P. Kögerler, L. Cronin, *Angew. Chem. Int. Ed.*, **2005**, *44*, 3415-3419.

124. Q. Zheng, L. Vilà-Nadal, C. Busche, J. S. Mathieson, D.-L. Long, L. Cronin, *Angew. Chem. Int. Ed.*, **2015**, *54*, 7895-7899.

125. M. J. Manos, J. D. Woollins, A. M. Z. Slawin, T. A. Kabanos, *Angew. Chem. Int. Ed.*, **2002**, *41*, 2801-2805.

126. H. N. Miras, D. J. Stone, E. J. L. McInnes, R. G. Raptis, P. Baran, G. I. Chilas, M. P. Sigalas, T. A. Kabanos, L. Cronin, *Chem. Commun.*, **2008**, 4703-4705.

127. J. Yan, D.-L. Long, L. Cronin, *Angew. Chem., Int. Ed.*, **2010**, *49*, 4117-4120.

128. J. Yan, J. Gao, D.-L. Long, H. N. Miras, L. Cronin, *J. Am. Chem. Soc.*, **2010**, *132*, 11410-11411.
129. M. N. Corella-Ochoa, H. N. Miras, D.-L. Long, L. Cronin, *Chem. Eur. J.*, **2012**, *18*, 13743-13754.
130. J. Gao, J. Yan, S. G. Mitchell, H. N. Miras, A. G. Boulay, D.-L. Long, L. Cronin, *Chem. Sci.*, **2011**, *2*, 1502-1508.
131. J. Gao, J. Yan, S. Beeg, D.-L. Long and L. Cronin, *Angew. Chem. Int. Ed.*, **2012**, *51*, 3373-3376.
132. M. N. Corella-Ochoa, H. N. Miras, A. Kidd, D.-L. Long, L. Cronin, *Chem. Commun.*, **2011**, *47*, 8799-8801.
133. A. Macdonell, N. A. B. Johnson, A. J. Surman, L. Cronin, *J. Am. Chem. Soc.*, **2015**, *137*, 5662-5665.
134. G. Rozantsev, S. Radio, N. Gumerova, V. Baumer, O. Shishkin, *J. StrucT. Chem.*, **2009**, *50*, 296-305.
135. (a) A. Perloff, *Inorg. Chem.*, **1970**, *9*, 2228-2239; (b) C.-G. Lin, W. Chen, D.-L. Long, L. Cronin, Y.-F. Song, *Dalton Trans.*, **2014**, ***43***, 8587-8590.
136. A. L. Nolan, R. C. Burns, G. A. Lawrance, D. C. Craig, *Acta Crystllogr. C*, **2000**, *56*, 729-730.
137. D.-L. Long, P. Kögerler, A. D. C. Parenty, J. Fielden, L. Cronin, *Angew. Chem., Int. Ed.*, **2006**, *45*, 4798-4803.
138. J. Yan, D.-L. Long, E. F. Wilson, L. Cronin, *Angew. Chem., Int. Ed.*, **2009**, *48*, 4376-4380.
139. D.-L. Long, Y. F. Song, E. F. Wilson, P. Kögerler, S. X. Guo, A. M. Bond, J. S. J. Hargreaves, L. Cronin, *Angew. Chem., Int. Ed.*, **2008**, *47*, 4384-4387.
140. L. Vilà-Nadal, K. Peuntinger, C. Busche, J. Yan, D. Lüders, D.-L. Long, J. M. Poblet, D. M. Guldi, L. Cronin, *Angew. Chem. Int. Ed.*, **2013**, *52*, 9695-9699.
141. Müller, E. Krickemeyer, H. Bögge, M. Schmidtmann, C. Beugholt, P. Kögerler, C. Lu, Angew. Chem. Int. Ed., 1998, 37, 1220-1223.
142. A. Müller, E. Krickemeyer, H. Bögge, M. Schmidtmann, F. Peters, *Angew. Chem. Int. Ed.*, **1998**, *37*, 3359-3363.
143. A. Müller, E. Krickemeyer, H. Bögge, M. Schmidtmann, P. Kögerler, C. Rosu, E. Beckmann, Angew. Chem. Int. Ed. 2001, 40, 4034-4037.
144. A. Müller, C. Beugholt, H. Bögge, M. Schmidtmann, Inorg. Chem. 2000, 39, 3112-3113.
145. L. Cronin, C. Beugholt, E. Krickemeyer, M. Schmidtmann, H. Bögge, P. Kögerler, T. K. K. Luong, A. Müller, *Angew. Chem. Int. Ed.* **2002**, *41*, 2805-2808.

146. (a) A. Müller, S. Sarkar, S. Q. N. Shah, H. Bögge, M. Schmidtmann, S. Sarkar, P. Kögerler, B. Hauptfleisch, A. X. Trautwein, V. Schünemann, *Angew. Chem. Int. Ed.*, **1999**, *38*, 3238-3241; (b) A. Müller, S. Q. N. Shah, H. Bögge, M. Schmidtmann, P. Kögerler, B. Hauptfleisch, S. Leiding, K. Wittler, *Angew. Chem. Int. Ed.* **2000**, *39*, 1614-1616.

147. (a) P. Gouzerh and M. Che, *Actual Chim.*, **2006**, 9-22; (b) A. Müller and C. Serain, *Acc. Chem. Res.*, **1999**, *33*, 2-10; (c) P. Kögerler, B. Tsukerblat and A. Müller, *Dalton Trans.*, **2010**, *39*, 21-36; (d) A. Müller and P. Gouzerh, *Chem. Soc. Rev.*, **2012**, *41*, 7431-7463.

148. (a) C. Tanielian, *Coord. Chem. Rev.*, **1998**, *178–180, Part 2*, (0), 1165-1181; (b) N. Mizuno, K. Kamata, *Coord. Chem. Rev.*, **2011**, *255*, (19–20), 2358-2370; (c) B. Hasenknopf, *Front Biosci-LandmrkI*, **2005**, *10*, 275-287; (d) J. T. Rhule, C. L. Hill, D. A. Judd, R. F. Schinazi, *Chem. Rev.* **1998**, *98*, (1), 327-358; (e) D. E. Katsoulis, *Chem. Rev.*, **1998**, *98*, 359-387.

149. D.-L. Long, R. Tsunashima, L. Cronin, *Angew. Chem. Int. Ed.*, **2010**, *49*, 1736-1758.

150. S.-S. Wang, G.-Y. Yang, *Chem. Rev.*, **2015**, *115*, 4893-4962.

151. J. E. Lyons, P. E. Ellis Jr., H. K. Myers Jr., G. Suld, W. A. Langdale, *U.S. Patent 4803187*, Feb. 7, **1989**.

152. (a) B. S. Dzhumakaeva, W. A. Golodov, *J. Mol. Catal.*, **1986**, *35*, 303-307; (b) (a) M. K. Harrup and C. L. Hill, *Inorg. Chem.*, **1994**, *33*, 5448-5455; (c) M. K. Harrup and C. L. Hill, *J. Mol. Catal. A: Chem.*, **1996**, *106*, 57-66.

153. (a) N. M. Okun, T. M. Anderson, C. L. Hill, *J. Am. Chem. Soc.*, **2003**, *125*, 3194-3195; (b) N. M. Okun, M. D. Ritorto, T. M. Anderson, R. P. Apkarian, C. L. Hill, *Chem. Mater.*, **2004**, *16*, 2551-2558.

154. K. Yonehara, K. Kamata, K. Yamaguchi, N. Mizuno, *Chem. Commun.*, **2011**, *47*, 1692-1694.

155. T. Hirano, K. Uehara, K. Kamata, N. Mizuno, *J. Am. Chem. Soc.*, **2012**, *134*, 6425-6433.

156. Y. Kikukawa, K. Suzuki, M. Sugawa, T. Hirano, K. Kamata, K. Yamaguchi, N. Mizuno, *Angew. Chem., Int. Ed.*, **2012**, *51*, 2434-2437.

157. A. Muller, F. Peters, M. T. Pope, D. Gatteschi, Chem. Rev., 1998, 98, 239-272.

158. D. Gatteschi, L. Pardi, A. L. Barra, A. Müller, J. Doring, Nature, 1991, 354, 463-464.

159. M. J. Manos, H. N. Miras, V. Tangoulis, J. D. Woollins, A. M. Z. Slawin, T. A. Kabanos, Angew. Chem., Int. Ed., 2003, 42, 425-427.

160. J. Lehmann, A. Gaita-Arino, E. Coronado, D. Loss, *Nat. Nanotechnol.* **2007**, *2*, 312-317.

161. X. Fang, P. Kögerler, M. Speldrich, H. Schilder, M. Luban, *Chem. Commun.*, **2012**, *48*, 1218-1220.

162. C. Ritchie, A. Ferguson, H. Nojiri, H. N. Miras, Y. F. Song, D.-L. Long, E. Burkholder, M. Murrie, P. Kögerler, E. K. Brechin, L. Cronin, *Angew. Chem., Int. Ed.*, **2008**, *47*, 5609-5612.

163. M. Ibrahim, Y. Lan, B. S. Bassil, Y. Xiang, A. Suchopar, A. K. Powell, U. Kortz, Angew. Chem., Int. Ed., 2011, 50, 4708-4711.

164. H. El Moll, A. Dolbecq, J. Marrot, G. Rousseau, M. Haouas, F. Taulelle, G. Rogez, W. Wernsdorfer, B. Keita and P. Mialane, Chem. Eur. J., **2012**, *18*, 3845-3849.

165. M. A. AlDamen, J. M. Clemente-Juan, E. Coronado, C. Marti-Gastaldo, A. Gaita-Arino, *J. Am. Chem. Soc.*, **2008**, *130*, 8874-8875.

166. C. Ritchie, M. Speldrich, R. W. Gable, L. Sorace, P. Kögerler, C. Boskovic, Inorg. Chem., **2011**, *50*, 7004-7014.

167. B. Botar, A. Ellern, R. Hermann and P. Kögerler, Angew. Chem., Int. Ed., **2009**, *48*, 9080-9083.

168. R. Neumann, A. M. Khenkin, *Inorg. Chem.*, **1995**, *34*, 5753-5760.

169. M. Murakami, D. C. Hong, T. Suenobu, S. Yamaguchi, T. Ogura, S. Fukuzumi, *J. Am. Chem. Soc.*, **2011**, *133*, 11605-11613.

170. F. M. Toma, A. Sartorel, M. Iurlo, M. Carraro, P. Parisse, C. Maccato, S. Rapino, B. R. Gonzalez, H. Amenitsch, T. Da Ros, L. Casalis, A. Goldoni, M. Marcaccio, G. Scorrano, G. Scoles, F. Paolucci, M. Prato, M. Bonchio, *Nature Chemistry* **2010**, *2*, 826-831.

171. N. Kawasaki, H. Wang, R. Nakanishi, S. Hamanaka, R. Kitaura, H. Shinohara, T. Yokoyama, H. Yoshikawa, K. Awaga, *Angew. Chem. Int. Ed.* **2011**, *50*, 3471-3474.

172. L. Vilà-Nadal, S. G. Mitchell, S. Markov, C. Busche, V. Georgiev, A. Asenov, Leroy Cronin, *Chem. Eur. J.* **2013**, *19*, 16502-1651.

173. C. Robl, K. Haake, *J.Chem. Soc., Chem. Commun.*, **1993**, 397-399.

174. N. I. Kapakoglou, B. I. Panagiotis, S. E. Kazianis, C. E. Kosmidis, C. Drouza, M. J. Manos, M. P. Sigalas, A. D. Keramidas, T. A. Kabanos, *Inorg. Chem.*, **2007**, *46*, 6002-6010.

175. N. Fay, A. M. Bond, C. Baffert, J. F. Boas, J. R. Pilbrow, D.-L. Long, L. Cronin, *Inorg. Chem.*, **2007**, *46*, 3502-3510.

176. N. Casan-Pastor, J. Bas-Serra, E. Coronado, G. Pourroy, L. C. W. Baker, *J. Am. Chem. Soc.*, **1992**, *114*, 10380-10383.

177. S. G. Mitchell, S. Khanra, H. N. Miras, T. Boyd, D.-L. Long, L. Cronin, *Chem. Commun.*, **2009**, 2712-2714.
178. K. Nomiya, T. Takahashi, T. Shirai, M. Miwa, *Polyhedron*, **1987**, *6*, 213-218.
179. F.-X. Liu, C. Marchal-Roch, D. Dambournet, A. Acker, J. Marrot, F. Sécheresse, *Eur. J. Inorg. Chem.*, **2008**, *2008*, 2191-2198.
180. H. N. Miras, M. Sorus, J. Hawkett, D. O. Sells, E. J. L. McInnes, L. Cronin, *J. Am. Chem. Soc.*, **2012**, *134*, 6980-6983.
181. N. E. Brese, M. O'Keeffe, *Acta Cryst.*, **1991**, B47, 192-197.
182. C. Baffert, S. Feldberg, A. M. Bond, D.-L. Long, L. Cronin, *Dalton Trans.*, **2007**, *48*, 4599-4607.
183. (a) H. N. Miras, A. R. de la Oliva, H. Zang, V. Sans, L. Paramonov, H. Makatsoris, R. Inglis, E. K. Brechin, D.-L. Long, L. Cronin, *Nature Chem.*, **2012**, *4*, 1037-1043; (b) H.-Y. Zang, A. R. de la Oliva, H. N. Miras, D.-L. Long, R. T. McBurney, L. Cronin, *Nature Commun.*, **2014**, *5*, 3715.
184. T. Scientific, http://www.tricontinent.com/products/cseries-syringe-pumps/.
185. N. I. Corp., http://www.ni.com/trylabview/
186. J. Yue, J. C. Schouten, T. A. Nijhuis, *Ind. Eng. Chem. Res.*, **2012**, *51*, 14583-14609.
187. (a) D. F. Evans, *J. Chem. Soc.*, **1959**, 2003-2005; (b) J. Loliger, R. Scheffold, *J. Chem. Educ.*, **1972**, *49*, 646-647.
188. (a) L. Goerigk, S. Grimme, *WIREs Comput. Mol. Sci.*, **2014**, *4*, 576-600; (b) A. Hansen, C. Bannwarth, S. Grimme, P. Petrovic, C. Werl, J.-P. Djukic, *Chemistry Open*, **2014**, *3*, 177-189.
189. G. M. Sheldrick, *Acta. Crystallogr. Sect. A*, **2008**, *64*, 112-122.
190. P. Müller, *Crystal structure refinement: a crystallographer's guide to SHELXL*, Oxford University Press, Oxford, **2006**.
191. L. J. Farrugia, *J. Appl. Crystallogr.*, **2012**, *45*, 849-854.
192. R. C. Clark, J. S. Reid, *Acta. Crystallogr. Sect. A*, **1995**, *51*, 887-897.
193. R. Blessing, *Acta Crystallogr. Sect. A*, **1995**, *51*, 33-38.
194. H. Wu, J. Biol. Chem., **1920**, *43*, 189.